2016

Recoverable resources calculation using non-linear methods: a comparative study

Matthew Cobb
Edith Cowan University

Recoverable Resources Calculation Using Non-Linear Methods: A Comparative Study

by

Matthew Cobb

A Thesis Submitted to the
School of Science
Edith Cowan University
Perth, Western Australia

In Partial Fulfilment of the Requirements for the
Masters of Science (Mathematics and Planning)

Supervisors:
Associate Professor U Mueller
Dr J Lo

16th May 2016

Edith Cowan University

Copyright Warning

COPYRIGHT AND ACCESS DECLARATION

I certify that this thesis does not, to the best of my knowledge and belief:

(i) incorporate without acknowledgement any material previously submitted for a degree or diploma in any institution of higher education;

(ii) contain any material previously published or written by another person except where due reference is made in the text; or

(iii) contain any defamatory material.

Signed (signature not included in this version of the thesis)

Date…….

Abstract

The prediction of recoverable resources at an operating manganese mine is currently undertaken using univariate ordinary kriging of the target variable manganese, and 5 deleterious variables. Input data densities at the time of this calculation are considerably lower than at the time of final selection (grade control), and the potential for unnacceptable conditional bias to be introduced through the use of linear geostatistical methods when determining grade estimates over a small support has led to assessment of the potential benefit of employing the local change of support methods Localised Uniform Conditioning (LUC) and Conditional Simulation (CS). Allowances for the operating conditions, including time frames for estimation / simulation, and likely software limitations are accounted for by also requiring decorrelation to be used in instances where the data are considered in a multivariate sense. A novel method for decorrelation of geostatistical datasets, Independent Components Analysis (ICA), is compared against the more common method of Minimum-Maximum Autocorrelation Factorisation (MAF). ICA performs comparably against MAF in terms of its ability to diagonalise the variance-covariance matrix of the test dataset over multiple lags, for a variety of input data densities and treatments (log-ratio transformed and raw oxide data).

Based on these results, ICA decorrelated data were incorporated into a comparative study of LUC and CS against block ordinary kriging (BOK), using an input dataset of reduced density, treated variously as raw univariate oxide data, decorrelated oxide data, and log-ratio transformed decorrelated data. The use of the log-ratio transform, designed to account for the 100% sum constraint inherent to the input data, proved impractical for LUC due to difficulties associated with the discrete Gaussian model change of support method employed by this technique. Log-ratio data transformation was restricted to use with CS where back transformation to raw oxide space could take place on a pseudo-equivalent

support to the input data, prior to change of support. While use of the log-ratio transformation for CS guaranteed adherence to the sum constraint for results (the only method to do so) it resulted in distortion to both the spatial and grade distribution of results.

Decorrelation by ICA also posed difficulties, with biases introduced to final back transformed results as a result of the decorrelation algorithm in both log-ratio transformed and oxide data, which in some instances caused impossible negative values to be returned for some variables in the final results. In a comparison of net profit calculations for each method, the distortions introduced from both log-ratio transformation, and decorrelation become evident in either overly optimistic or conservative profit distributions for methods in which they were used. Of the results presented, only BOK, CS and LUC of non-decorrelated oxide data appear to show results similar to those which would be used at the operation during final selection (based on ordinary kriging of a complete dataset). Based on the comparison of spatial grade distributions and both net profit spatial distribution and summary, the decision to employ a non-linear method of recoverable resource calculation at the operation under question would be questionable in terms of its reward for effort, given that the current method of BOK appears to produce equivalent results.

Acknowledgements

As the old saying goes; Insanity is defined as doing the same thing over-and-over, and each time expecting a different result. I disagree, and now instead think that insanity is perhaps better defined as willfully subjecting ones-self to a higher degree by research while raising a young family and working full-time with a partner who is also studying full-time. The very fact that this thesis now exists is therefore not so much solely the end product of my efforts, but more a result of the collective efforts of those who by choice or otherwise agglutinated around me in support of its creation (I couldn't resist throwing in a geology joke). And so...Sonya, thankyou for believing that what I was doing was worthwhile and supporting me unquestioningly despite your own study load. For Penelope, thankyou sweetheart for showing understanding beyond your years when dad was stressed out at home, and may not have had time to play as much as he wanted. And Lawrence, thanks for being an awesome recent addition to the clan, and making me smile when I didn't feel like it. To Ute and Johnny, your patience and insight when discussing statistics and linear algebra with a geologist knows no bounds. Both of you have a knack of explaining complex matters in a way that is clear and simple, but not patronising, and that is a real talent. Your enthusiasm for what you do is clear and infectious, and I could not have reached this point without either of you. Lastly, thankyou to Consolidated Minerals Australia for provision of a great dataset with which to work, and the opportunity to put some of this newfound knowledge into practice.

Contents

List of Figures

List of Tables

Chapter 1

Introduction

The mathematical theory that has become known as geostatistics has its beginnings in the mining industry. Krige's foundational work in the gold mines of the Witswatersrand [38], and its formalisation in the work of Matheron [42] have since established what is now an almost ubiquitous approach to the determination of grade and tonnage characteristics for orebodies. At the core of these methodologies is the desire to define as accurately and precisely as possible the location and grade of portions of an orebody that meet specific grade requirements for profitability (the basic definition of recoverable resources calculation). Just as importantly, from a practical point of view, the characterisation of grade distribution within an orebody typically needs to be at a resolution (area in 2 dimensions / volume in 3 dimensions) that equates to a realistically mineable portion commonly referred to as the *selective mining unit* (SMU) which is typically much smaller than the total orebody size.

In certain mining operations, classification of SMUs as ore or waste does not depend solely on the grade of a single attribute. For a manganese mining operation, deleterious attributes such as iron, silicon, aluminium, phosphorous and lead must also be considered. These variables are correlated to varying degrees, which must be accounted for during resource estimation to preserve the most realistic combination of attributes within the resultant model, and thus maintain a suitable degree of accuracy and precision in ore/waste discrimination. Common techniques for estimation of grade can be extended to multivariate environments accounting for cross-variable correlation, however practical implementation in commercial software can often be cumbersome, and compromises in parameters dictating the spatial relationships between variables may be required in order for the process to be mathematically permissible. The solution to circumvent some of these potential difficulties is decorrelation

of the multivariate input dataset prior to use, via one of a variety of recognised mathematical transformations [45, 44, 63, 10] though any given decorrelation method may not be free itself from limitations.

Finally, in operations such as a manganese mine, the compositional nature of the input data and resultant estimates must be considered. The values of each variable in the multivariate set represent parts of a whole, and as such are subject to a sum constraint where these parts must sum to unity. This requirement also places specific conditions upon the treatment of a dataset during geostatistical studies, which often dictate the need to operate within compositional space, known as the *Simplex* [3].

The following sections define more specifically the problems associated with recoverable resources calculation, and also the additional complexities of compositional, multivariate data. Subsequent to these definitions the objectives and structure of the thesis are outlined, and a tabulation of the notation specific to the document is presented.

1.1 General Statement of Problem

An important feature of the recoverable resources paradigm is that the selection between ore and waste is not made on the actual grade of the material being selected, which cannot be known until after extraction and processing, but instead on the estimate of that grade. It is also therefore important that the methods used to estimate these grades are unbiased, i.e. the expected value of an estimate is equal to the true grade. The common method of kriging aims to achieve unbiasedness on a global scale, such that the average grade from an estimate over a gloablly defined region (eg. an entire orebody) is equal to the average grade of the input data from which the estimate was derived, under the assumption that the input data form a representative sample from the entire orebody. However, global unbiasedness does not guarantee local unbiasedness, particularly where strict stationarity cannot be assumed. In such cases, it is possible that at a smaller scale (a subset region of the orebody), the data distribution and therefore the expected value for that region may differ substantially from the global expected value, and so an estimate that prioritises global unbiasedness, may be severely locally biased compared to the locally expected grade.

Methods based on the computation of weighted averages, such as kriging, inevitably have a normalising/deskewing effect on results when compared to input data. In the case of kriging, weights for input data are derived on the basis of their proximity and orientation to the location at which the value is to be estimated. Depending on the model chosen to represent this spatial relationship, for locations at distances greater than a specified threshold, weights for input data will become uniform and the resultant estimate will simply be their arithmetic average [4]. Where data are sparse, it may be difficult to obtain an estimate using data within the specified range. In this worst case scenario, the normalising effect of the kriging algorithm is at its maximum. While the expected grade over the entire orebody will be unibaised, and any volume / area smaller than this, the estimate is likely to be significantly different to the true grade; local conditional bias, and relates directly to how representative the estimate may truly be when compared to the real (but unknown) value at that location. Further, where input data grade distributions are skewed, misrepresentation of grade due to normalisation may be severe [4]. Therefore, when such an estimate is made at a SMU scale, the existence of conditional bias can potentially severely misrepresent the proportion of an orebody which is recoverable, and there are numerous studies published which warn of the consequences of such estimations at a fine scale with sparse data [4, 39, 36, 35, 34].

The issue of available data and their location defines a phenomenon termed the *information effect* [37] where only limited input data are available to make the required estimate, and which may not be dense enough to avoid severe conditional bias within an estimate at the resolution required. The simplest solution is to increase the volume (*support*) over which an estimate is conducted. For any specified volume within an orebody, the expected grade is simply the average of the grades for any smaller divisions within that volume. In simplistic terms, the larger the volume over which a grade estimate is made, the closer the true grade of that volume is likely to be to the global average, and therefore the lower the conditional bias will be for that estimate. While this resolves the issue of conditional bias, the larger support necessarily reduces the overall variance between estimates within the modeled orebody. This *support effect* in turn makes it more difficult to adequately discriminate between mineable volumes (i.e. SMUs) that may be ore or waste.

Two antagonistic issues thus define the main problem with recoverable resource calculation, and dictate the utility of any estimate of grade(s) within an orebody. The desire for grade discrimination at a suitably small support (SMU) needs to be balanced against potential misrepresentation of grades by the estimate. While the problem would be easily mitigated by

increasing the density of input data to the estimate, the issue must often be considered with an overriding context of commercial viability. In practical terms for a potential mining operation, additional data are obtained usually through additional drilling and sample assaying, which represents a significant expenditure, and is unlikely to be undertaken until viability of the deposit as a mine is made. Consequently, the decision-to-mine is normally made on an estimate based on substantially less data, and for this reason a range of methodologies has been developed known as *change of support*, designed to permit determination of grade distribution at the SMU scale while limiting the issues of conditional bias. The following section summarises published work relating to these various methods in a multivariate environment and, given the requirements for compositional considerations, also offers a background on the treatment of compositional data in a geostatistical sense.

1.2 Change of Support

The concept of change of support derives its name from the support effect, recognising that the variance of the distribution of grades for specific volumes of material within an orebody is directly related to the volume under consideration. As noted in the previous section, larger supports will show decreased grade variance, and modelling this behaviour yields the simplest tools for recoverable resources calculation; global change of support methods. The basis for global change of support methods is permanence of distribution [36], which asserts that for a given region (in this case an orebody) changing from one support to another does not fundamentally change the type of distribution, but only its variance [36]. Operating under this principle, determination of recoverable resources requires knowledge of the distribution of a representative sample, and a means by which to adjust the variance of the distribution as a function of the desired new support. Journel and Huijbregts, Wackernagel, Isaaks and Srivastava [63, 36, 29] present a number of options for variance adjustment including the "affine correction", the indirect lognormal correction (where the underlying grade distribution approximates lognormal), and variance adjustment via Hermite expansion. In the multivariate case, Wackernagel [63] presents only the affine correction, however each of the alternative measures (indirect lognormal / Hermite expansion) may also be applied, as no consideration for the *spatial* distribution of grades is made.

The lack of consideration of the spatial distribution of grade within the orebody is the principal drawback of the global change of support methods. In a decision to mine process,

feasibility for profitable extraction must be considered. Most commonly, the derivation of a specific target value such as maximum profit or maximum ore (product) tonnage is used to determine this feasibility. Objective functions such as the well known Lerchs-Grossman algorithm are routinely applied in the mining industry to optimise the desired parameter, given a set of input assumptions regarding all influencing factors which importantly include grade, tonnage and spatial distribution of the target orebody [40]. This algorithm requires the spatial distribution of grades to be determined on the desired support. Consequently, methods of *local* change of support have been developed.

Multiple Indicator kriging (MIK) offers local grade distribution by kriging not the discrete grade values of the input data, but indicator values defined by the exceedance or otherwise of a particular cutoff grade at each location, for n cutoffs. This non-parametric method effectively provides a set of kriged probabilities of exceeding a given threshold for a particular location, which may be used to define a cumulative distribution function of grade at that location. Once local distributions are defined, their variance may be adjusted to account for the change in support to SMU by means of applying a variance correction factor (such as the affine correction) to the local distribution [14]. MIK is cited as useful for real-world scenarios where multiple discrete grade populations may exist, which cannot be adequately separated on the basis of the spatial information available, and has been used in recoverable resources calculations for both gold and silver at a mine in British Columbia [46]. However, the method also has several limitations; for a set of n cutoff thresholds, a corresponding number of semivariograms must be developed. Additionally, in a mining context, with increasing grade the proportion of a dataset exceeding said grade reduces leaving fewer points on which to define a robust semivariogram. The possibility of negative kriging weights (a risk with all kriging estimators) might lead to negative probabilties for a given threshold, and further there is no guarantee that probabilities of exceedance for increasing threshold values will form a decreasing sequence of values [16]. Indicator co-kriging can be implemented to avoid such order relation problems, however it presents a far greater level of complexity and requires the joint modelling of cross covariances between all indicators. While some authors have achieved success with this method [48] results from Goovaerts [24] anecdotally suggest the benefit from Indicator co-kriging does not significantly outweigh the increased complexity of the method. In a practical sense for the mining industry, recent authors have noted that Indicator co-kriging has largely been relegated to the realms of academia due to its high level of theoretical complexity [52].

Disjunctive kriging (DK), defined by Rivoirard [50] is similar to Indicator co-kriging, in that multiple indicator kriging amounts to an approximation of kriging some function of the target variable distribution for a given location. Given enough indicator thresholds, co-kriging of the indicators is effectively kriging of the function itself. Through the use of a polynomial expansion (typically the Hermite expansion), the kriging of the function defining the variable at each location can then be estimated, by kriging of the factors comprising the polynomial. Variance correction for DK estimates follows the discrete Gaussian model, by means of a variance correction factor applied as a coefficient to each polynomial factor within the resulting expansion [16]. In practical application, DK requires an assumption that the function describing the distribution of the variable under study is invariant within the study area regardless of sample subset size or spatial location (strict stationarity) [16]. Such conditions are rarely encountered within real-world orebodies, and similar to Indicator co-kriging, DK is rarely utilised within the mining industry due to its theoretical constraints.

More commonly within the mining industry, Uniform Conditioning (UC) has been applied for localised change of support calculation. A variant of disjunctive kriging, UC relaxes the stationarity assumptions of DK, by conditioning the distribution of SMU grades to a more spatially localised *panel* comprising a number of SMUs. In this instance, the distribution function for the target variable is only assumed to be stationary over the panel, the average grade of which is determined usually by Ordinary kriging. Given the larger size of a panel with respect to the SMU, careful selection of its size will yield ordinary kriging (OK) estimates that do not exhibit significant conditional bias. Humphreys [25] presents a real-world case for a gold mine where UC has been applied effectively to address the issue of recoverable resources estimation with limited input data. The limitation of the UC method is the restriction of spatial variability to the panel scale, i.e. while UC yields a distribution function of grades within a panel at SMU support, it does not offer indication of the *spatial* distribution of grades within the panel. In the case where input data are sparse, and the panel used for conditioning is quite large, the resulting loss of spatial resolution may limit the utility of UC for mining optimisation studies. Abzalov [1] extends the utility of UC, by addressing this limitation of spatial resolution with an extension of UC known as Localised Uniform Conditioning (LUC). An OK estimate of the SMU grades within a panel, instead of representing the grade of the unit, is used to rank and spatially locate average values of the discretised panel grade distribution derived from UC. There are now numerous studies where LUC has demonstrated to be an effective method of addressing recoverable resources calculation. Abzalov [2] presents two case studies of LUC application at an iron ore mine

and a bauxite mine. Results from the iron ore mine comparative study revealed significantly greater resolution of grade variability from the LUC method when compared to OK results at the SMU scale, while the bauxite study shows the ability for LUC to be utilised in the vertical distribution of Al_2O_3 grades within a panel at an appropriate resolution for current mining practices, where previous estimates were unable to due to the use of historic drilling which was not sampled at a similarly appropriate resolution. Assibey-Bonsu et al. [8, 6, 7] present multiple studies for the successful use of LUC, with comparisons of LUC estimates against production data showing better reconciliation than those of a simple kriging estimate for the same input dataset.

Indicator kriging, DK and UC all offer estimates of the recoverable resources at SMU support by applying (variance) adjustment factors to a function defining the distribution of the target variable grades on point support. An alternative method is that presented by conditional simulation. Different to variance correction, conditional simulation defines a number of equiprobable "realisations" of the value of the target variable at a support similar to the input data. Collectively, these realisations may be considered to define the distribution for the given grade variable at the current support. Changing to a greater support is then simply a matter of averaging the values for each realisation over the number of discrete input values contained within the new support volume / area. By extension, the newly defined suite of realisations on the larger support now define the probable grade distribution for that volume / area. Simulation methods for recoverable resources calculation are advantageous in that, while assumptions regarding permanance of distribution between different supports are implicit, the block averaging method of change of support requires more relaxed assumptions of stationarity than either DK or UC. Their principal drawback is that execution can be cumbersome due to the much larger volumes of data generated, and the greater computational requirements for their production. Journel and Kyriakidis [37] present a comparative study of volume variance correction methods for local change of support (MIK) and simulation and note a number of advantages to simulation. Simulation is not affected by the limitations of MIK, since the change of support is derived from an underlying base of data on quasi-point support, generally equivalent to that of the input data. This common base permits sensitivity analysis to recoverable resources as a function of a variety of SMU sizes, while the existence of a grade distribution function for each SMU also allows for risk sensitivity analysis on the basis of probability of recovered grade. Additionally, results from (L)UC are heavily dependent on panel size selection, as this has an overarching bearing on the degree of conditional bias which may be carried through to the conditioning of the results. Simulation is not constrained in a such a way, and panels may be tailored to any particular requirements.

In the case of open pit mining, this may be advantageous with a panel corresponding to a mining block; the unit on which medium term scheduling is conducted and which is variable depending on pit design and depth (level). Assibey-Bonsu and Muller [5] make the pertinent observation that no localised change of support model, including conditional simulation, is able to account for existing bias resulting from sampling methods / distribution within the data available at the time of estimation / simulation.

1.3 Multivariate Considerations

In a mining scenario, co-products or deleterious elements often require consideration along with the primary target variable. Where these secondary variables show a correlation to the target variable, this needs to be accounted for during estimation. For basic linear geostatistical methods, this is achieved by co-kriging, using cross-variogram models (linear models of coregionalisation - LMC) to account for not only univariate, but also cross-variate spatial correlations. Given that methods such as indicator co-kriging (and MIK), and DK are effectively co-kriged estimates already, application to a multivariate scenario results in very large variance-covariance matrices between not only indicator factors of a distribution function of a single variable, but also between those across different variables. The size of the resultant system of equations to be solved for kriging makes such a practice impractical. The alternatives; LUC and conditional simulation both have more tractable multivariate applications. Desraime and Assibey-Bonsu and Assibey-Bonsu et al. [20, 6, 7] detail the successful use of Localised Multivariate Uniform Conditioning (LMUC), though Desraime and Assibey-Bonsu [20] note that in this case, conditioning of the target variable is achieved under the assumption that its SMU grade is conditionally independent of the panel estimates for secondary variables, given its own panel estimate and that SMU grades of secondary variables are considered conditional only to the primary target variable. In the Multivariate Conditional Simulation method (MCS), all bi-variate cross correlations are taken into account. Both of the multivariate methods mentioned still require the definition of a multivariate models of spatial correlation, which themselves are subject to specific assumptions regarding the nature of spatial (cross-) correlations (e.g. the assumption that the semivariance and cross-semivariance for all variables are adequately modelled using the same number of structures with equal ranges) and may result in sub optimal model representations of the true spatial correlation.

Decorrelation of the variables for estimation/ simulation is a means by which a dataset may

be freed from the limitations associated with using an LMC. Wackernagel [63] proposed the use of Principal Components Analysis (PCA) to decorrelate a dataset, diagonalising its general variance-covariance matrix, however notes that *spatial* correlation between variables would only be completely removed in very specific circumstances (the intrinsic case) uncommon in real world spatial datasets. Desbarats and Dimitrakopolous [19] improved upon this spatial decorrelation using Minimum-Maximum Autocorrelation Factorisation (MAF); a technique for image processing initially proposed by Switzer and Green [57]. MAF ensures very good decorrelation for co-located variables, and also between variables at one specific (user defined) separation distance for variable locations, but is incomplete for all other spatial configurations. Despite these limitations, MAF has seen common use in geostatistical contexts [21, 22, 67, 23, 13].

Subsequent to the introduction of MAF to geostatistical applications, other alternative methods of decorrelation for spatial datasets have been sought, in an attempt to address the incomplete spatial decorrelation shortcomings of MAF. Bandarian [9], Mueller and Ferreira [45] and Mueller [44] present methods of approximate joint diagonalisation which seek optimal, though not necessarily complete, diagonalisation for variance-covariance matrices of multivariate spatial datasets at a suite of selected separation distances. Decorrelation will be jointly maximised accross all chosen separation distances, but will not be complete for any of them. Leuangthong and Deutsch [41] developed a method known as Stepwise Conditional Transformation, where variables are sequentially transformed into Gaussian factors, conditional to the distribution of the variable preceding them in a user defined order. The main objective of this transform is the production of a multivariate Gaussian distribution, however a by product is the independence of transformed variables. While simple to implement, and able to decorrelate variables even in the presence of non-linear relationships, complete decorrelation with stepwise conditional transform will only be achieved at separation distances of zero. Further, the technique is sensitive to the ordering of the variables, and also the number of samples available [17].

A more recently applied method of decorrelation for spatial datasets is that of Independent Components Analysis (ICA). Similar to the other forms of decorrelation, ICA is derived from the field of signal processing, and is a form of Blind Source Separation (BSS). The basis of BSS is the derivation of maximally independent "source" signals (variables) from a series of mixed signals, where there is no a priori knowledge of either the "source" signals themselves, or their mixture compositions. ICA seeks maximally independent signals via objective func-

tion iteration and in doing so, satisfies the less stringent statistical phenomenon of producing maximally decorrelated signals (variables). The fields of communications, image filtering, neuroscience and economics have all demonstrated the utility of ICA [11, 43, 15, 62]. In the context of geostatistics, Tercan and Sohrabian [59] demonstrate the use of ICA as a means of decorrelating coal quality parameters prior to simulation, and their conclusions note an acceptable level of performance for decorrelation. The authors do however note specifically that while results were acceptable in the case presented, the nature of the ICA algorithm cannot ensure adequate decorrelation of variables at distances greater than zero. This highlights both the principal advantage and limitation of ICA for geostatistical decorrelation; since the algorithm operates on the general measure of dependence between variables (and by extension the general variance-covariance matrix), no assumption need be made regarding spatial cross-variable correlations as in the case of MAF. Conversely, the decorrelation based solely on the general variance-covariance matrix allows for no guarantee that decorrelation will be adequate at separation distance greater than zero (as in the case of PCA). Nonetheless, Sohrabian and Ozcelik [55] utilised ICA to decorrelate facing stone quality parameters (water content, permeability, porosity, compressive strength and tensile strength) prior to estimating the independent factors throughout an andesite quarry, and in a comparative study their conclusions indicate that at all spatial separation distances considered, ICA showed better overall performance than PCA.

1.4 Compositional Data in Geostatistics

Compositional datasets are multivariate data that are subject to a sum constraint, where each individual value must be non-negative, and represents a ratio to the whole [66]. Measurements of percentage and parts per million are both compositional. In the context of a mining environment, any estimation or simulation of the grades within an orebody must be bound by this sum constraint in order, not only to be stoichiometrically reasonable, but also to preserve the relative proportions of one component to the others. This latter point can be very important in multivariate operations such as a manganese mine, where deleterious elements must be appropriately represented in conjunction with the main target variable. Methods such as compositional kriging have been developed [64], which preserve the relative proportions of each variable against others, but are difficult to implement, and due to their methodology can lead to negative kriging estimates; a practical impossibility [65].

Using a log-ratio approach, in accordance with the work of Aitchison, Pawlowsky-Glahn et

al. and Tolosana-Delgado et al. [3, 49, 60] resolves the issue of preserving compositions in results, and ensuring positive only results adhering to the sum constraint. This approach is not however, without difficulties. The change of support from point input data to SMU or panel introduces a bias into estimation results when log-ratio data are back transformed [65]. Depending on both the back transform method used and the magnitude of difference in support, this bias may be severe [65, 30]. Consequently, compositional methods are not easily applied in UC where an estimate over a panel is required.

Compositional considerations are however, necessary for change of support methods based upon simulation. Unlike kriging and estimation based methods, simulation algorithms permit values with greater and lesser extremes than the input data (for any given variable). This presents the possibility that stoichiometrically impossible values for any given variable may result. To prevent this, and ensure compliance with the sum constraint, a log-ratio approach may be taken. Given that the basis for simulation is a quasi-equivalent support between input and output, back transformation can be conducted without introduction of significant bias. Change of support can then be undertaken on the back-transformed data.

1.5 Objectives and Research Questions

The research presented in this thesis addresses multiple objectives. Initially, a comparative study of two methods of decorrelation for spatial datasets are presented. The objectives of this part of the thesis are: Firstly, to determine whether Independent Components Analysis (ICA) is a viable means of decorrelation for multivariate spatial datasets; secondly to address what limitations might be inherent to the method in its application to a dataset from a real-world mining operation. ICA is compared against the method of Minimum-Maximum Autocorrelation Factorisation (MAF), which has a more established history of successful usage for decorrelation of geostatistical data. This study is not a full evaluation of the ICA algorithm, and is not designed to identify all possible shortcomings of the method for geostatistical application. Instead, this study is comparative between the novel method of ICA, and more established MAF. While ICA has previously been demonstrated to yield acceptable results in other geostatistical studies, and has been noted to yield better results that PCA, it has yet to be compared against MAF in the same way.

Secondly, a comparative study of 3 methods of recoverable resources calculation is undertaken; Block Ordinary kriging (BOK), Localised Uniform Conditioning, and Conditional

Simulation. Specifically, these methods are studied using the same real-world dataset utilised in part one of the thesis. Current practices at the operation from which data were sourced have recoverable resources calculations made using BOK in a univariate sense. The workflow from recoverable resources calculation through to grade control estimation and final selection immediately prior to mining is well established, and the time constraints placed on grade control estimation and selection require a standardised set of software scripts (macros) that preclude joint estimation / simulation methods. Parameters for this grade control estimation are taken from the prior recoverable resources work, and so this earlier work must also be limited to the univariate case for utility and reconciliation consistency. The non-linear methods trialled in this study are conducted within the framework of limitations that would be imposed, were the method to be employed across the greater operations of the mine from which the data were extracted. Namely, work is restricted to application of univariate geostatistical methods either through intentional disregard of the potential multivariate nature of the dataset, or through decorrelation.

With these considerations, the objective in undertaking this comparative study is to assess the merits or otherwise of each potential method of recoverable resources calculation, against each other and the status-quo at the current mining operation; Block Ordinary kriging.

Specifically, this thesis seeks to answer a series of questions:

1. How effective is ICA for decorrelating spatial datasets, when compared to MAF?
2. Given the constraint of univariate consideration only, how do Conditional Simulation and Localised Uniform Conditioning perform in comparison to each other?
3. What effect on predicted profitability would result from using one of the above methods, when compared to the current forecasting practices at both the decision-to-mine stage and at final selection?
4. What specific limitations might exist with any of the above proposed methods, should they be applied at the currently operating mine from which data were sampled?

1.6 Thesis Structure

Subsequent to the introductory Chapter 1, Chapter 2 provides a summary of the mathematical concepts on which the presented study is based. Chapter 3 provides a geological background

for the deposit under study, and how the geology potentially influences the data arrangement as they are presented. Chapter 4 details treatment of the input data prior to analysis. Chapter 5 focuses on methods of decorrelation, and assesses their performance. Chapters 6 and 7 present the results and conclusions of the various methods of recoverable resources calculation; Ordinary kriging, Localised Uniform Conditioning and Conditional Simulation.

1.7 Notation

The list of symbols and notation used in this thesis are as follows:

Table 1.1: Notation used in this thesis

Symbol	Definition
A	The (Global) area under study.
$\mathbf{B}$	Variance-covariance matrix.
C	Two-point covariance.
c	core / chip volume. The volume of a single sample of material from a drillhole, which is considered so insignificant in proportion to A that it is considered to have point support.
$\tilde{c}$	Quasi-point support volume. A volume of material that is greater than c, but sufficiently small with respect to V and A, that may be considered to have an essentially equivalent dispersion variance to that of c. Conditional Simulations are generated on $\tilde{c}$.
$\mathscr{C}[\cdot]$	Closure operation on the compositional dataset.
$\sigma^2_D(c\|A)$	Dispersion variance between two random functions defined on supports c and A.
$\sigma^2_d(c\|A)$	Experimental dispersion variance between realisations of the random variables $z_c(u)$ and $z_A(u)$ on the differing supports c and A.
den	Density.
$E\cdot$	Theoretical expectation.
$f(z)$	A mathematical function of the variable z.
g	Model semivariogram.
G	Gaussian variable.
γ	Theoretical semivariogram, describing the two-point semivariance between all possible values of $Z(u)$, mapped over A.
$\hat{\gamma}_c$	Experimental semivariogram, calculated from the two point semivariance measurements between realisations $z(u_i)$ and $z(u_j)$ on support c, most commonly determined at multiples of a specified separation vector h.
Γ	Multivariate experimental semivariogram.

Continued on next page

Table 1.1 – *Continued from previous page*

Symbol	Definition
$H(z)$	Entropy of the random variable z.
h	Lag - A vector of specified length used to quantify the two-point semi-variance / covariance of a regionalised variable $\mathbf{z}(u)$.
$J(z)$	Negentropy of random variable z.
$\kappa(h)$	Diagonalisation efficiency for the variance-covariance matrix at lag h.
$\Lambda_{\mathbf{B}}$	Eigenvalues resulting from the decomposition of matrix $\mathbf{B}$.
m	Experimental mean derived from $z(u)$.
$P\cdot$	Probability.
$p_{G/N}$	Profit (Gross / Net).
$Q_{\mathbf{B}}$	Eigenvectors resulting from decomposition of matrix $\mathbf{B}$.
$\mathbb{R}$	Real vector space.
$_{\text{l/f}}$	Price (lump / fines).
$_{\text{p}}^{\text{Fe}}$	Price penalty, superscript defines the deleterious oxide (abbreviated) from which the value is determined.
$s_n(u)$	Simulated realisation n at location u.
vol	Volume (area in 2 dimensions) of a block.
$\tau(h)$	Relative deviation from diagonality of the variance-covariance matrix at lag h.
u	Location within A. i.e. $u \in A$.
σ_c^2	Population variance on support $c; c \in A$.
V	Panel volume. A volume comprising multiples of $v; v, V \in A$.
v	SMU volume. A non trivial volume of material defined as the smallest volume on which discrimination between grades must be made within A.
$\mathbf{W}_{ICA}$	A decorrelation, or "unmixing" matrix. The subscript defines the technique.
$\mathbf{w}$	A single vector from the matrix $\mathbf{W}$.
$\mathrm{X}(u)$	The vector of random variables resulting from the emphadditive log-ratio transformation of multivariate random variable $\mathrm{Z}(u)$.
$\mathbf{Y}_{MAF}$	Random function of decorrelated multivariate random variable $Y_{MAF}(u)$. The subscript denotes the decorrelation method. Individual univariate random variables of the set are denoted by a numerical subscript; $Y_{MAF_N}(u)$.

Continued on next page

Table 1.1 – *Continued from previous page*

Symbol	Definition
$y_{l/f}$	Product yield expressed as a decimal (lump / fines).
$\mathrm{z}(u)$	Realisation of the random variable $\mathrm{Z}(u), u \forall A$.
z	Realisation of a Gaussian random variable, with zero mean and unit variance.
$\mathrm{Z}(u)$	Random variable Z at locations $u \forall A$.
$\mathbf{Z}$	The random function $\mathbf{Z}$.

Chapter 2

Mathematical Background

Presented within this chapter are the mathematical concepts on which the subsequent work is based. Specifically the theory of regionalised variables is described, and the use of a random function model to describe them is explained. The mathematical theory of kriging, conditional simulation and uniform conditioning are outlined in a univariate sense, and it is important to note that only the univariate cases are presented, as this study has been specifically designed to assess the applicability of non-linear geostatistical methods for use in the mining operation from which the data were drawn. Current grade control and mining reconciliation workflows are restricted to univariate methods through a combination of operational time constraints, software limitations and long prevailing historic methodologies. The possible impact of changing operational systems to permit multivariate treatment of data is beyond the scope of the study. Consequently, this chapter also addresses the mathematical methods for dealing with the additional complexities of the dataset being both multivariate and compositional, and the means by which such a dataset may be treated in a univariate geostatistical sense through decorrelation.

2.1 Regionalised Variables

A *regionalised variable* [42], is a function that depends on a continuous variable in 2 or 3D space, and shows variation across space that may be irregular. Characteristically, this variation also tends to show broad scale (longer distance) trends over the defined space in addition to localised, less structured, variability. The metal grade within an orebody is a typical example of a regionalised variable, and for the purposes of decisions such as determining whether

or not an orebody is of sufficient size / grade to mine, it is desirable to be able to define a model to describe the behaviour of this variable. The difficulty in this is that geological features such as orebodies are the product of highly complex interactions between innumerable different factors (eg. host rock chemistry, ore fluid temperature, metal type, duration of mineralising event, size of ore system etc...).

Consider a series of samples of metal grade taken from a collection of drillholes within an orebody. Collectively these samples define the incomplete dataset available to represent the behaviour of metal grade over the entire orebody (incomplete because the orebody is not exhaustively sampled - which would effectively constitute mining). One method of defining a model for such a system is to consider defining a regression function for the large scale trends observed within the regionalsed data, coupled with a measurement of error at each locality to account for the local scale variability. The problems with this approach are that the assumption is made that the local scale variability in values is unrelated to the complex geological processes involved, and the adjustments to the regression function to account for the errors often result in very large, cumbersome equations that are difficult to adequately fit to all of the available data [4].

The alternative is to acknowledge the highly complex interaction of many unknown parameters in the generation of the measured data, and to consider the variability in the measured samples as inherent to the complex (and unknown) function which may describe them.

2.2 The Random Function Model

Now consider the available drillhole samples as a non-repeatable (the exact sample cannot be drilled out twice) set of measurements of an attribute $\{\mathrm{z}(u_a) : u_a \in A, a = 1,\ldots,N\}$ within a study area A. Each measurement $\mathrm{z}(u_a)$ can be thought of as a single realisation of a random variable $\mathrm{Z}(u_a)$ defined at $u_a \in A$, and which describes the continuous (but unknown) distribution of all possible values for the attribute in question at that point. Similarly, the (unknown) value $\mathrm{z}(u)$ of the attribute z can be considered as a realisation of $\mathrm{Z}(u)$ at the unsampled location $u \in A$. The random variable $\mathrm{Z}(u)$ may be defined by its *cumulative distribution function* (cdf):

$$F(u;\mathrm{z}) = P\{\mathrm{Z}(u) \leq \mathrm{z}\} \tag{2.1}$$

which gives the probability that $\mathrm{Z}(u)$ does not exceed a specified threshold z. This cdf is a non-decreasing function for all possible ordered increasing values of z. A *random function* is

a mapping from the study area A into the set of all random variables defined on A:

$$\mathbf{Z} : A \rightarrow \{\mathrm{Z}(u) : u \in A\} \tag{2.2}$$

The random function is characterised by all possible n-point cdfs, and models the joint uncertainty of all random variables across all unsampled locations within the study area:

$$F(u_1 \ldots u_n; \mathrm{z}_1, \ldots, \mathrm{z}_n) = P\{\mathrm{Z}(u_1) \leq \mathrm{z}_1, \ldots, \mathrm{Z}(u_n) \leq \mathrm{z}_n\} \tag{2.3}$$

In the multivariate case, $\mathrm{z}(u) = [\mathrm{z}_1(u), \ldots, \mathrm{z}_K(u)]^T$ is a vector of single realisations for K variables at location u, of the vector $\mathrm{Z}(u) = [\mathrm{Z}_1(u), \ldots, \mathrm{Z}_K(u)]^T$. The random function, $\mathbf{Z}$, in the multivariate case is now a function whose values are vectors of random functions; $\mathbf{Z} : A = \{[\mathrm{Z}_1(u), \ldots, \mathrm{Z}_K(u)] : u \in A\}$. The marginal (univariate) cdf of the k^{th} random function is given by:

$$F_k(u; \mathrm{z}_k) = P\{\mathrm{Z}_k(u) \leq \mathrm{z}, k = 1, \ldots, K \tag{2.4}$$

and the bivariate cdf:

$$F_{jk}(u, u'; z_j, z_k) = Prob(Z_j(u) \leq z_j, Z_k(u') \leq z_k) \tag{2.5}$$

The remaining multivariate cdfs are defined in the same fashion. Together, all K-variate, N-point cdfs for all sampled locations within A define the joint uncertainty of the N unsampled vectors [24]. Knowing each and all univariate, bivariate and multivariate N-point cdfs, for every possible set of locations within the study area A would completely define a spatial model for the behaviour of the K-variate random function. In reality, there is only a single realisation at each of a limited set of locations u for each random function $\mathbf{Z}_K(u)$, and so any comment on the spatial behaviour of a K-variate random function $\mathbf{Z}$, must be made from models which rely on certain assumptions. The main assumption to be held is that of stationarity. A (multivariate in this case, but need not be) random function $\mathbf{Z}$, is said to be strictly stationary if for every positive integer the N-point cdf is invariant under translation [63] . Given the lack of an exhaustively sampled random function (a practical impossibility), the assumption of strict stationarity is relaxed to that of secondary stationarity for geostatistical modelling. Second order stationarity requires only the assumptions that the expected value of a random function $E\{\mathbf{Z}\}$, exists, and is constant, and that the covariances of all possible

pairs of random variables $\mathrm{Z}(u)$ and $\mathrm{Z}(u+h)$ depend only on their separation vector, h [24]. The two point covariance for any given random function $\mathbf{Z}$ is given by:

$$C(h) = E\{\mathrm{Z}(u)\mathrm{Z}(u+h)\} - E\{\mathrm{Z}(u)\}E\{\mathrm{Z}(u+h)\} \tag{2.6}$$

and the corresponding bivariate cross-covariance:

$$C_{ik}(h) = E\{\mathrm{Z}_i(u)\mathrm{Z}_k(u+h)\} - E\{\mathrm{Z}_i(u)\}E\{\mathrm{Z}_k(u+h)\}, i,k = 1,\ldots,K \tag{2.7}$$

In the instance where $i = k$, the cross-covariance is simply the covariance. Another measure of the spatial relationship between two random functions is the semivariogram:

$$2\gamma(h) = E\{(\mathrm{Z}(u) - \mathrm{Z}(u+h))^2\} \tag{2.8}$$

which describes the semivariance between two realisations of the same random function, for any given vector h. When the random function is second-order stationary, the semivariogram is related to the covariance function by:

$$C(h) = C(0) - \gamma(h) \tag{2.9}$$

Extended to the multivariate case $\mathrm{z}_i, \mathrm{z}_k (k = 1,\ldots,K)$ between any two random functions in Z, the cross-semivariogram is given by:

$$2\gamma_{(i,k)}(h) = E\{(\mathrm{Z}_i(u) - \mathrm{Z}_i(u+h)).(\mathrm{Z}_k(u) - \mathrm{Z}_k(u+h))\} \tag{2.10}$$

Note that for any given separation vector h, it is not necessarily true that $\gamma_{(i,k)}(h)$ and $\gamma_{(i,k)}(-h)$ are equal, however conventionally any asymmetry is ignored.

In the multivariate case the semivariogram function for a set of K variables is defined by:

$$\Gamma(h) = \begin{bmatrix} \gamma_{(1,1)}(h) & \cdots & \gamma_{(1,K)}(h) \\ \vdots & \ddots & \vdots \\ \gamma_{(K,1)}(h) & \cdots & \gamma_{(K,K)}(h) \end{bmatrix} \tag{2.11}$$

The covariance function for K variable is defined similarly:

$$\mathrm{C}(h) = \begin{bmatrix} C_{(1,1)}(h) & \cdots & C_{(1,K)}(h) \\ \vdots & \ddots & \vdots \\ C_{(K,1)}(h) & \cdots & C_{(K,K)}(h) \end{bmatrix} \tag{2.12}$$

Similar to the univariate case, the semivariogram and covariance functions for the multivariate case are related by:

$$\mathrm{C}(h) = \mathrm{C}(0) - \Gamma(h) \tag{2.13}$$

In practice, the (cross-)semivariance (and cross-covariance) functions are unknown for the random function $\mathbf{Z}$, and are approximated by calculation of the experimental covariance and semivariance from the measured realisations of each $\mathrm{Z}_i, i = 1, \ldots, K$.
The experimental cross-covariance is defined as:

$$\hat{C}_{(i,k)}(h) = \frac{1}{(N(h))} \sum_{(a=1)}^{N(h)} (\mathrm{z}_i(u_a)\mathrm{z}_k(u_{a+h}) - m_i m_k), i, k = 1, \ldots, K \tag{2.14}$$

where m_i and m_k are the means of $\mathrm{z}_i(u)$ and $\mathrm{z}_k(u)$ respectively, calculated from those realisations that satisfy the separation criteria imposed by given lag h.
The experimental cross-semivariance is defined as:

$$\hat{\gamma}_{(i,k)}(h) = \frac{1}{2(N(h))} \sum_{(a=1)}^{N(h)} (\mathrm{z}_i(u_a) - \mathrm{z}_i(u_{a+h}))(\mathrm{z}_k(u_a) - \mathrm{z}_k(u_{a+h})), i, k = 1, \ldots, K \tag{2.15}$$

A model function is then fitted to the resulting $\hat{\gamma}_{(i,k)}(h)$ plotted for a range $h \geq 0$, using a variety of structures to enable the definition of semivariance between measured sample locations, and those locations to be simulated / estimated. In the multivariate case, where cokriging or co-simulation might be undertaken to account for the multivariate nature of a dataset, this amounts to fitting not only semivariogram models in the univariate cases but also permissible models for each of the cross-semivariance instances leading to a Linear Model of Co-regionalisation (LMC). The fitting of a valid LMC is a non-trivial exercise that becomes increasingly difficult with increasing numbers of correlated variables due to the requirement for positive semi-definiteness of the semivariogram matrix [51]. Advancement in the effectiveness of automatic model fitting algorithms in some modern geostatistical software packages has reduced the difficulty of LMC fitting substantially, but as yet such automated model fitting is not ubiquitous to all common software packages.

2.3 Kriging

For the purposes of this study, given the univariate methods limitation, the principles of kriging are presented here only in the univariate sense. The algorithms do extend to the multivariate case, but are beyond the scope of this work. Kriging is the term given to a group of

algorithms that provide the best unbiased estimate via linear weighted averaging. In context, "best" means that the algorithm minimises the variance of the estimation error, and "unbiased" refers to the expected value of the estimation error being zero [4]. The basic premise of kriging is to derive an estimate of z at an unsampled location u, from the weighted average of n nearby known samples $\mathrm{z}(u_\alpha), \alpha = 1,\ldots,n$. The kriged estimate; $\mathrm{Z}^*(u)$ is determined by

$$\mathrm{Z}^*(u) - m(u) = \sum_{\alpha=1}^{n} \lambda_\alpha(u)[\mathrm{Z}(u_\alpha) - m(u_\alpha)] \tag{2.16}$$

where λ_α are the weights attached to each known value, and are determined such that the estimation error variance

$$\sigma^2_{err} = Var[\mathrm{Z}^*(u) - \mathrm{Z}(u)] \tag{2.17}$$

is minimised. Additionally, the expected value of the estimation error is zero.

$$\mathrm{E}[\mathrm{Z}^*(u) - \mathrm{Z}(u)] = 0 \tag{2.18}$$

The kriging algorithm is an exact interpolator, since the estimated value of an attribute at a sampled location u_α will be equal to the sampled value at that location for all locations.

$$\mathrm{Z}^*(u_\alpha) = \mathrm{z}(u_\alpha) \tag{2.19}$$

The weights λ_α used within the kriging system are determined by pre-multiplication of the vector of covariances (semivariances) from known samples to the estimate location, as determined from the semivariogram model, by the inverse of the known sample-to-known sample covariances (semivariances). In the case of Simple kriging, the mean is known and assumed stationary and so eq. 2.20 completely solves the weights for a single location.

$$\begin{bmatrix} \lambda_{u_1} \\ \vdots \\ \lambda_{u_n} \end{bmatrix} = \begin{bmatrix} C_{(u_1,u_1)} & \cdots & C_{(u_1,u_n)} \\ \vdots & \ddots & \vdots \\ C_{(u_n,u_1)} & \cdots & C_{(u_n,u_n)} \end{bmatrix}^{-1} \begin{bmatrix} C_{(u,u_1)} \\ \vdots \\ C_{(u,u_n)} \end{bmatrix} \tag{2.20}$$

With Ordinary kriging, while the mean is assumed to be stationary it is unknown, and so to preserve unbiasedness the kriging weights are forced to sum to one. This is achieved through

the use of a Lagrange multiplier [24] (eq. 2.21).

$$\begin{bmatrix} \lambda_{u_1} \\ \vdots \\ \lambda_{u_n} \\ \mu \end{bmatrix} = \begin{bmatrix} \gamma_{(u_1,u_1)} & \cdots & \gamma_{(u_1,u_n)} & 1 \\ \vdots & \ddots & \vdots & 1 \\ \gamma_{(u_n,u_1)} & \cdots & \gamma_{(u_n,u_n)} & 1 \\ 1 & 1 & 1 & 0 \end{bmatrix}^{-1} \begin{bmatrix} \gamma_{(u,u_1)} \\ \vdots \\ \gamma_{(u,u_n)} \\ 1 \end{bmatrix} \tag{2.21}$$

2.4 (Localised) Uniform Conditioning

Uniform conditioning (UC) is a method of defining the conditional expectation of some non linear function of Z (commonly a Hermite expansion) on support v, conditional to the grade of a larger support V [63, 16]. The grade at support V is typically not known, but may be approximated by a kriged estimation while, selection of a suitable size / volume for V, minimises conditional bias of this estimate.

Under the assumptions of the Discrete Gaussian Model (DGM) [50, 16], the point anamorphosis is used to derive the anamorphosis on SMU support.

$$\mathrm{Z}_v = \phi_v(\mathrm{Y}_v) = \sum_{k=1}^{\infty} \frac{\varphi_k}{k!} H_k r^k(\mathrm{Y}_v) \tag{2.22}$$

and on panel support

$$\mathrm{Z}_V = \phi_V(\mathrm{Y}_V) = \sum_{k=1}^{\infty} \frac{\varphi_k}{k!} H_k r'^k(\mathrm{Y}_V) \tag{2.23}$$

Given that Z_V is approximated by Z_V^*, the proportional tonnage within a specified panel which exceeds a given cutoff, may be then extracted on SMU support

$$T_v(cut) = E[I_{z_v \geq cut} \mid \mathrm{Z}_V^*] = E[I_{y_v \geq y(cut)} \mid \mathrm{Y}_V^*] = 1 - G\left\{ \frac{y(cut) - \frac{r'}{r}\mathrm{Y}_V^*}{\sqrt{1-(\frac{r'}{r})^2}} \right\} \tag{2.24}$$

One of the limitations of UC is that while a conditional cumulative distribution function (*ccdf*) of the extractable tonnage on SMU support may be defined for any given panel, the spatial location within that panel of high and low grade portions is not defined. The Localised

Uniform Conditioning (LUC) variant overcomes this with a post-processing step, whereby the *ccdf* for each panel is discretised into a number of intervals corresponding to the number of SMUs within a panel. A kriged estimate of grade on SMU support is then used to rank the SMUs within a panel, and the average grades from each discretised interval of the panel *ccdf* are assigned according to rank. In this way, the spatial distribution of the SMU grades (conditional to the panel grade) is derived for every panel [1].

2.5 Turning Bands Simulation

Of the many simulation algorithms that exist for use in geostatistical studies two tend to be more prevalent than others within common mining packages; Sequential Gaussian Simulation (SGS) and Turning Bands Simulation (TBS). SGS provides a directly conditioned simulation at each node visited on a random path that is changed for each realisation, by kriging the neighbouring values and selecting a realisation from the resulting Gaussian distribution defined by the estimate and its estimation variance. While the directly conditioned result may be advantageous, the need for unique random paths through the study area for each realisation (in order to avoid spurious correlation between realisations) and the multiple kriging steps for each realisation can significantly increase computation time.

The Turning Bands method is a non-conditional simulation algorithm to simulate Gaussian variables in real space. It proceeds by projection of the 2- or 3- dimensional covariance (or semivariance) function of a variable onto an arbitrary line in $\mathbb{R}$, to define the corresponding 1- dimensional covariance function. Independent covariance functions are determined for a set of n lines then, the coordinates of each point to be simulated are projected onto each of the lines. The simulated value for any point u within $\mathbb{R}$ is determined from the weighted sum of simulated values at projections $u_1, u_2, \ldots, u_n$ determined from each independent 1-dimensional covariance function along each line [16]:

$$s_n(u) = \frac{1}{\sqrt{n}} \sum_{i=1}^{n} s(u_i) \tag{2.25}$$

Once a non-conditional simulation has been completed for all desired points, the data are conditioned. To achieve this, the error between the unconditional simulated value and the true value at each known point is kriged, using the same model of spatial covariance (semivariance) used to generate the simulations. The final conditioned simulated value at each point is then the additive combination of the simulated value and the kriged error. While the

process of Turning Bands has an extra conditioning step post-simulation for each realisation, this kriging step need only take place once. Additionally, there is no need to continually define new random paths through the study area, and both of these points reduce computation time in comparison to SGS.

2.6 Compositional Data

Compositional data are defined as multivariate data, with each component representing a proportion of some defined whole. In this context each variable carries only relative information, must be non-negative and the set must have at least one negatively correlated variable pair [3, 30]. An important feature of compositional datasets is the phenomenon of *spurious correlation* as first described by [3]; due to the data representing proportions which share a common denominator (the sum constraint value).

Common geostatistical methods such as kriging and simulation characteristically ignore the compositional nature of multivariate data [66]. Consequently, there can be no guarantee that the sum constraint at any estimated point u will be preserved for the multivariate random function Z. To alleviate this issue, the data may be transformed via use of the logarithms of ratios between components, which removes the sum-constraint limitation from the data while ensuring it remains in multivariate real space $\mathbb{R}$ [49].

A multivariate compositional vector z comprising N parts (known as the N dimensional simplex S^N) will sum to a constant (which in this study is 100%)

$$\sum_{n=1}^{N} \mathrm{z}_n = 100\% \tag{2.26}$$

and may be transformed via the *additive logratio* (alr) transform (here presented relative to the N^{th} component of $\mathbf{Z}$

$$alr(\mathrm{z}) = \mathrm{x} = (ln(\frac{\mathrm{z}_1}{\mathrm{z}_N}), \ldots, ln(\frac{\mathrm{z}_{N-1}}{\mathrm{z}_N})) \tag{2.27}$$

The alr transform also reduces the number of variables to be modelled by one.

Back transformation of logratio data from $S^{N-1} \rightarrow \mathbb{R}^N$ is achieved through the additive generalised logistic (*agl*) function

$$agl(\mathrm{x}) = \mathrm{z} = 100 * \frac{(\exp(x_1), \ldots, \exp(x_{N-1}), 1)}{1 + \sum_{n=1}^{N-1} \exp(x_n)} \tag{2.28}$$

2.7 Decorrelation

The potential difficulties relating to fitting of an LMC commonly require compromises in the fit of the resulting model in order to be admissible. For example, permissible structures which may be used for modelling the (cross-)covariance are limited to those common between all univariate covariance models, and therefore may result in sub-optimal compromises between in representivity of the covariance model used and the underlying experimental data. Additionally, the computational power required for intensive operations such as conditional simulation while not prohibitive, is far more onerous for co-simulation, and may be restricted by available memory and processing power of available computers. To alleviate these issues, it is possible to transform a multivariate regionalised dataset into uncorrelated factors. Each factor may then be modelled / estimated / simulated independently in a univariate sense, with the results back-transformed to reinstate spatial correlation.

2.7.1 Min-Max Autocorrelation Factorisation

The method of Minimum-Maximum Autocorrelation Factorisation (MAF) has origins in signal processing, and was first described as a method for separating signals in Landsat data [57]. Desbarats [19] introduced MAF for decorrelating geostatistical datasets. Since this time, multiple other works have cited the utility of MAF as a means of geostatistical decorrelation [21, 22, 67, 23, 13, 56, 55, 61]. It proceeds through two rotations and a scaling of the data, based on decompositions of the variance covariance matrix.

The multivariate random variable $\mathrm{Z}(u) = [\mathrm{z}_1(u), \ldots, \mathrm{z}_N(u)]^T$ has a variance-covariance matrix $\mathbf{B}$. The spectral decomposition of $\mathbf{B}$ into its eigenvalues and eigenvectors can be used to define a transformation matrix, which when applied to $\mathrm{Z}(u)$ yields N principal components of the dataset.

$$\mathbf{B} = \mathrm{Q}^T \Lambda \mathrm{Q} \tag{2.29}$$

defines the rotation and scaling matrix

$$\mathbf{W}_{PCA} = \Lambda^{-1/2}\mathrm{Q} \tag{2.30}$$

and the transformed random variable

$$\mathrm{Y}_{PCA}(u) = \mathbf{W}_{PCA}\mathrm{Z}(u) \tag{2.31}$$

MAF then proceeds via a second decomposition, this time of the semivariogram matrix of $\mathrm{Y}_{PCA}(u)$ at a specified lag h

$$\Gamma_{\mathrm{Y}_{PCA}}(h) = \mathrm{Q}_{\Gamma}^{T}\Lambda_{\Gamma}\mathrm{Q}_{\Gamma} \tag{2.32}$$

to yield a second rotation, which when applied to the first scaling and rotation defines the MAF transformation matrix [51]

$$\mathbf{W}_{MAF} = \mathrm{Q}_{\Gamma}\Lambda^{-1/2}\mathrm{Q} \tag{2.33}$$

and the resultant transformed factors

$$\mathrm{Y}_{MAF} = \mathbf{W}_{MAF}\mathrm{Z}(u) \tag{2.34}$$

Decorrelation using MAF ensures complete decorrelation at both lag distance zero and h, however decorrelation will be incomplete at any other lag. Thus, selection of an appropriate lag distance at which to determine the second rotation for MAF is an important decision for which no general answer exists. It is possible to improve decorrelation at all lags, by fitting a valid 2 structure LMC to $\mathrm{Z}(u)$

$$\Gamma(h) = \mathbf{B}_1 g_1(h) + (\mathbf{B} - \mathbf{B}_1)g_2(h) \tag{2.35}$$

The resulting LMC for the PCA factors then can be computed as

$$\Gamma_{Y_{PCA}}(h) = \mathbf{I}g_2 + \mathbf{W}_{PCA}\mathbf{B}_1\mathbf{W}_{PCA}^{T}(g_1(h) - g_2(h)) \tag{2.36}$$

and this can be used to derive Q_{Γ} where

$$\mathbf{W}_{PCA}\mathbf{B}_1\mathbf{W}_{PCA}^{T} = \mathrm{Q}_{\Gamma}^{T}\Lambda_{\Gamma}\mathrm{Q}_{\Gamma} \tag{2.37}$$

Working with a valid LMC in this instance allows Q_{Γ} to be determined independent of lag

h, and so decorrelation from the resultant matrix will be improved [51]. However, in many instances, avoidance of fitting an LMC either due to unacceptable compromises in structure, or due to more practical considerations such as software limitations, moots the application of this latter method.

2.7.2 Independent Components Analysis (ICA)

Independent Components Analysis is a means of blind source separation (BSS), which operates under the premise that available data are mixed signals resulting from the linear combination of a number of *independent* source signals. It is best represented by the 'cocktail party problem' where multiple microphones situated around a room simultaneously record the mixed voices of multiple people within that room. Due to their differing locations within the room, each microphone records a different mix of voices. ICA seeks to derive the signals of the individual voices with no *a priori* knowledge of either them, or their combinations at each microphone. The key is that each voice is independent, i.e. the speech from each individual offers no information on the voice of any other.

Now consider the multivariate random variables $\mathrm{Z}(u) = [\mathrm{z}_1(u), \ldots, \mathrm{z}_K(u)]^T$ and $\mathrm{Y}(u) = [\mathrm{y}_1(u), \ldots, \mathrm{y}_K(u)]^T$ as mappings of the multivariate random functions $\mathbf{Z}$ and $\mathbf{Y}$, where $\mathrm{Z}(u)$ is the K-variate original (mixed) data, and $\mathrm{Y}(u)$ is the K independent "source" signals. ICA seeks to find a matrix $\mathbf{M}$ such that

$$\mathrm{Z}(u) = \mathbf{M}\mathrm{Y}(u) \tag{2.38}$$

which allows the determination of matrix $\mathbf{W} = \mathbf{M}^{-1}$, yielding

$$\mathrm{Y}(u) = \mathbf{W}\mathrm{Z}(u) \tag{2.39}$$

The determination of $\mathbf{M}$ and $\mathbf{W}$ is complicated by the fact that no information is available on $\mathrm{Y}(u)$. However, the assumption that $\mathrm{y}_1(u), \ldots, \mathrm{y}_K(u)$ are *independent* permits the deduction of $\mathbf{M}$. Quantitative assessment of independence of the source components is possible in a variety of ways; with the commonly utilised methods being infomax [11], maximum likelihood estimation [53], and minimisation of mutual information / maximisation of negentropy [26, 28]. Each of these cases is based on the definition of an objective function for maximisation / minimisation of a particular feature as a proxy for independence.

The method under consideration here is FastICA [26]. It is a consequence of central limit

theorem that the sum of two or more independent datasets will yield a more Gaussian result than any of the inputs [47] therefore, determining the maximum "non-Gaussianity" of each source $\mathrm{y}_k(u) : k = 1,\ldots,K$ would also ensure their maximal independence. FastICA uses the measurement of negentropy for the discrete distribution of each variable (based on the vector of available measurements) as an indication of their non-Gaussianity. FastICA as a method of implementation has been chosen for this study due to its speed and the robustness of the measure of non-Gaussianity used. (For a more complete review of all of the mentioned methods of ICA, the reader is referred to Hyvärinen and Oja, and Hyvärinen et al. [28, 27]).

For implementation of FastICA, consider a single source component y:

$$\mathrm{y} = \mathbf{w}^T \mathbf{Z}(u) = \sum_{i=1}^{K} \mathrm{w}_i \mathrm{z}_i(u) \tag{2.40}$$

where $\mathbf{w}$ is one of the columns of $\mathbf{M}^{-1} = \mathbf{W}$. Now let $\mathbf{v} = \mathbf{M}^T \mathbf{w}$ and:

$$\mathrm{y} = \mathbf{w}^T \mathbf{Z}(u) = \mathbf{w}^T \mathbf{M} \mathrm{Y}(u) = \mathbf{v}^T \mathrm{Y}(u) \tag{2.41}$$

This describes a single source component y as a linear combination of *all* source components $\mathrm{Y}(u)$, and will be more Gaussian than any of them individually. When $\mathrm{y} = \mathbf{w}^T \mathrm{Z}(u)$ is maximally non-Gaussian, it will also represent one of the source components. The FastICA algorithm utilises measurement of negentropy due to its ease of implentation and speed. Given that a Gaussian random variable of zero mean and unit variance contains maximum entropy H [54], for any given function $f(z)$ of the random variable $\mathrm{Z}(u)$:

$$H(z) = -\int f(z) \ln f(z) dz \tag{2.42}$$

The negentropy J may be defined as a non negative measure which is zero only when z is Gaussian:

$$J(z) = H(z_{Gauss}) - H(z) \tag{2.43}$$

and for given experimental data is approximated by:

$$J(z) \propto [E\{G(z)\} - E\{G(v)\}]^2 \tag{2.44}$$

where G is a non-quadratic function, and $\mathbf{v}$ is a Gaussian random variable of zero mean and unit variance.

Hyvärinen and Oja [28] propose to maximise independence in FastICA, using measurement of negentropy by using a fixed point iteration scheme:

1. Consider g as the derivative of G
2. For $i = (1, \ldots, n)$, Select a random initial vector $\mathbf{w}_i$
3. Let $\mathbf{w}_i^+ = E\{\mathrm{Z}(u)g(\mathbf{w}_i^T\mathrm{Z}(u))\} - E\{g'(\mathbf{w}_i^T\mathrm{Z}(u))\}\mathrm{w}_i$
4. Let $\mathbf{w}_i = \mathbf{w}_i^+ / \|\mathbf{w}_i^+\|$
5. Orthogonalise full matrix $\mathbf{W}$ by
   (a) $\mathbf{W} = \mathbf{W}/\sqrt{\|\mathbf{W}\mathbf{W}^\mathbf{T}\|}$
   (b) $\mathbf{W} = \frac{3}{2}\mathbf{W} - \frac{1}{2}\mathbf{W}\mathbf{W}^\mathbf{T}\mathbf{W}$
6. Repeat until convergence.

2.7.3 Decorrelation Performance Measures

The decorrelation performance of both MAF and ICA is assessed via two measures:

1: Relative deviation from diagonality τ; the ratio of the sum of absolute values of the off-diagonal elements, against the sum of absolute values of the diagonal elements for the experimental semivariogram matrix, at any lag h:

$$\tau(h) = \frac{\sum_j \sum_k |\gamma(h,j,k)|}{\sum_j |\gamma(h,j,j)|}, j \neq k \tag{2.45}$$

2: Diagonalisation efficiency κ; 1 minus the ratio of the sum of squared off-diagonal *decorrelated* experimental semivariogram elements to the sum of squared off-diagonal elements for the experimental semivariogram matrix of *original* data at any lag h:

$$\kappa(h) = 1 - \frac{\sum_j \sum_k (\gamma_Y(h,j,k)^2}{\sum_j \sum_k (\gamma_Z(h,j,k)^2}, j \neq k \tag{2.46}$$

The value τ is theoretically unbounded, but when decorrelation is good will be close to zero, while the value κ assumes values between 0 and 1 inclusive, and when decorrelation is good will show values close to one [44, 58, 9].

The discrimination of 'good' versus 'poor' decorrelation is arbitrary. There are no specifically set thresholds by which one determines at what point decorrelation becomes poor, however expectations for adequate decorrelation are that τ will show values very close to zero, and that κ will show values very close to one. With this frame of reference, and knowing that established methods such as MAF have already been sucessfully used in a geostatistical context, these decorrelation measure can provide a good comparative means by which to assess the utility of ICA.

2.8 Conventional Profit Calculation

Conventional profit calculations for models used at the current operation are based upon a product grade and yield algorithm. Each block is classified into one of 5 categories, based upon $Mn_3O_4\%$, which determines the processed product able to be generated from that block (and therefore unpenalised initial product price). Price is determined in *dmtu* (Dry Metric Tonnage Units) of Mn, which equates to 0.01 tonnes (10 kg). Total block tonnages are calculated via a regression formula based upon $Mn_3O_4\%$ and $Fe_2O_3\%$. Grade categories are defined thus:

Table 2.1: Product category classifications, with price data.

Ore category	Mn_3O_4 Grade		Lump price	Fines price
	Min	Max		
1	66.64	100	\$4.45	\$3.58
2	58.31	66.64	\$3.99	\$3.58
3	41.65	58.31	\$3.99	\$3.58
4	20.82	41.65	\$3.99	\$2.95
5	0	20.82	\$0.00	\$0.00

Yields for each product are the result of a regression formula based upon the Mn / SiO_2 ratio of the material under examination. Two formulae are used, corresponding to lump yield and fines yield.

Yield to Lump:

$$y_l = \begin{cases} \frac{\ln\left(\frac{\mathrm{Mn}}{\mathrm{SiO_2}}\right)}{4} + 0.3 & \frac{\mathrm{Mn}}{\mathrm{SiO_2}} \leq 5 \\ 0.7 & else \end{cases} \tag{2.47}$$

Yield to Fines:

$$y_f = \begin{cases} 0.0115 \times \ln \dfrac{\text{Mn}}{\text{SiO}_2} + 0.0914 & \dfrac{\text{Mn}}{\text{SiO}_2} > 5 \\ 0.114 & else \end{cases} \tag{2.48}$$

From the product price and tonnage yield calculations, an unpenalised profit for each block is determined:

$$p_G = (\$_l \times vol \times den \times y_l \times 100) + (\$_f \times vol \times den \times y_f \times 100) \tag{2.49}$$

To this profit calculation, penalties are subsequently applied based on the grades of the deleterious elements. The penalty applied differs in mode of calculation and final penalty dependent on the variable under examination.

$$\$_p^{Fe} = \begin{cases} 0 & 0 \leq \text{Fe}_2\text{O}_3 < 8.64 \\ 0 - (p_G \times \dfrac{(\text{Fe}_2\text{O}_3)}{43.21} & 8.64 \leq \text{Fe}_2\text{O}_3 < 43.21 \\ -p_G & \text{Fe}_2\text{O}_3 \geq 43.21 \end{cases} \tag{2.50}$$

$$\$_p^{P} = \begin{cases} (den \times vol \times y_l \times 100) + (den \times vol \times y_f \times 100) & \dfrac{\text{P}_2\text{O}_5}{y_l} \geq 0.23 \\ 0 & else \end{cases} \tag{2.51}$$

$$\$_p^{Al} = \begin{cases} 0 - p_G & \dfrac{\text{Al}_2\text{O}_3}{y_l} \geq 9 \\ 0 & else \end{cases} \tag{2.52}$$

$$\$_p^{Pb} = \begin{cases} (den \times vol \times y_l \times 100) + (den \times vol \times y_f \times 100) & \dfrac{\text{PbO}}{y_l} \geq 0.11 \\ 0 & else \end{cases} \tag{2.53}$$

$$\$_p^{Si} = \begin{cases} 0 - p_G & \text{SiO}_2 \geq 45 \\ 0 & else \end{cases} \tag{2.54}$$

Net profit is then simply the greater of zero or the sum of gross profit and all penalties. Where net profit returns a negative number, these values are set to zero. This has been done

for consistency between methods. While negative or zero-profit blocks would nominally be mined as waste, and would indeed typically have a negative profit (mining cost) associated with them, the focus of this study is calculation of gross revenue as a straight comparative measure.

$$p_N = \begin{cases} p_g + \sum \$_p & p_N \geq 0 \\ 0 & else \end{cases} \tag{2.55}$$

2.9 Evaluation of Recoverable Resources Results

Individual methods of recoverable resources calculation are assessed through examination of the summary statistics and distributions (spatial and non-spatial) of their results. Comparisons are made both between methods, and against the input data used. Under the assumption of permanence of distribution, quantile-quantile plots are used to assess the bias within the results for each variable compared to the input data. Histograms and summary statistics including variance and skewness are also reviewed to comment on the likely representivity of results. Spatially, the results for each variable for each method are compared against each other, with general comment.

Net profit results for each method are compared against each other, and also against the net profit determined from univariate ordinary kriging of a complete dataset (see Chapter 4) which would represent the expected net profit at the time of mining (the grade control estimate). A better measure of performance of each method would be to compare calculated net profit results to the true net profit realised from the flitch from which the study data were extracted. However, the nature of the workflow within the beneficiation plant, which includes the blending of material from multiple open pits on a day-to-day, case-by case basis introduces a disconnect in the reconciliation of the product from a single pit with the material produced through the plant. Additionally, the practice of permitting ore spotters to make ad-hoc decisions to up and down grade ore parcels at the active face during the time of mining further reduces the ability to quantitatively track ore mined in a single pit against product produced for sale. The closest representation of true net profit from a single pit therefore becomes the estimate derived from the most complete dataset immediately prior to mining.

Net profits from simulations are considered both in terms of the distribution of expected net profits from the set of 100 realisations, and also in the context of the single realisation which yields the median net profit when ranked. LUC and OK methods are assessed based on their

singular results.

Chapter 3

Geological Setting of Woodie Manganese Deposits

3.1 Regional Stratigraphy

The Manganese (Mn) of the Woodie Mine is hosted within the Neoarchaean to Mesoproterozoic Oakover Basin; situated on the eastern margin of the Pilbara Craton in north-western Australia. It comprises a basal Archaean sequence sequence of shales, siltstones and carbonate units, which are then unconformably overlain by a series of Mesoproterozoic sediments deposited subsequent to a ca. 1300Ma hiatus (Figure 3.1) [32]. Upper portions of the Archaean units are dominated by the Carawine dolomite, which is variably silicified to produce the Pinjian Chert Breccia, and which crops out as bedding sub-parallel bands of angular silicified dolomite and chert fragments that often preserve internal relict bedding and are cemented by a fine grained chert matrix. Formation of the Pinjian Chert Breccia is attributed to silicification of parts of the upper Carawine Dolomite during prolonged sub-aerial exposure and weathering, with dissolution of less silicified portions causing the *in-situ* collapse and brecciation of the silicified bands contemporaneous with siliceous cementation [18]. This process represents the gradual shallowing of the eastern Hamersley basin, and the eventual cessation of deposition with protracted sub-aerial exposure (and subsequent karst weathering) between *ca*2630Ma - 1300Ma. The Mesoproterozoic upper portions of the Oakover basin are represented within the Woodie Mine region by the Manganese Subgroup [31, 33]. Basal lithologies of the Subgroup are poorly sorted, matrix supported conglomerates derived from the underlying Pinjian Chert Breccia. The formation fines upwards into a poorly sorted ferruginous sandstone and siltstone, and gradationaly contacts the well sorted, medium, grained

sandstones of the upper portions of the Subgroup [31]. The complete stratigraphic column of the Oakover Basin is presented in Figure 3.1.

3.2 Structural Development

Five principal deformation events are recognised within the Oakover Basin: 1) The D_1 northwest-southeast directed rifting of initial basin formation during the Archaean, 2) Protracted Mesoproterozoic D_2 northwest-southeast extension resulting in renewed basin development 3) D_3 strong northeast-southwest compression 4) D_4 east-northeast - west-southwest extension and 5) north-south directed compression [32]. The most relevant activity for deposition of the Woodie orebodies occurred during D_1 and D_2.

Basin initiation was during D_1 extension, and occurred during rift-related development of the Hamersley Basin [12]. The Achaean units of the Oakover Basin were deposited during a transition to sag-related subsidence within the post-rift basin [32]. The north-northwest strike of the normal faulting during this period also set the framework for subsequent tectonic activity. Following a protracted period of quiescence, during which the Pinjian Chert Breccia developed, renewed extensional activity (D_2) occurred; related to the growth of the Bangemall Basin. This northwest-southeast oriented extension saw reactivation of the major northwest striking normal faults of D_1, and the development of an additional network of lesser north-northwest, northeast and and east-southeast extension faults associated with basin growth. The Mesoproterozoic sediments of the Manganese subgroup were deposited contemporaneously with D_2 extension, with the basal conglomerate of the Manganese Subgroup sourced from the flanks of graben and half graben structures formed between the new dilational extensional fault network. Extension during D_2 may be divided into D_{2a} and D_{2b}, with the first period principally associated with fault formation, active tectonism and large scale hydrothermal activity responsible for the formation of the Woodie Manganese deposits. The second period has been associated with coalesence and the intrusion of dolerite into the upper units of the Manganese Subgroup. To a lesser extent, hydrothermal activity during D_{2b} also resulted in Manganese mineralisation, seen within the shales of the upper units of the Manganese Subgroup.

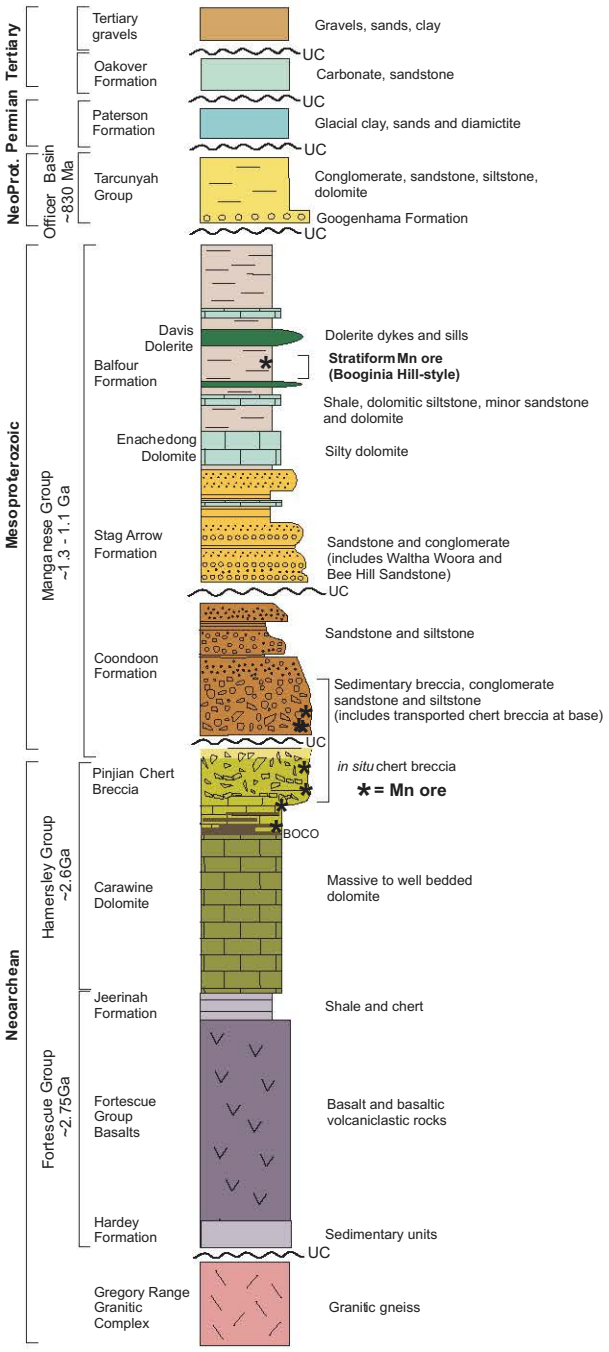

Figure 3.1: Stratigraphic representation of the Oakover Basin, showing mineralised horizons [31]

3.3 Ore Deposit Geology

The Greensnake deposit is a broadly coherent, massive orebody that is principally controlled by 4 faults; the Bells, Greensnake, Channel and Python faults (Figure 3.2). Stratigraphically it is situated within both the Pinjian Chert Breccia, and the overlying Manganese Subgroup. Minor mineralisation is seen within the basal Carawine dolomite. The manganese orebody is partially surrounded by a partially concentric, incomplete shell of Iron (Fe) mineralisation (hematite). Petrogenetic models for the formation of manganese deposits at Woodie propose a predominantly hydrothermal origin for ore fluids, with fault controlled fluid flow. Changing pH / eH conditions due to the buffering effect of dolomite composition caused early stage precipitation of less soluble Fe, resulting in remnant, highly fractionated, manganese (Mn) rich ore bearing fluids finally precipitating Mn bearing ores in the later stages of the mineralising event. Of the other elements of importance, silicon (Si) is partially controlled by host rock lithology, and partially by the composition of the ore bearing fluids. Aluminium (Al) is predominantly related to clay content within the orebody, which in turn is related to both hydrothermal argillacous alteration during mineralisation, and post-mineralisation weathering of the area. Lead (Pb) is largely controlled by ore fluid composition, while phosphorous (P) is controlled by factors similar to Al. These mechanisms for mineralisation are responsible for the appearance of the Fe halo, as pervasive early stage Fe mineralisation is subsequently overprinted by later stage, more confined Mn mineralisation [31]. The fault-related fluid flow and host rock pH control for mineralisation have resulted in the elongate, steeply dipping nature of the orebody and its pseudo-concentric layering and are likely to be expressed within grade data as spatial anisotropy. The overprinting (replacement) nature of Mn with respect to both host lithologies and earlier Iron mineralisation implies a negative correlation between Fe, Si and Al, while the differing controls on concentration for each of these sub-ordinate elements suggest a potentially weaker spatial correlation between Mn and Si / Al.

The Greensnake orebody is dominated by four Mn bearing minerals and hematite (Fe_2O_3). Generally, higher grade (>40% Mn by weight) ores comprise a combination of haussmanite $(Mn)_3O_4$, bixbyite $(Mn,Fe)_2O_3$, cryptomelane $K(Mn^{4+},Mn^{2+})_8O_{16}$, and pyrolusite MnO_2, with the remaining comprising gangue minerals including quartz SiO_2, dolomite $(Mg,Ca)CO_3$ and kaolinite $Al_2Si_2O_5(OH)_4$. Lower grade ores, including those with high Fe content (>6% by weight) are dominated by cryptomelane (50%), with varying contributions from both hematite and quartz ca. 15%, and minor contributions from pyrolusite and bixbyite ($\sim$5% each). The remaining balance comprises goethite FeO(OH), quartz, dolomite and kaolinite. Trace element contaminant Pb is predominantly contained within the mineral coronadite;

$Pb(Mn^{4+}Mn^{2+})_8O_{16}$, while the contaminant P is contained within an as yet unidentified mineralogical phase. Given the complex solid substitution relationships in coronadite, and the unknown phase of P, both are represented within analytical data as their major oxides PbO and P_2O_5. Similarly Al, which is contained mostly within hydrated clay minerals of variable true stoichiometric compositions, is also represented by its major oxide Al_2O_3. It is important to note that mineralogical composition varies widely, and these generalisations do not represent conclusive assemblages.

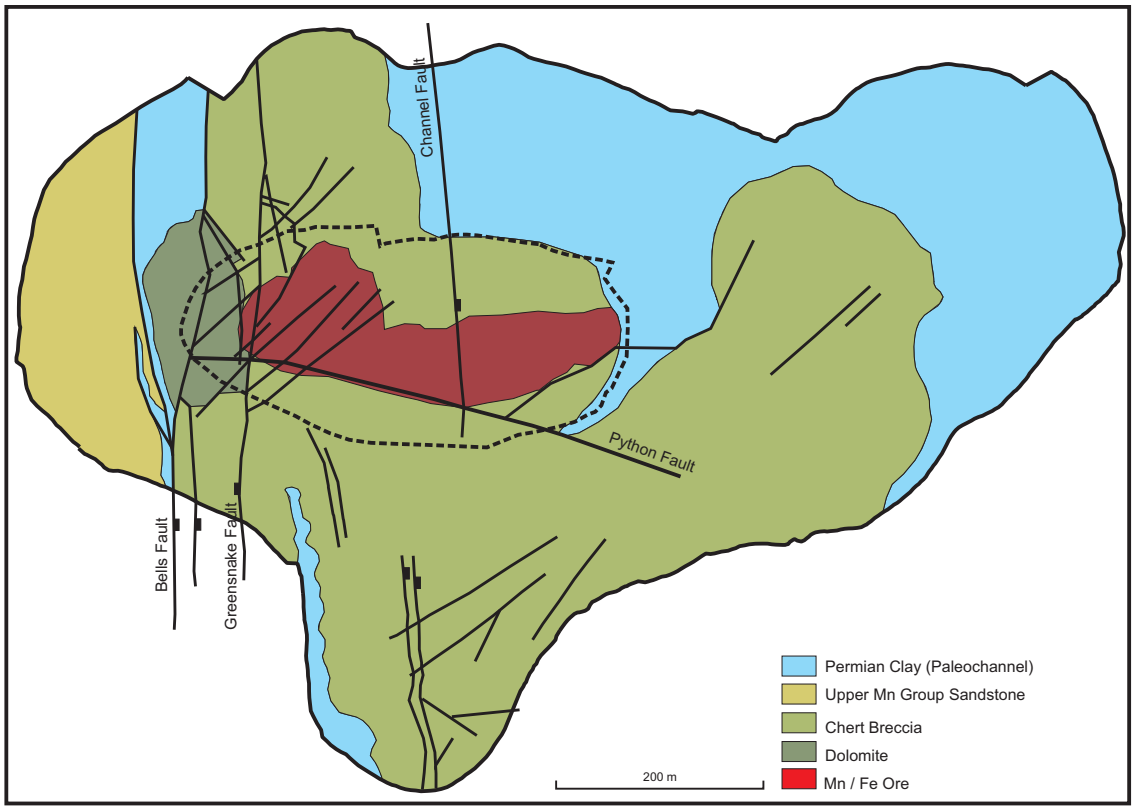

Figure 3.2: Geology of the Greensnake Pit. Dashed outline represents extent of pit floor for data under study

Chapter 4

Input Data

4.1 Background

Data were sourced from drilling information from a single mining flitch of the Greensnake pit at Consolidated Minerals' Woodie Woodie Operations. Data comprised multi-element assays from 1 m RC drillhole samples. Samples are a mix of both resource development and grade-control drilling. In both cases, samples were collected via a rotating cone splitter attached directly to the exhaust hose from the inner-tube return. Samples were collected based on a 12.5% split from the main return. The drillhole database contained holes drilled both vertically and at a dip of -60°, with varying azimuths. For this study, the 1 m sample assay values were composited downhole over 3 vertical metres (flitch height) by selecting those sample intervals whose centroid co-ordinates fell between the two elevations marking the upper and lower limits of the flitch. The co-ordinates of the centroid of the newly created composite were taken as the location data for that single sample. Elevation values were discarded, and data were subsequently considered in the horizontal 2 dimensional plane of the flitch. Both the easting and northing components of the data were subject to linear translation to remove reference to their true location in real space.

A "complete" dataset, and a reduced "resource development" dataset were considered. The complete dataset comprises every sample within the mining flitch, and is representative (in 2 dimensions) of the density of data available immediately prior to mining. For the purposes of this study this constitutes the grade-control dataset, on which final selection prior to mining would be based. The resource development dataset comprises predominantly those intercepts resulting from resource development drilling (no grade-control). Due to the nature

of the exploration process this yields a dataset of lower density (approximately 50% of the complete set) and heterogeneous spatial distribution, and is more representative of the realistic data configuration that would be encountered at this stage of the mining life-cycle. Each dataset is further divided into two domains (eastern - 1 and western - 2) as they exist in the complete 3 dimensional model for the Greensnake orebody. Domaining has been based upon structural controls of mineralisation and overall morphology. The western domain is largely controlled by the Bells and Greensnake faults, while the main eastern domain is controlled by the generally east-west striking Python fault and its splay. Figure 4.1 presents the distribution comparison between complete and resource-development datasets, and also the domain extents. All treatments of the data, including estimation, simulation, transformation, variogram modelling and neighbourhood analysis were conducted on a per-domain basis. Domaining of the data was undertaken on the data recognising differences in orientation of the main mineralisation controlling features in both Domain 1 (eastern, horizontal domain) and Domain 2 (western northerly striking domain), with separation of the two domains taken from the 3-dimensional models of the full orebody from which the study data were sampled. It is the reduced "Resource Development" dataset that is used predominantly within this study to assess the performance of each method of recoverable resources calculation (BOK, LUC and CS) against the others. The complete datset is used only for generation of the "grade-control" estimate, used as a benchmark for the comparison between the other methods.

Assay data at Consolidated Minerals' Woodie Operations are collected via fused disc XRF, with a multi-element suite collected that includes the 6 principal target elements that are utilised within this study. These elements (or their major oxides) comprise the primary commodity, and the five most significant deleterious elements which determine ore grade; Mn (primary commodity), Fe, Al, Si, Pb and P. Six raw variables are routinely reported from the on-site assay laboratory: Mn, Fe, SiO_2, Al_2O_3, Pb and P. Major oxide back-calculations were made for Mn_3O_4, Fe_2O_3, PbO and P_2O_5, which ensures preservation of stoichiometric constraints and prevents elemental concentrations greater than those realistically permitted during subsequent simulation of the data, particularly for Mn_3O_4 and Fe_2O_3 major oxide data.

The scaling factors applied in order to determine major oxide percentages were derived from the common average atomic weights of each element. The scaling factors are presented in Table 4.1

Table 4.1: Conversion ratios for major oxide percentages to elemental values

From	To	Ratio
Mn_3O_4	Mn	0.720309
Fe_2O_3	Fe	0.6994307
P_2O_5	P	0.436427
PbO	Pb	0.92832

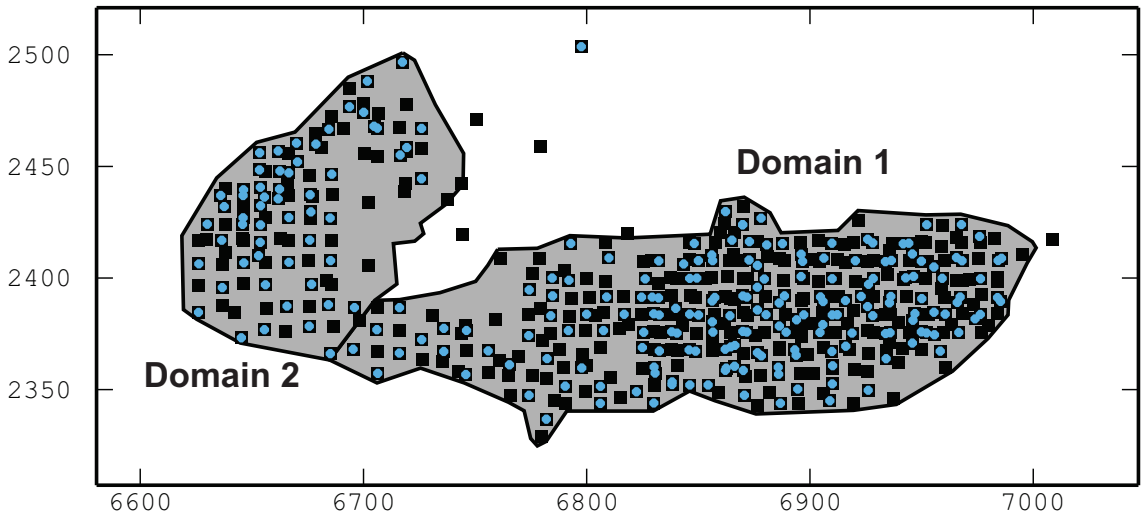

Figure 4.1: Data spatial distribution. Black: Complete (grade control) dataset. Blue: Resource Development dataset

4.2 Summary

Summary statistics for the complete and reduced input data are detailed in Tables 4.2 to 4.5. Both domains generally show broadly similar ranges of values and variance. Exceptions of note are P_2O_5, which shows a much higher maximum and associated greater variance in Domain 1 due to higher value outlier data, and SiO_2, with a higher maximum in Domain 1, making it nearly the sole contributor to the data composition at 96.66%. The main target variable Mn_3O_4 shows moderate to strong negative correlations with Al_2O_3, Fe_2O_3 and SiO_2. A weak to moderate correlation is seen between Mn_3O_4 and deleterious variable PbO, while P_2O_5 shows weak to moderate correlation to Al_2O_3 and SiO_2. The deleterious elements Al_2O_3 and SiO_2 show a moderate positive correlation. Petrogenetically, these correlations are consistent with the known development of the Greensnake orebody. Mn_3O_4, Fe_2O_3 and PbO are all of epigenetic hydrothermal origin, and are emplaced through replacement of the host

rock, which is the primary contributor of SiO_2, Al_2O_3 and P_2O_5. Fe_2O_3 is emplaced earliest, with pH/eH buffering via the dolomitic host rock causing this mineralisation to then be overprinted by minerals bearing Mn_3O_4 and PbO. This replacement system induces the negative correlation between these elements. The reduced dataset shows very similar correlations between variables to the complete dataset, as expected given its predominantly petrogenetic control.

Table 4.2: Summary statistics for the full dataset

VARIABLE	Count	Minimum	Maximum	Mean	Variance	Skewness
All Domains						
Al_2O_3	490	0.07	10.55	1.29	2.22	2.70
Fe_2O_3	490	0.22	90.54	15.92	419.17	1.74
Mn_3O_4	490	0.44	86.22	49.96	809.48	-0.54
P_2O_5	490	0.00	16.59	0.16	0.78	15.76
PbO	490	0.00	0.71	0.06	0.01	3.91
SiO_2	490	0.18	96.66	20.98	467.87	1.54
Domain 1						
Al_2O_3	381	0.07	8.97	0.96	1.36	3.15
Fe_2O_3	381	0.22	90.54	15.2	432.76	1.80
Mn_3O_4	381	0.44	86.22	50.89	860.79	-0.58
P_2O_5	381	0	16.59	0.18	1	13.92
PbO	381	0	0.71	0.05	0.01	4.32
SiO_2	381	0.18	96.66	20.71	487.96	1.57
Domain 2						
Al_2O_3	109	0.33	10.55	2.41	3.59	2.03
Fe_2O_3	109	1.17	88.93	18.44	363.52	1.56
Mn_3O_4	109	1.18	80.68	46.72	616.6	-0.51
P_2O_5	109	0	0.44	0.08	0.01	1.96
PbO	109	0.01	0.62	0.08	0.01	2.67
SiO_2	109	0.57	87.78	21.96	396.42	1.40

Table 4.3: Correlation Matrix for the full dataset, by domain: Upper triangle - Domain 1, Lower triangle - Domain 2

VARIABLE	Al_2O_3	Fe_2O_3	Mn_3O_4	P_2O_5	PbO	SiO_2
Al_2O_3		0.1	-0.47	0.17	-0.08	0.52
Fe_2O_3	-0.01		-0.64	0.08	-0.08	0.05
Mn_3O_4	-0.36	-0.68		-0.16	0.18	-0.73
P_2O_5	0.04	-0.03	-0.02		-0.02	0.1
PbO	0.41	-0.18	-0.01	0.23		-0.18
SiO_2	0.38	0.01	-0.73	0.05	0.13	

Table 4.4: Summary statistics for the reduced (RD) dataset

VARIABLE	Count	Minimum	Maximum	Mean	Variance	Skewness
All Domains						
Al_2O_3	233	0.1	10.55	1.32	2.21	2.41
Fe_2O_3	233	0.22	84.14	14.45	329.28	1.75
Mn_3O_4	233	0.71	85.4	50.29	821.88	-0.57
P_2O_5	233	0	16.59	0.18	1.22	14.16
PbO	233	0	0.68	0.06	0.01	3.46
SiO_2	233	0.18	96.66	21.94	526.46	1.46
Domain 1						
Al_2O_3	177	0.1	5.88	0.89	0.97	2.62
Fe_2O_3	177	0.22	84.14	13.47	337.23	1.88
Mn_3O_4	177	0.71	85.4	52.5	847.83	-0.67
P_2O_5	177	0	16.59	0.2	1.6	12.35
PbO	177	0	0.68	0.05	0.01	4.06
SiO_2	177	0.18	96.66	20.46	518.57	1.6
Domain 2						
Al_2O_3	56	0.56	10.55	2.7	3.61	1.72
Fe_2O_3	56	1.17	67.13	17.55	291.49	1.44
Mn_3O_4	56	1.26	80.68	43.29	675.4	-0.38
P_2O_5	56	0	0.44	0.1	0.01	1.45
PbO	56	0.01	0.62	0.09	0.02	2.31
SiO_2	56	0.57	87.78	26.62	522.56	1.13

Table 4.5: Correlation Matrix for the reduced (RD) dataset, by domain: Upper triangle - Domain 1, Lower triangle - Domain 2

VARIABLE	Al_2O_3	Fe_2O_3	Mn_3O_4	P_2O_5	PbO	SiO_2
Al_2O_3		0.23	-0.51	0.2	-0.09	0.53
Fe_2O_3	0.11		-0.62	0.07	-0.04	0.12
Mn_3O_4	-0.4	-0.61		-0.17	0.16	-0.78
P_2O_5	-0.05	-0.02	0.02		-0.02	0.14
PbO	0.47	-0.23	0.04	0.26		-0.18
SiO_2	0.3	0.03	-0.8	-0.01	0.05	

Table 4.6: Relative erros between complete and reduced datasets

VARIABLE	Minimum	Maximum	Mean	Variance	Skewness
All Domains					
Al_2O_3	43%	0%	2%	0%	11%
Fe_2O_3	0%	7%	9%	21%	1%
Mn_3O_4	61%	1%	1%	2%	-6%
P_2O_5	-	0%	13%	56%	10%
PbO	-	4%	0%	0%	12%
SiO_2	0%	0%	5%	13%	5%
Domain 1					
Al_2O_3	43%	34%	7%	29%	17%
Fe_2O_3	0%	7%	11%	22%	4%
Mn_3O_4	61%	1%	3%	2%	-16%
P_2O_5	-	0%	11%	60%	11%
PbO	-	4%	0%	0%	6%
SiO_2	0%	0%	1%	6%	2%
Domain 2					
Al_2O_3	70%	0%	12%	1%	15%
Fe_2O_3	0%	25%	5%	20%	8%
Mn_3O_4	7%	0%	7%	10%	-25%
P_2O_5	-	0%	25%	0%	26%
PbO	0%	0%	13%	100%	13%
SiO_2	0%	0%	21%	32%	19%

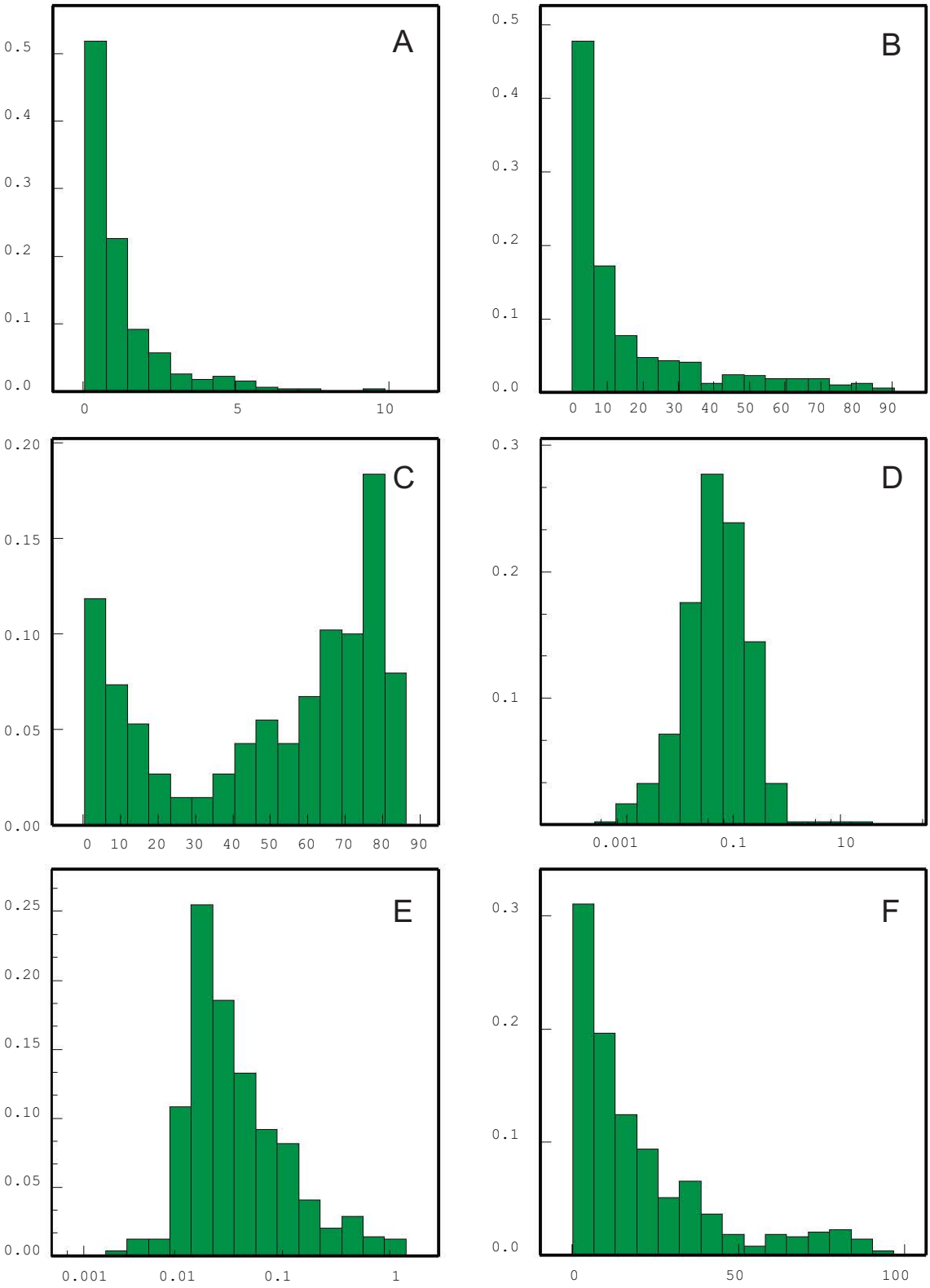

Figure 4.2: Histograms of input data distributions combined domains (Complete Dataset). A - Al_2O_3, B - Fe_2O_3, C - Mn_3O_4, D - P_2O_5, E - PbO, F - SiO_2,

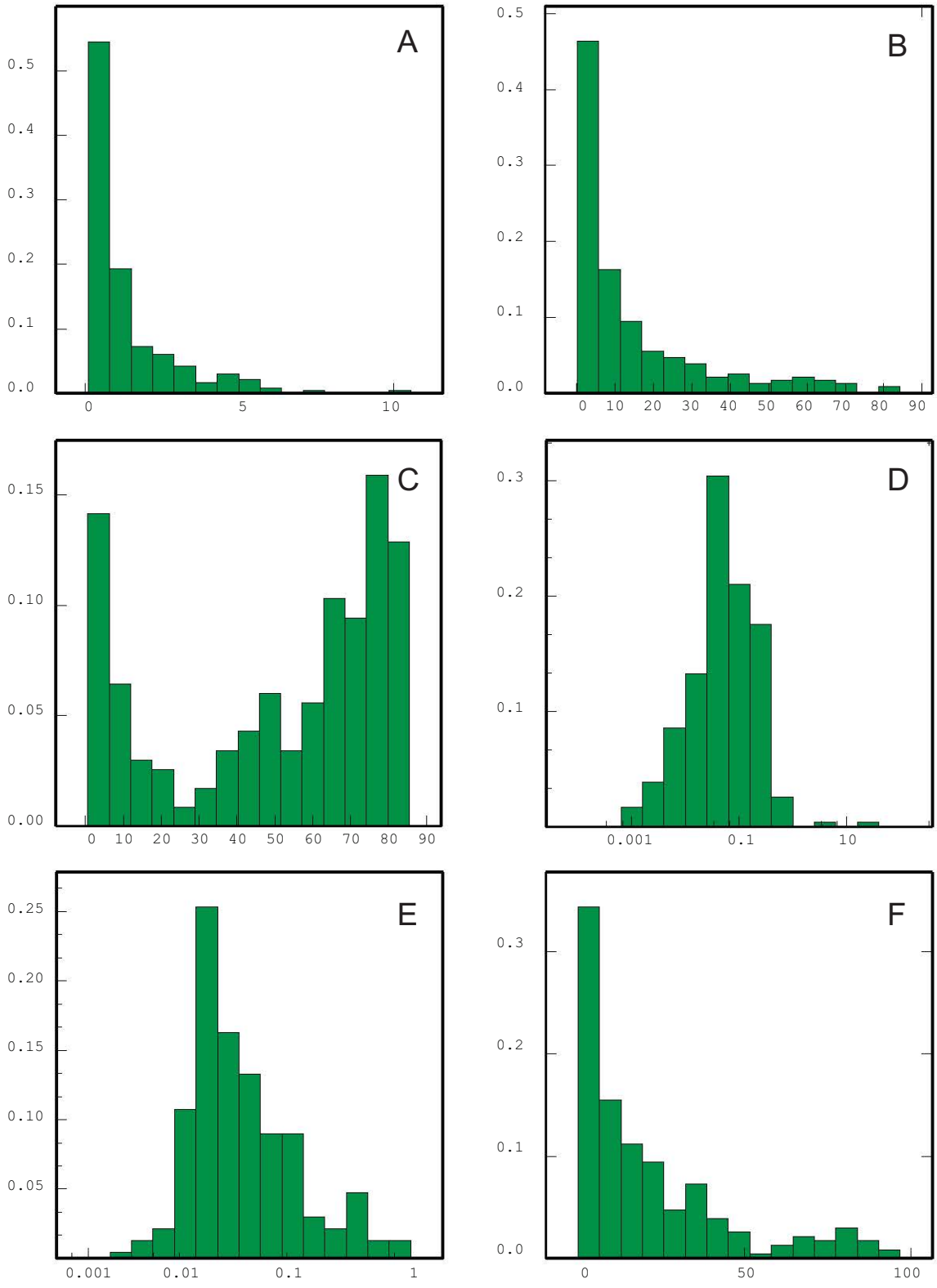

Figure 4.3: Histograms of input data distributions combined domains (Reduced Dataset). A - Al_2O_3, B - Fe_2O_3, C - Mn_3O_4, D - P_2O_5, E - PbO, F - SiO_2,

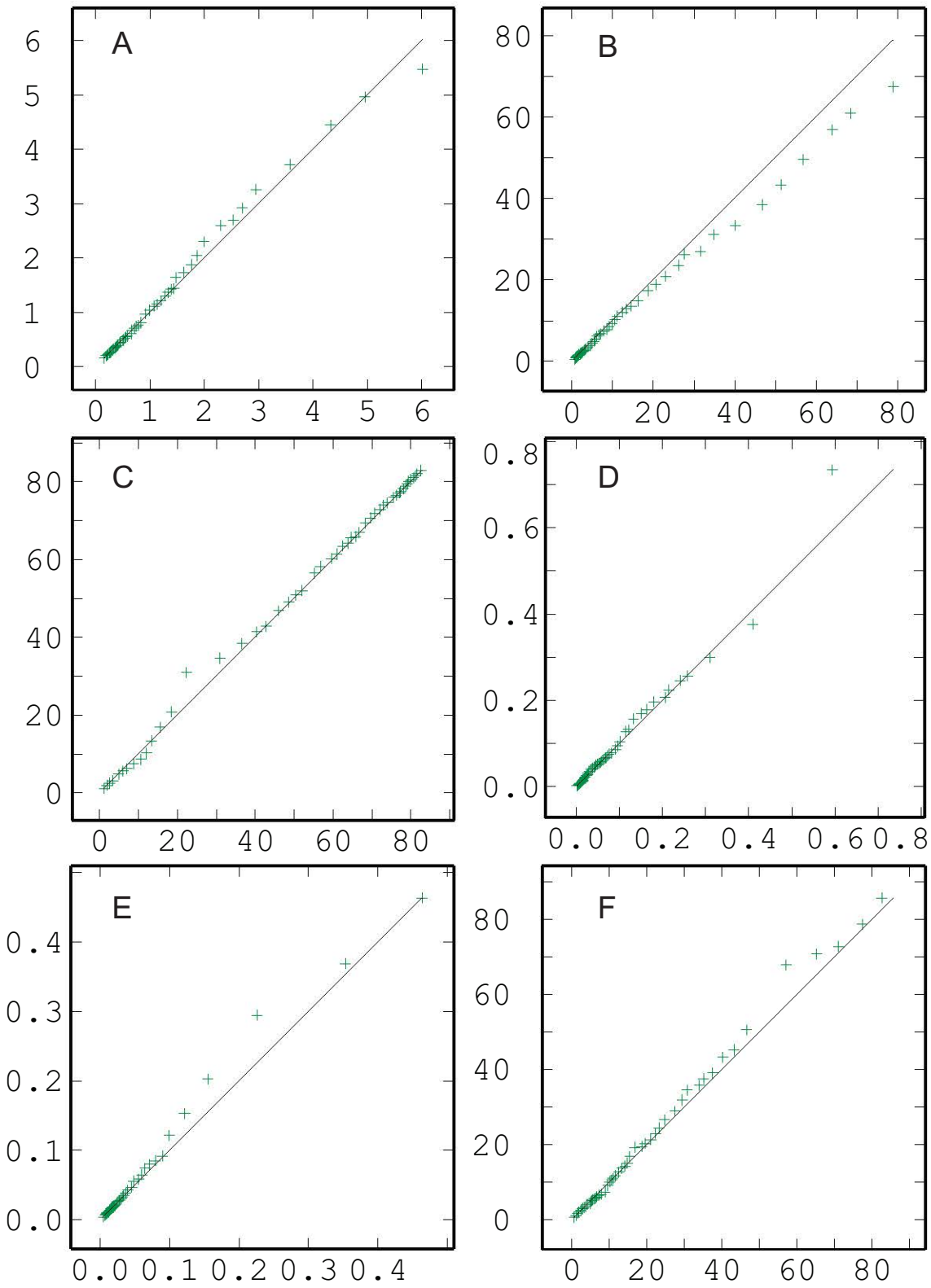

Figure 4.4: Comparative Q-Q plot of input datasets: Reduced Data Ordinate, All Data Abcissa. A - Al_2O_3, B - Fe_2O_3, C - Mn_3O_4, D - P_2O_5, E - PbO, F - SiO_2,

Histograms of the distributions for both domains combined, between the complete and RD dataset (Figures 4.2 to 4.3) are very similar. All variables, with the exception of Mn_3O_4 which appears bimodal, have strongly positively skewed distributions. The distribution of Mn_3O_4 corresponds to potential minor waste inclusions within the orebody, with peak values between 0 and 5%, and also at 80%. The same also holds true for individual domains Appendix B. Q-Q plots of the complete dataset against the reduced dataset in Figure 4.4 and Appendix B generally confirm the similarities in distributions observed in the histograms though they do show some bias as do the relative errors statistics of Table 4.6, particularly in the values of Al_2O_3, Mn_3O_4, P_2O_5, PbO and SiO_2 for Domain 2. Generally the reduced dataset is considered suitably representative of the complete set, showing minimal overall global bias, and closely approximates the likely differences observed between datasets available at the time of resources calculation and final selection.

4.3 Compositional Data Transformation

The oxide variables of the dataset used in this study are described in percentages; portions of a whole. This defines their compositional nature, and also indicates that they are subject to a sum constraint (parts measured in percentages cannot sum to more than 100%). Given the possibility for violating the sum constraint through the estimation / simulation of multiple compositional variables [65] the use of a log-ratio approach has been employed where appropriate as a treatment of the input data.

The compositional vectors (z) of the major oxide input data (RD dataset only) were first closed using a service variable

$$\mathrm{z}_N = 100 - \sum_{i=1}^{N-1} \mathrm{z}_i \tag{4.1}$$

and subsequent to closure, data were then transformed by the additive log-ratio (alr) approach.

$$alr(\mathrm{z}) = \mathrm{x} = (\ln(\frac{\mathrm{z}_1}{\mathrm{z}_N}), \ldots, \ln(\frac{\mathrm{z}_{N-1}}{\mathrm{z}_N})) \tag{4.2}$$

The alr transform also reduces the dimensionality of the data by 1, $S^N \rightarrow \mathbb{R}^{N-1}$, however the resulting final dataset for use in this study comprised six oxide variables, and also six *alr* transformed variables with the service variable used as the ratio denominator, (and therefore

removed from the variable count). Summary statistics for alr transformed data are presented in Tables 4.7 and 4.8. The log-ratio transformation has a normalising effect on the resultant variables which is suggested in the small skewness values for transformed variables, however histograms and Q-Q plots against a Gaussian distribution for the log-ratio transformed data, when considered as combined domains or individually appear non-normal for both the complete and reduced data (Figures 4.5 and 4.6 and Appendix B).

Table 4.7: Summary statistics for log-ratio transformed RD data of Domains 1 and 2

VARIABLE	Count	Minimum	Maximum	Mean	Variance	Skewness
Domain 1						
alrAl_2O_3	177	-5.58	0.99	-2.78	1.65	0.74
alrFe_2O_3	177	-4.06	4.72	-0.57	3.44	0.51
alrMn_3O_4	177	-3.35	2.61	1.29	0.89	-2.48
alrP_2O_5	177	-9.34	1.77	-5.3	2.75	0.59
alrPbO	177	-9.59	-2.45	-6.01	1.35	0.3
alrSiO_2	177	-4.55	5.86	0.11	3.15	0.47
Domain 2						
alrAl_2O_3	56	-3.28	0.24	-1.37	0.76	0.08
alrFe_2O_3	56	-2.28	2.98	0.24	1.72	0.3
alrMn_3O_4	56	-1.3	1.83	1.19	0.58	-1.71
alrP_2O_5	56	-8.72	-2.88	-5.19	2.02	-0.45
alrPbO	56	-7.31	-3.01	-5.3	1.24	0.5
alrSiO_2	56	-3.22	4.11	0.66	2.3	-0.17

Table 4.8: Summary statistics for log-ratio transformed Complete data of Domains 1 and 2

VARIABLE	Count	Minimum	Maximum	Mean	Variance	Skewness
Domain 1						
alrAl_2O_3	381	-5.58	0.99	-2.73	1.48	0.65
alrFe_2O_3	381	-4.06	4.72	-0.46	3.43	0.50
alrMn_3O_4	381	-4.00	2.61	1.24	0.98	-2.51
alrP_2O_5	381	-10.06	1.77	-5.28	2.59	0.27
alrPbO	381	-10.34	-2.45	-6.01	1.27	0.18
alrSiO_2	381	-4.55	5.86	0.18	2.70	0.29
Domain 2						
alrAl_2O_3	109	-3.88	0.57	-1.59	0.87	0.05
alrFe_2O_3	109	-2.28	4.99	0.18	1.90	0.67
alrMn_3O_4	109	-1.30	1.83	1.29	0.38	-2.11
alrP_2O_5	109	-8.72	-2.24	-5.38	1.76	-0.18
alrPbO	109	-7.40	-2.82	-5.42	1.10	0.62
alrSiO_2	109	-3.29	4.11	0.35	2.36	-0.21

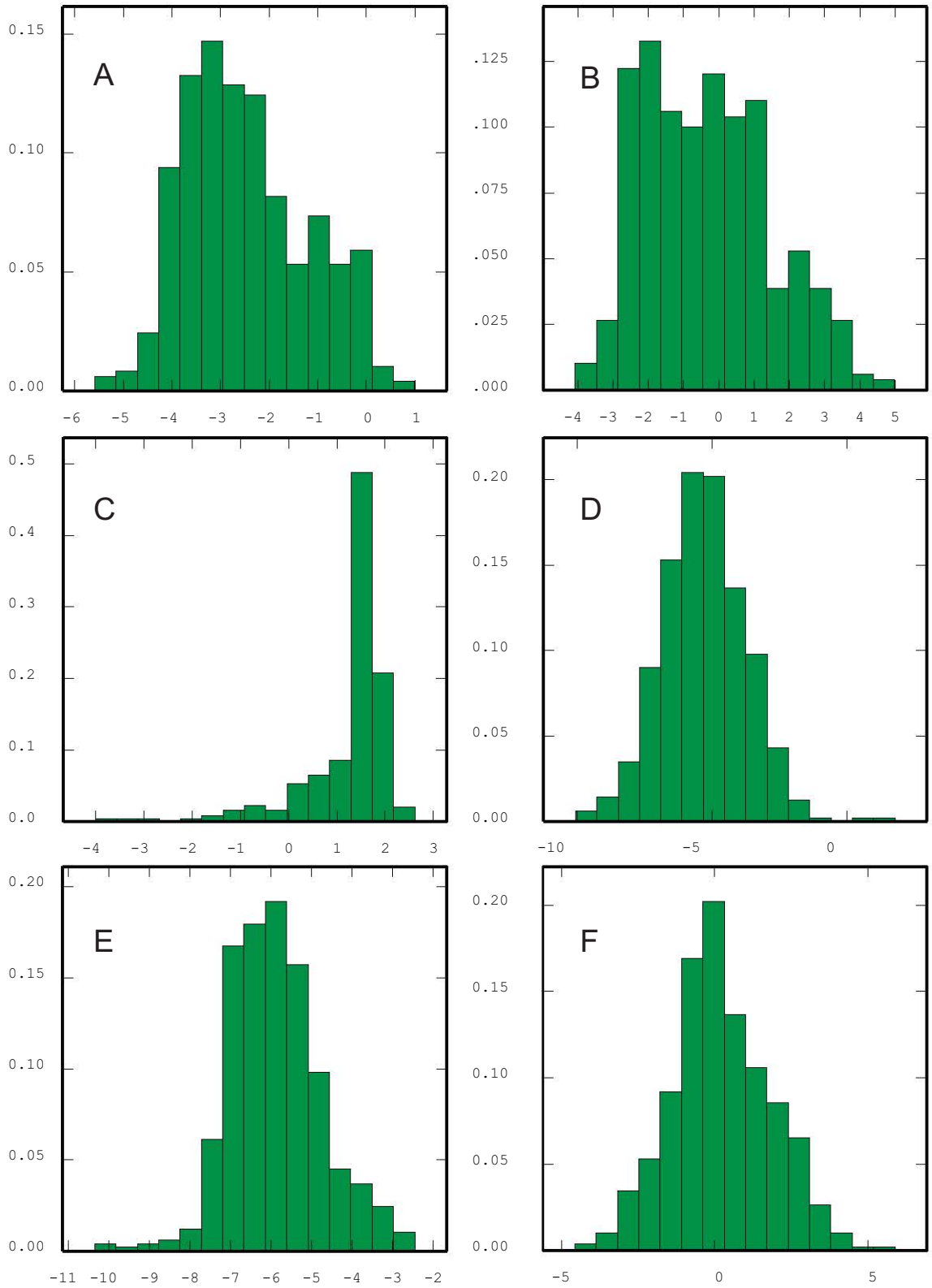

Figure 4.5: Distributions of log-ratio transformed input data; Complete dataset both domains. A - alrAl_2O_3, B - alrFe_2O_3, C - alrMn_3O_4, D - alrP_2O_5, E - alrPbO, F - alrSiO_2

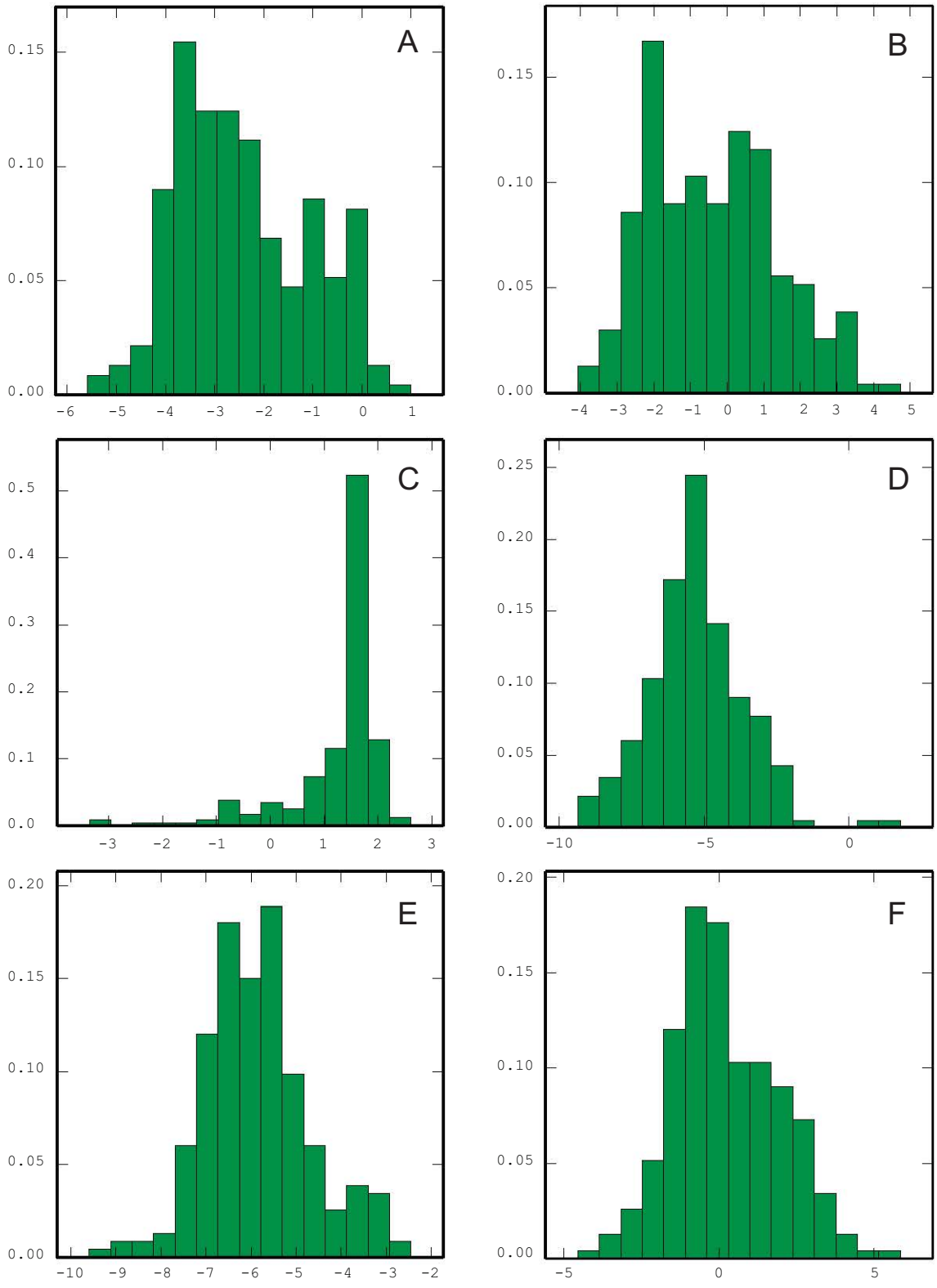

Figure 4.6: Distributions of log-ratio transformed input data; RD dataset both domains. A - alrAl_2O_3, B - alrFe_2O_3, C - alrMn_3O_4, D - alrP_2O_5, E - alrPbO, F - alrSiO_2

Chapter 5

Multivariate Decorrelation

For both Min/Max Autocorrelation Factorisation (MAF) and Independent Components Analysis (ICA), two datasets comprising either the six *alr* transformed variables or the six raw oxide variables (no log-ratio transformation) were subject to decorrelation, followed by assessment of the performance of each method in removing spatial cross-correlation. Performance was measured by the degree to which the covariance matrices at various lags h were diagonalised. MAF factors were produced for both data treatments for the complete dataset using a lag spacing of 7.5 m, and 10 m for the reduced (RD) dataset; representing the general minimum distance between sample points. Two sets of MAF transformation matrices were generated utilising both an omnidirectional, and a directional semivariogram matrix (main continuity direction of 085). Independent components were derived from each dataset using the FastICA algorithm [27, 28]. A maximum of 300 iterations were permitted to achieve convergence during derivation of $\mathbf{W}_{ICA}$, with a tolerance of 1.0×10^{-5} as the acceptable limit between iterations to define convergence.

Data were categorised by three criteria; Complete (All) / Reduced (RD) data densities, Raw Oxide (OX) / additive log-ratio (ALR) transformation applied, and Domain 1 / 2. Each method of decorrelation (ICA and MAF) was tested for each combination of data categories. Measures of decorrelation performance; κ and τ were determined from the experimental semivariance / cross-semivariance matrices calculated for up to 12 lags of 7.5 m for the complete dataset, and up to 7 lags of 10 m for the RD dataset. Performance of each decorrelation was measured in both an omnidirectional (isotropic) sense, and also in a directional (anisotropic) sense, using a main direction of continuity of 085. While anisotropy along 085 may not individually best represent each variable in each domain, it is the most common

direction of maximum continuity across all combinations of classifications of the data for both domains. The experimental semivariograms of the input (non-decorrelated) data are presented in Appendix B. The degree of spatial cross-covariance (semivariance) changes between variable pairs in all configurations of the data, but clear spatial structure is seen in the majority of instances.

5.1 Decorrelation Performance

For all categories of data, MAF transformation matrices were generated using both the variance-covariance matrix of the first lag from both an omnidirectional experimental variogram (MAF), and the same matrix from the main direction of an anisotropic (directional) experimental variogram (DMAF). The comparison between MAF and DMAF decorrelation in each measure of performance are largely equivocal. Omnidirectional MAF presents slightly better performance at short lags and consequently, given the close similarities between the two types of MAF, was selected as the representative method for further comparison against ICA. The code for decorrelation via MAF and DMAF is presented in Appendix Chapter F

Decorrelation performance is plotted on a per-lag basis for all combinations of data. In general, both the complete and reduced datasets show similar trends in performance of each decorrelation method. Decorrelation via both techniques, when measured by κ across a range of lag distances, is generally very good, with values consistently very close to one. The exception to this is the performance of ICA at the first lag for log-ratio transformed data, which shows varying performance dependent on domain (and therefore per-lag pair count), that is consistently lower than that for MAF on the same data. Similarly, τ values for ICA decorrelated data at the first lag are higher than for MAF, but for all other lags the results are comparable.

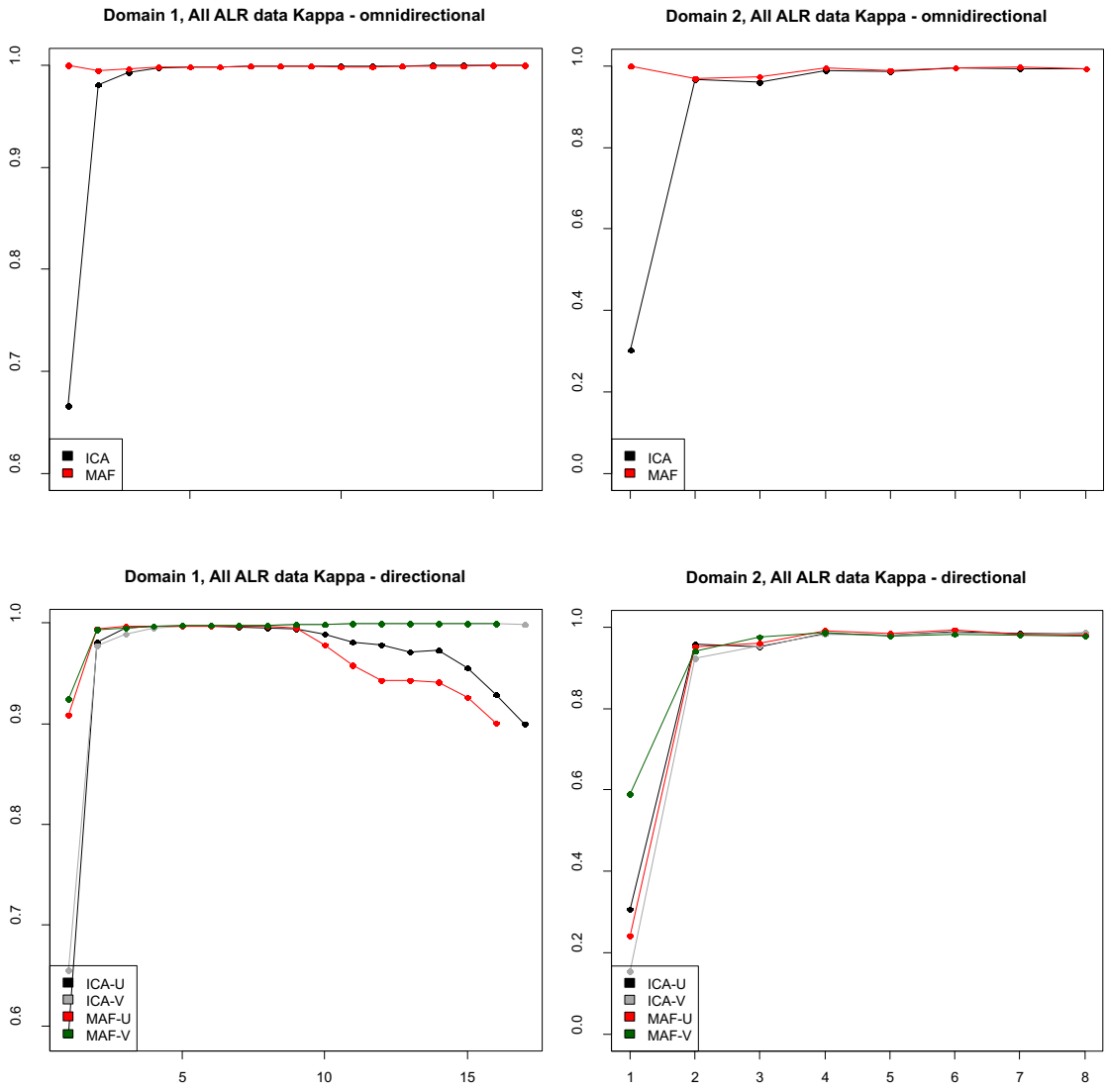

Figure 5.1: Kappa values by lag, complete data ALR transformed

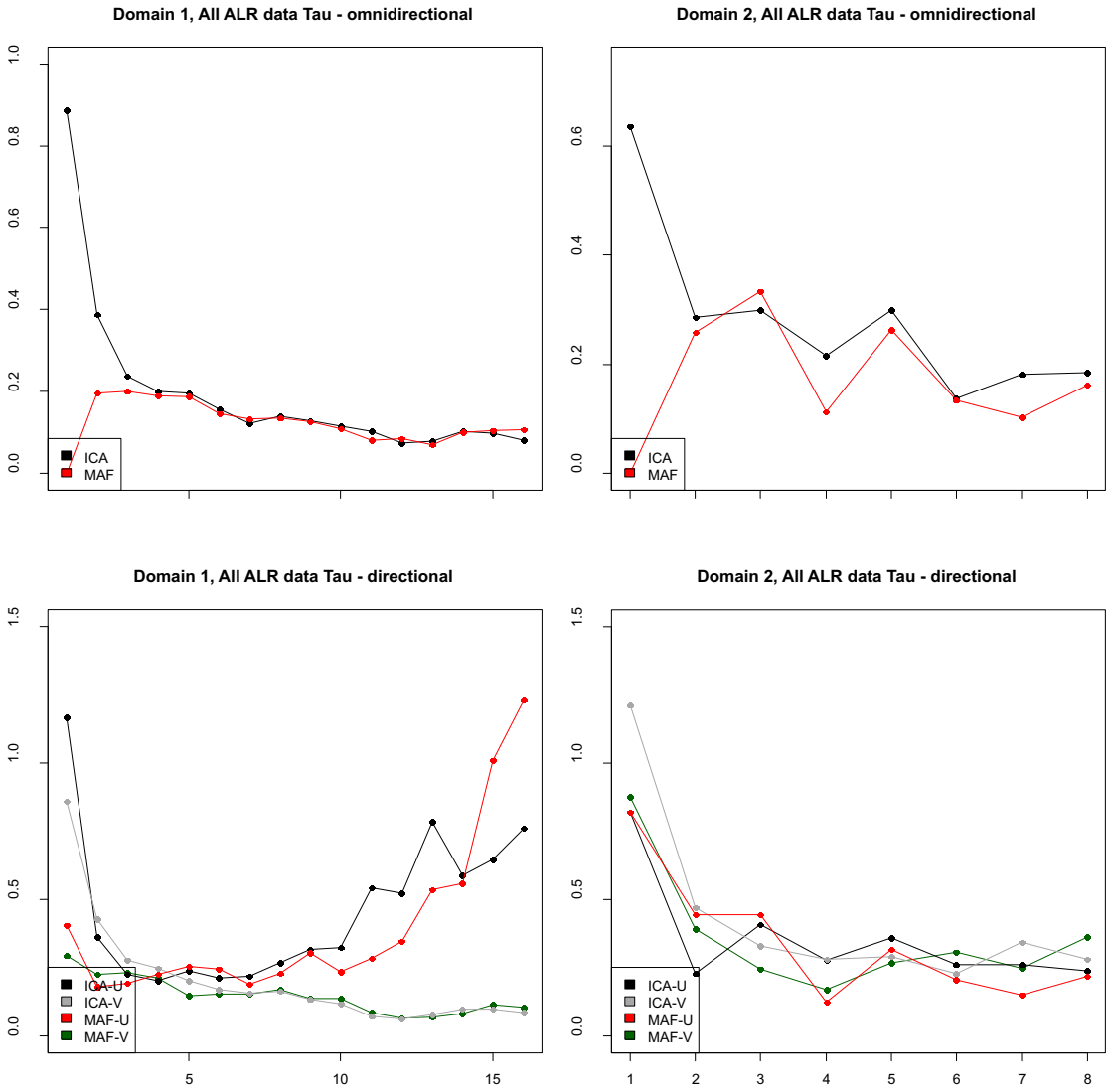

Figure 5.2: Tau values by lag, complete data ALR transformed

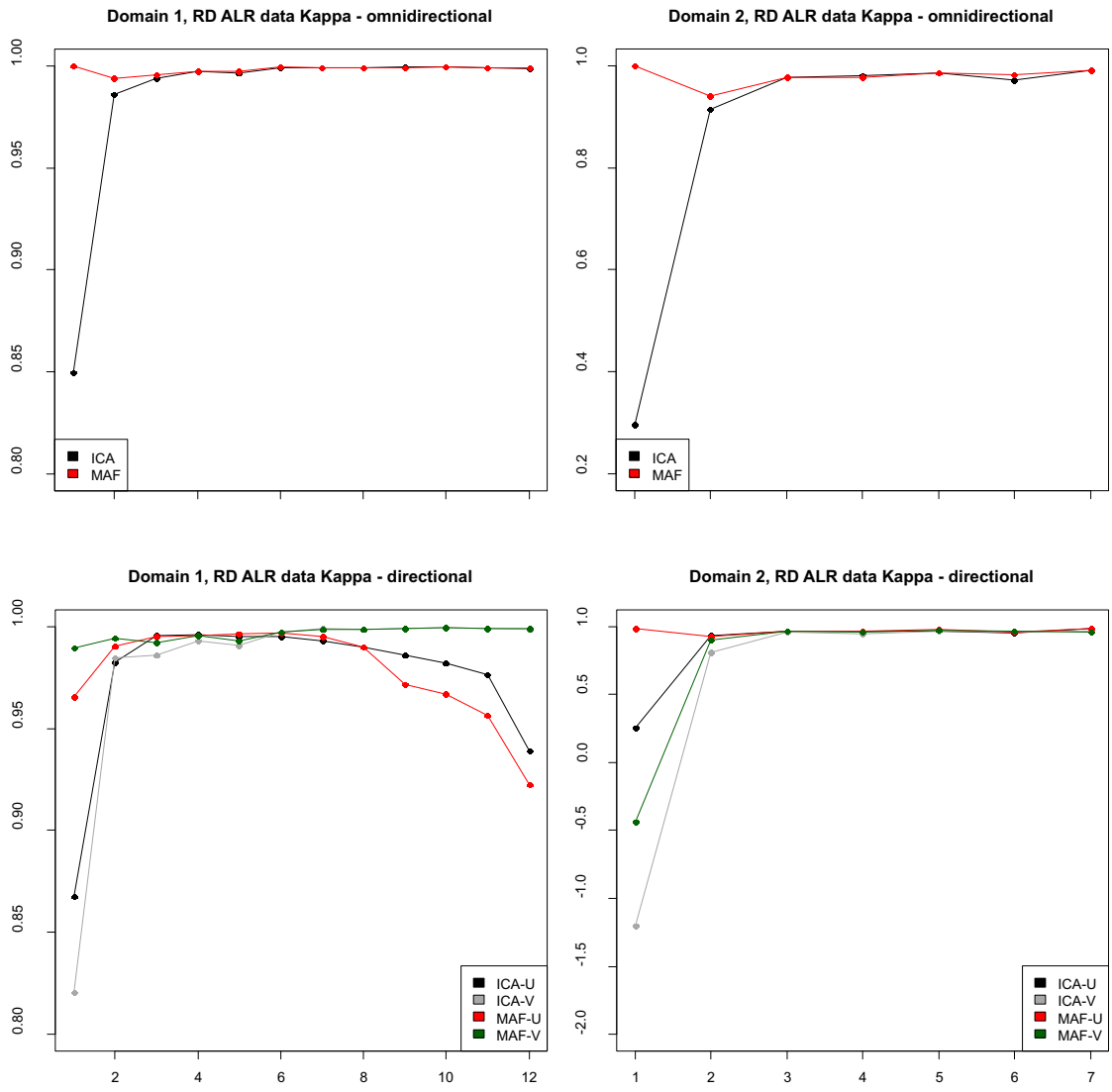

Figure 5.3: Kappa values by lag, RD data ALR transformed

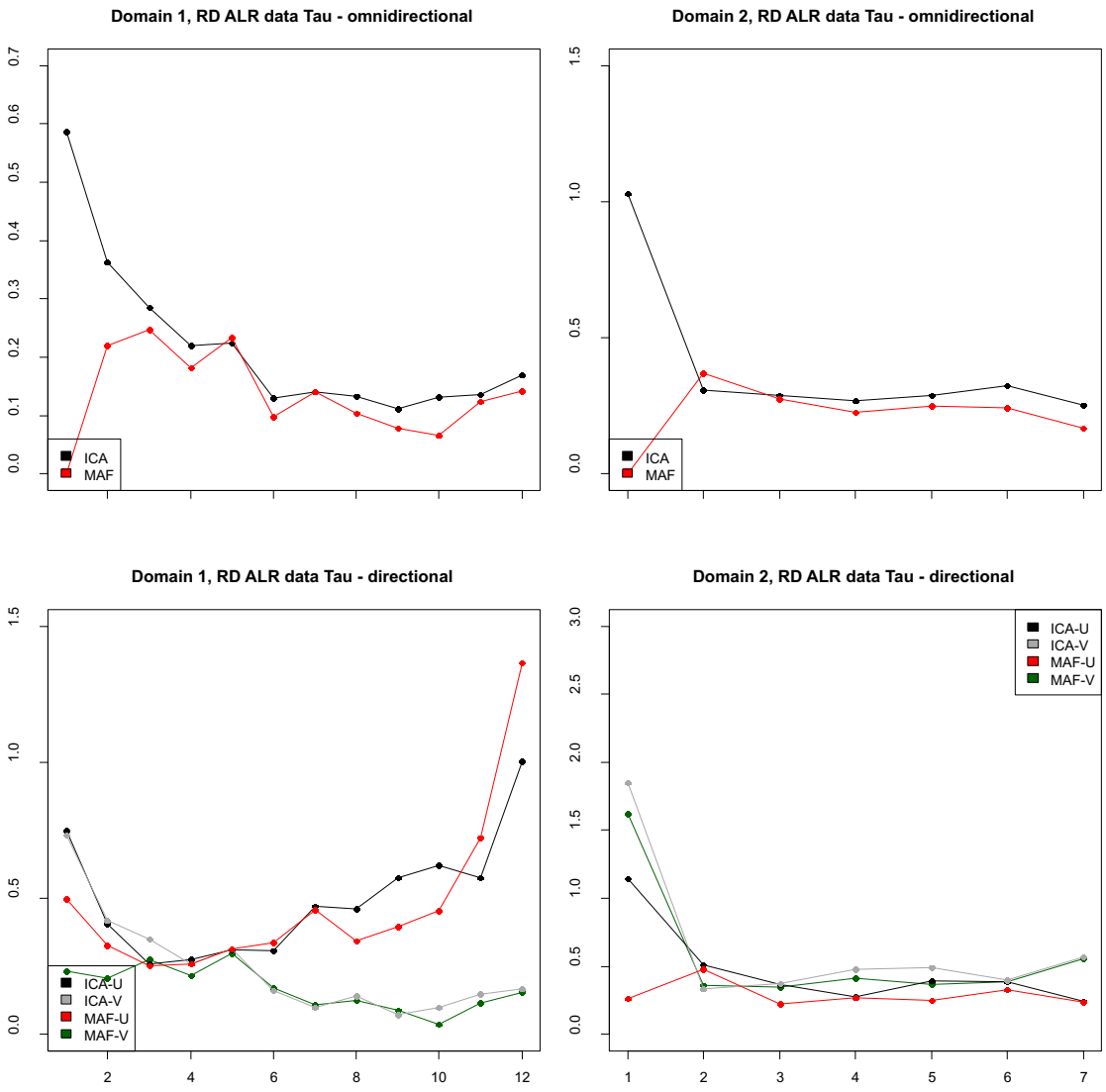

Figure 5.4: Tau values by lag, RD data ALR transformed

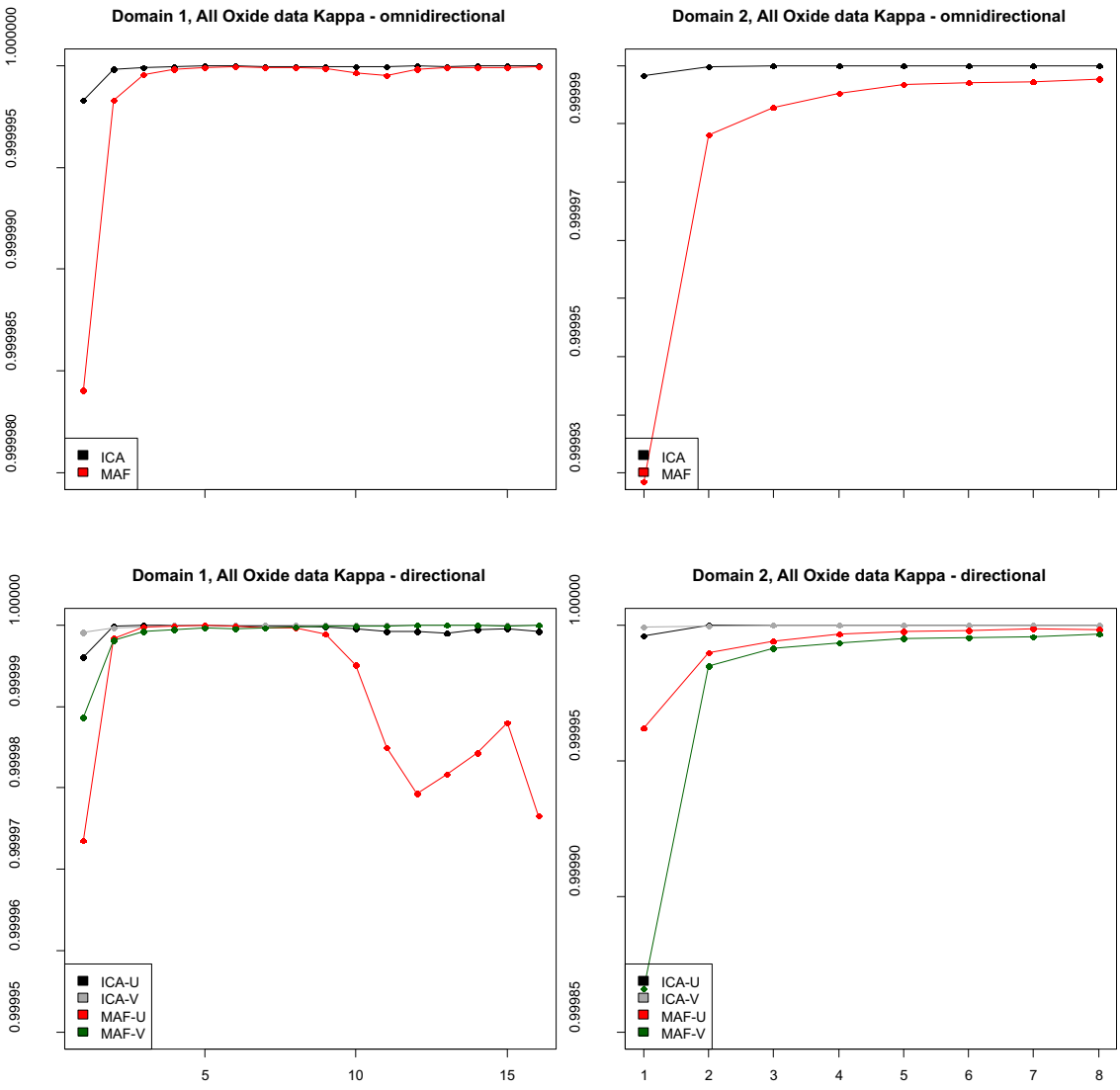

Figure 5.5: Kappa values by lag, complete oxide data

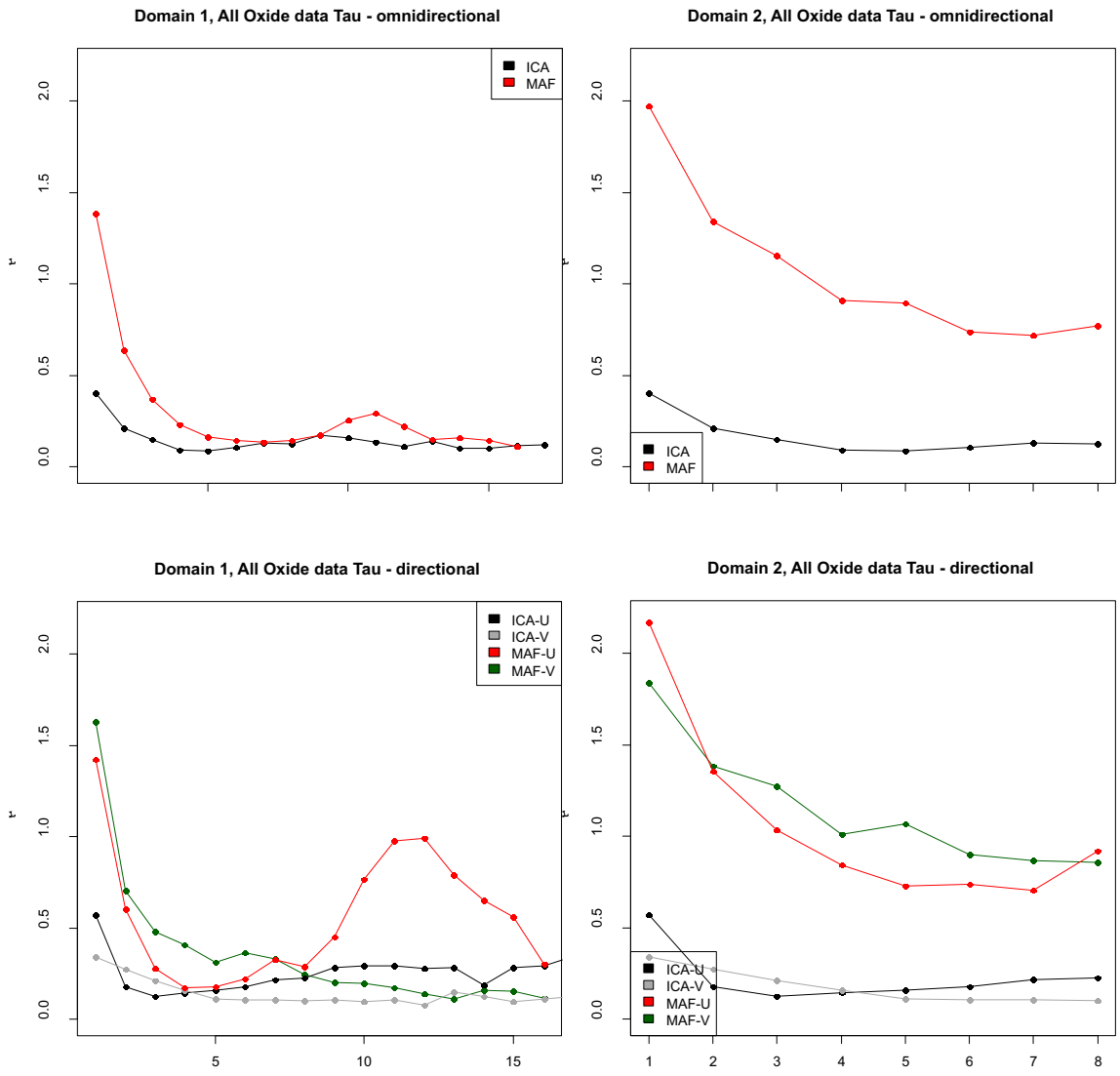

Figure 5.6: Tau values by lag, complete oxide data

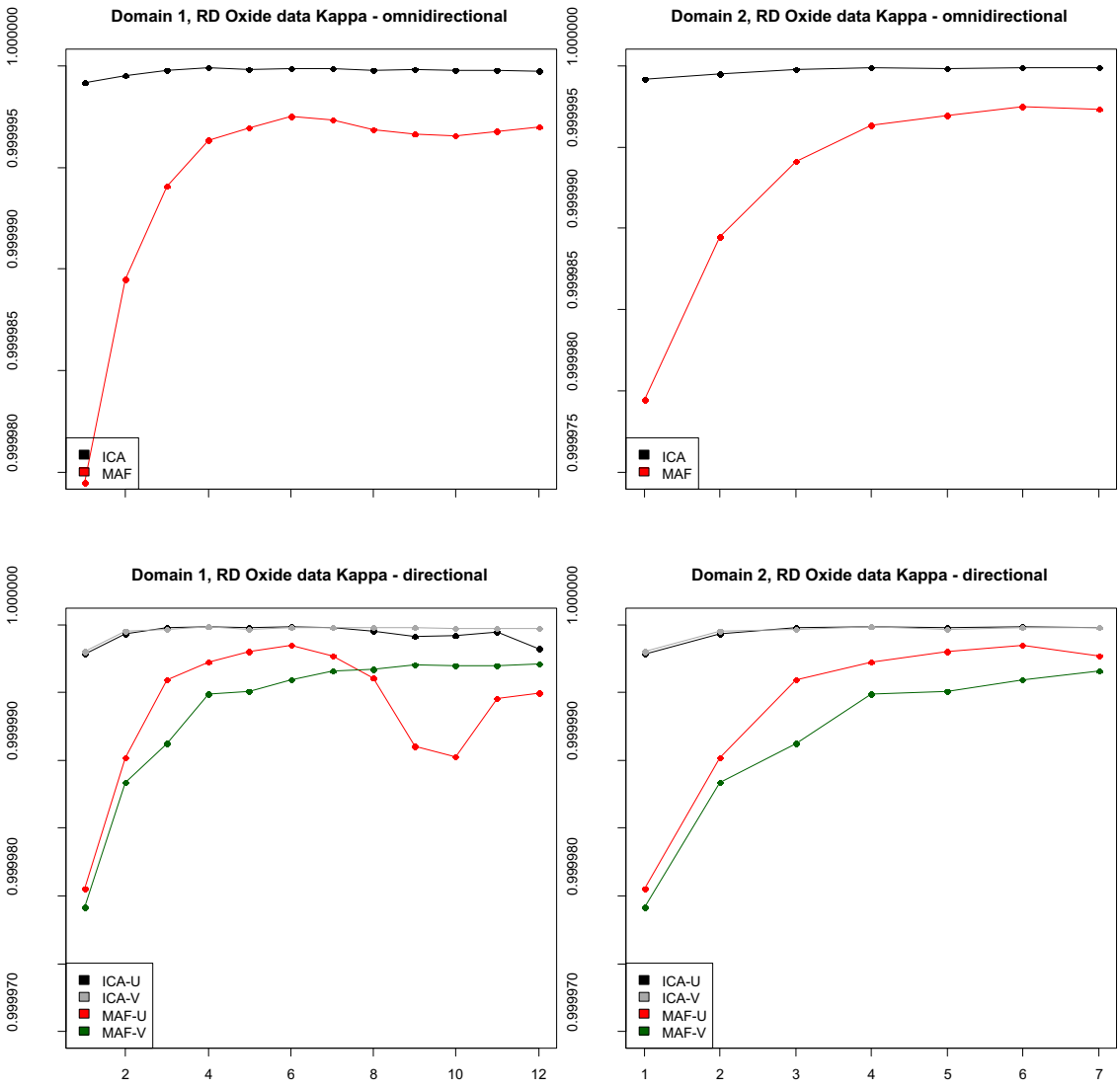

Figure 5.7: Kappa values by lag, complete oxide data

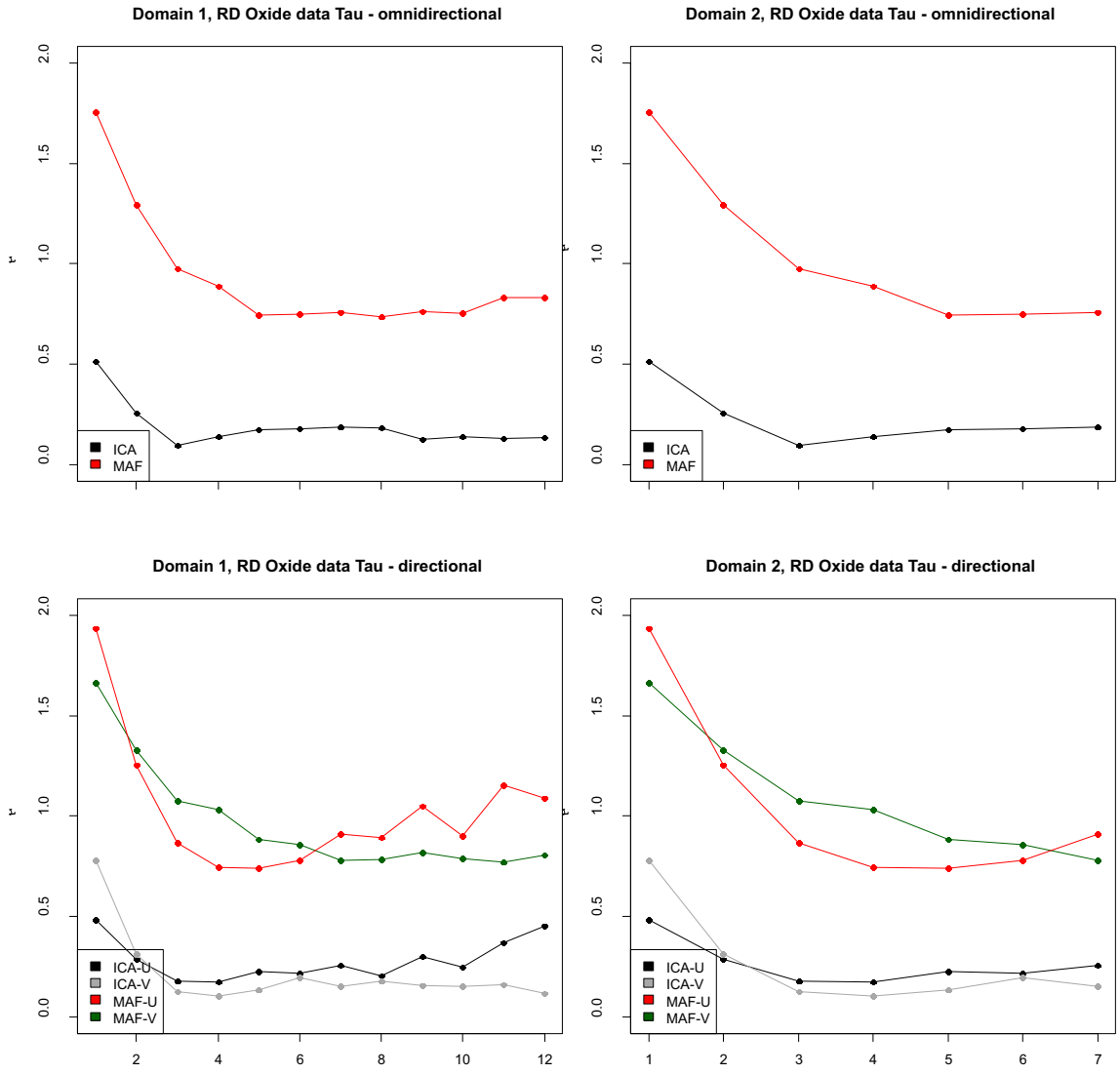

Figure 5.8: Tau values by lag, complete oxide data

For data that are not log-ratio transformed, a number of features become evident. Firstly, decorrelation performance as measured by κ is very high for both MAF and ICA methods. Secondly, ICA performs better for the raw data at the first lag than for the transformed data. Next, the performance of ICA, as measured by τ varies less between log-ratio transformed data and raw oxide data than does the performance of MAF. Lastly, the performance of MAF for decorrelation of the raw oxide data is consistently worse than that of ICA. The differences in performance at the first lag may be attributed to MAF being optimised for decorrelation at this distance due to its variance / covariance matrix being that selected for decomposition in the second part of the generation of $\mathbf{W}_{MAF}$. Additionally, the performance of ICA is known to degrade with increasing normality of the input "mixed" signals (Hyvärinen, pers. comm.). The process of generating log-ratios partially normalises the data, and part of the differing performance for MAF and ICA, particularly at shorter lags where MAF is optimised, can also be attributed to this potential degradation in ICA performance.

On the basis of decorrelation performance it would be valid to select either ICA or MAF as an appropriate method for subsequent geostatistical studies. Both methods return consistenly good results, that are very similar, with the only exception being the first lag performance of ICA on log-ratio transformed data. Additionally, with ICA there is no fundamental underlying assumption of the spatial covariance structure of the data, as there is with MAF, where an assumption is made that the spatial covariance of the given dataset can be adequately modelled by two model structures (see Section 2.7.1). On the basis of this, and given the novelty of ICA as a geostatistical decorrelation tool, it has been selected as the method by which to decorrelate for the subsequent portions of this study.

5.2 Decorrelated Data Summary

The datasets resulting from ICA decorrelation of both raw oxide data and log-ratios are presented in Tables 5.1 and 5.2. Histogram distributions of the decorrelated factors derived from both oxide and log-ratio input data are presented in Figures 5.9 and 5.10. All factor means are zero for both datasets, and all variances are scaled to one; this relates directly to the preliminary "centering and whitening" step in the FastICA process, which is in fact transformation into principal components. Minima and maxima are asymmetrically distributed about the zero mean and both the skewness and the kurtosis deviate from zero and three respectively describing two sets of variables that are non-normal, as is expected from ICA.

Table 5.1: Summary statistics of the factors from ICA decorrelation of RD dataset oxides

Combined Domains	Count	Minimum	Maximum	Mean	Variance	Skewness	Kurtosis
ICA_ox1	233	-2.23	5.74	0	1	3.03	16.11
ICA_ox2	233	-3.37	5.1	0	1	2.19	11.02
ICA_ox3	233	-6.54	1.42	0	1	-3.65	19.92
ICA_ox4	233	-2.17	4.09	0	1	1.58	5.93
ICA_ox5	233	-12.96	3.38	0	1	-9.11	122.39
ICA_ox6	233	-4.03	3.34	0	1	-1.35	6.63
Domain 1							
ICA_ox1	177	-0.54	5.74	0	1	4.06	20.53
ICA_ox2	177	-2.08	5.1	0	1	2.76	12.59
ICA_ox3	177	-6.54	0.79	0	1	-4.74	25.7
ICA_ox4	177	-1.23	4.09	0	1	1.86	6.14
ICA_ox5	177	-12.96	0.28	0	1	-12.39	159.68
ICA_ox6	177	-4.03	1.32	0	1	-2.08	7.04
Domain 2							
ICA_ox1	56	-2.23	1.77	0	1	-0.25	2.17
ICA_ox2	56	-3.37	2.97	0	1	0.39	6.08
ICA_ox3	56	-1.69	1.42	0	1	-0.18	1.63
ICA_ox4	56	-2.17	3.39	0	1	0.71	5.26
ICA_ox5	56	-1.88	3.38	0	1	1.24	4.52
ICA_ox6	56	-2.12	3.34	0	1	0.95	5.36

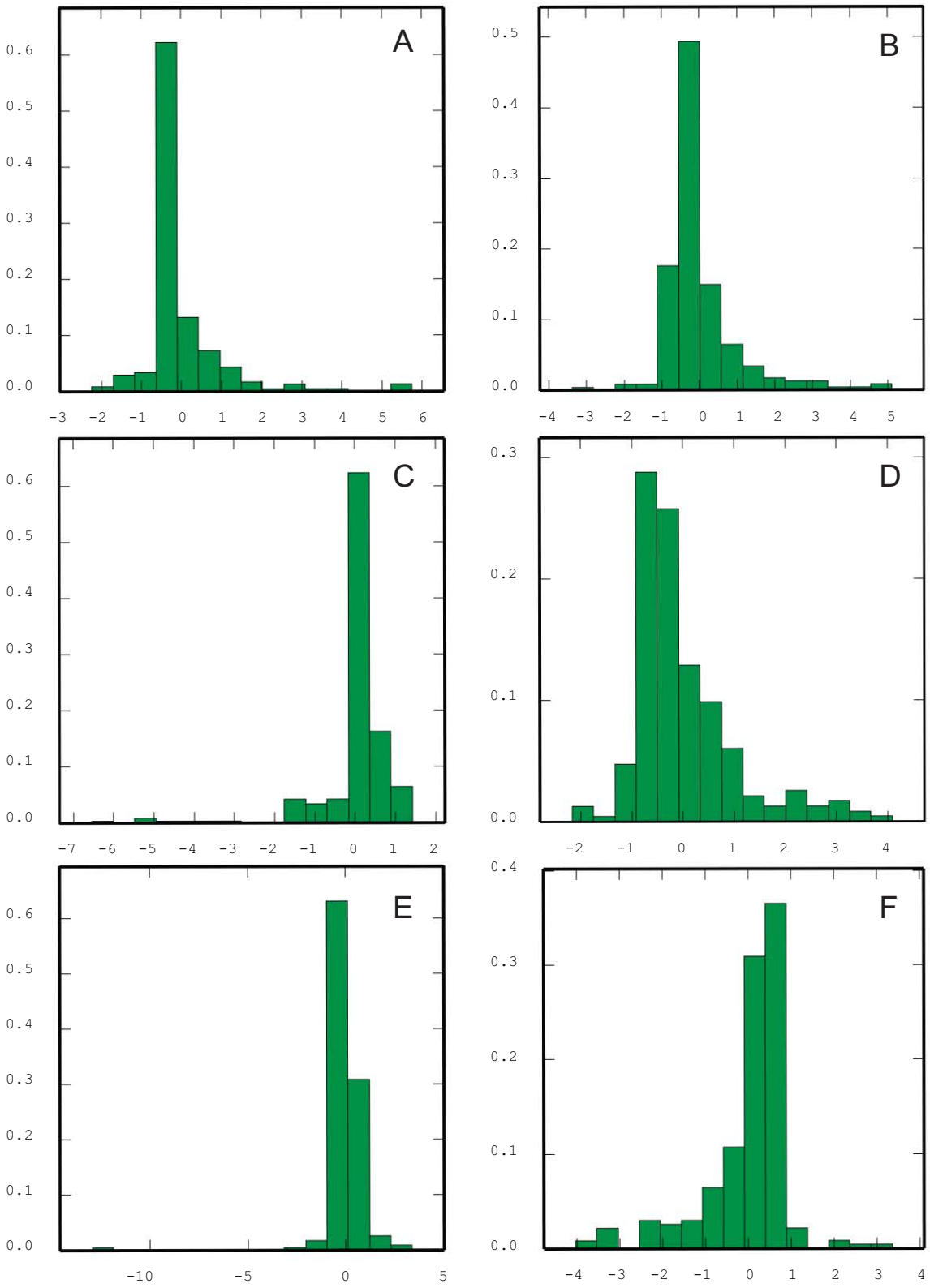

Figure 5.9: Distributions of ICA decorrelated oxide input data. A - Factor 1, B - Factor 2, C - Factor 3, D - Factor 4, E - Factor 5, F - Factor 6

Table 5.2: Summary statistics of the factors from ICA decorrelation of RD dataset log-ratios

Combined Domains	Count	Minimum	Maximum	Mean	Variance	Skewness	Kurtosis
ICA_alr1	233	-5.73	2.4	0	1	-2.75	14.48
ICA_alr2	233	-3.98	3.17	0	1	-0.51	5.24
ICA_alr3	233	-3.26	2.77	0	1	-0.34	4.06
ICA_alr4	233	-2.17	2.57	0	1	0.29	2.36
ICA_alr5	233	-2.33	2.84	0	1	-0.07	2.53
ICA_alr6	233	-2.91	3.56	0	1	0.26	3.79
Domain 1							
ICA_alr1	177	-5.73	1.43	0	1	-3.58	18.2
ICA_alr2	177	-3.68	3.17	0	1	-0.02	4.65
ICA_alr3	177	-3.26	2.77	0	1	-0.57	4.22
ICA_alr4	177	-1.97	2.57	0	1	0.35	2.37
ICA_alr5	177	-2.32	2.21	0	1	-0.24	2.16
ICA_alr6	177	-2.91	3.56	0	1	0.33	3.93
Domain 2							
ICA_alr1	56	-2.44	2.4	0	1	-0.11	2.72
ICA_alr2	56	-3.98	1.12	0	1	-2.04	7.11
ICA_alr3	56	-2.43	2.65	0	1	0.38	3.55
ICA_alr4	56	-2.17	2.19	0	1	0.07	2.34
ICA_alr5	56	-2.33	2.84	0	1	0.45	3.71
ICA_alr6	56	-2.62	2.46	0	1	0.06	3.34

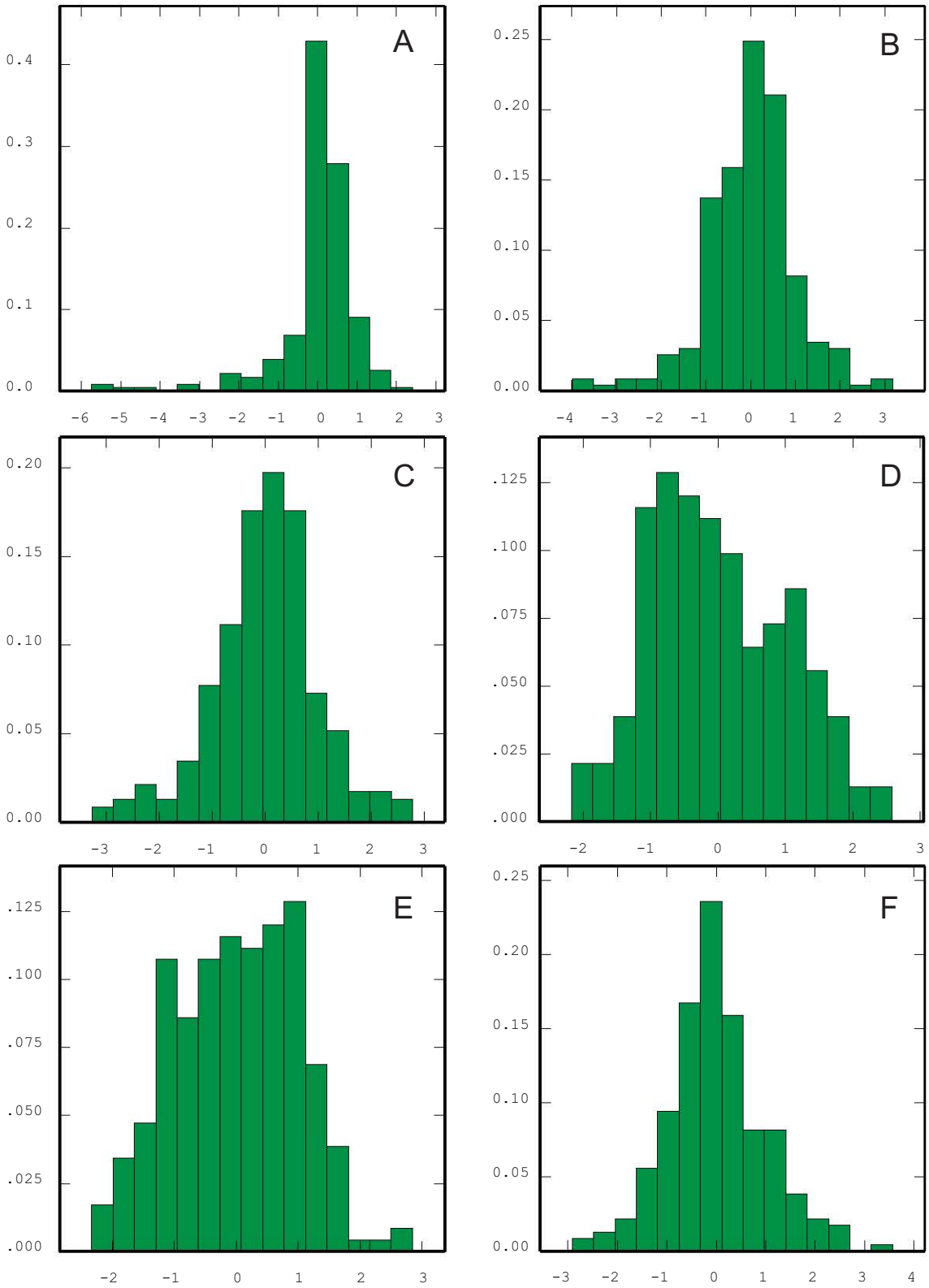

Figure 5.10: Distributions of ICA decorrelated, log-ratio transformed input data. A - Factor 1, B - Factor 2, C - Factor 3, D - Factor 4, E - Factor 5, F - Factor 6

Chapter 6

Estimation, Simulation and LUC

Using the reduced density (RD) dataset, which is representative of the typical input data density available at the decision-to-mine, recoverable resources were calculated in a variety of ways using varied treatments of the original input data for comparison:

Using the non-transformed, raw oxide values, block ordinary kriging (BOK), Localised Uniform Conditioning, and Turning Bands Conditional Simulation were applied. In the case of these raw oxide block estimations / simulations, an assumption of no spatial cross-correlation between variables is made. This is in direct keeping with the restrictions in practice that would be encountered at the real-world mining operation from which the data were sampled, and relates directly to software limitations within the current operating framework of the mine. Using oxide data decorrelated by ICA, LUC was applied as was Turning Bands Conditional Simulation. Next, using log-ratio transformed (ALR) oxide data that were subsequently decorrelated via ICA, Turning Bands Conditional Simulation was applied. This series of estimations / simulations yields results that compare directly to current methods of recoverable resources calculation at the operation under study (BOK), as well as results from the non-linear methods under trial. Finally, using the complete dataset, BOK was applied on the raw oxide data. This final estimation represents a benchmark estimate, closest to the results that would typically be produced at the time of grade control, immediately prior to mining. Table 6.1 lists the methods applied for comparison in this study.

Table 6.1: Summary of estimation / simulation methods being compared

Summary of Methods Compared	
Block Ordinary Kriging	
Localised Uniform Conditioning of Oxide Data	6m Panel
Localised Unifrom Conditioning of Decorrelated Oxide data	6m Panel
Localised Uniform Conditioning of Oxide Data	12m Panel
Localised Uniform Conditioning of Decorrelated Oxide Data	12m Panel
Conditionial Simulation of Decorrelated Log-ratio data	
Block Ordinary Kriging (Complete Dataset - Reference Estimate)	

6.1 Implementation Parameters

In keeping with current practices at the minesite from which they were taken, data for BOK were not subject to any transformation. Block estimates were made on a 3×3 m grid, discretised to 1 m nodes. This represents the current practice for recoverable resources calculation at the mine from which the data were sampled. For both raw oxide and ICA decorrelated LUC, estimation was conducted over both a 12×12 m and 6×6 m panel, discretised to 1 m. Change of support was applied to the local grade tonnage curves on the basis of a 3×3 m final block size. Post processing yielded localised estimates over this block size for each panel size. In both cases, data were treated in a univariate sense, similar to BOK, and in accordance with likely operating restrictions at the Woodie Woodie mine.

For all Conditional Simulations, data were again treated in the univariate sense; for raw oxides this meant no transformation other than Gaussian anamorphosis (via Hermite expansion) prior to simulation. Simulations were conducted on a quasi-point support grid ($\tilde{c} = 1$ m), with Gaussian back transformation taking place on this grid to maintain similar supports for forward and backward transformations. For ICA decorrelated data simulation, the decorrelation first took place, with subsequent Gaussian anamorphosis immediately prior to simulation. All back transformations were undertaken on quasi-point support. Conditional simulation of ALR data proceeded in a similar fashion; oxide data were log-ratio transformed, decorrelated, and then subject to Gaussian anamorphosis. Back transformation took place on the quasi-point support grid in the reverse order to forward transformations. In all cases, after complete back transformation, all simulations were averaged up to a 3 m grid.

Finally, using the complete non-transformed raw major oxide dataset, another BOK was undertaken over a 3×3 m grid, discretised to 1 m nodes. The estimates of each variable were completed in the univariate sense, with the results representing the estimate that would be available at the current mining operation at final selection (immediately prior to mining).

Each variant of the data used in the above estimations / simulations was modelled for spatial covariance, and a search neighbourhood to be used in all subsequent geostatistical algorithms was determined. Neighbourhood selection was made by iterative quantitative analysis of various neighbourhood dimensions, and input sample numbers through "leave-one-out" cross validation using ordinary kriging at each of the available input data locations. Covariance modelling and neighbourhood selection were conducted on a per-domain basis to acknowledge the influence of their differing geometries. Experimental and subsequent model variographic parameters, along with neighbourhood cross validation results are available in Appendices C to E.

Models for for decorrelated log-ratio, decorrelated oxide and oxide datasets all shared commonalities in their resulting semivariogram models. In general each factor / oxide was adequately fitted with a nugget and two spherical structures, which displayed varying degrees of zonal anisotropy. Variography for the oxide PbO was the exception, being generally omnidirectional for both Domains 1 and 2.

6.2 Non-Spatial Results

Summary statistics for each method of recoverable resources calculation are presented in Tables 6.2 to 6.9. For simulation results, these include a selection of the results from individual simulations, and also the post processed results accross 100 simulations, reported at the 50^{th} percentile. Histograms of the distributions of results are presented in Figures 6.1 to 6.6. Graphical representations of the spatial distribution of results for estimation, simulation and localised uniform conditioning are presented in Figures 6.21 to 6.26.

Table 6.2: Summary Statistics: Raw Oxide Simulations

VARIABLE	Count	Minimum	Maximum	Mean	Variance	Skewness
Simulation 10						
Al_2O_3	3471	0.11	8.41	1.51	1.88	1.49
Fe_2O_3	3463	0.24	83.72	15.49	246.89	1.42
Mn_3O_4	3463	0.80	84.36	47.35	566.17	-0.41
P_2O_5	3472	0.00	4.25	0.17	0.09	5.83
PbO	3471	0.00	0.56	0.06	0.01	2.44
SiO_2	3423	0.30	95.82	23.99	484.05	1.29
Simulation 41						
Al_2O_3	3471	0.12	8.34	1.52	1.67	1.44
Fe_2O_3	3463	0.22	81.52	16.70	289.73	1.37
Mn_3O_4	3463	0.71	84.95	47.45	644.59	-0.41
P_2O_5	3472	0.00	6.50	0.20	0.19	6.20
PbO	3471	0.01	0.49	0.06	0.00	2.18
SiO_2	3423	0.30	94.99	21.92	421.67	1.42
Simulation 61						
Al_2O_3	3471	0.13	7.33	1.46	1.54	1.28
Fe_2O_3	3463	0.30	83.53	15.70	278.11	1.45
Mn_3O_4	3463	0.71	84.71	48.09	659.49	-0.41
P_2O_5	3472	0.00	5.12	0.17	0.12	7.04
PbO	3471	0.00	0.60	0.06	0.01	2.47
SiO_2	3423	0.18	94.25	22.52	439.92	1.38
Simulation 84						
Al_2O_3	3471	0.13	6.36	1.42	1.31	1.24
Fe_2O_3	3463	0.25	81.45	13.86	234.89	1.72
Mn_3O_4	3463	0.71	84.64	46.66	644.80	-0.40
P_2O_5	3472	0.00	7.02	0.20	0.17	6.66
PbO	3471	0.01	0.62	0.05	0.00	2.99
SiO_2	3423	0.26	96.12	23.63	475.82	1.33

Table 6.3: Summary Statistics: ICA Simulations

VARIABLE	Count	Minimum	Maximum	Mean	Variance	Skewness
Simulation 10						
Al_2O_3	3472	-4.12	6.94	1.56	2.14	0.34
Fe_2O_3	3472	-36.05	74.34	14.94	251.77	0.61
Mn_3O_4	3472	-22.25	112.27	49.21	573.90	-0.35
P_2O_5	3472	-0.17	10.20	0.17	0.34	8.87
PbO	3472	-0.18	0.65	0.06	0.01	2.10
SiO_2	3472	-26.85	97.31	22.22	383.62	0.60
Simulation 41						
Al_2O_3	3472	-2.30	6.31	1.57	1.67	0.32
Fe_2O_3	3472	-43.61	75.40	16.28	254.46	0.47
Mn_3O_4	3472	-30.52	105.57	45.73	609.03	-0.36
P_2O_5	3472	-0.14	12.02	0.16	0.26	11.67
PbO	3472	-0.15	0.66	0.06	0.01	2.15
SiO_2	3472	-41.05	106.57	25.21	403.10	0.62
Simulation 61						
Al_2O_3	3472	-4.40	7.36	1.42	1.95	0.27
Fe_2O_3	3472	-47.60	85.52	15.29	248.11	0.39
Mn_3O_4	3472	-27.88	106.01	47.37	557.91	-0.27
P_2O_5	3472	-0.17	7.75	0.18	0.28	7.50
PbO	3472	-0.15	0.62	0.06	0.01	2.08
SiO_2	3472	-44.52	99.72	23.71	379.95	0.49
Simulation 84						
Al_2O_3	3472	-3.73	7.39	1.40	1.89	0.38
Fe_2O_3	3472	-42.89	72.26	12.49	207.56	0.50
Mn_3O_4	3472	-29.86	110.92	50.70	597.28	-0.47
P_2O_5	3472	-0.18	10.86	0.15	0.35	9.68
PbO	3472	-0.15	0.66	0.06	0.01	2.13
SiO_2	3472	-31.85	100.81	22.41	419.71	0.74

Table 6.4: Summary Statistics: ALR Simulations

VARIABLE	Count	Minimum	Maximum	Mean	Variance	Skewness
Simulation 10						
Al_2O_3	3472	0.07	17.15	2.08	4.15	2.22
Fe_2O_3	3472	0.28	83.28	16.15	219.85	1.55
Mn_3O_4	3472	0.16	90.22	44.20	496.16	-0.05
P_2O_5	3472	0.00	4.49	0.09	0.02	12.31
PbO	3472	0.00	0.54	0.04	0.00	2.99
SiO_2	3472	0.22	93.97	26.89	370.71	0.89
Simulation 41						
Al_2O_3	3472	0.03	17.93	2.01	3.78	2.44
Fe_2O_3	3472	0.19	81.70	14.37	194.44	1.70
Mn_3O_4	3472	0.38	93.10	44.98	488.40	-0.06
P_2O_5	3472	0.00	2.29	0.09	0.02	5.71
PbO	3472	0.00	0.81	0.05	0.00	4.53
SiO_2	3472	0.10	96.13	27.15	377.23	0.85
Simulation 61						
Al_2O_3	3472	0.04	10.60	1.63	1.71	1.83
Fe_2O_3	3472	0.12	88.11	16.56	265.93	1.45
Mn_3O_4	3472	0.13	94.94	44.45	491.07	-0.11
P_2O_5	3472	0.00	3.54	0.09	0.03	10.22
PbO	3472	0.00	0.53	0.04	0.00	3.52
SiO_2	3472	0.39	94.98	26.44	328.60	0.97
Simulation 84						
Al_2O_3	3472	0.04	9.44	1.64	1.80	1.64
Fe_2O_3	3472	0.12	80.78	16.40	288.63	1.42
Mn_3O_4	3472	0.34	93.30	44.76	594.02	0.06
P_2O_5	3472	0.00	5.03	0.09	0.03	15.32
PbO	3472	0.00	0.59	0.04	0.00	3.73
SiO_2	3472	0.24	88.86	26.97	353.18	0.77

Table 6.5: Summary Statistics: Ordinary kriging

VARIABLE	Count	Minimum	Maximum	Mean	Variance	Skewness
Al_2O_3	3469	0.15	8.14	1.51	1.31	1.39
Fe_2O_3	3469	-0.83	67.7	16.41	146.64	1.21
Mn_3O_4	3469	0.1	85.53	46.09	451.69	-0.37
P_2O_5	3469	0	15.28	0.23	0.92	10.27
PbO	3469	0.01	0.48	0.06	0	2.35
SiO_2	3469	0.92	85.63	23.63	299.44	1.34

Table 6.6: Summary Statistics: Oxide LUC 12 m panel

VARIABLE	Count	Minimum	Maximum	Mean	Variance	Skewness
Al_2O_3	3310	0.19	9.34	1.5	1.51	1.80
Fe_2O_3	3310	0.86	78.17	16.09	249.71	1.42
Mn_3O_4	3310	0.06	82.76	47.01	564	-0.42
P_2O_5	3310	0	17.19	0.2	0.88	13.33
PbO	3310	0.01	0.35	0.06	0	1.94
SiO_2	3310	1.15	95.73	23.2	418.81	1.38

Table 6.7: Summary Statistics: Oxide LUC 6 m panel

VARIABLE	Count	Minimum	Maximum	Mean	Variance	Skewness
Al_2O_3	3463	0.17	7.71	1.51	1.44	1.39
Fe_2O_3	3463	0.08	64.1	16.43	209.44	0.98
Mn_3O_4	3463	0.33	82.8	46.08	537.94	-0.33
P_2O_5	3463	0	16.76	0.22	0.91	10.37
PbO	3463	0.01	0.43	0.06	0.01	2.00
SiO_2	3463	1.41	84.87	23.65	365.48	1.08

Table 6.8: Summary Statistics: ICA LUC 12 m panel

VARIABLE	Count	Minimum	Maximum	Mean	Variance	Skewness
Al_2O_3	3310	-1.21	6.44	1.49	1.51	1.02
Fe_2O_3	3310	-12.5	61.53	16.32	161.6	0.89
Mn_3O_4	3310	-9.86	91.7	47.71	476.53	-0.42
P_2O_5	3310	-0.11	8.05	0.14	0.12	9.90
PbO	3310	-0.09	0.44	0.06	0.01	1.95
SiO_2	3310	-15.12	75.22	22.22	280.74	1.02

Table 6.9: Summary Statistics: ICA LUC 6 m panel

VARIABLE	Count	Minimum	Maximum	Mean	Variance	Skewness
Al_2O_3	3454	-1.35	6.87	1.51	1.43	0.97
Fe_2O_3	3454	-8.4	67.5	16.75	165.15	0.93
Mn_3O_4	3454	-12.38	90.11	46.72	479.05	-0.36
P_2O_5	3454	-0.1	16.71	0.17	0.37	16.08
PbO	3454	-0.07	0.45	0.06	0.01	2.07
SiO_2	3454	-10.86	76.57	22.97	287.05	1.05

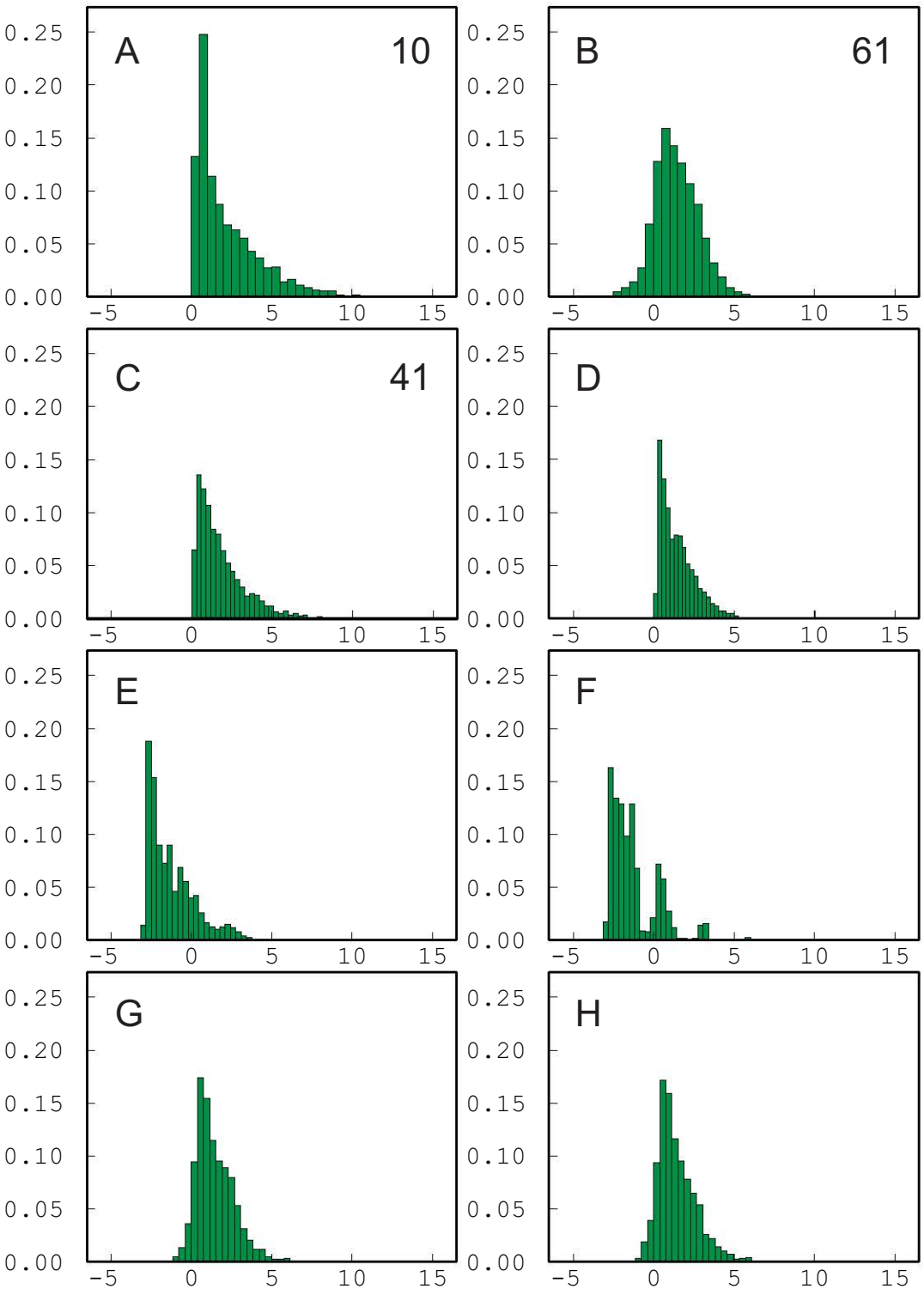

Figure 6.1: Distribution of results for Al_2O_3. A - Raw Oxide Simulation 10, B - Decorrelated Oxide Simulation 61, C - Decorrelated Log-ratio Simulation 41, D - Block Ordinary kriging, E - 12 m Panel LUC, F - 6 m panel LUC, G - 12 m Panel Decorrelated LUC, H - 6 m panel Decorrelated LUC.

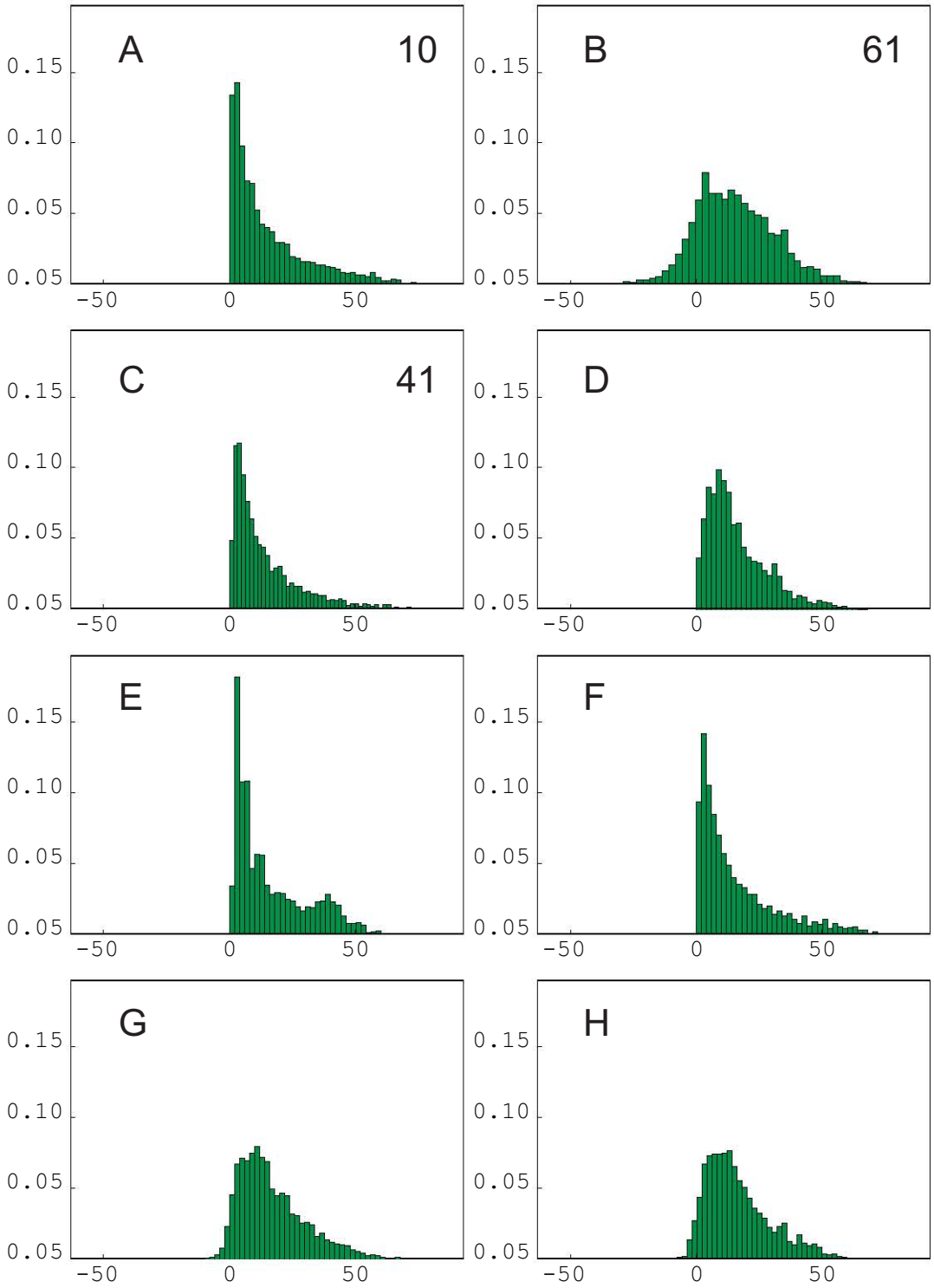

Figure 6.2: Distribution of results for Fe_2O_3. A - Raw Oxide Simulation 10, B - Decorrelated Oxide Simulation 61, C - Decorrelated Log-ratio Simulation 41, D - Block Ordinary kriging, E - 12 m Panel LUC, F - 6 m panel LUC, G - 12 m Panel Decorrelated LUC, H - 6 m panel Decorrelated LUC.

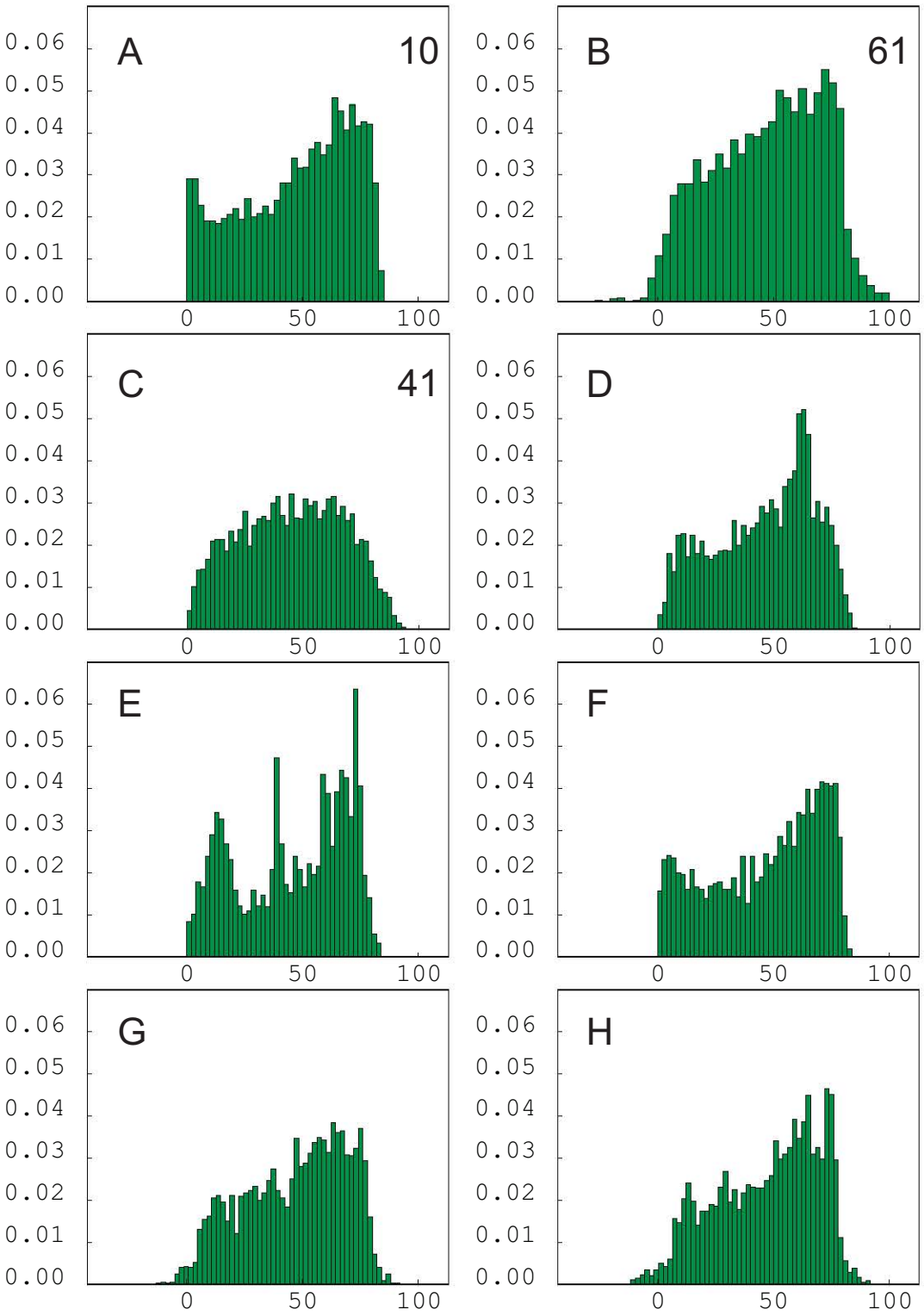

Figure 6.3: Distribution of results for Mn_3O_4. A - Raw Oxide Simulation 10, B - Decorrelated Oxide Simulation 61, C - Decorrelated Log-ratio Simulation 41, D - Block Ordinary kriging, E - 12 m Panel LUC, F - 6 m panel LUC, G - 12 m Panel Decorrelated LUC, H - 6 m panel Decorrelated LUC.

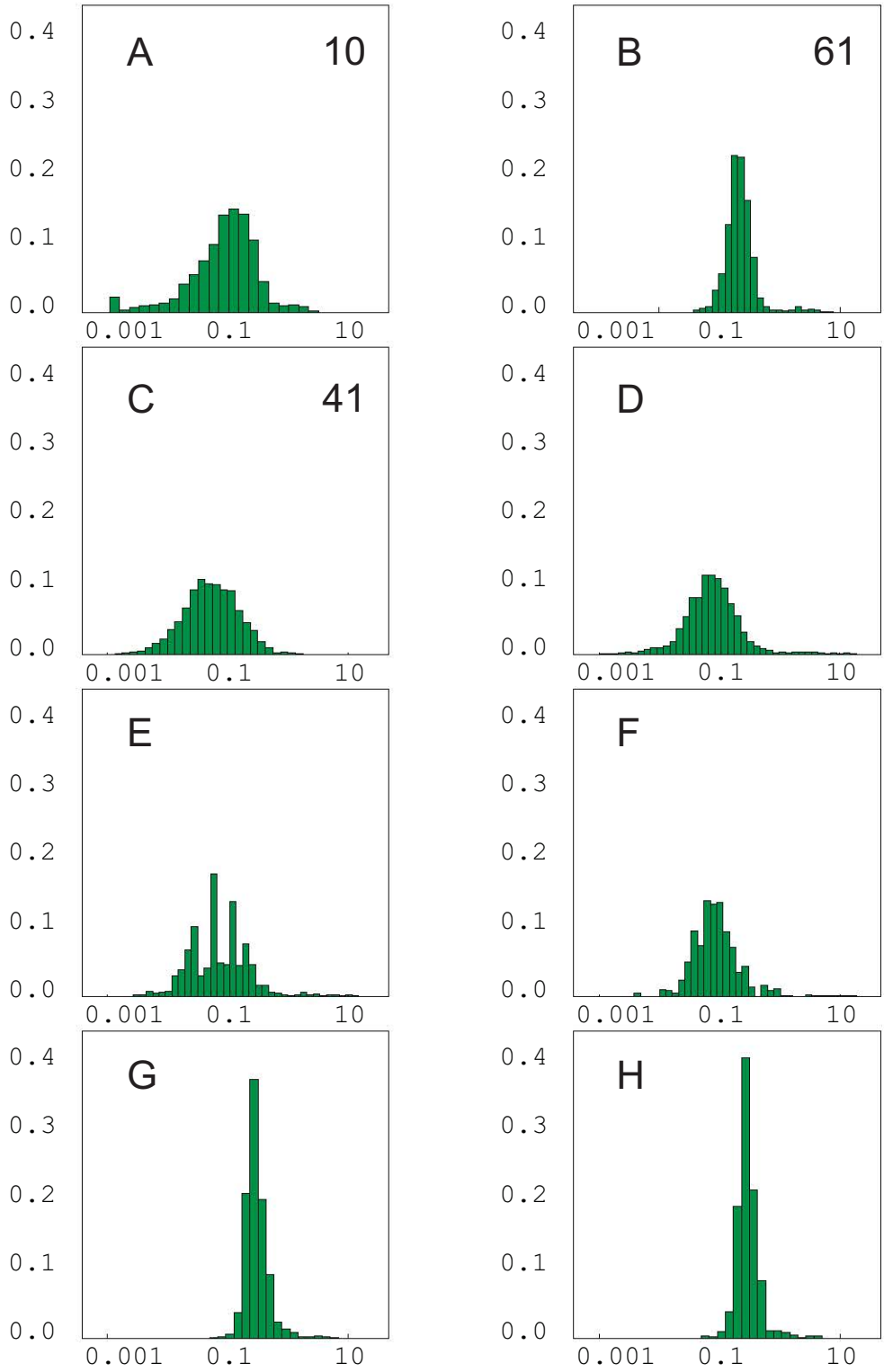

Figure 6.4: Distribution of results for P_2O_5. A - Raw Oxide Simulation 10, B - Decorrelated Oxide Simulation 61, C - Decorrelated Log-ratio Simulation 41, D - Block Ordinary kriging, E - 12 m Panel LUC, F - 6 m panel LUC, G - 12 m Panel Decorrelated LUC, H - 6 m panel Decorrelated LUC.

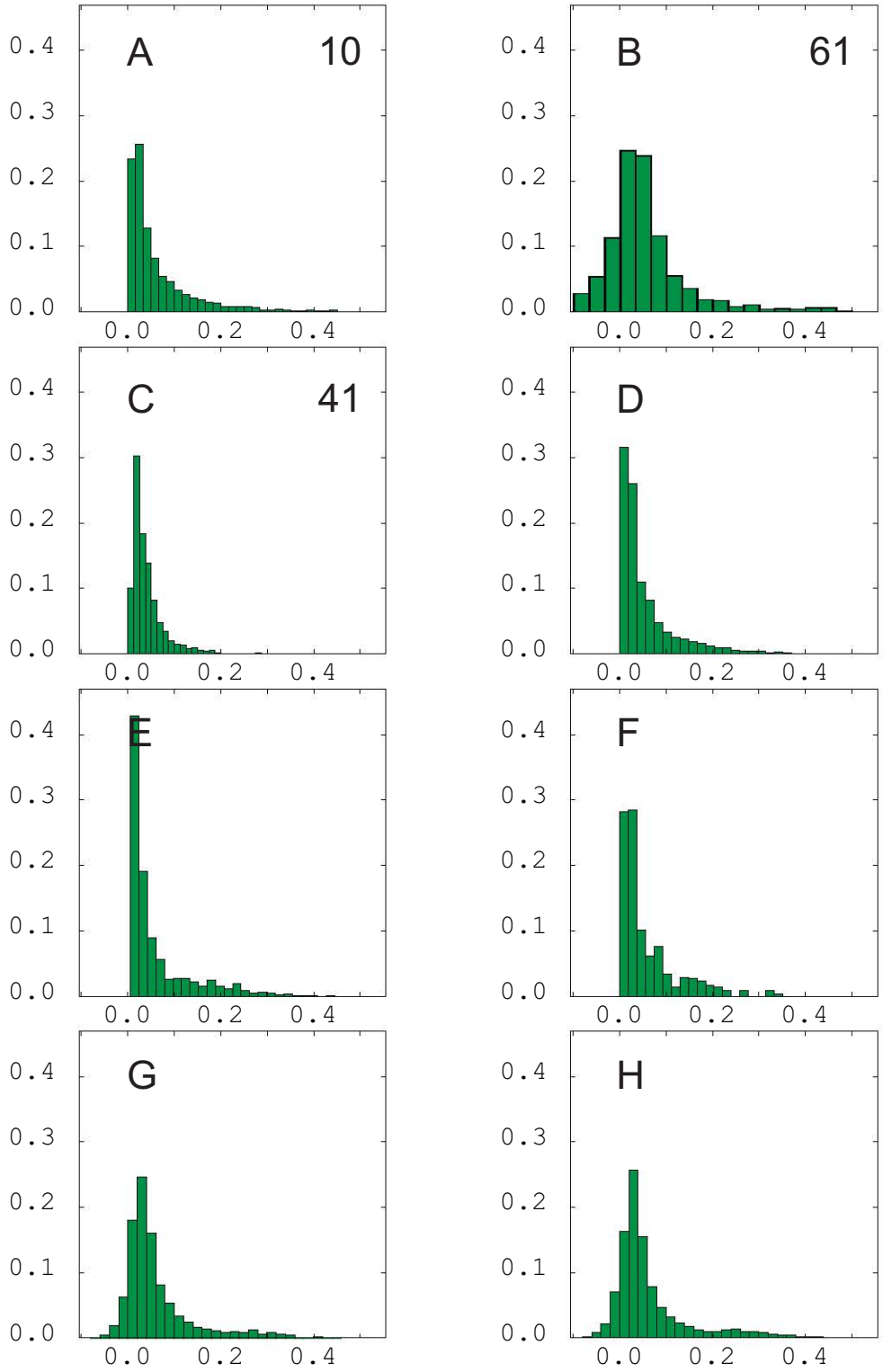

Figure 6.5: Distribution of results for PbO. A - Raw Oxide Simulation 10, B - Decorrelated Oxide Simulation 61, C - Decorrelated Log-ratio Simulation 41, D - Block Ordinary kriging, E - 12 m Panel LUC, F - 6 m panel LUC, G - 12 m Panel Decorrelated LUC, H - 6 m panel Decorrelated LUC.

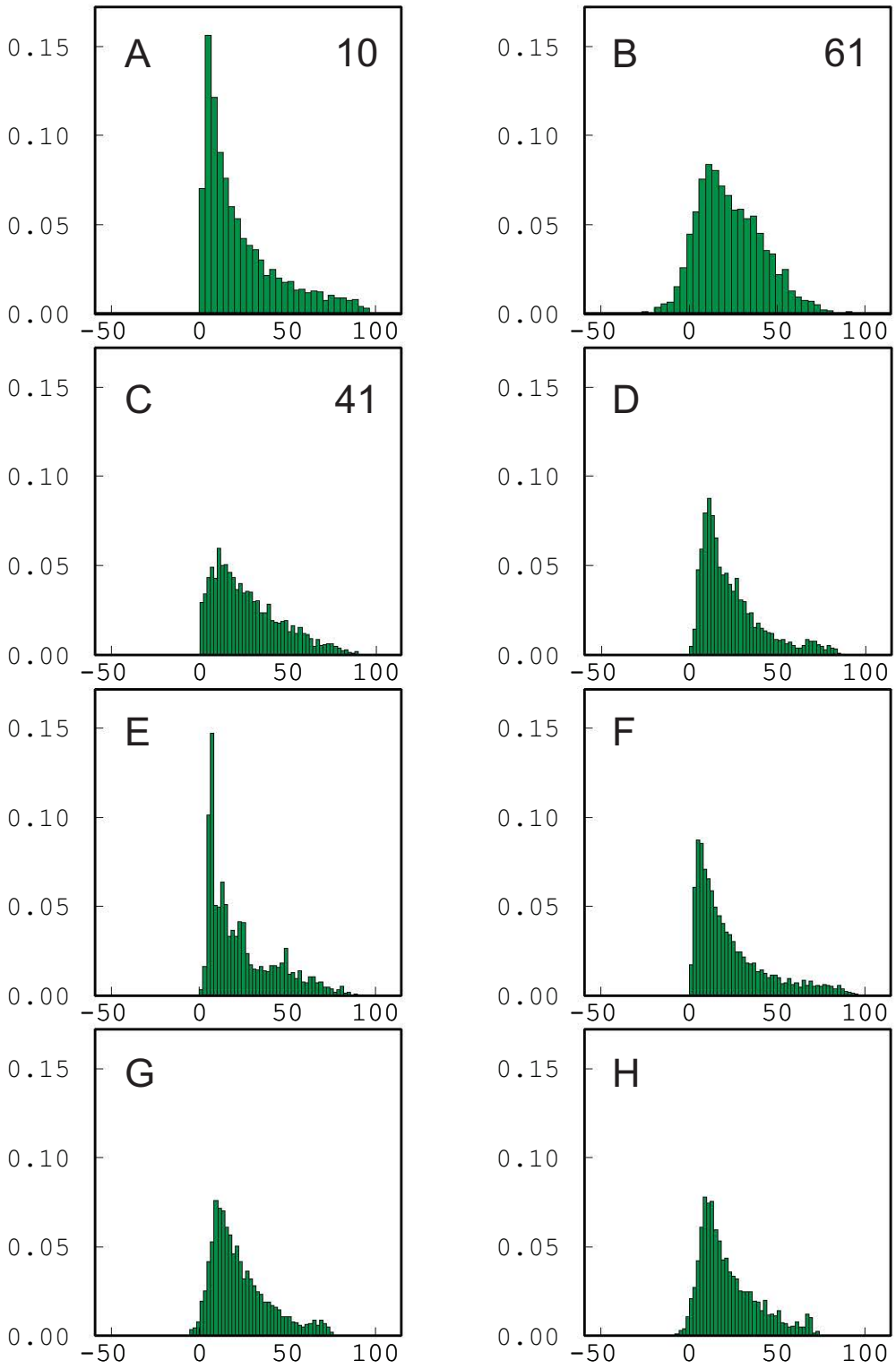

Figure 6.6: Distribution of results for SiO_2. A - Raw Oxide Simulation 10, B - Decorrelated Oxide Simulation 61, C - Decorrelated Log-ratio Simulation 41, D - Block Ordinary kriging, E - 12 m Panel LUC, F - 6 m panel LUC, G - 12 m Panel Decorrelated LUC, H - 6 m panel Decorrelated LUC.

Results for simulation are presented using individual simulations corresponding to median net profit result or each method (see Section 6.6). The ability of each method to reproduce the histogram of input data varies between methods. Generally, simulation of oxides results in reasonable reproduction of the input data distribution. In contrast, both the decorrelated oxides and the decorrelated log-ratio data show poorer reproduction of input distributions. The bimodal distribution of Mn_3O_4 is lost almost entirely within both of the decorrelated simulation methods (Figure 6.3). Decorrelated oxide results also show substantial deskewing of both Fe_2O_3 and SiO_2 results (Figures 6.2 and 6.6). BOK reproduces input data distributions moderately well, with some deskewing. LUC on both a 6 m and 12 m panel reproduce input distributions very well, with the exception of an anomalous spike in the distribution of Mn_3O_4 results at the average ($\approx 45\%$) within the 6 m panel results (Figure 6.3). Decorrelated oxide LUC performs poorly in terms of both the reproduction of input data histograms with substantial deskewing, but also a much more evident degree of loss of variance within the results, when compared to other methods (Tables 6.2 to 6.9 and Figures 6.1 to 6.6). Further, results from the estimation / simulation of ICA decorrelated oxides present impossible negative percentages for some elements when back-transformed into $\mathbb{R}^N$ (Table 6.10).

From these general comments, it is clear that the poorest reproduction of input data distribution generally occurs where transformation is involved. Potentially, this may be attributable to the way in which the tails of each distribution are modelled during Gaussian anamorphosis for both simulation and LUC. Gaussian transformations (via hermite anamorphosis) in Isatis for the purposes of simulation and LUC model the tails of each distribution using linear functions. The possibility that the Gaussian anamorphosis plays a role in distorting the results distribution is discussed further in Section 6.3

Table 6.10: Percentages of negative values for each estimation / simulation

	Al2O3	Fe2O3	Mn3O4	P2O5	PbO	SiO2
ICA LUC 6 m	6%	4%	1%	8%	11%	2%
ICA LUC 12 m	5%	3%	1%	8%	9%	2%
Individual Simulations						
ICA 10	11%	16%	1%	18%	16%	9%
ICA 41	9%	11%	3%	16%	16%	6%
ICA 61	13%	15%	1%	16%	21%	8%
ICA 84	13%	18%	2%	22%	19%	10%

Figure 6.7 presents the results of each of the methods as a series of grade tonnage curves, with the deterministic methods of LUC and BOK presented as lines, while the range of val-

ues defined by each series of simulations is described by a differently shaded area. Each plot also shows the grade tonnage curve for the BOK of the complete dataset, and also the block anamorphosis of the input data, presented on the same 3 m block support over which the results of each studies method have been produced. Negative results have been ignored in the determination of grade tonnage curves.

When plotted on grade tonnage curves, LUC methods and both BOK of the RD data and the complete dataset show similar patterns. Simulations tends to show more divergent characteristics, both from the deterministic methods of LUC and BOK, but also from each other. Considering the curves for variable Al_2O_3, raw simulations are generally close to curves of the other methods, but those for the ICA decorrelated oxides show a general overstatement of grade at any given percentile. Simulations of the decorrelated log-ratio (ALR) data show an even more pronounced overstatement of grade, with greater maxima and range than for any of the other methods. For the results of Fe_2O_3, most methods overstate lower cutoff grades when compared to the block anamorphosis of the input data, most clearly by the ALR simulations. Decorrelated oxide (ICA) simulations show roughly evenly distribution around the block anamorphois. Raw oxide simulations show that for the majority, grades are overstated at each cutoff level. Mn_3O_4 results of most methods show dissimilarity from the input distribution described by the 3 m block anamorphosis. ALR simulations show a general understatement of grades at all cutoff levels, except the maximal cutoffs, where grades tend to be overstated. ICA simulations overstate the grades at lower cutoff levels, an then tend to understate grades at cutoffs betwen 50% and 10% of the study region. The highest grade portions (90th percentile and above) are overstated similar to ALR simulation. Of the deterministic methods, all tend to to show over statement of grades for the $\tilde{3}$0th percentile and lower, and then significant understatement of grades for all percentiles greater than this value. Phosphorous values all appear to be generally similar in trends on the grade tonnage curve, though the highly positively skewed results may mask some detail.

For PbO, cutoff grades for ALR simulations are understated in all percentiles, with a noticeably lower maximal grade. All other methods tend to plot similarly to the input data anamorphosis, excepting generally lower maximal grades. ICA simulations tend to overstate cutoff grades at all percentiles. SiO_2 shows significant overstatement of cutoff grades for all percentiles in both ALR simulations and ICA simulations. Generally all other methods tend to moderately overstate grade for cutoff up to the 70th percentile, and then display similar grades henceforth to those of the input data anamorphosis.

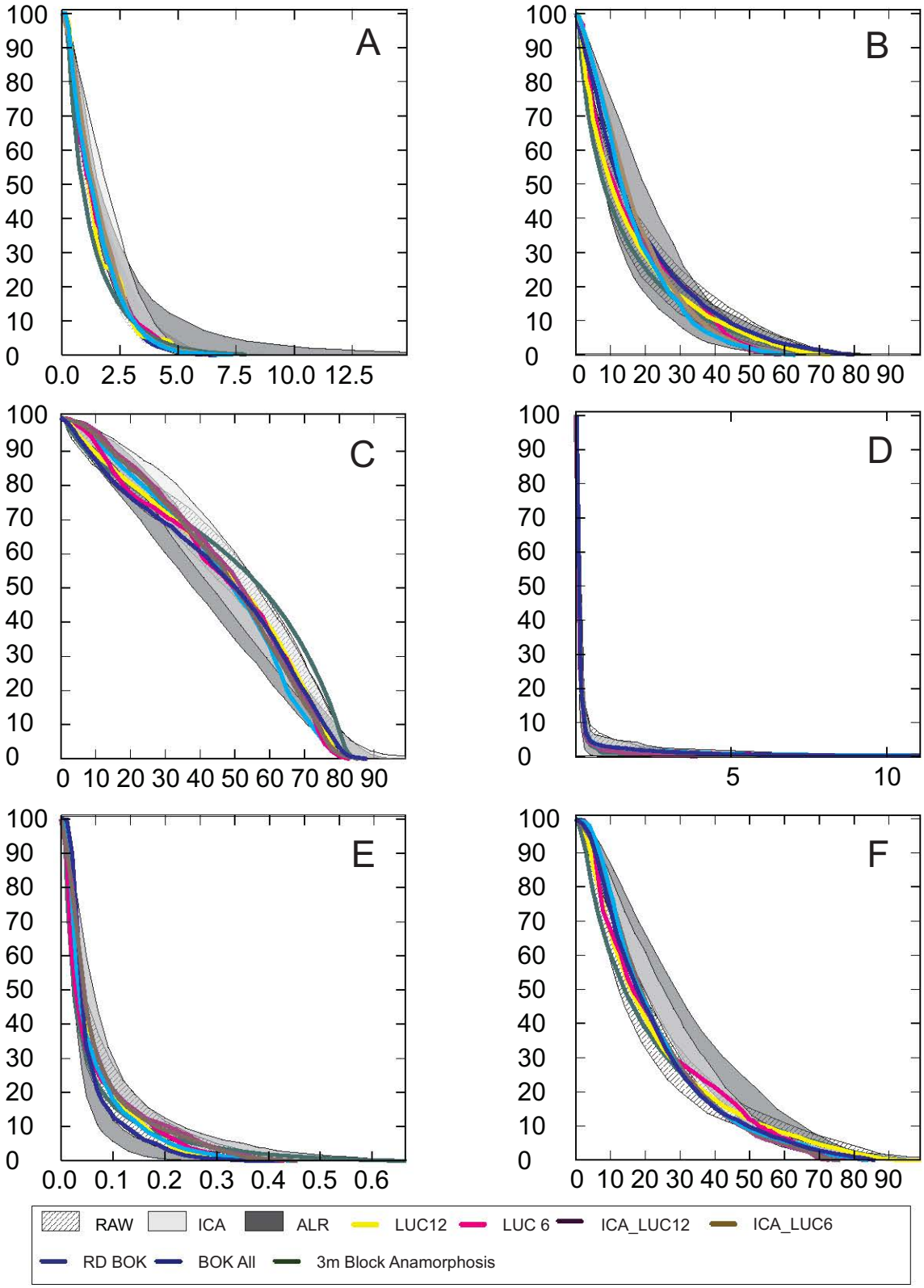

Figure 6.7: Grade-Tonnage curves for each variable, presenting the results of each method. A - Al_2O_3, B - Fe_2O_3, C - Mn_3O_4, D - $P2O_5$, E - PbO, F - SiO_2

6.3 Specific Comment On Simulation Results

The differences observed between the deterministic methods (LUC and BOK) and those of simulation become even more pronounced when considering the average results of each individual simulation in comparison to the results from each of the other methods. While the average values from raw and decorrelated oxide simulations show broadly similar values to those of the other methods, ALR simulation results show obvious bias, for all variables (Figure 6.8). While both the ICA simulations, and raw oxide simulations generally display averages similar to both the input data and ordinary kriged results, Al_2O_3, and Mn_3O_4 show substantial high and low bias respectively for approximately half of the ALR simulations. Average values per simulation of both P_2O_5 and PbO are substantially low biased compared to the input data and all other simulations. Finally, SiO_2 is consistently high-biased for the ALR simulations.

Why this might occur, given that one of the key features of geostatistical simulation is input histogram reproduction, can only be attributed to one or more of the transformations which this set of simulation results has undergone. On a Q-Q plot, simulation results in transformed space (ICA decorrelated factors of log-ratio transformed variables) show very close reproduction of the input data (Figure 6.9), however, the re-correlated log-ratio transformed results show a distinct departure from the input data distributions (Figure 6.10). A very similar distortion is observed in the decorrelated only (no log-ratio transform) simulations. Histogram reproduction for the simulated results of the decorrelated factors is very good (Figure 6.12), yet back transformed raw oxide distributions for the simulated results are markedly distorted (Figure 6.13). It is likely therefore, that the ICA transform is responsible for introduction of a significant bias. One possible reason, is that the rotation matrix by which ICA seeks to yield maximally independents factors assumes unimodal (singular) source signals. The unmixing matrix by which ICA decorrelates therefore seeks maximally independent unimodal factors. The histogram of Mn_3O_4 values in the input data shows a distinct bimodal distribution. Once simulation has taken place on the unimodal factors resulting from ICA transformation, their back transform is unlikely to yield a similarly bimodal distribution. Additionally, the distribution of any distortion from the bimodality of Mn_3O_4 is likely to be distributed through all fo the decorrelated factors via the unmixing matrix, which will be carried through the results when back transformed once again. For comparison, the histogram reproduction is substantially better for simulations of the raw oxide data (Figure 6.14). The exception is the distribution of results for P_2O_5, which are spuriously bimodal in the simulated results with an over-representation of very low values.

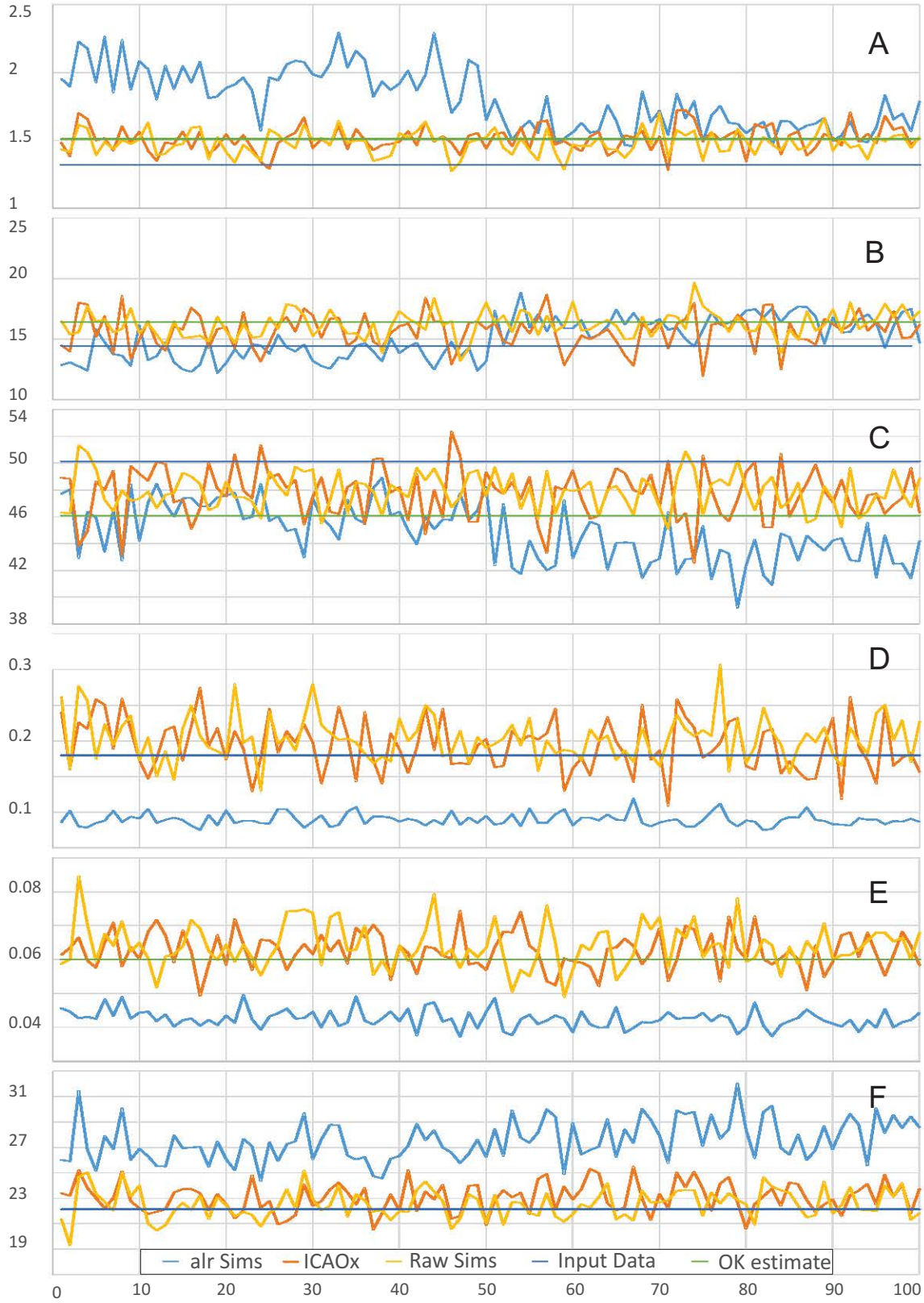

Figure 6.8: Average values, per-simulation, compared to average results of OK and LUC for each variable. A - Al_2O_3, B - Fe_2O_3, C - Mn_3O_4, D - P_2O_5, E - PbO, F - SiO_2

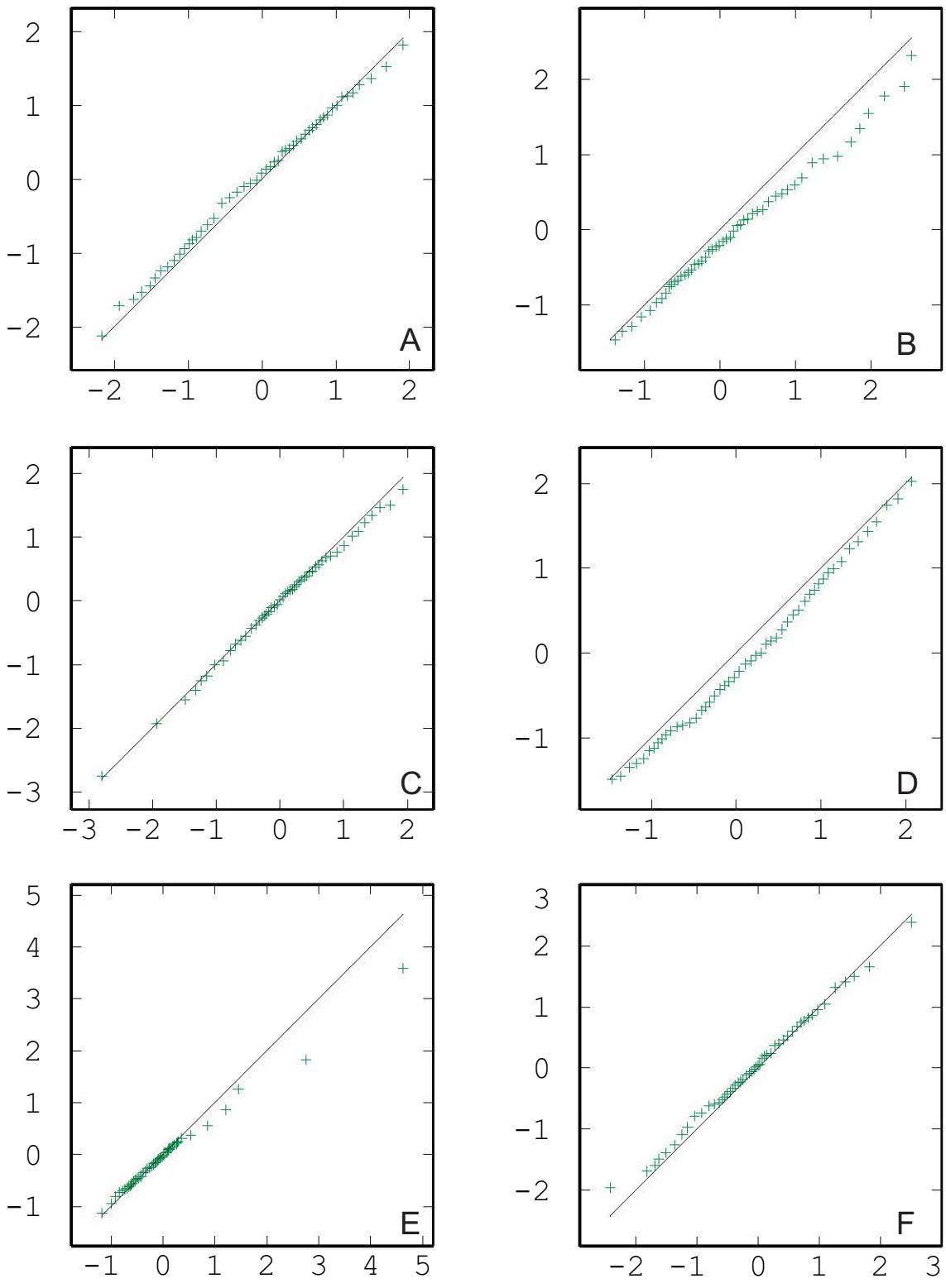

Figure 6.9: Decorrelated, log-ratio transformed factor results for simulation 41 (horizontal axis) against input data (reduced dataset, vertical axis) A - Factor 1, B - Factor 1, C - Factor 3, D - Factor 4, E - Factor 5, F - Factor 6

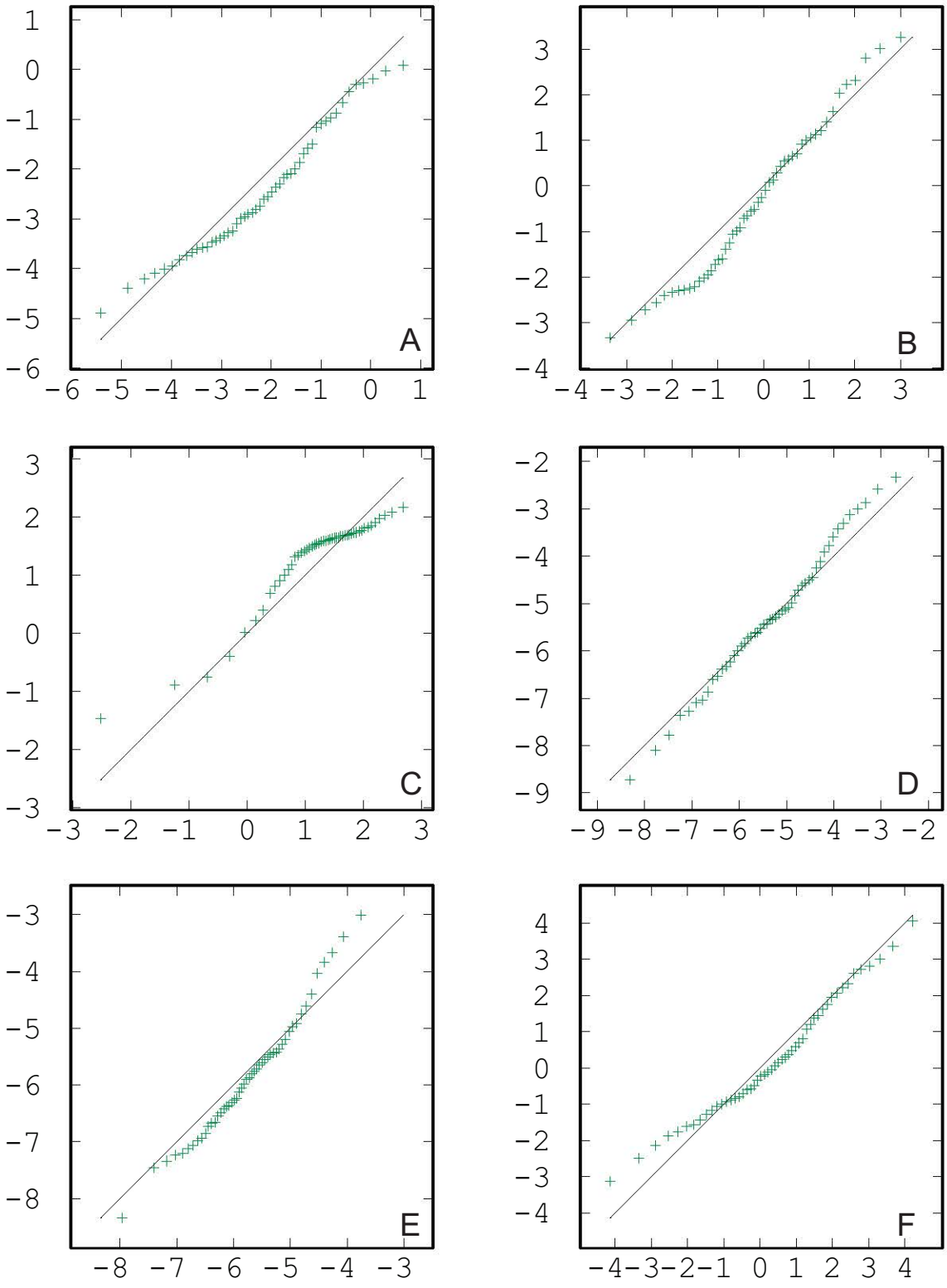

Figure 6.10: Back transformed log-ratio results against input log-ratio data; simulation 41. A - alrAl_2O_3, B - alrFe_2O_3, C - alrMn_3O_4, D - alrP_2O_5, E - alrPbO, F - alrSiO_2

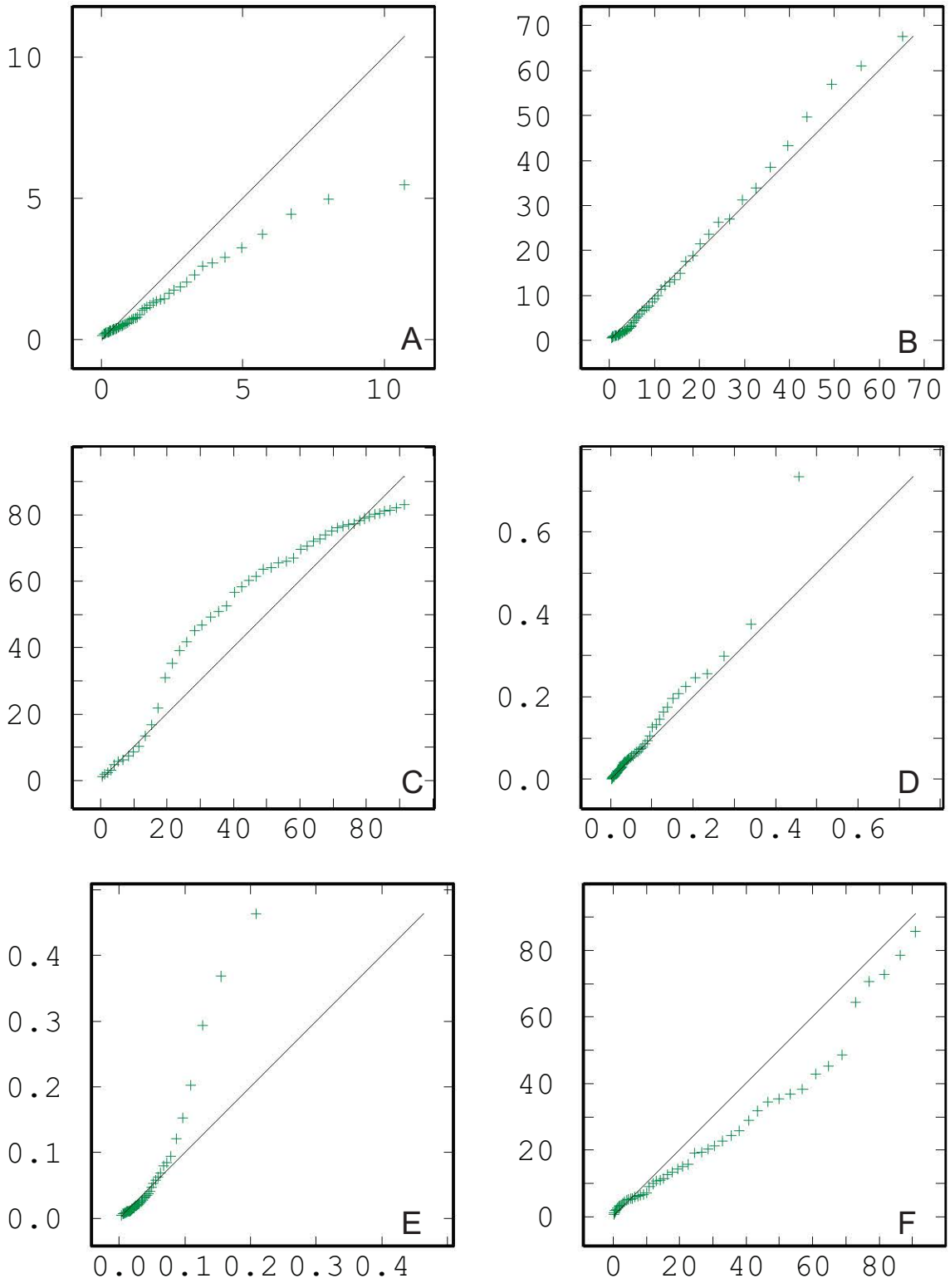

Figure 6.11: Fully back transformed results from simulation of decorrelated log-ratios against input oxide data; simulation 41. A - Al_2O_3, B - Fe_2O_3, C - Mn_3O_4, D - P_2O_5, E - PbO, F - SiO_2

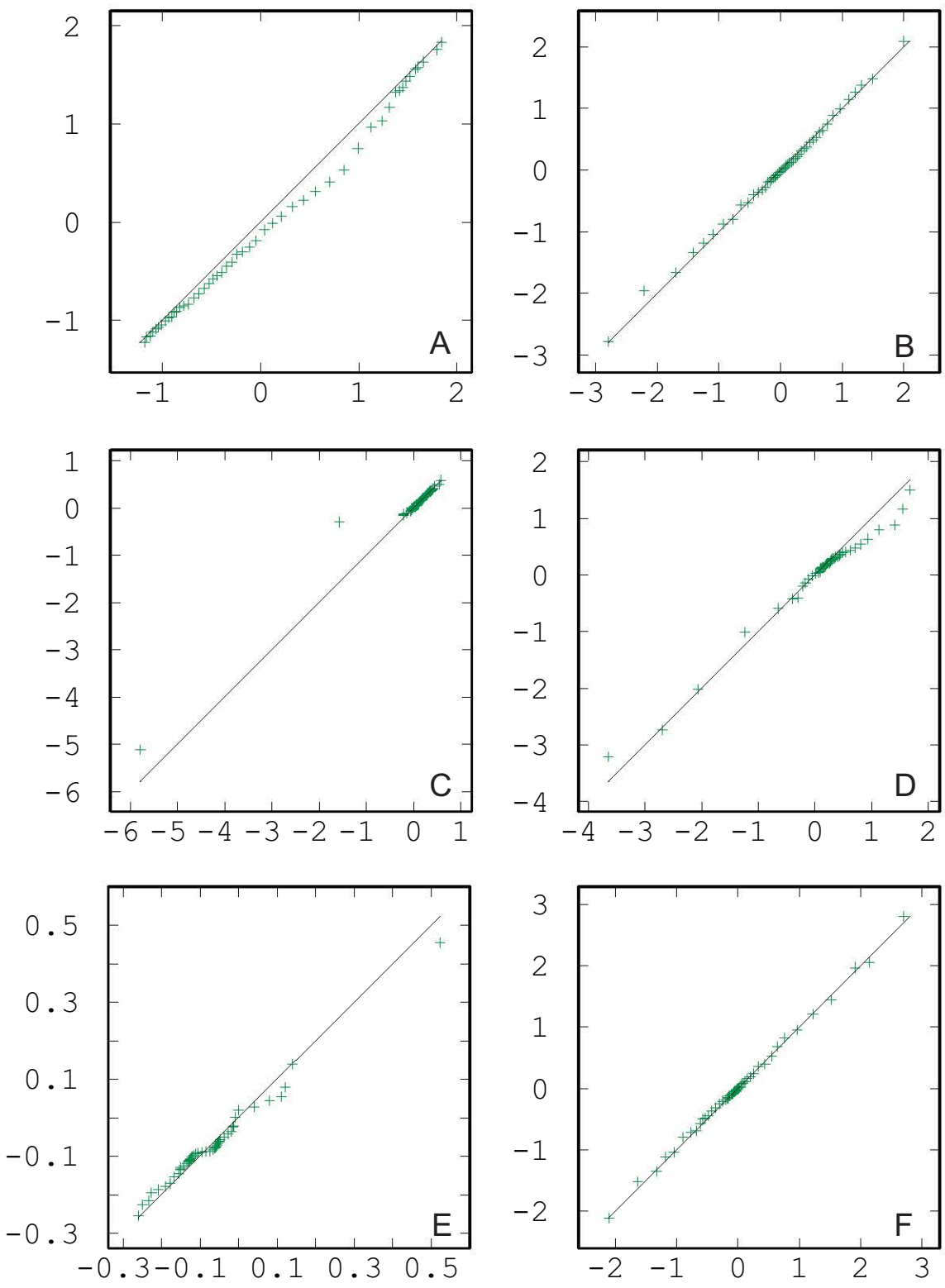

Figure 6.12: Decorrelated Oxide Factors (horizontal axis) against input factors (vertical axis); simulation 61. A - Factor 1, B - Factor 2, C - Factor 3, D - Factor 4, E - Factor 5, F - Factor 6

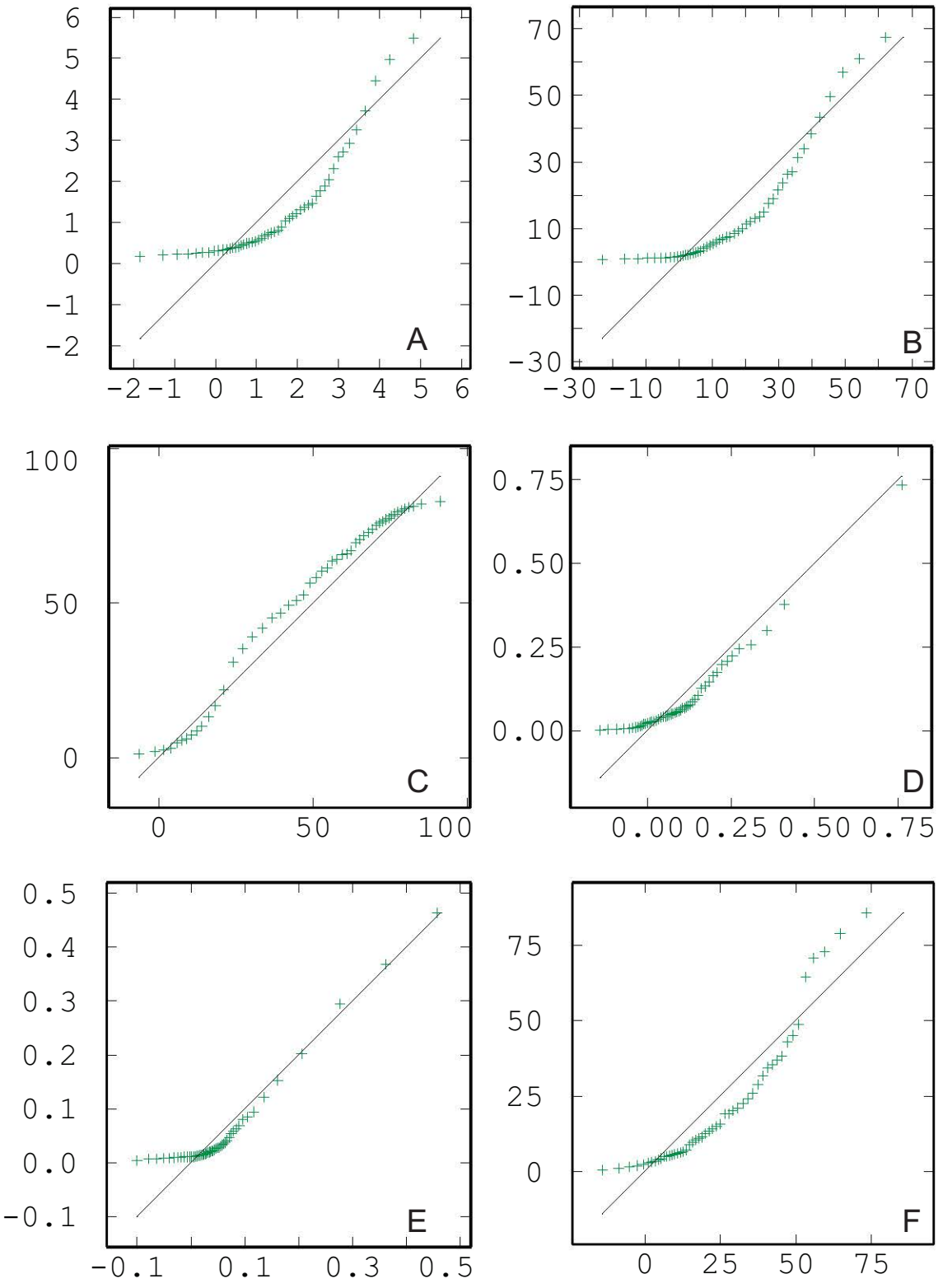

Figure 6.13: Back transfomred oxide results from simulation of decorrelated oxide factors; simulation 61. A - Al_2O_3, B - Fe_2O_3, C - Mn_3O_4, D - P_2O_5, E - PbO, F - SiO_2

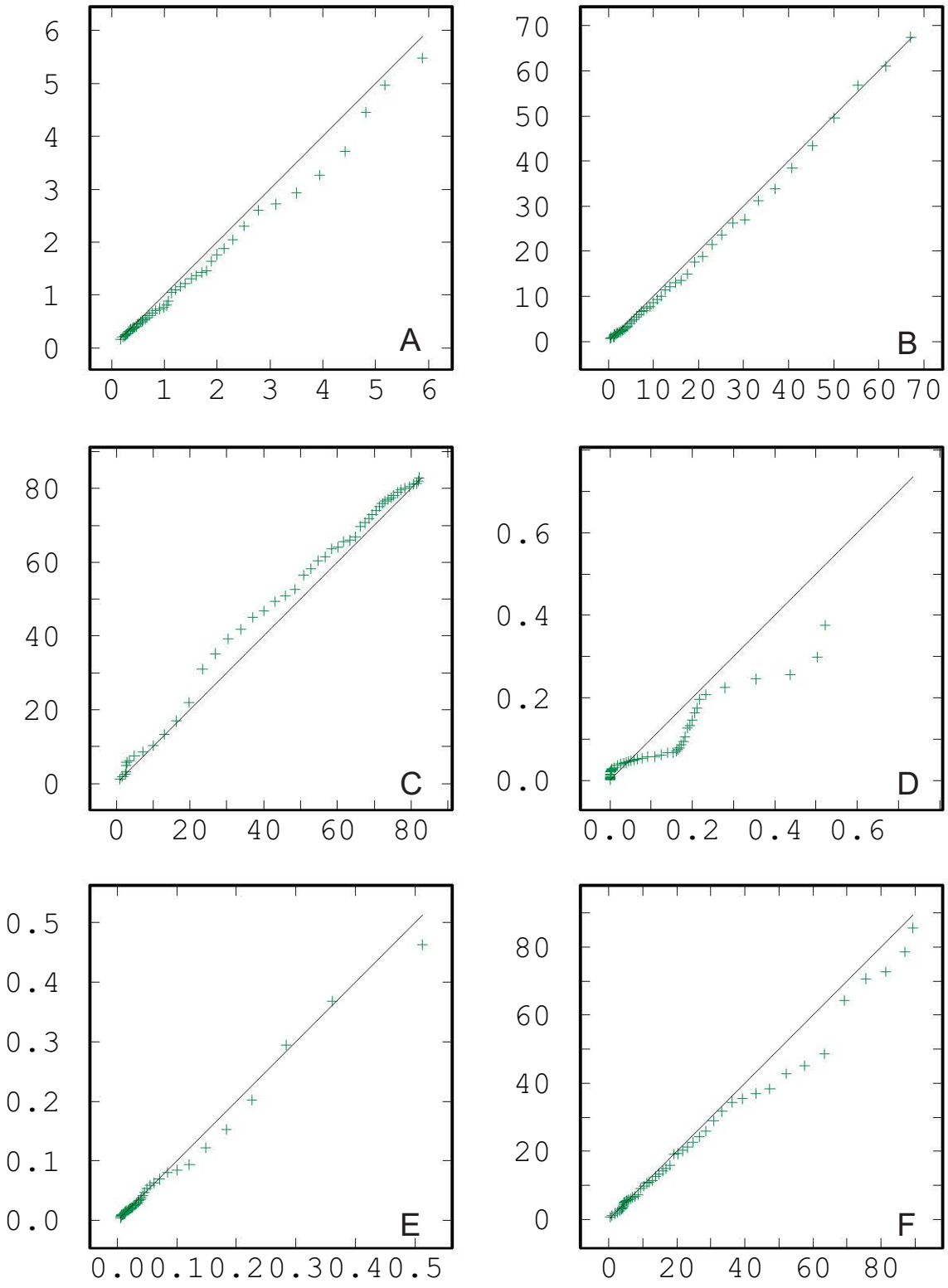

Figure 6.14: Oxide simulation results (horizontal axis) against input oxide data (vertical axis); simulation 10. A - Al_2O_3, B - Fe_2O_3, C - Mn_3O_4, D - P_2O_5, E - PbO, F - SiO_2

6.4 Spatial Results

Generally speaking, all methods and all data treatments show similar spatial patterns within their results, for all variables (Figures 6.15 to 6.26). Simulated results tend to be "noisier" than either BOK or LUC, since simulation is not subject to the same degree of smoothing from the linear averaging inherent in the other methods. Note that those results whose labels are highlighted in red in Figures 6.15 to 6.20, relate to the median net profit results presented later in Section 6.6.

Al_2O_3 results for both the oxide and decorrelated oxide (RAW and ICA) data treatments show good visual correlation to the distribution of input data, with the exception of slightly under-representing the high grade outliers evident in the input data in the southern part of Domain 2. Decorrelated log-ratio (ALR) simulation results conversely show an over-representation of high grade material in Domain 2, inconsistent with the input data distribution. BOK, LUC (6 and 12 m panels) and decorrelated ICA (6 and 12 m panels) all show very good visual correlation to the input data. All of these latter methods also record the high grade outlier in domain 2. Similar trends are observed in Fe_2O_3 results where, while general spatial distributions are reproduced, ALR simulations, particularly in Domain 2 over-represent high grade material. Mn_3O_4 results for ALR simulation tend to under-represent the grades within Domain 2, while over-representing the extent of high grade material along the south east and north east margins in Domain 1. P_2O_5 results from all simulations fail to capture the presence of a high grade outlier in the north east of Domain 1. Additionally, simulation methods appear to generally over-represent the distribution of higher grades within the central portions of Domain 1. In contrast BOK and LUC methods all capture the existence of the outlier (though may over-represent its influence through smoothing of the linear averaging algorithm), and generally have very good reproduction of the spatial distribution of input data. Decorrelated LUC results do exhibit a high proportion of negative values distributed throughout the very low grade portions of Domain 1 in the south west, and also through the central portion of Domain 2, where there are fewer sample locations. Distribution of PbO results for all methods appears to be good, with the exception of ALR simulation, which appears to fail in capturing the sporadic distribution of isolated higher grade material throughout both domains. These higher grade areas are seen as discrete "patches" within all other methods. Note that for the P_2O_5 and PbO results of LUC over a 6 m panel, often the SMU support grade tonnage curve is unable to be discretised adequately within the precision of the panel results and so all blocks receive the panel grade. SiO_2 results all reproduce the distribution of input data reasonably well, capturing the discrete high grade zones within both Domain 1 and 2. Once

again the exceptions are the ALR simulation results, which overstate the occurrence of high grade material in Domain 2.

Assessing the total sum of all variables Figures 6.27 and 6.28, noting that the data are compositional, RAW simulations can be seen to severely violate the sum constraint with a high proportion of regions exceeding sums of 105%. These are interspersed with regions of very low total sums, and in combination, this pattern also bears little resemblance to the spatial distribution of total sums observed in the input data. Directly, this is a result of the selection of values for each realisation, for each variable, occuring independently of any knowledge of the values selected for all other variables. All other methods are reasonable in the reproduction of total sum distribution, and in not violating the sum constraint. The worst of the other methods for violation of the sum constraint is appears to be LUC of raw oxides, however the adherence of decorrelated LUC and decorrelated simulation (ICA) to the total sum will be influenced unduly by the presence of spuriously negative results for some variables potentially masking poor sum constraint adherance. Only the ALR simulations, through the use of log ratios, will guarantee both positive only results and adherence to the sum constraint.

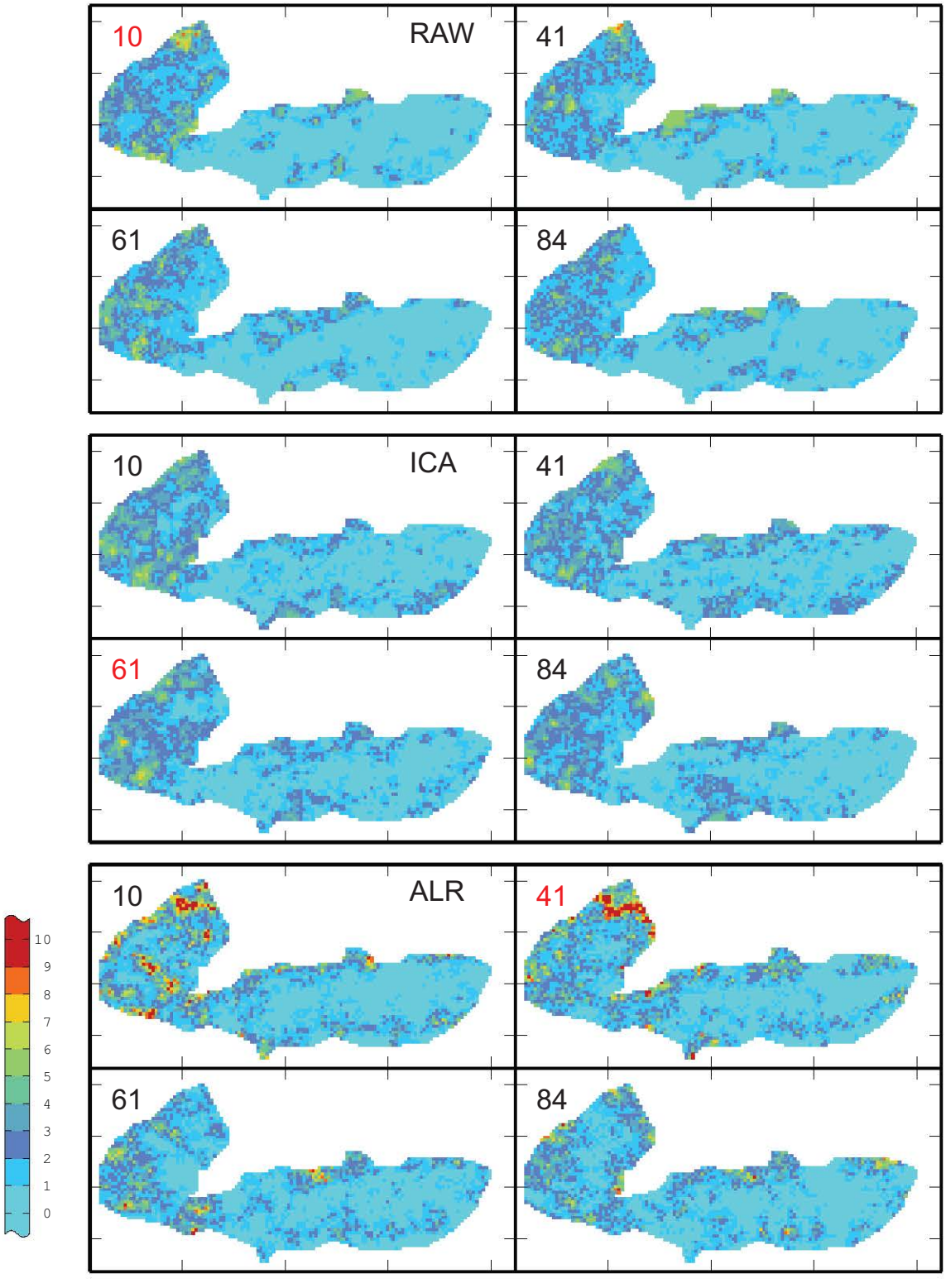

Figure 6.15: Al_2O_3 individual simulation results.

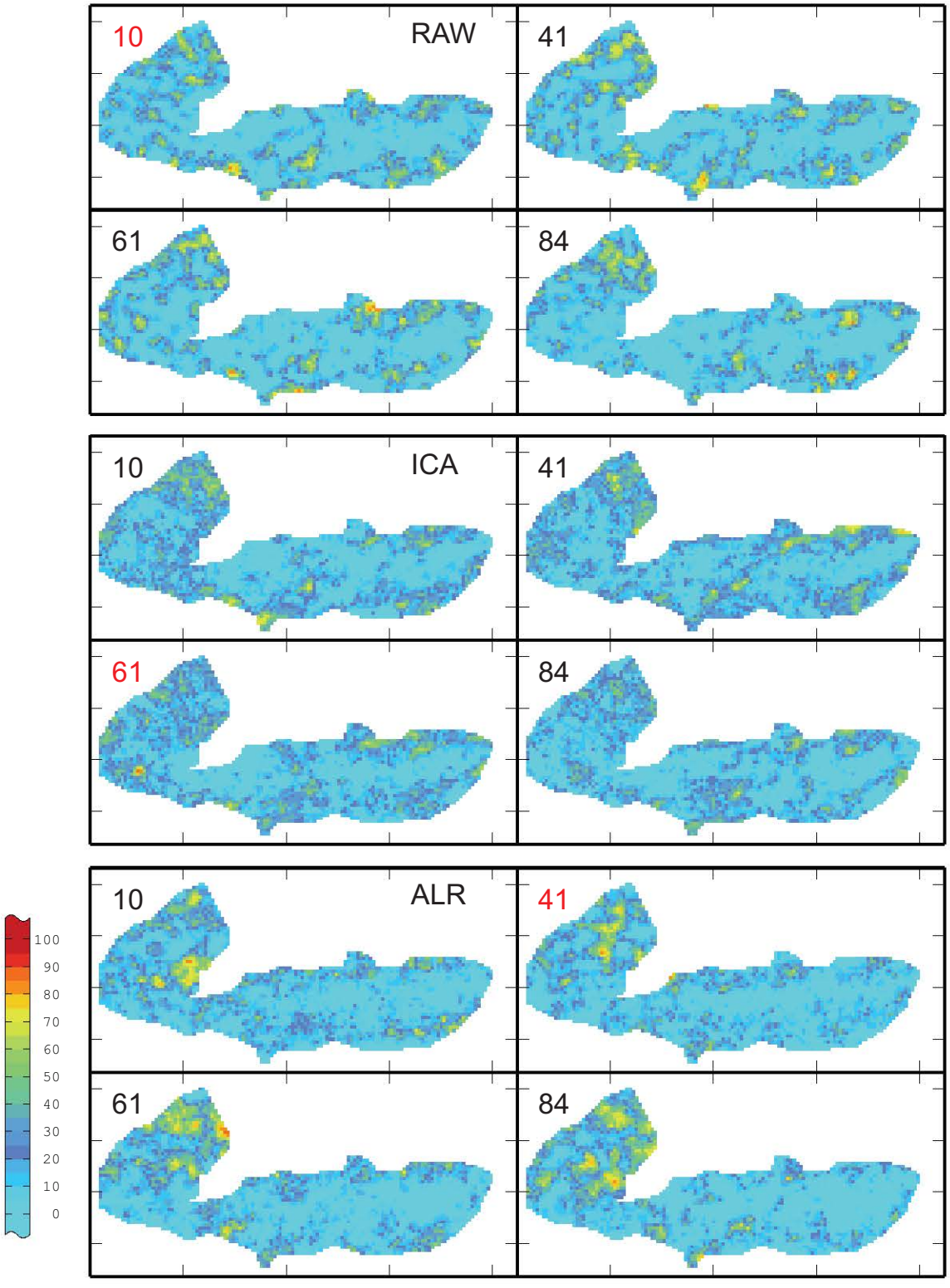

Figure 6.16: Fe_2O_3 individual simulation results.

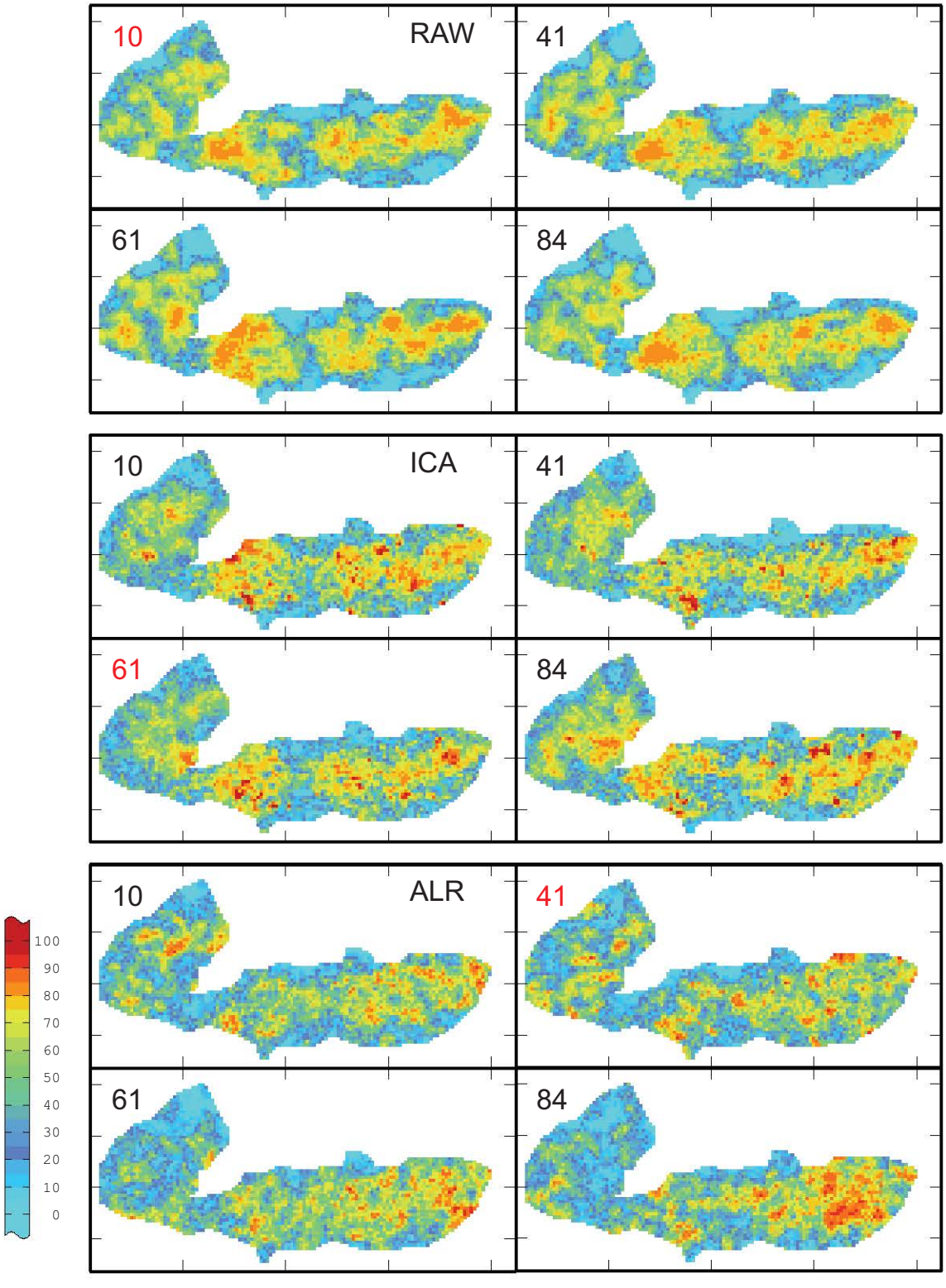

Figure 6.17: Mn_3O_4 individual simulation results.

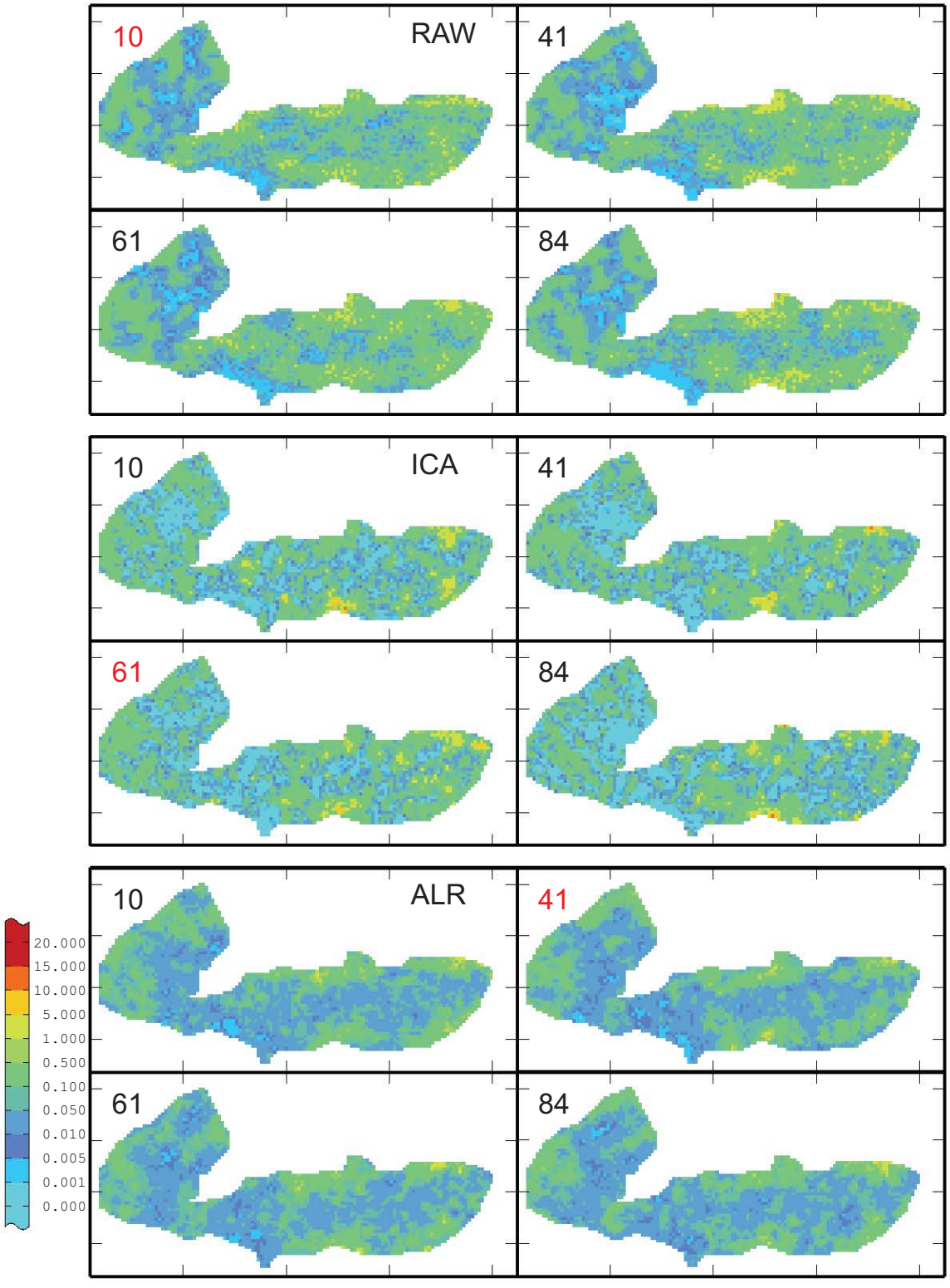

Figure 6.18: P_2O_5 individual simulation results.

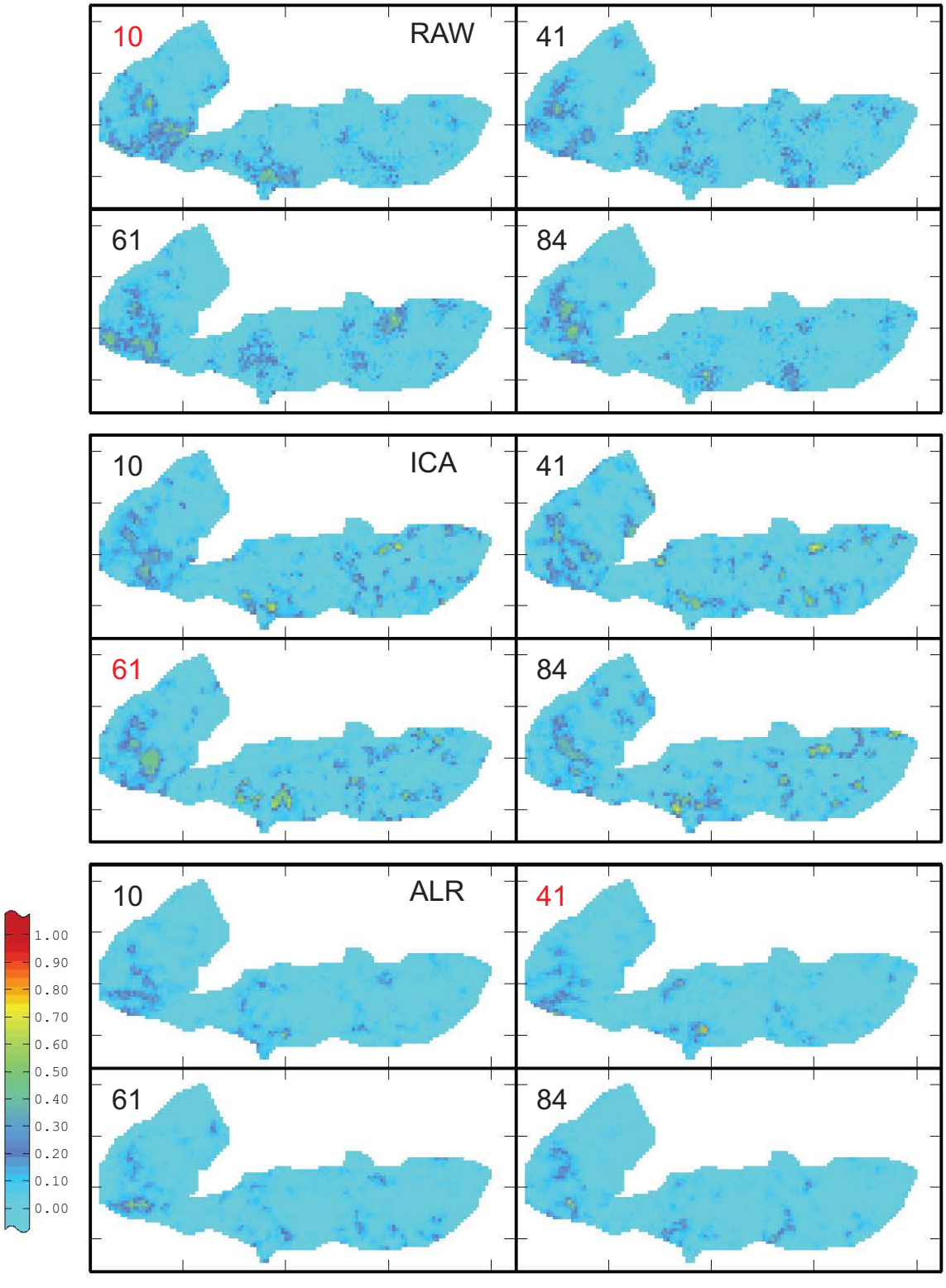

Figure 6.19: PbO individual simulation results.

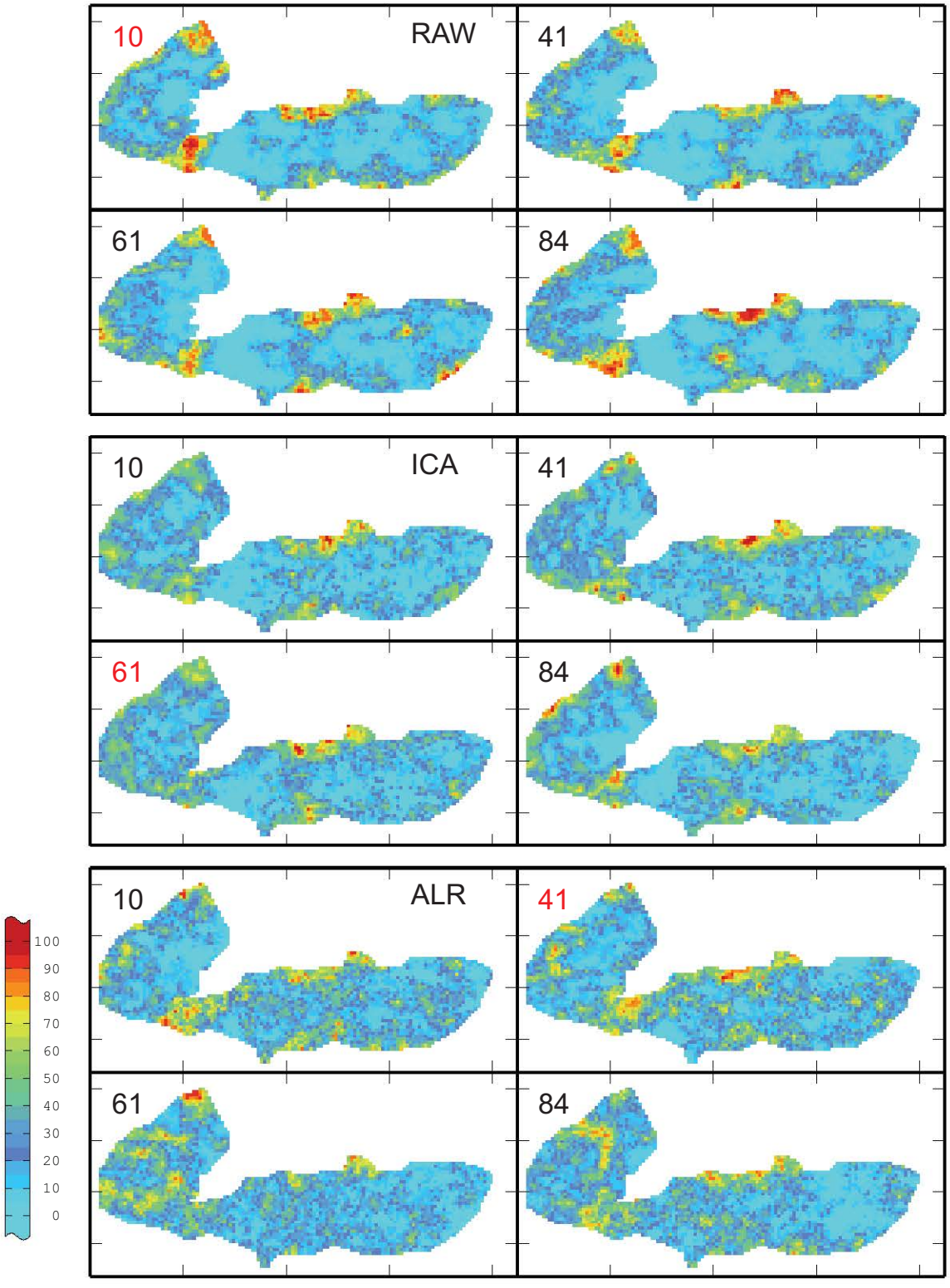

Figure 6.20: SiO_2 individual simulation results.

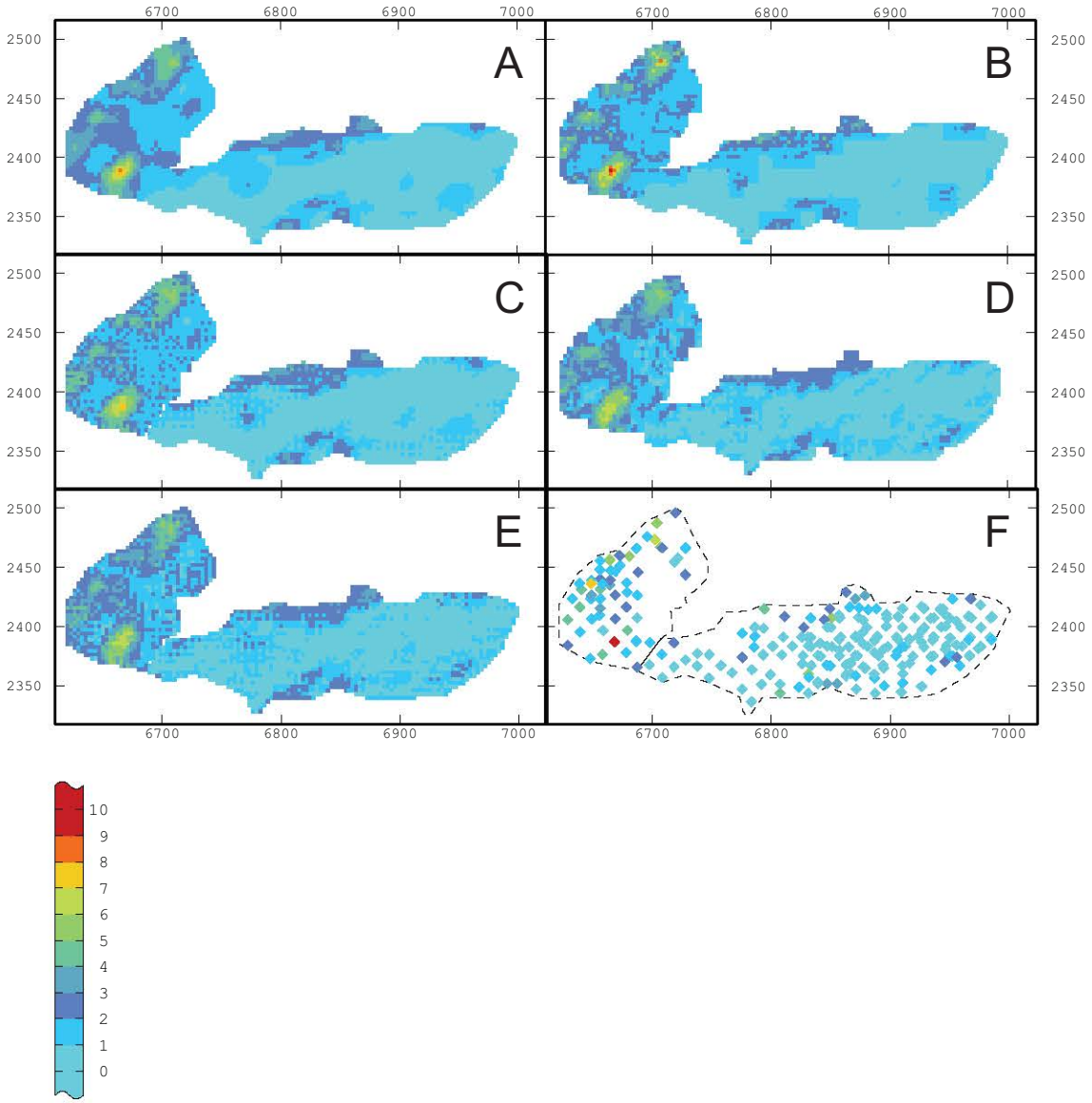

Figure 6.21: Al_2O_3 results. A - Ordinary kriging, B - LUC 12 m panel, C - LUC 6 m panel, D - Decorrelated LUC 12 m panel, E - Decorrelated LUC 6 m panel, F - Input Data

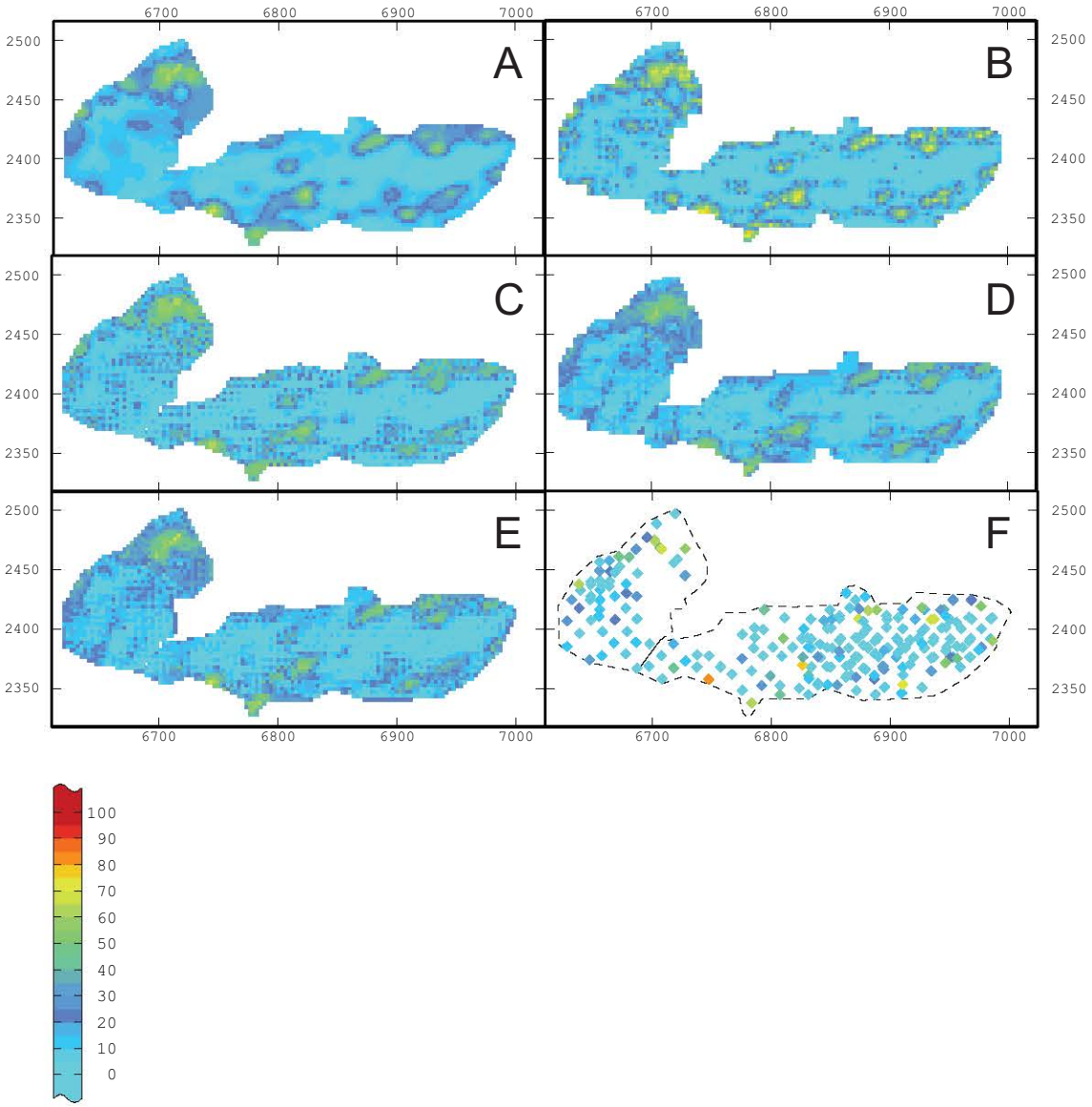

Figure 6.22: Fe_2O_3 results. A - Ordinary kriging, B - LUC 12 m panel, C - LUC 6 m panel, D - Decorrelated LUC 12 m panel, E - Decorrelated LUC 6 m panel, F - Input Data

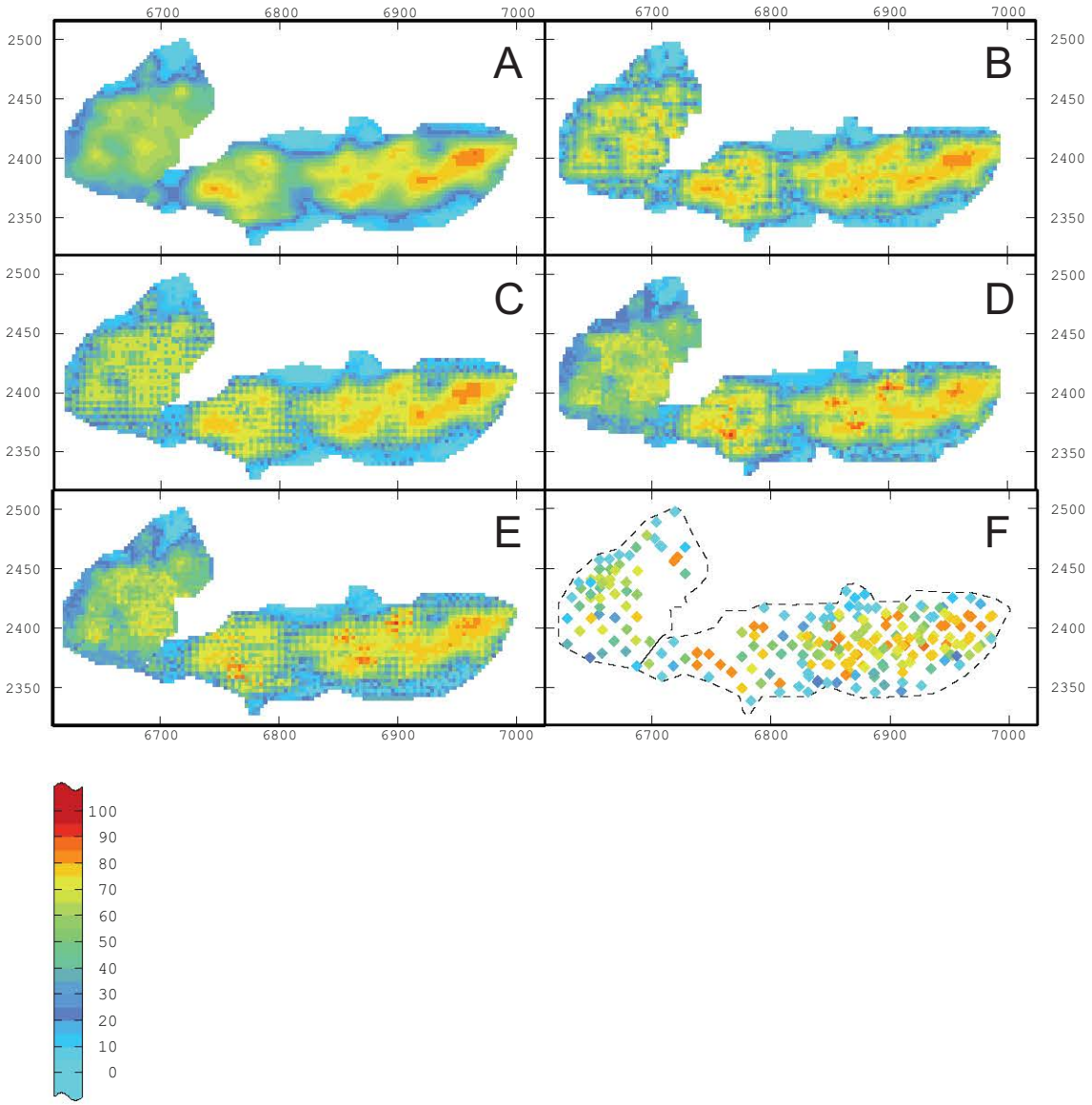

Figure 6.23: Mn_3O_4 results. A - Ordinary kriging, B - LUC 12 m panel, C - LUC 6 m panel, D - Decorrelated LUC 12 m panel, E - Decorrelated LUC 6 m panel, F - Input Data

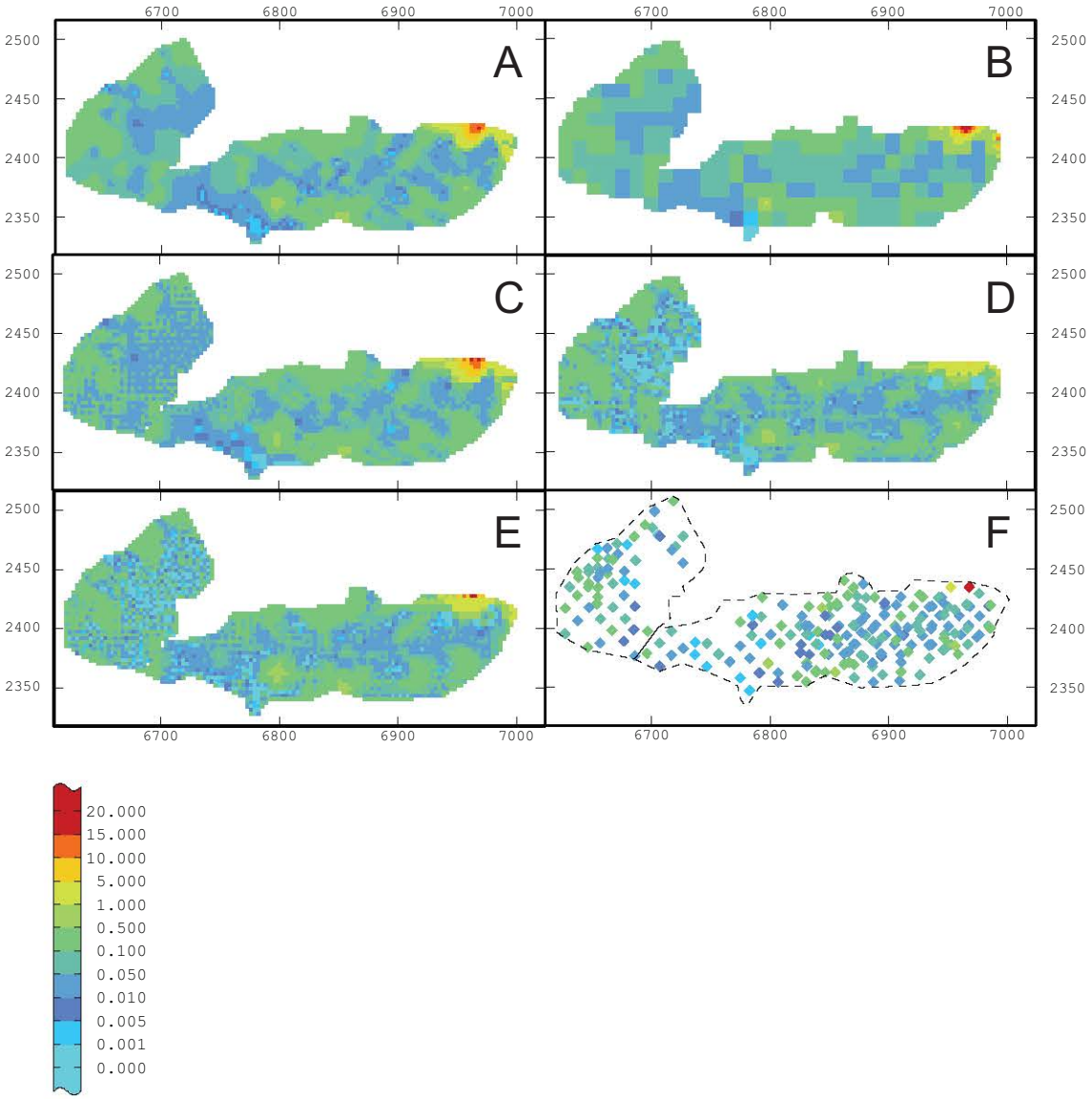

Figure 6.24: P_2O_5 results. A - Ordinary kriging, B - LUC 12 m panel, C - LUC 6 m panel, D - Decorrelated LUC 12 m panel, E - Decorrelated LUC 6 m panel, F - Input Data

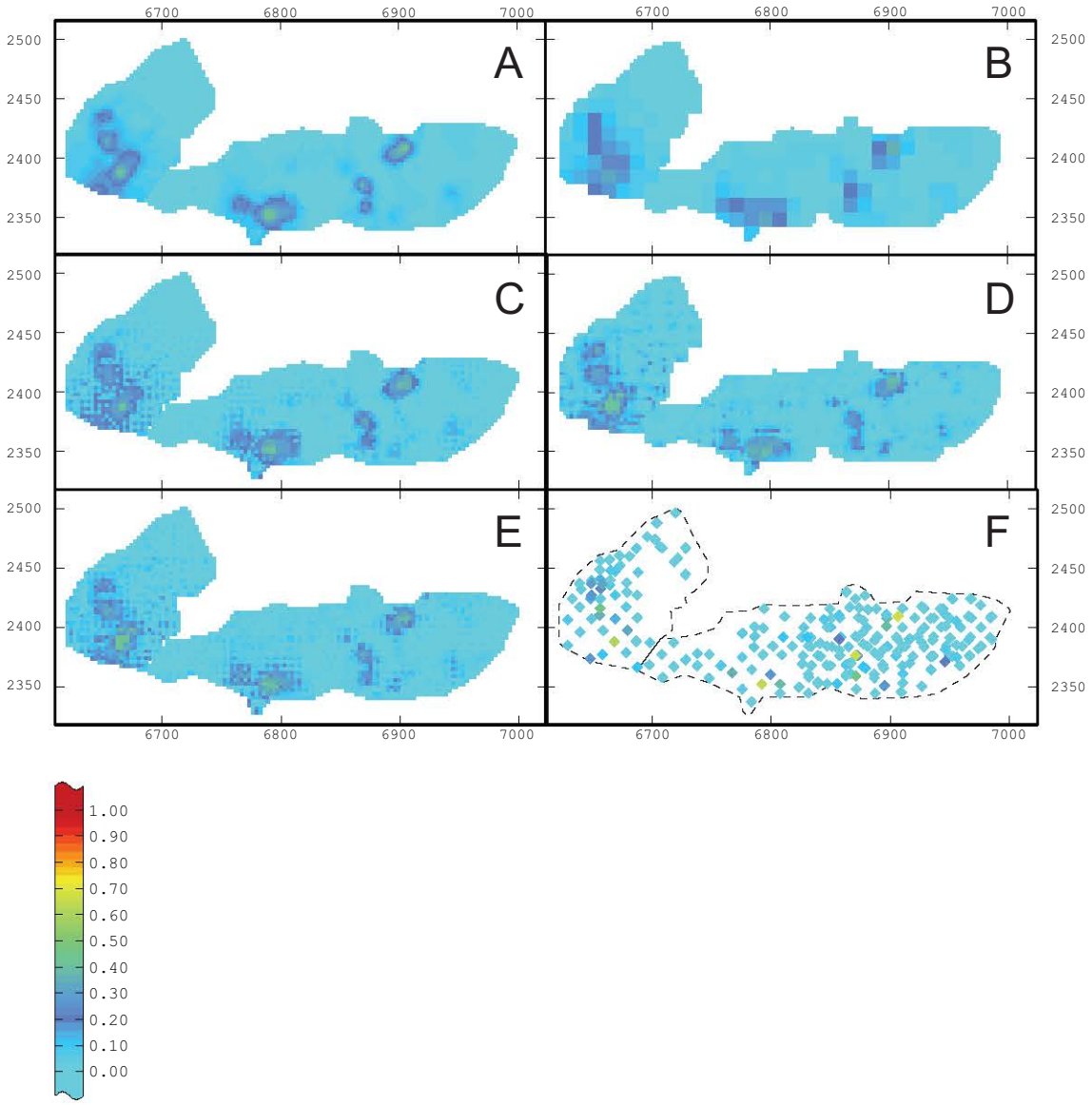

Figure 6.25: PbO results. A - Ordinary kriging, B - LUC 12 m panel, C - LUC 6 m panel, D - Decorrelated LUC 12 m panel, E - Decorrelated LUC m panel, F - Input Data

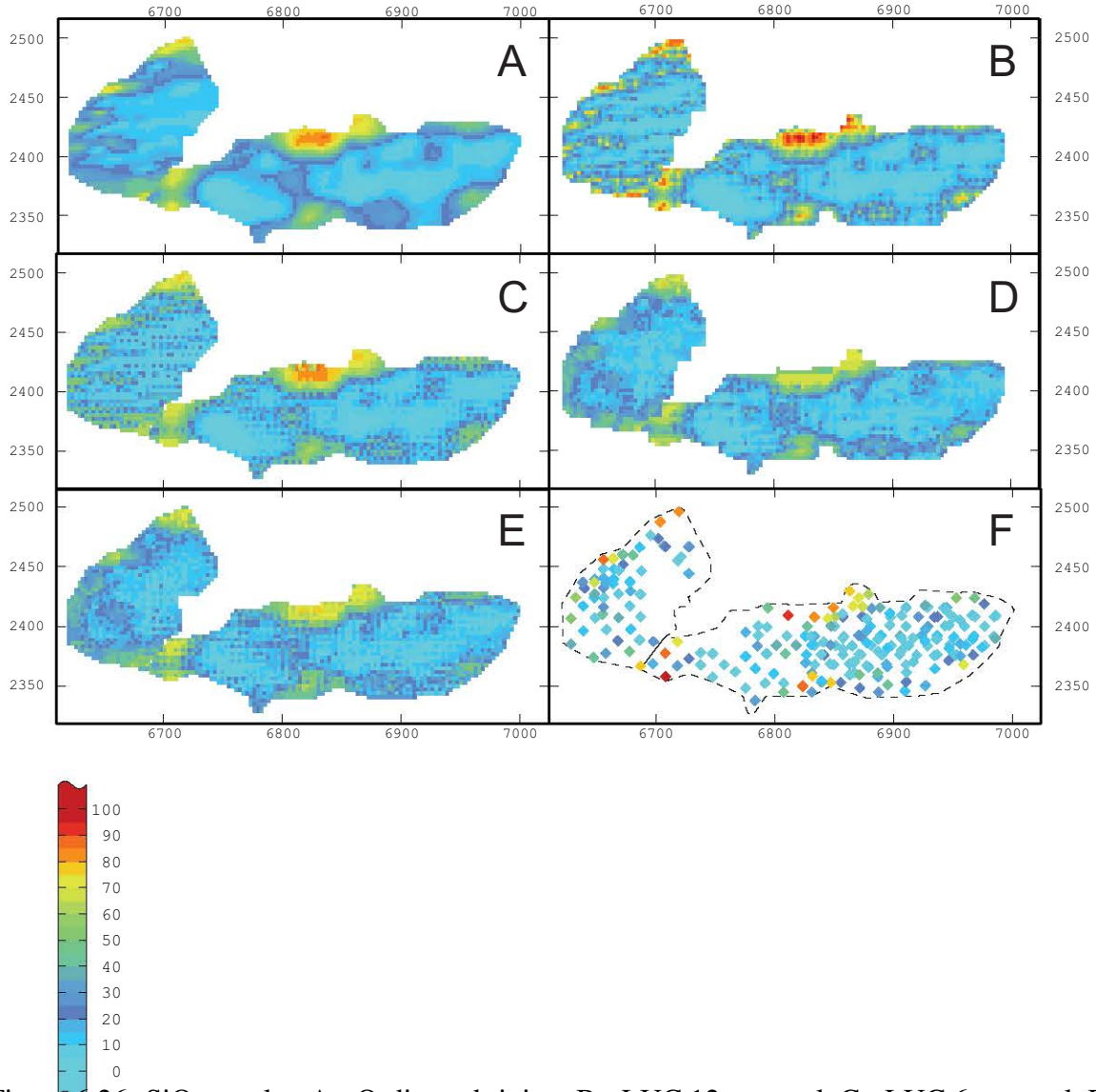

Figure 6.26: SiO_2 results. A - Ordinary kriging, B - LUC 12 m panel, C - LUC 6 m panel, D - Decorrelated LUC 12 m panel, E - Decorrelated LUC 6 m panel, F - Input Data

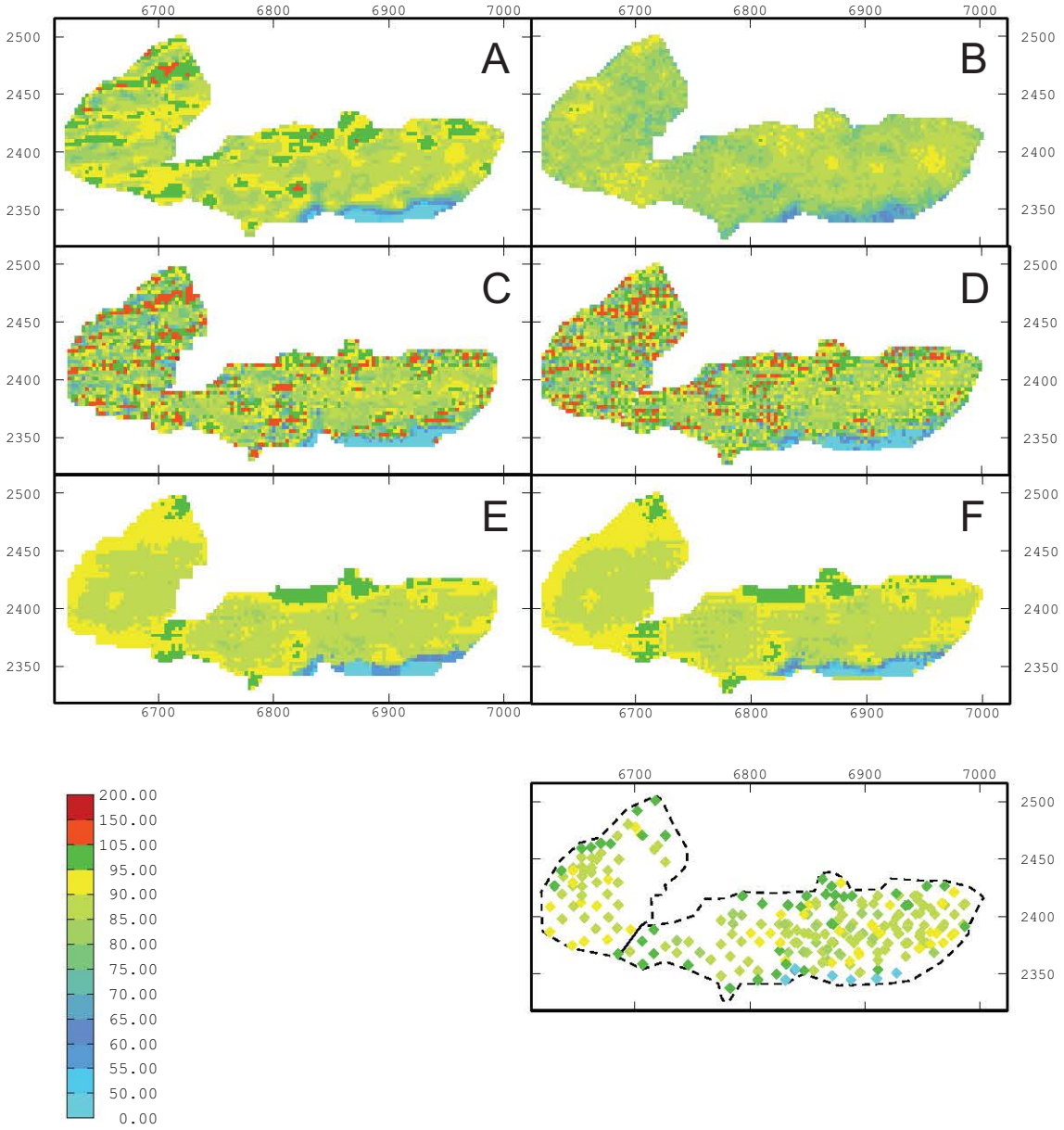

Figure 6.27: Total sums from all six oxide variables. A - Ordinary kriging, B - LUC 12 m panel, C - LUC 6 m panel, D - Decorrelated LUC 12 m panel, E - Decorrelated LUC 6 m panel, F - Input Data

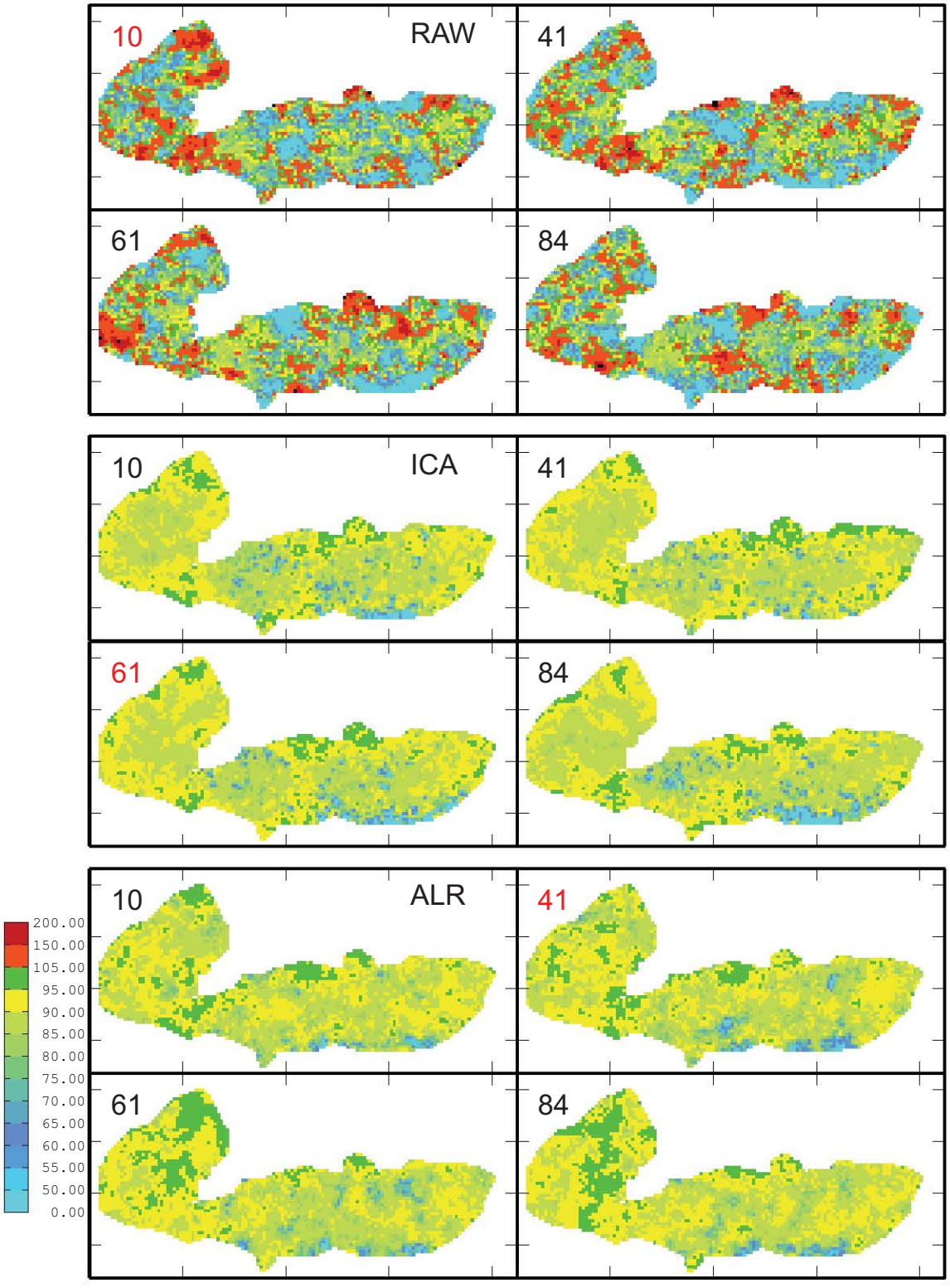

Figure 6.28: Total sums from individual simulations.

6.5 Bias Assessment

The presence of negative estimates and the observed distortion of spatial grade distributions in various simulations (such as the ALR simulations) indicates a degree of bias in the results for some methods, which is also observed in Quantile-Quantile (Q-Q) plots of the input data plotted against the results of each method. Results from the closest grid node were assigned to each input data point to yield Figures 6.29 to 6.40. A comparison of the plots shows that decorrelated results deviate far more than those results of non-decorrelated methods. Given the SMU dimensions of 3 x 3m used, this meant no inut / result data pair were separated by a distance greater than 1.5m. By using this method, the issues of clustering within the input data, and the well known issue of smoothing in kriged estimates are largely negated (due to the exact interpolator nature of kriging) allowing a better direct comparison between all methods.

Quantile-Quantile plots for individual simulations for Al_2O_3 show that results are generally biased high against the input data. ALR simulations maintain this high bias at higher percentiles, while ICA and RAW simulations then tend to become slightly low biased. Simulations of Fe_2O_3 are all generally biased low, but more so for log-ratio simulations. All Mn_3O_4 results suggest a reduction in variance, with results tending towards the mean resulting in high biased results at lower input grades (30-40%) and low biased results above these values. P_2O_5 results are typically high-biased for RAW and ICA simulations, but are low-biased for log-ratio simulations. PbO results show varying high and low bias between individual simulations however ALR simulation results are consistently low biased. SiO2 results show minimal bias, but are clearly high-biased for ALR simulations. The Q-Q plots also show the presence of negative results in the ICA simulations.

BOK and LUC results generally show minimal levels of bias (the exception being P_2O_5), and exhibit the same trends as simulation methods for each variable. The range of P_2O_5 values in BOK and LUC methods is substantially smaller, with less extreme outliers than for simulations. Similar to the ICA simulations, the ICA decorrelated LUC results show spurious negative values, particularly for Fe_2O_3, P_2O_5 and PbO. To a minor degree, BOK and all UC results for Mn_3O_4 exhibit centralisation of results, and the resulting high-bias at lower grades and low-bias at higher grades. The inflection point in all cases is 40% Mn_3O_4 in input grades. This is most extreme in the decorrelated oxide LUC, where the high bias at input grades 40% is greater than for the other methods. BOK and oxide LUC results show minimal levels of bias.

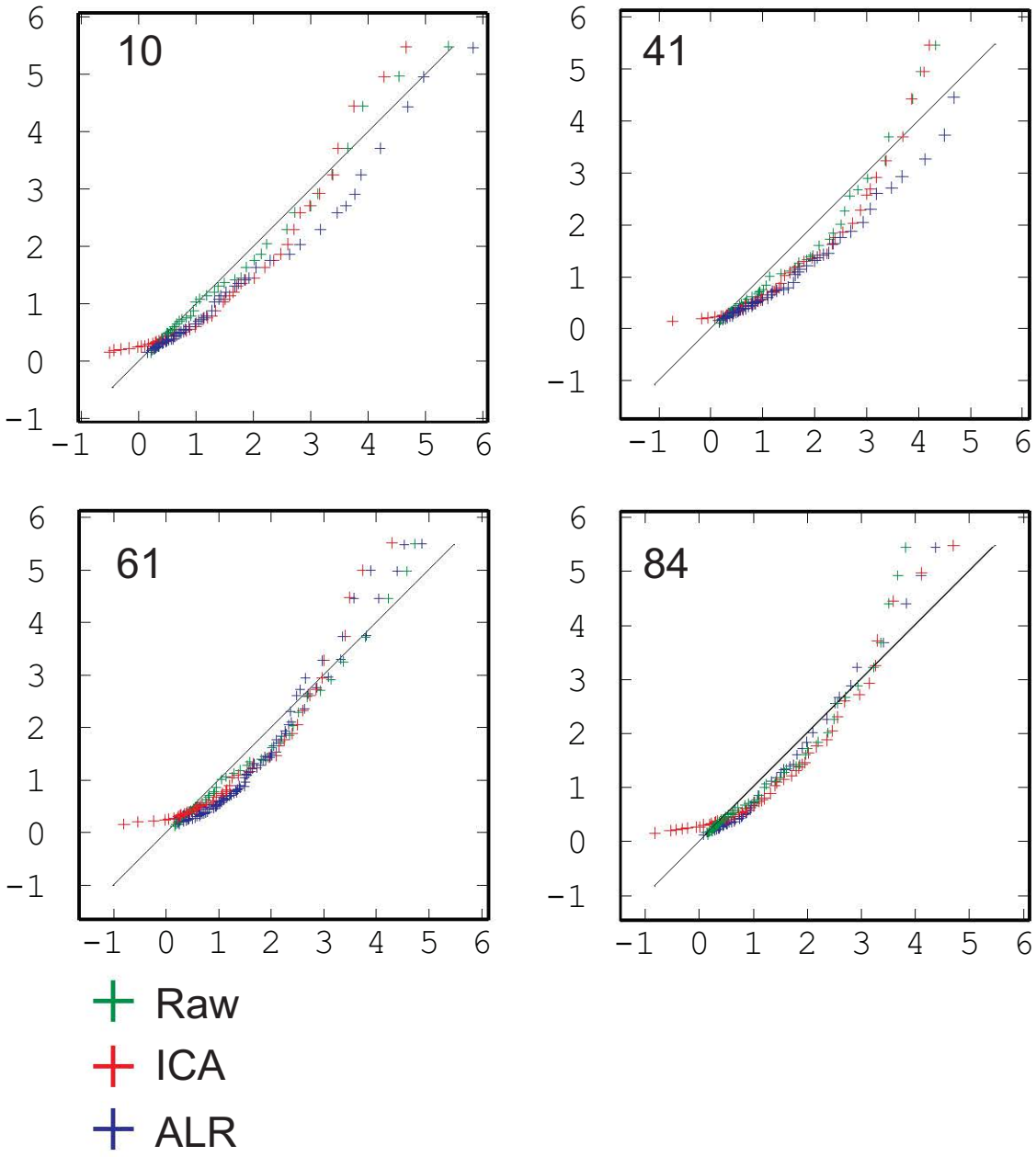

Figure 6.29: Quantile-quantile (Q-Q) plots of individual Al_2O_3 simulation results against input (RD) data

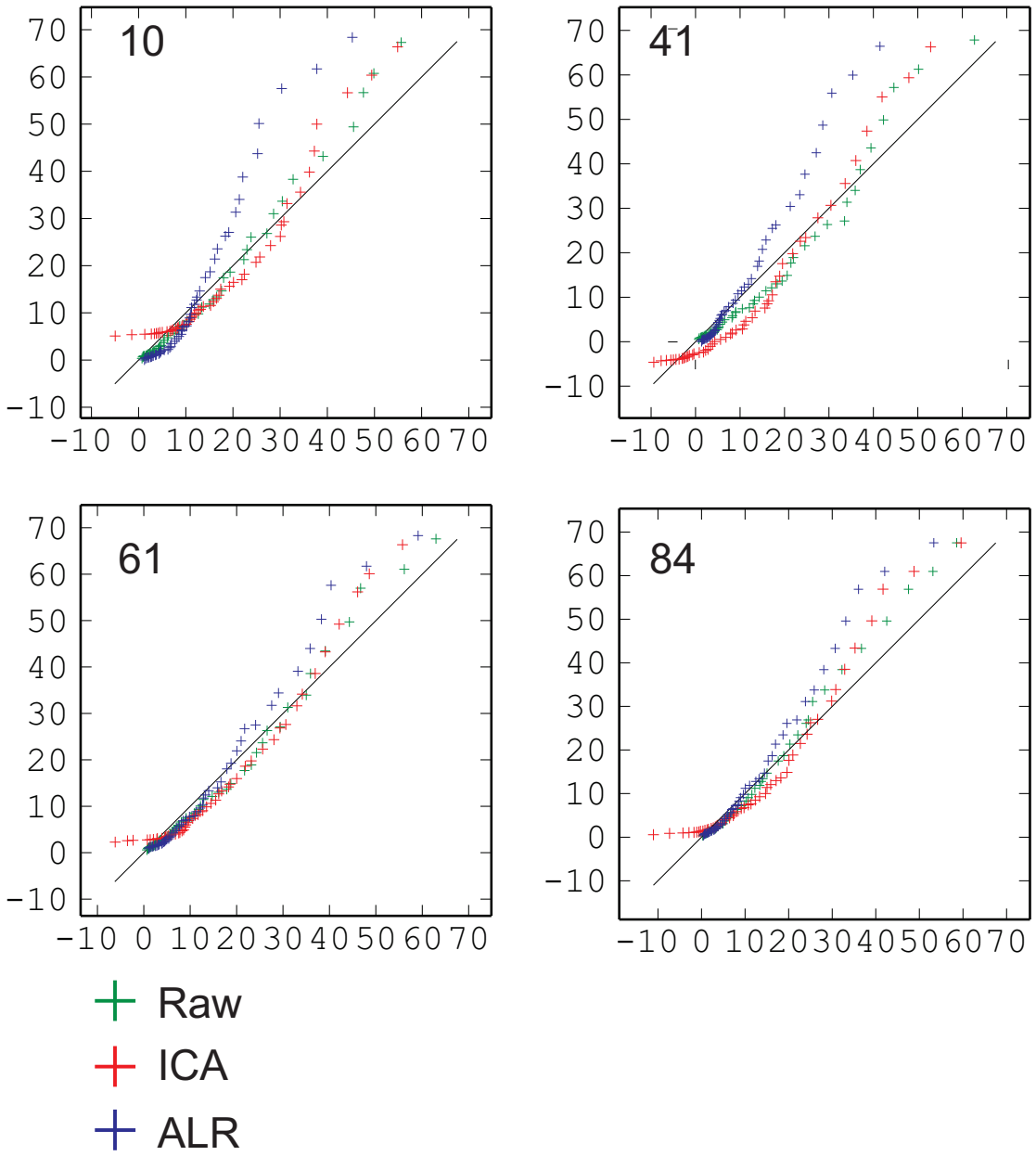

Figure 6.30: Quantile-quantile (Q-Q) plots of individual Fe_2O_3 simulation results against input (RD) data

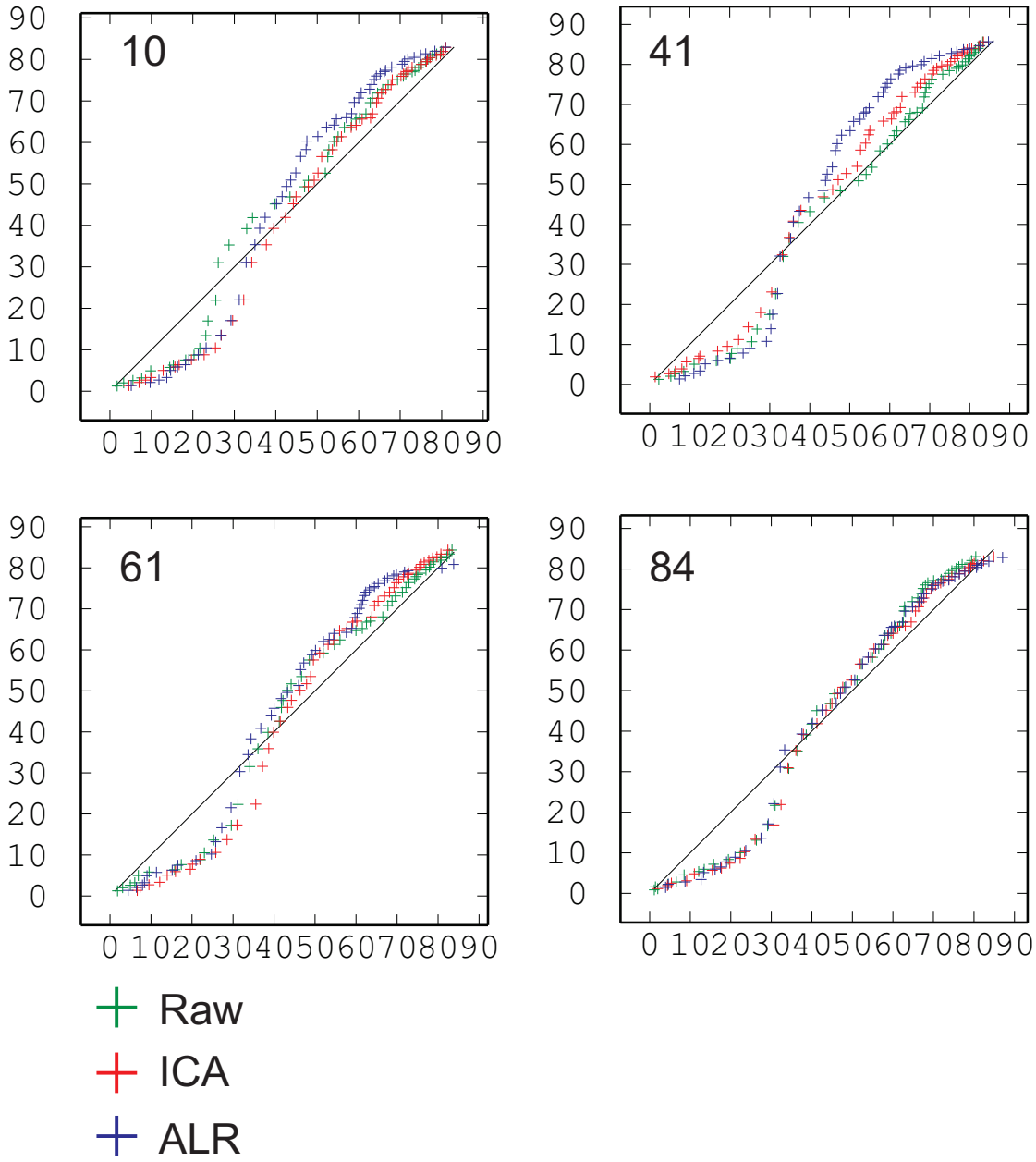

Figure 6.31: Quantile-quantile (Q-Q) plots of individual Mn_3O_4 simulation results against input (RD) data

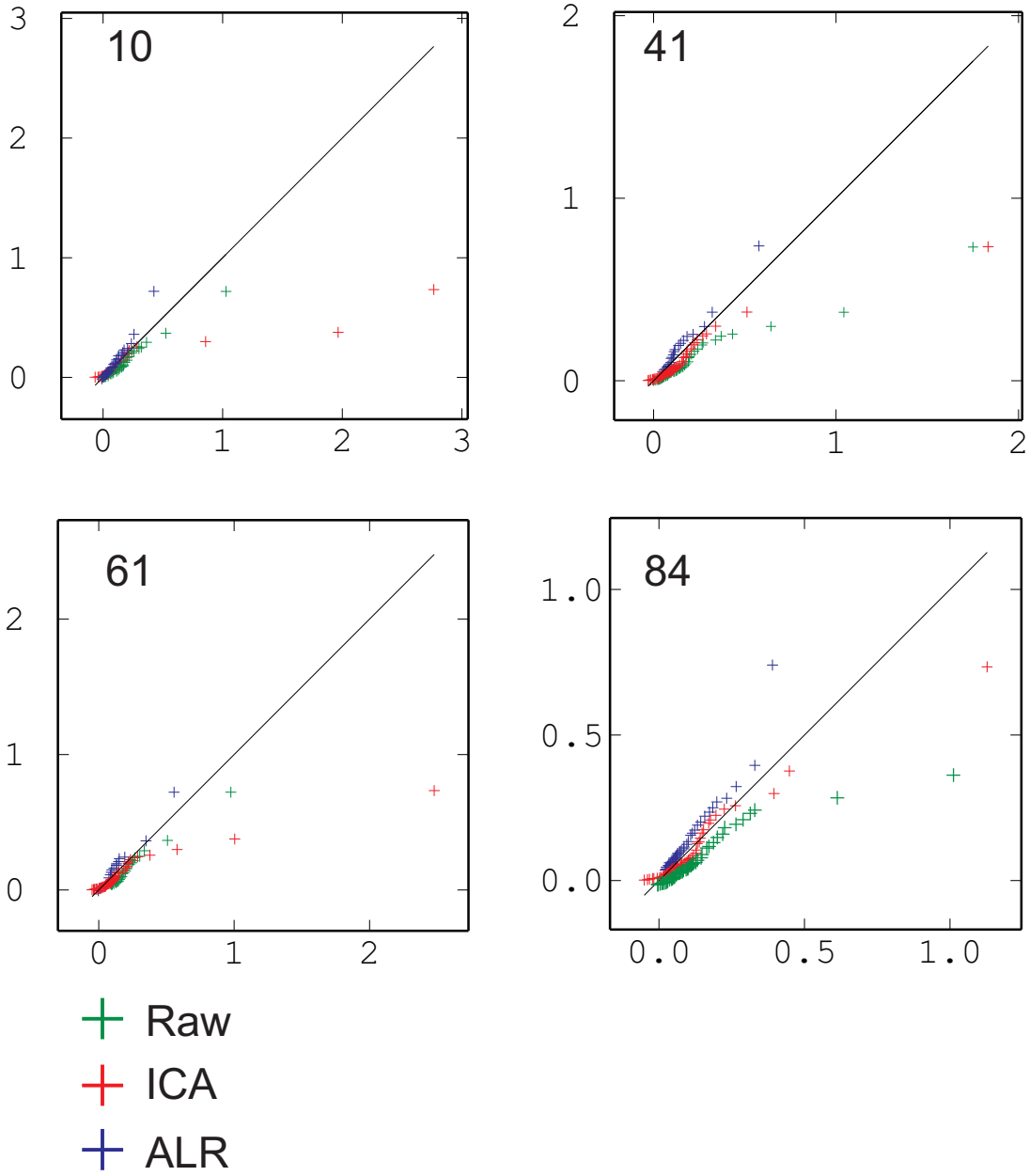

Figure 6.32: Quantile-quantile (Q-Q) plots of individual P_2O_5 simulation results against input (RD) data

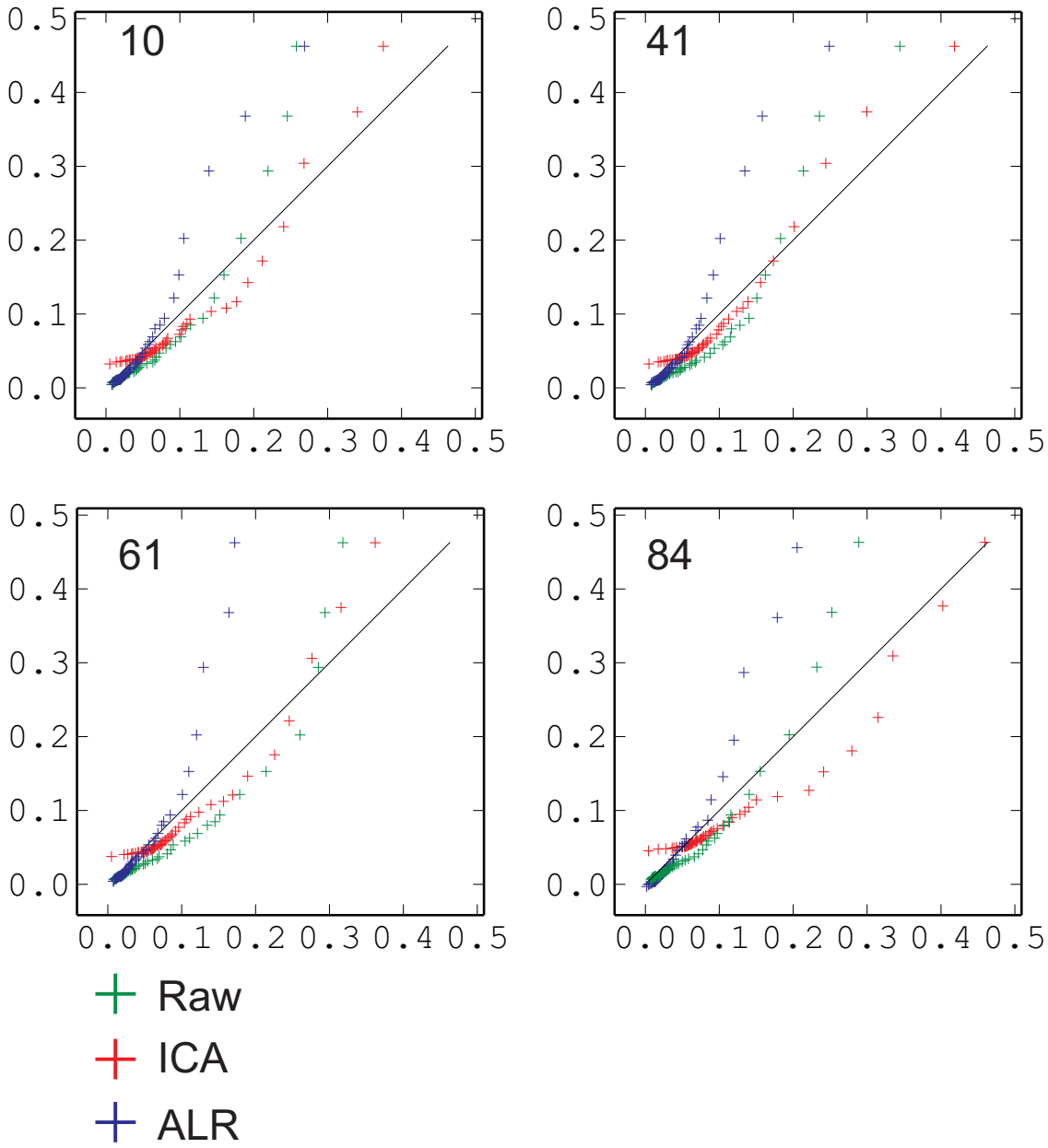

Figure 6.33: Quantile-quantile (Q-Q) plots of individual PbO simulation results against input (RD) data

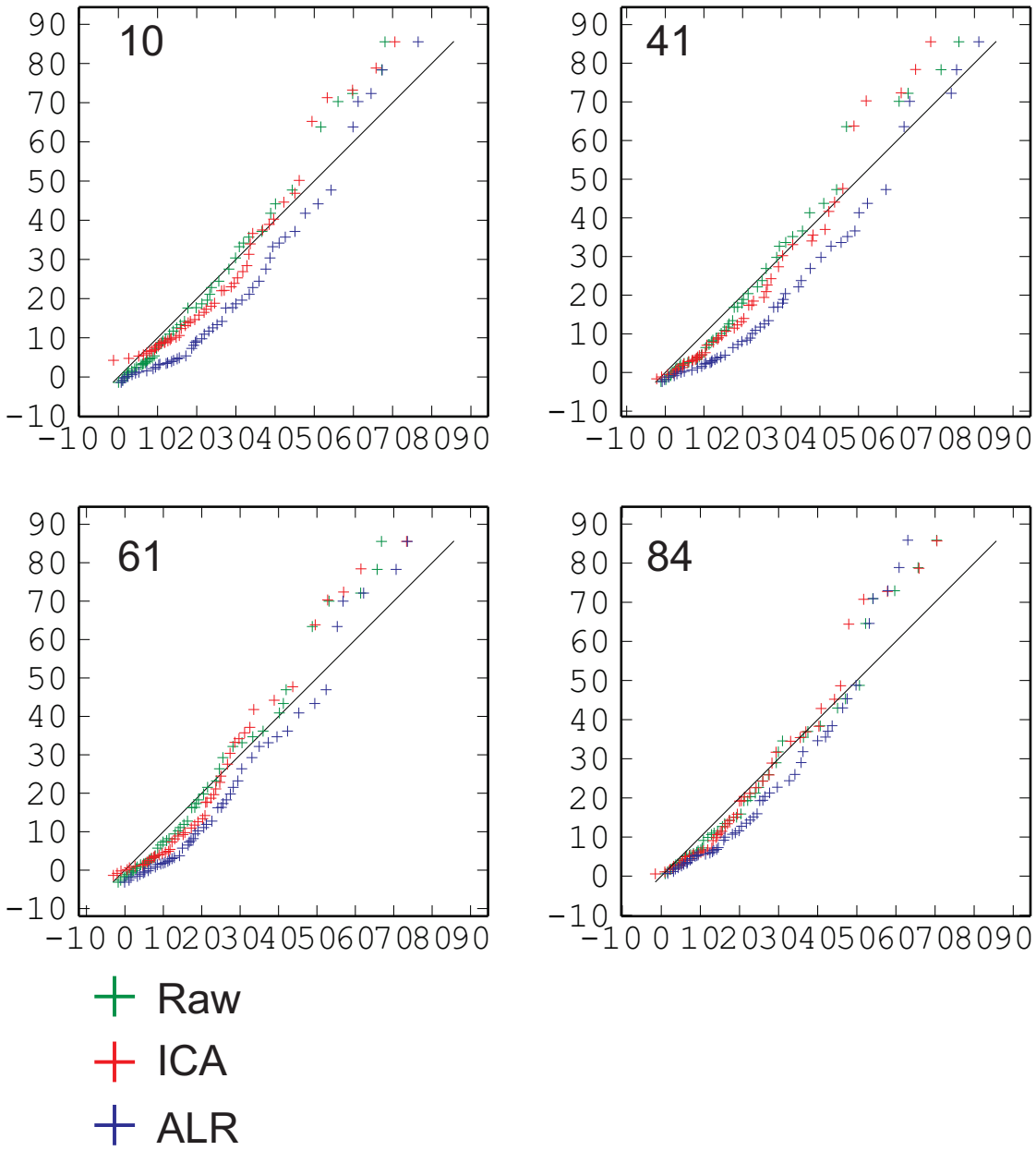

Figure 6.34: Quantile-quantile (Q-Q) plots of individual SiO_2 simulation results against input (RD) data

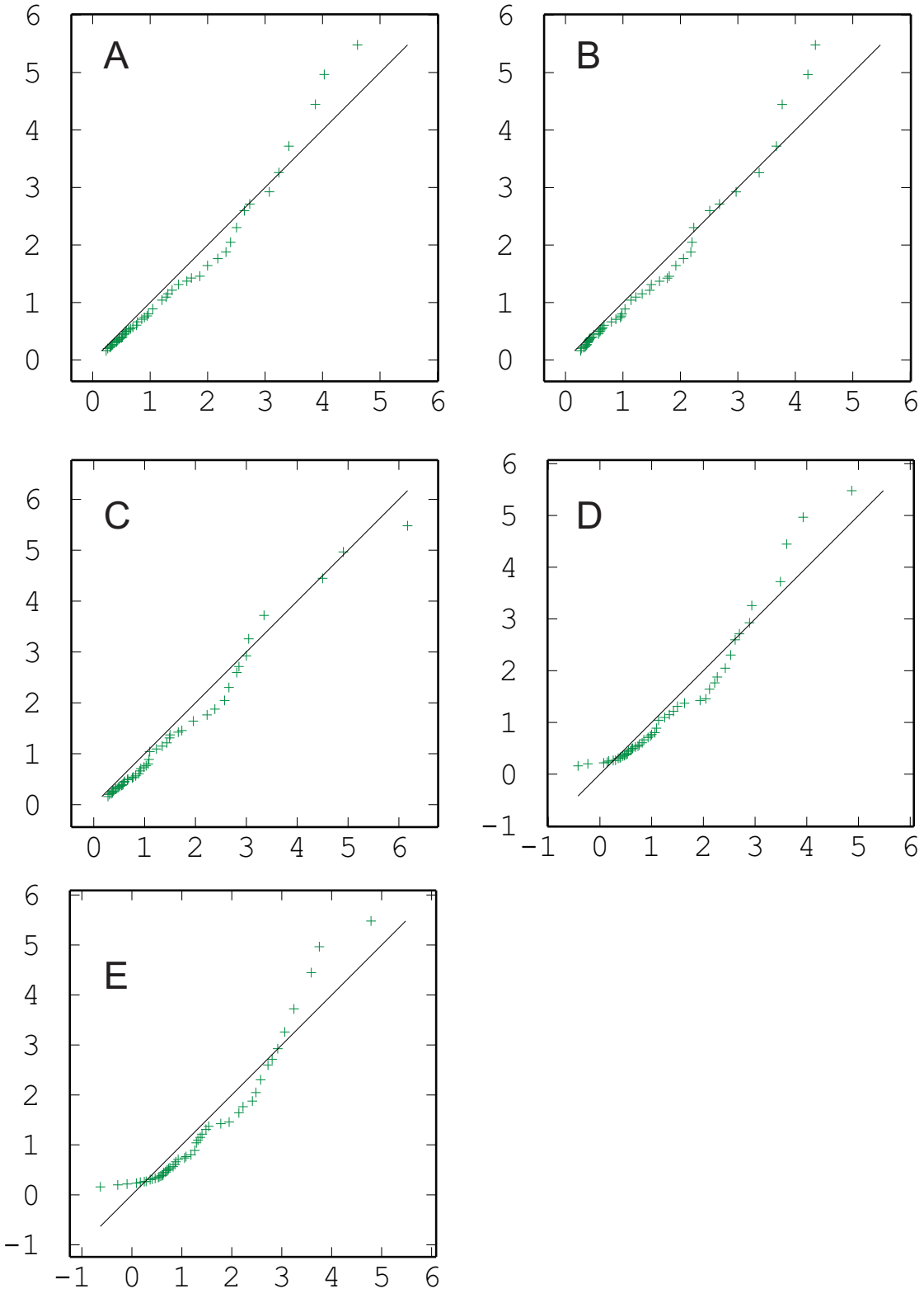

Figure 6.35: Quantile-quantile (Q-Q) plots of Al_2O_3 results against input (RD) data. A - BOK, B - LUC 6 m panel, C - LUC 12 m panel, D - LUC decorrelated oxides 6 m panel, E - LUC decorrelated oxides 12 m panel

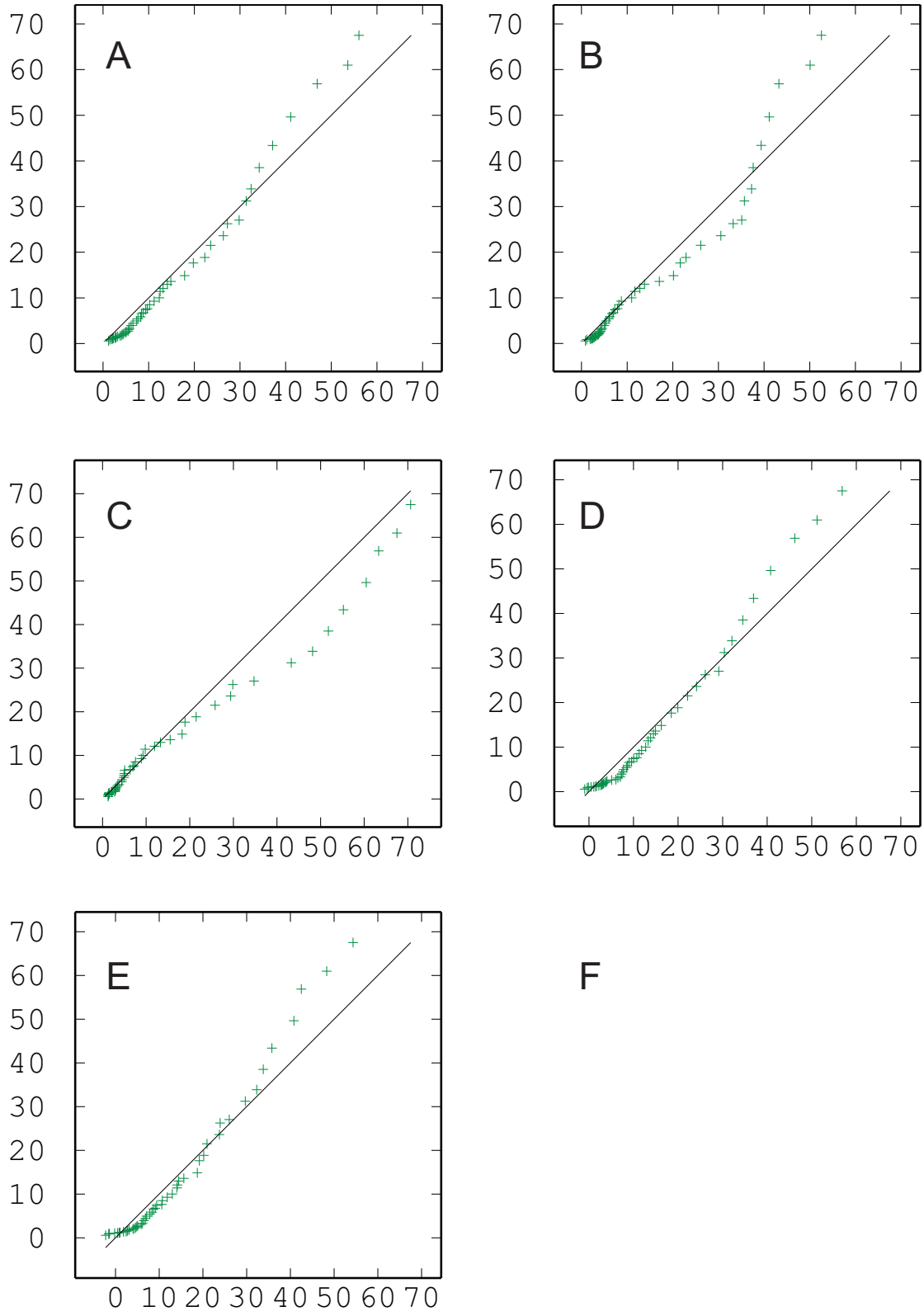

Figure 6.36: Quantile-quantile (Q-Q) plots of Fe_2O_3 results against input (RD) data.A - BOK, B - LUC 6 m panel, C - LUC 12 m panel, D - LUC decorrelated oxides 6 m panel, E - LUC decorrelated oxides 12 m panel

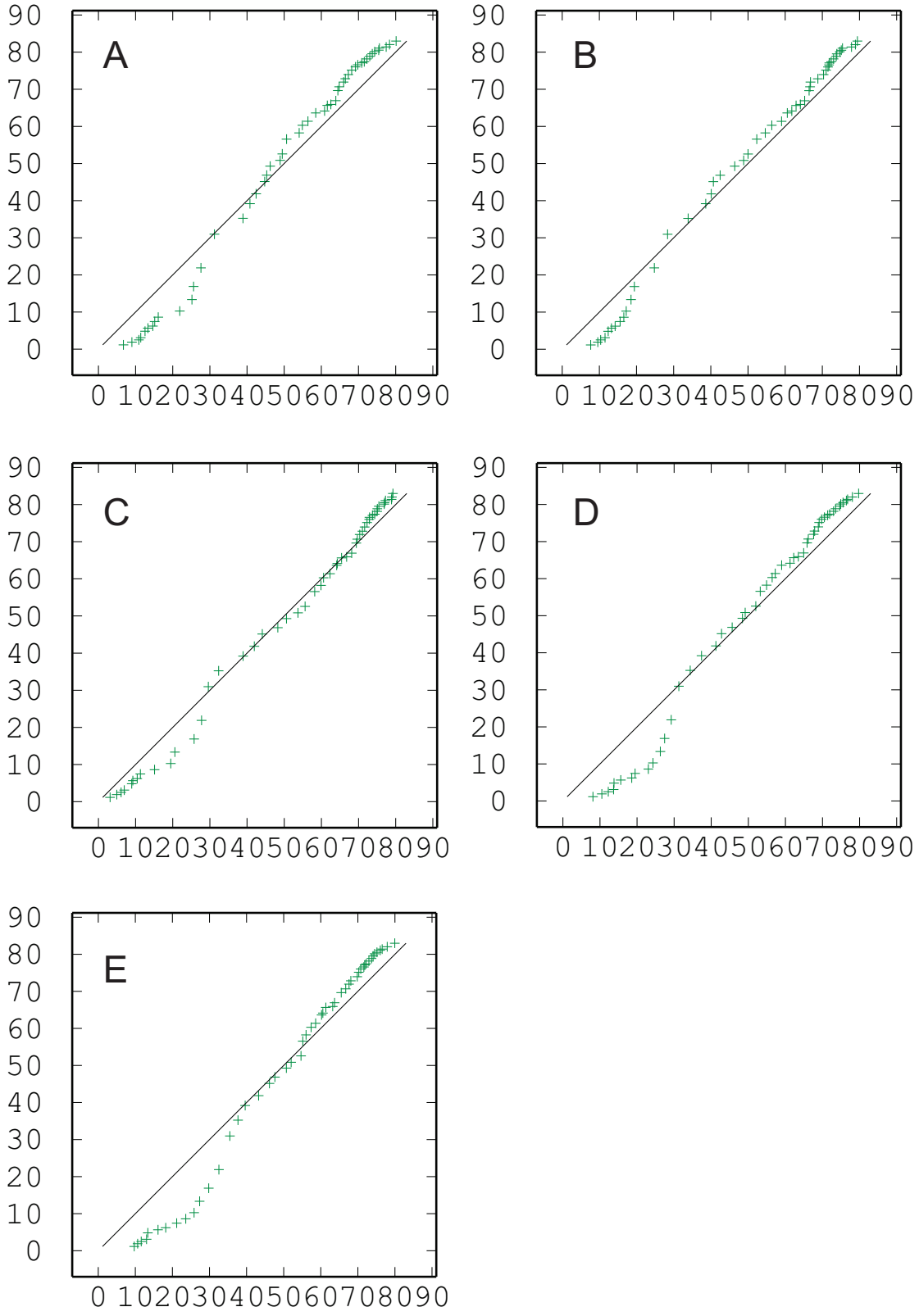

Figure 6.37: Quantile-quantile (Q-Q) plots of Mn_3O_4 results against input (RD) data. A - BOK, B - LUC 6 m panel, C - LUC 12 m panel, D - LUC decorrelated oxides 6 m panel, E - LUC decorrelated oxides 12 m panel

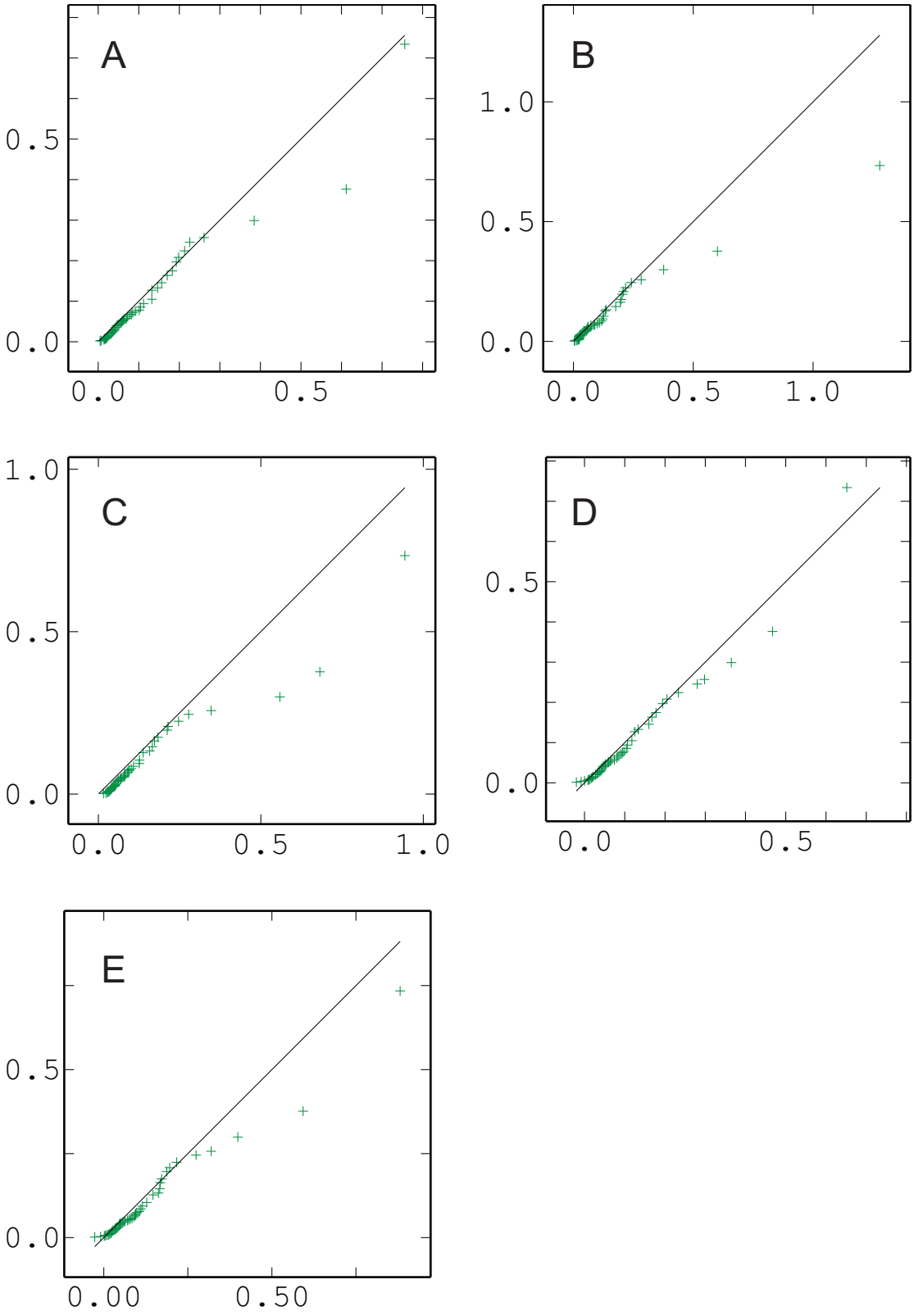

Figure 6.38: Quantile-quantile (Q-Q) plots of P_2O_5 results against input (RD) data. A - BOK, B - LUC 6 m panel, C - LUC 12 m panel, D - LUC decorrelated oxides 6 m panel, E - LUC decorrelated oxides 12 m panel

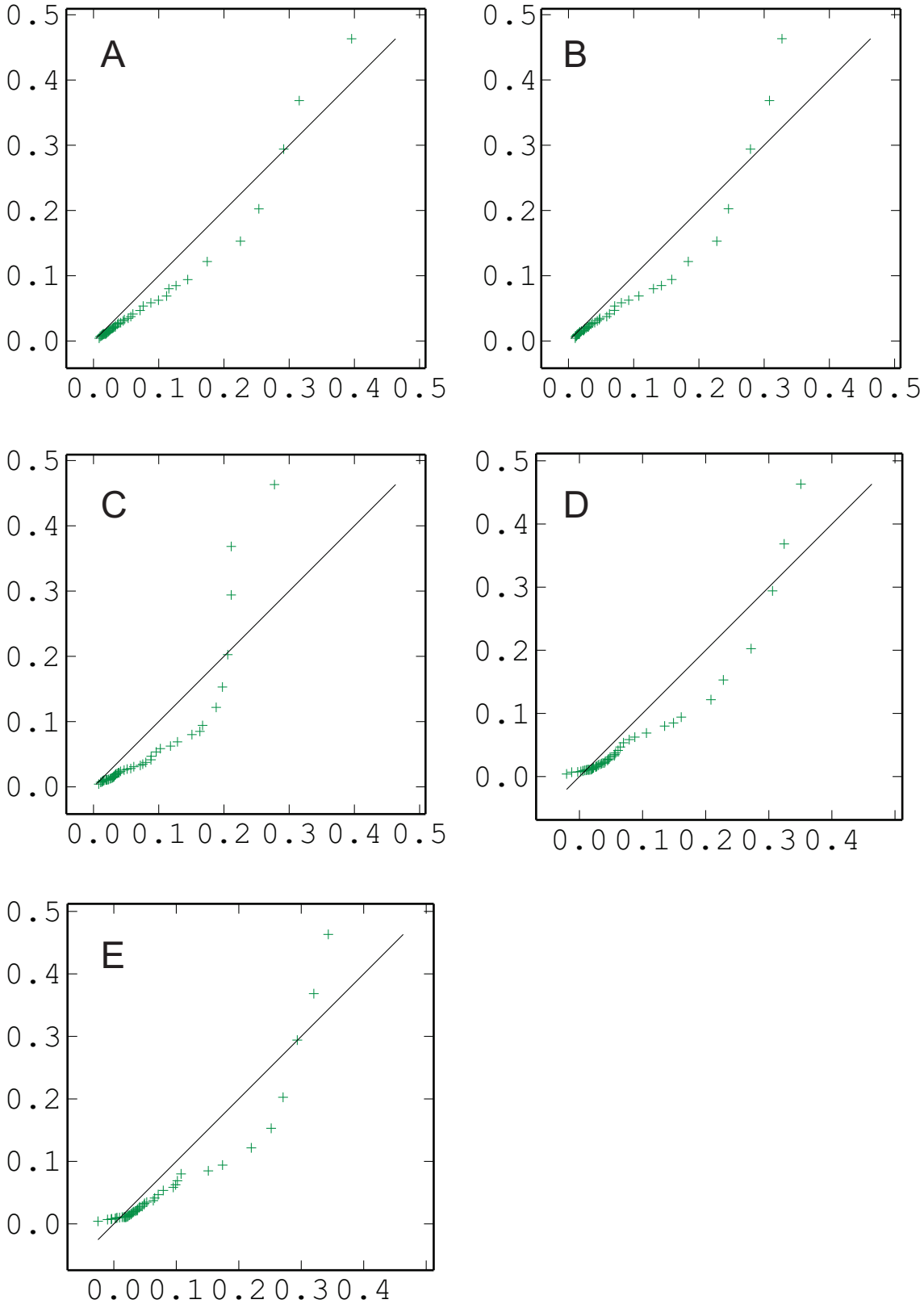

Figure 6.39: Quantile-quantile (Q-Q) plots of PbO results against input (RD) data. A - BOK, B - LUC 6 m panel, C - LUC 12 m panel, D - LUC decorrelated oxides 6 m panel, E - LUC decorrelated oxides 12 m panel

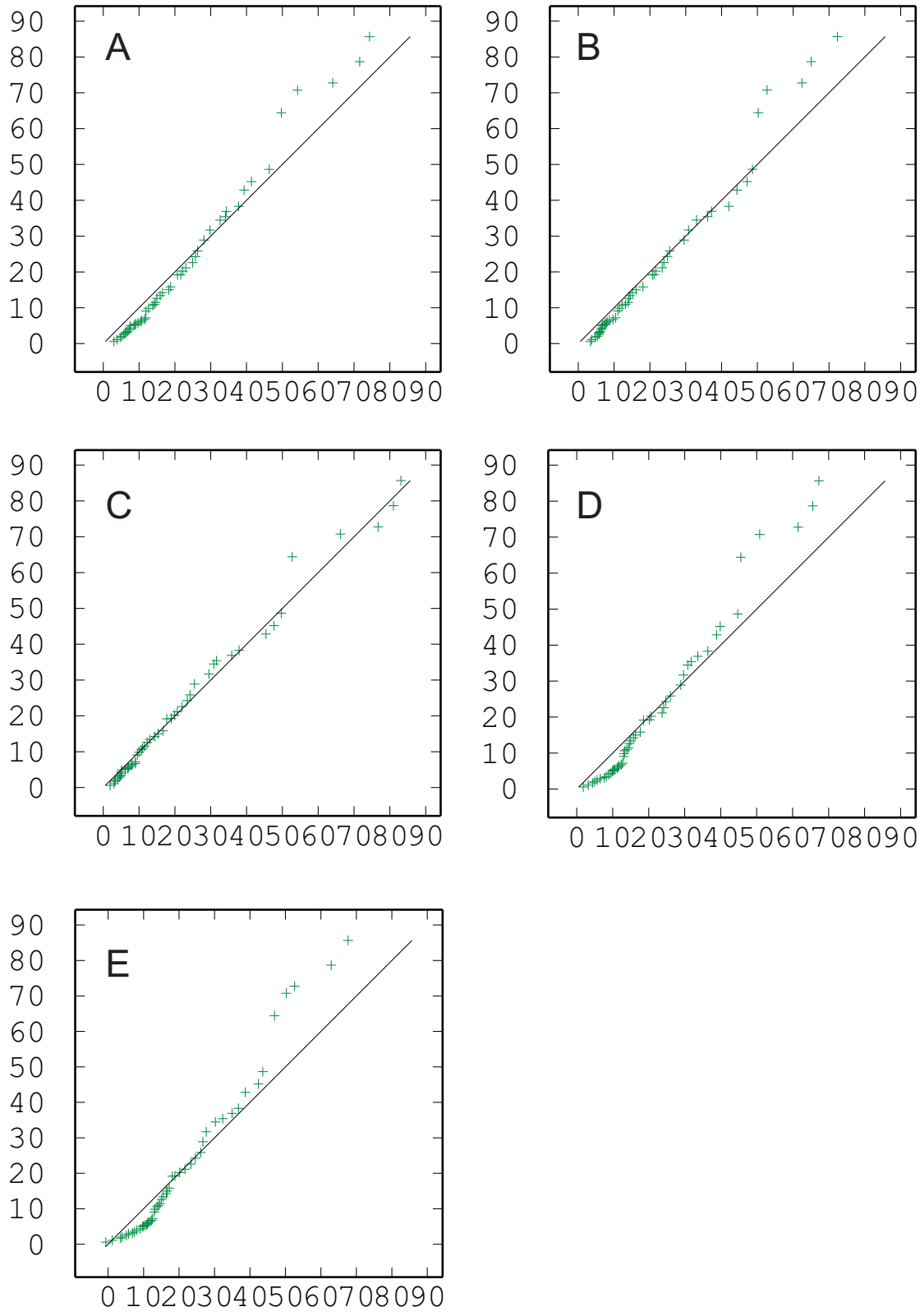

Figure 6.40: Quantile-quantile (Q-Q) plots of SiO_2 results against input (RD) data. A - BOK, B - LUC 6 m panel, C - LUC 12 m panel, D - LUC decorrelated oxides 6 m panel, E - LUC decorrelated oxides 12 m panel

6.6 Conventional Profit Results

A net profit value was determined at each block within the study area, for each method of recoverable resources calculation that had been applied. In the case of simulations, net profits were determined on each individual simulation, and then ranked from lowest to highest. Where negative values existed for any given variable, net profit for that particular grid node was set to zero. As a benchmark, and representing the results that would be used during final selection, net profits were also determined for BOK using the complete input dataset. Net profit results are presented in Tables 6.11 and 6.12 and Figures 6.41 to 6.43. Figure 6.42 presents the net profit results from the selection of simulations that have been presented in results previous. Those simulations highlighted in red are the simulations which yield the median profit result for that particular method.

It is immediately apparent that ALR simulation results are overly optimistic in Domain 1 when compared to all other methods (Figure 6.41). The most conservative of all simulations yields net profit that is well in excess of the next two most profitable methods - BOK (with RD dataset), and the ICA simulations. Domain 2 however, presents a profit from ALR simulations far more conservative than all *but* the ICA simulations. Nonetheless in total, ALR simulations yield far more optimistic overall net profit results that any other method. The results of the deleterious elements (other than SiO_2) in ALR simulation are all predominantly low biased, sometimes in contradiction to the results of other methods. The slightly higher SiO_2 results enhance both unpenalised profit and yield, and combined with the low biases in other deleterious variables, all contribute to the overly optimistic net profit of ALR simulations. Similar to the ALR simulations, the ICA simulations are overly optimistic compared to most other methods in Domain 1, and similarly overly conservative in Domain 2. Also similar, is the generally overly optimistic total net profit. LUC methods, the reduced dataset BOK, and the complete dataset BOK, all show much more similar estimates.

Unlike ALR and ICA simulation profits, which range mostly from above all other methods, to significantly above all other methods and with a very wide range, the simulation of non transformed oxide data yields results more aligned with those of ordinary kriging and LUC, and with a much more reduced range of values Figure 6.41. Raw simulation results are also generally more conservative than either LUC or BOK in both domains, with equivalent profits only seen in the simulation range of results between the 70^{th} and 85^{th} percentiles.

Spatially, the differences in net profit Figures 6.42 and 6.43 observed in ALR and ICA simulations compared to other methods are seen in a wider distribution and greater prevalence of very high profit individual blocks in the eastern portion of Domain 1, and a paucity of high net profit values overall in Domain 2. For the other methods tested, the results all tend to show similar distributions of net profit, with a central east west 'core' of high value material on Domain 1, and a central high value region along the eastern edge of Domain 2, surrounded by very low value material.

Lastly, given the similarities in spatial distribution of net profit in oxide simulations and BOK / LUC methods (Figure 6.41), it is interesting to note the suggestion of downside risk presented in the results. Such is the nature of simulation methods, that given enough simulations (an arbitrary determination but 100 should suffice), the mean value of a simulation set should approximate the ordinary kriged estimate for the same given area. It follows that the mean net profit determined from such a suite of simulations should then also approximate the net profit estimate from ordinary kriging, but in this case it does not (Tables 6.11 and 6.12). All other things being equal (variography, search ellipse) and taken at face value, the results from raw oxide simulation may suggest that current methods of recoverable resources calculation may be optimistic. However, the serious violation of the sum constraint for this simulations set makes such an observation generally unreliable.

Table 6.11: Summary of total net profit from Ordinary kriging and Localised Uniform Conditioning method.

	Domain 1	Domain 2	Combined
Ordinary kriging	$37,723,602	$17,534,313	$55,257,914
LUC			
12 m	$36,540,751	$15,651,458	$52,192,209
6 m	$36,043,238	$15,437,674	$51,480,911
Decorrelated LUC			
12 m	$28,848,639	$10,738,474	$39,587,133
6 m	$29,498,818	$10,429,388	$39,928,207
OK All Data	$36,139,717	$18,788,658	$54,928375

Table 6.12: Summary of total net profit from Various Methods of Simulation.

	Domain 1	Domain 2	Combined
Oxide Simulation			
Mean	$35,575,121	$13,955,946	$49,531,066
Median	$35,496114	$13,815,461	$49,624,838
Variance	1,370,980	1,164,494	1,977,079
ICA Simulations			
Mean	$42,397,027	$10,800,426	$53,197,452
Median	$42,473,720	$11,199,964	$53,234,735
Variance	2,430,933	4,069,554	3,842,228
ALR Simulations			
Mean	$52,611,570	$13,354,110	$65,965,681
Median	$52,438,678	$13,779,903	$65,802,216
Variance	3,192,024	5,168,175	4,947,623

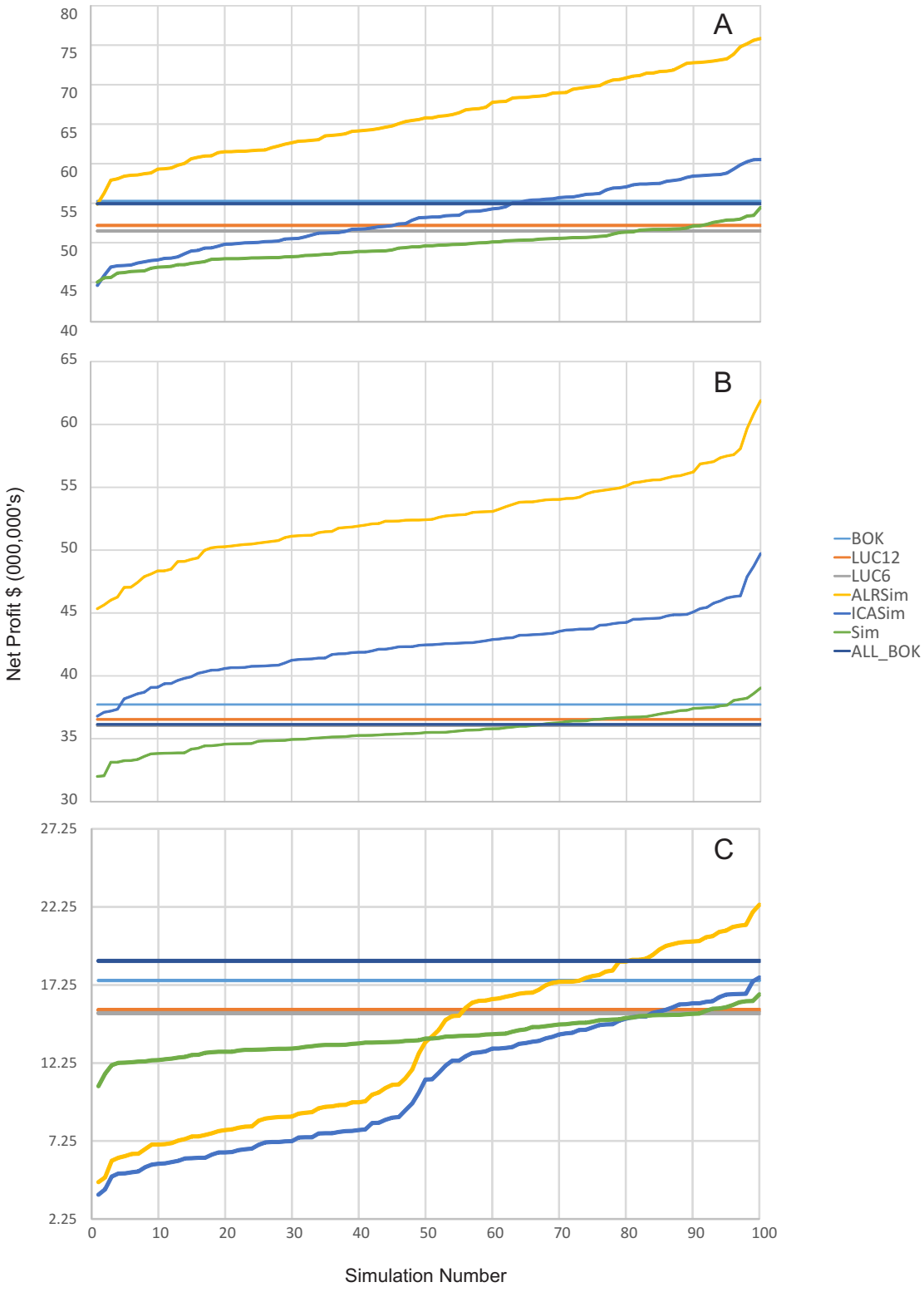

Figure 6.41: Net profit distributions, plotted for individual simulations. A: Combined Domains, B: Domain 1, C: Domain 2

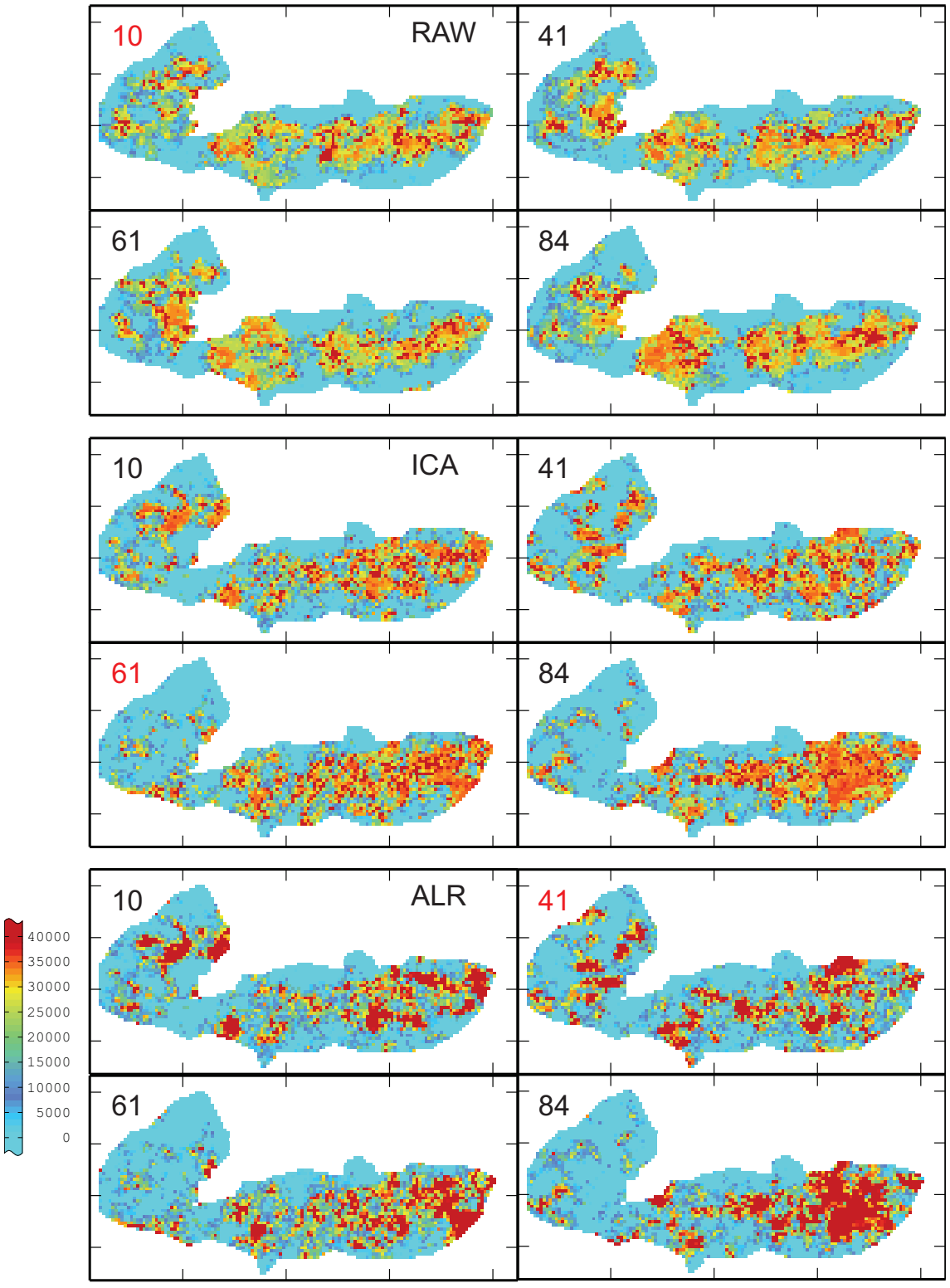

Figure 6.42: Net profit results for individual simulations. RAW - oxide simulations, ICA - Decorrelated factors of oxides simulation, ALR - Decorrelated log-ratio simulation results

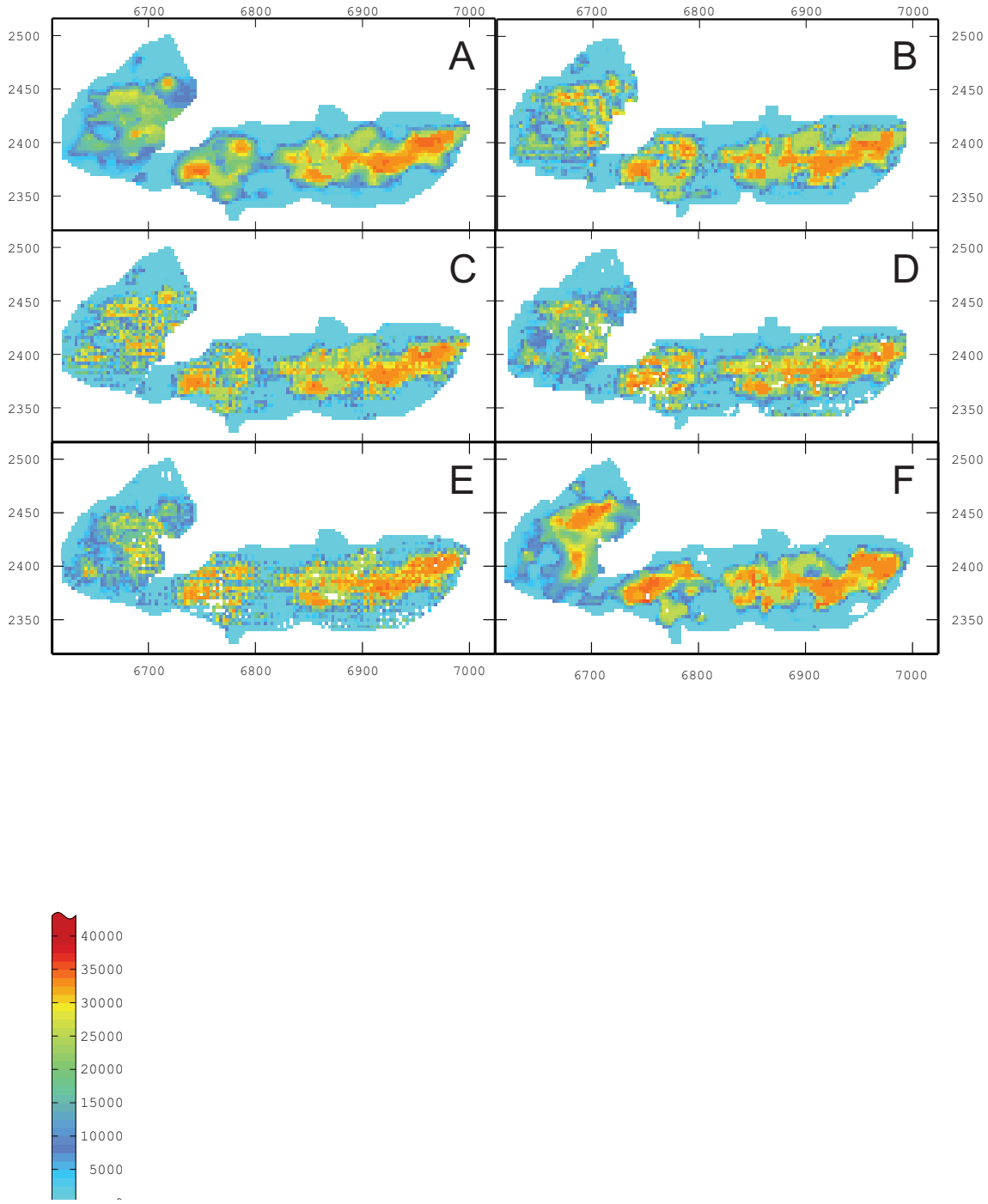

Figure 6.43: Net profit results. A - BOK, B - LUC 12 m panel, C - LUC 6 m panel, D - Decorrelated oxide LUC 12 m panel, E - Decorrelated oxide LUC 6 m panel. F - Full dataset BOK (reference estimate).

Chapter 7

Discussion

7.1 General Comment

The work presented in this study centres around two foci, with the first aiming to test the viability of using Independent Components Analysis as a means of decorrelating a multivariate dataset from a Western Australian Manganese mine. ICA was measured for decorrelation performance against the method of Minimum Maximum Autocorrelation Factorisation, which is a more widely established method for decorrelation of multivariate geostatistical datasets. The second part of this thesis compares three methods of recoverable resources calculation; Block Ordinary kriging, Localised Uniform Conditioning and Conditional Simulation. The second part of this thesis includes usage of the decorrelated data from part 1, and evaluates the benefit in decorrelation of the Manganese dataset prior to estimation / simulation. Of note is that the second part of this thesis is heavily influenced by the practicalities of implementation of each technique, in the context of the current limitations of both procedure and software availability at the operation from which the data were sampled. Comparative performance of each method in question was evaluated in this context, with not only the statistical performance of each method assessed, but also the ability to yield usable results in the framework of the current operations' procedures.

The results of Chapter 5 indicate that ICA as a means of decorrelation is potentially viable, produces generally equivalent results to that of MAF, and is not subject to the assumptions that are requisite with the use of MAF. However the choice to decorrelate, in terms of improvement to multivariate recoverable resources calculation, at least in the context of the data presented in this study, may be considered equivocal due to specific issues which arise during

estimation / simulation of the decorrelated data. It is evident from the results presented, that the use of ICA as a means of decorrelation may introduce a distortion to the final results when back-transformed. While such an observation is only preliminary it does highlight that the method, while free form the limitations and assumptions of MAF, is not free entirely of limitations in its use.

The treatment of the data of this study in a compositional sense also introduces a number of difficulties when attempting to use non-linear methods of change of support based on the discrete Gaussian Model (LUC), and also when compositional data are decorrelated for simulation. A further bias appears to be introduced into the results of decorrelated, log-ratio transformed data, which has the result of significantly distorting profitability calculations based on the simulated results.

7.2 Issues with ICA for Decorrelation

When dealing with the transformation to independent components, the resulting factors are maximally non-normal. Non-linear techniques such as simulation and LUC typically require the use of an anamorphosis function (commonly the Hermite expansion) to either transform the data into Gaussian distributions (for simulation), or for the purposes of volume variance corrections (change of support). In the case of simulation, given that the ICA factors are permissibly negative and that the authorised boundaries of an anamorphosis function must be adjusted to account for values lesser or greater than those of the input data, the selection of a lower authorised limit for anamorphosis is not a simple task as it would be with real-world data (with a hard lower boundary of zero). As this study demonstrates, realistically impossible negative percentages can occur in the final back transformed results. Problems with the change of support associated with UC can also arise in situations where the Ordinary kriged estimate for a given panel of the model will yield a negative value that appears to be valid. When a change of support factor is applied to the point anamorphosis function of the input data, which must then be conditioned to the panel estimate, the resulting grade tonnage curve may yield results outside the permitted bounds of the anamorphosis. Unlike a uniformly conditioned estimate of real grade data, which is limited realistically to a lower bound of zero for most attributes of interest, such errors within the UC estimate of decorrelated data are difficult to correct other than by onerous trial and error.

7.3 Issues with the use of log-ratio data

The use of log-ratio transformation is recognised to be the only means by which the sum-constraint of a compositional dataset might be preserved. In the case of the dataset used in this study, this would seem a logical choice, given that the sum of the six variables in question vary widely, and in some instances approach a complete 100% representation of the sample composition at a given point. However, the use of log-ratio data in non-linear application poses some difficulties. Job [30] notes that the use of log transformed data in geostatistical estimation (such as ordinary kriging) results in the introduction of bias into the results, as the linear averaging of the kriging algorithm would converge toward a geometric mean, rather than the true mean of the data and this bias may in some cases be severe. Ward, and Ward and Mueller [65, 66] present Gauss-Hermite quadrature as a means of minimising this bias, but the method requires substantial post-processing, and may not be practical for the operation under consideration. Further, the use of log-ratio data within non-linear application such as (Localised) Uniform Conditioning is not easily achieved. The variance correction applied to results of uniform conditioning is achieved via adjustment of the coefficients of an anamorphosis function (commonly the Hermite series expansion). Taking logarithmic data through such an adjustment would again introduce distortions to the results which are not easily accounted for (Mueller, Pers.comm.).

Within the limitations of the current mining operation, use of log-ratio data is generally restricted to simulation, since variance correction for change of support does not rely on algorithmic factor adjustment, and is instead a simple averaging of results. Complete back transformation can take place on quasi-point support prior to variance correction, and should substantially reduce the amount of bias carried over into the final results. Nonetheless, the requirement in the current instance to also decorrelate in order to make simulation practical shows that the use of log-ratio transformation also, can still introduce significant bias into the results. This bias is also often in direct contrast to the bias which is observed in other methods trialled.

7.4 Significant Findings

On the basis of net profit, the median case for simulation of decorrelated log-ratios appears to yield the highest estimate. This however comes at the significant cost of reproduction

of the spatial and non-spatial distribution of the input data, with results not being generally representative of the input distributions of the underlying variables. In comparison to all other methods, the total range of net profits derived from this suite of simulations also appears far more optimistic than the next most profitable method (BOK). Simulation of decorrelated factors of oxides shows similarly optimistic median values, spatially similar distortions of the results, and also yields spuriously negative percentages for some variables. The spatial distributions (including net profit) of results from oxide simulation are more in keeping with other methods trialled, though violation of the sum constraint is severe, and the median case appears to be more conservative in its range of profits than for BOK / LUC.

Localised uniform conditioning of decorrelated oxide data causes significant problems with spuriously negative variable estimates, and this is borne out in clearly overly conservative net-profit results. Of the non-linear methods trialled, LUC of non decorrelated oxide data appears to best provide both reproduction of the input data histogram distributions and spatial distributions, yet it remains block ordinary kriging using the reduced data at the decision-to-mine stage that shows the closest net profit results to those derived from the final selection estimate using a complete dataset.

In light of this, given the difficulties presented by operating limitations, and the issues identified in use of advanced method such as decorrelation via ICA and use of log-ratio data, it is difficult to justify the additional effort and complexity of implementing such methods at an operation similar to that under study.

7.5 Future Study and Concluding Remarks

The results of this study raise a number of questions that would warrant further study. The use of a log-ratio transform guarantees the back transformed results honour the sum constraints in a compositional dataset, something that none of the other methods trialled can do. However, utilisation of log-ratio data in methods such as Localised Uniform Conditioning is difficult due to the method by which the volume variance correction is made between panel estimate and SMU. A means of anamorphosis for the log-ratio transformed input data would potentially allow for far more realistic compositions at the SMU scale to be determined via LUC.

Decorrelation via ICA appears to be viable and comparable to MAF when considering only

covariance matrix diagonalisation, yet back transformation of results appears to distort their distributions. Defining the reasons for such a distortion may be beyond the scope of this preliminary study, but warrant further investigation.

Finally, the premise of this study has been to investigate recoverable resources calculation methods that would potentially be applicable within the constraints imposed by the operating framework of the mine from which the data were sourced. This requires univariate methods to be applied, either through decorrelation, or by ignoring spatial cross-correlation. While LUC of oxides, ignoring any spatial cross correlation and compositional nature of the input data yields data distributions most similar to the input data, sums constraints are commonly violated, and the net profit results do not compare as well as those of BOK. An expansion of this study to consider the effect which multivariate treatment of the input data may have on improving the efficacy of LUC would be worthwhile.

To conclude, of methods of recoverable resource trialled in this study, non linear methods appear to offer no significant benefit over ordinary kriging, and indeed appear subject to issues such as inappropriate distortion of spatial relationships between variables, leading to spurious net profit determinations. Accounting for the compositional nature of the input data, in addition to decorrelation of the data, introduces further distortions to these relationships, and results in unacceptably deviant net-profit results. Of the methods presented, univariate (non-decorrelated) block ordinary kriging appears to produce results, particularly in net profit, that are closest to the results that would be used for final selection at time of mining.

Chapter 8

References

[1] M. Z. Abzalov. “Localised uniform conditioning (LUC): A new approach to direct modeling of small blocks.” In: *Mathematical Geology* 38.4 (2006), pp. 393–411.

[2] M. Z. Abzalov. “Localized uniform conditioing (LUC): Method and application case studies”. In: *The journal fo the South African Institute of Mining and Metallurgy* 114 (2014), pp. 205–211.

[3] J. Aitchison. *The Statistical Analysis of Compositional Data*. Chapman and Hall, Ltd., 1986.

[4] M. Armstrong. *Basic Linear Geostatistics*. Springer-Verlag, 1998.

[5] C. Assibey-Bonsu W.Muller. “Limitations in accepting localised conditioning recoverble resource estimates for medium-term, long-term, and feasibility-stage mining projects, particularly for sections of an orebody.” In: *The Journal of the South African Institute of Mining and Metallurgy* 114 (2014), pp. 619–624.

[6] W. Assibey-Bonsu, C. Muller, and H. Pretorius. “Application of a localized uniform conditioning mineral resource modeling technique for medium- and long term planning of underground mining operations.” In: *The Journal of the South African Institute of Mining and Metallurgy* 114 (2014), pp. 659–665.

[7] W. Assibey-Bonsu, J. Searra, and M. Aboagye. “The use of indirect distributions of selective mining units for assesment of recoverable mineral resources designed for mine planning at Goldfields’ Tarkwa Mine, Ghana.” In: *The Journal of the South African Institute of Mining and Metallurgy* 115 (2015), pp. 51–57.

[8] W. Assibey-Bonsu et al. “Production reconciliation of a multivariate uniform conditioning technique for mineral resource modelling of a porphyry copper gold deposit.” In: *The Journal of the South African Institute of Mining and Metallurgy* 114 (2014), pp. 285–292.

[9] E. Bandarian. “Linear TransTransform MMethod for Multivariate Geostatistical Simulation”. PhD. Edith Cowan Univeristy, 2008.

[10] R. M. Barnett, J. G. Manchuk, and C. V. Deutsch. “Projection Pursuit Multivariate Transform”. In: *Mathematical Geosciences* 46.3 (2014), pp. 337–359.

[11] A. J. Bell and T. J. Sejnowski. “An information-maximisation approach to blind separation and blind deconvolution”. In: *Neural* 7.6 (1995), pp. 1129–1159.

[12] T. S. Blake. “Late Australia crustal extension, sedimentary basin formation, flood basalt volcanism and continental rifting: the Nullagine and Mount Jope supersequences, Western Australia.” In: *Precambrian Research* 60 (1993), pp. 185–241.

[13] A. Boucher and R. Dimitrakopolous. “Multivariate Block-Support Simulation of the Yandi Iron Ore Deposit, Western Australia.” In: *Mathematical Geosciences* 44.4 (2012), pp. 449–468.

[14] A. Chapman. “Application of Orthogonal Polynomials to Geostatistics”. Honours Thesis. Edith Cowan University, 2002.

[15] Y. Chen, W. Hardle, and V. Spokoiny. “Portfolio value at risk based on independent components analysis.” In: *Journal of Computational and Applied Mathematics* 205 (2007), pp. 594–607.

[16] J-P. Chilès and P. Delfiner. *Geostatistics: Modeling Spatial Uncertainty*. 2nd. Wiley Series in Probability and Statistics. John Wiley and Sons, 2012.

[17] C. De-Vitry. “Simulation of Correlated Variables: A Comparison of Approaches with a Case Study from the Yandi Channel Iron Deposit”. Master Thesis. University of Adelaide, 2010.

[18] L. E. DeLaHunty. “The geology of manganese deposits of Western Australia”. In: *Bulletin - Geological Survey of Western Australia* 116 (1963), p. 112.

[19] A. J. Desbarats and R. Dimitrakopolous. “Geostatistical Simulation of Regionalized Pore-Size Distributions Using Min/Max Austocorrelation Factors”. In: *Mathematical Geology* 32.8 (2000), pp. 919–942.

[20] J. Desraime and W. Assibey-Bonsu. “Comparative study of Localized Block Simulations and Localized Uniform Conditioning in the Multivariate case.” In: *Geostatistics Oslo, 2012*. Ed. by P. Abrahamsen, R. Hague, and J. Kolb. Quantitative Geology and Geostatstics 17. 2012.

[21] R. Dimitrakopolous and M. B. Fonseca. “Australia risk in grade-tonnage curves in a complex copper deposit, northern Brazil, based on an efficient joint simulation of mulmulti correlated variables.” In: *Application of Computers and Operations Research in the Minerals Industries*. South African Institute of Mining and Metallurgy. 2003.

[22] R. Dimitrakopolous and S. Mackie. “Stochastic simulation for the quantification of mine spoil variability and rehabilitation decision making”. In: *geoENV VI - Geostatistics for Environmental Applications.* Vol. 15. Quantitative Geology and Geostatistics. 2008, pp. 349–359.

[23] R. Goodfellow et al. “Quantifying multi-element and volumetric uncertainty ,Coleman McCreedy deposit, Ontario, Canada”. In: *Computers and Geosciences* 42 (2012), pp. 71–78.

[24] P. Goovaerts. *Geostaistics for Natural Resources Evaluation*. Applied Geostatistics Series. Oxford University Press, 1997.

[25] M. Humphreys. “Local recoverable estimation: A case study in uniform conditioning on the Wandoo Project for Boddington Gold Mine.” In: *Beyond Ordinary Kriging: Non-Linear Geostatistical Methods in Practice*. Geostatistical Association of Australiasia. 1998.

[26] A. Hyvärinen. “Fast and Robust Fixed-Point Algorithms for Independent Component Analysis”. In: *IEEE Transactions on Neural Networks* 10.3 (1999), pp. 626–634.

[27] A. Hyvärinen, J. Karhunen, and E. Oja. *Independent Components Analysis*. Wiley Series on Adaptive and Learning Systems for Signal Processing, Communications and Control. Wiley and Sons, 2001.

[28] A. Hyvärinen and E. Oja. “Independent Components Analysis: Algorithms and Applications”. In: *Neural Networks* 13.4-5 (2000), pp. 411–430.

[29] E. A. Isaaks and R. M. Srivastava. *An Introduction to Applied Geostatistics*. Oxford University Press, 1989.

[30] M. R. Job. “Application of logratios for geostatistical modelling of compositional data.” MSc. University of Alberta, 2012.

[31] S. Jones. “Geological setting of manganese deposits in the Woodie Woodie region”. Unpublished Internal Report. 2009.

[32] S. Jones. “Proterozoic deformation in the East Pilbara Craton and tectonic setting of fault-hosted manganese at the Woodie Woodie mine.” In: *Australian Journal of Earth Sciences* 58.6 (2011), pp. 639–673.

[33] S. Jones. “Geology and geochemistry of the sedimentary / stratabound deposits of the Oakover Basin”. Unpublished Internal Report. 2012.

[34] A. G. Journel. “The lognormal approach to predicting local distributions or selective mining unit grade.” In: *Mathematical Geology* 12.4 (1980), pp. 285–303.

[35] A. G. Journel. “Nonparametric estimation of spatial distributions”. In: *Mathematical Geology* 15.3 (1983), pp. 445–468.

[36] A. G. Journel and Ch. J. Huijbregts. *Mining Geostatistics*. 5th. The Blackburn Press, 1991.

[37] A. G. Journel and P. C. Kyriakidis. *Evaluation of Mineral Reserves: A Simulation Approach*. Applied Geostatistics Series. Oxford University Press, 2004.

[38] D. Krige. “A statistical approach to some basic mine valuation problems on the Witwatersrand”. In: *Journal of the Chemical, Metallurgical and Mining Society of South Africa* 52.6 (1951), pp. 119–139.

[39] D. Krige. “A practical analysis of the effects of spatial structure and of data available and accessed, on conditional bias in ordinary Kriging”. In: *Geostatistics Woollongong ’96*. Vol. 1. Kluwer, 1996, pp. 799–810.

[40] I. F. Lerchs H.Grossman. “Optimum Design of Open-Pit Mines”. In: *Transactions, CIM* 48 (1965).

[41] O. Leuangthong and C. V. Deutsch. “Stepwise Conditional TransTransform for SImulation of Multiple Variables”. In: *Mathematical Geology* 35.2 (2003), pp. 155–173.

[42] G. Matheron. “Principles of Geostatistics”. In: *Economic Geology* 58 (1963), pp. 1246–1266.

[43] M. J. McKeown et al. “Analysis of fMRI Data by Blind Source Separation Into Independent Spatial Components”. In: *Human Brain Mapping* 6 (1998), pp. 160–188.

[44] U. A. Mueller. “Spatial Decorrelation MMethod: Beyond MAF and PCA”. In: *Geostatistics Oslo 2012*. Ed. by P. Abrahamsen, R. Hague, and J. Kolb. Vol. 17. Quantitative Geology and Geostatistics. 2012.

[45] U. A. Mueller and J. Ferreira. “The U-WEDGE TransTransform Method for Multivariate Geostatistical Simulation”. In: *Mathematical Geosciences* 44.4 (2012), pp. 427–448.

[46] M. S. Nowak, A. J. Sinclair, and A. Randall. “Multiple Indicator Kriging of precious metals at Silbak Premier Mine, British Columbia.” In: *Geostatistics for the Next Century*. Ed. by R. Dimitrakopolous. Vol. 6. Quantitative Geology and Geostatistics. 1993.

[47] A. Papoulis and U. Pillai. *Probability, Random Variables and Stochastic Processes*. McGraw-Hill, 2002.

[48] E. Pardo-Igúzquia and P. A. Dowd. “Multiple Indicator co-Kriging with application to optimal sampling for environmental monitoring”. In: *Computers and Geosciences* 31 (2005), pp. 1–13.

[49] V. Pawlowsky-Glahn, J. J. Egozcue, and R. Tolosana-Delgado. *Modeling and Analysis of Compositional Data*. Chichester, UK: Wiley, 2015.

[50] J. Rivoirard. *Introduction to Disjunctive Kriging and Non-Linear Geostatistics*. Oxford, 1994.

[51] O. Rondon. “Teaching Aid: Minimum / Maximum Autocorrelation Factors for Joint Simulation of Attributes”. In: *Mathematical Geosciences* 44.4 (2012), pp. 469–504.

[52] M. E. Rossi and C. V. Deutsch. *Mineral Resource Estimation*. Springer-Verlag, 2014.

[53] R. J. Samworth and M. Yuan. “Independent Component Analysis Via Nonparametric Maximum Likelihood Estimation”. In: *The Annals of Statistics* 40.6 (2012), pp. 2973–3002.

[54] C. E. Shannon and W. Weaver. *The Mathematcal Theory of Communication*. Urbana: The University of Illinois Press, 1998.

[55] B Sohrabian and Y. Ozcelik. “Determination of exploitable blocks in an andesite quarry using independentcomponent kriging”. In: *International Journal of Rock Mechanics & Mining Sciences* 55 (2012), pp. 71–79.

[56] B Sohrabian and Y. Ozcelik. “Joint simulation of building stone deposit using minimum / maximum autocorrelation factors”. In: *Construction and Building Materials* 37 (2012), pp. 257–268.

[57] P. Switzer and S. Green. *Min/Max Autocorrelation Factors for Multivariate Spatial Imagery*. Technical Report 6. C.S.I.R.O. Australia, 1984.

[58] A. E. Tercan. “Importance of OrthogoOrthogonal Algorithm in Modeling Conditional Distributions by Orthogonal Transform Indicator Methods”. In: *Mathematical Geology* 31.2 (1999), pp. 155–173.

[59] A. E. Tercan and B. Sohrabian. “Multivariate geostatistical simulation of coal quality data by independent components”. In: *International Journal of Coal Geology* 112.2 (2013), pp. 53–66.

[60] R. Tolosana-Delgado, K. G. van den Boogaart, and V. Pawlowsky-Glahn. “Compositional Data Analysis”. In: ed. by V. Pawlowsky-Glahn and A. Buccianti. John Wiley and Sons, 2011. Chap. 6. Geostatistics for Compositions, pp. 73 –86.

[61] T. T. Tran, M. Murphy, and I. Glacken. “Semivariogram structures used in multivariate conditional simulation via maximum/minimum autocorrelation factors”. In: *International Association for Mathematical Geology, XIth International Congress*. 2006.

[62] S. Vahdat et al. “Shared and specific ndependent component analysis for between-group comparison.” In: *Neural Computation* (2012), pp. 3052–3090.

[63] H. Wackernagel. *Multivariate Geostatistics*. 3rd. Springer-Verlag, 2003.

[64] D. J. J. Walvoort and J. J. de Gruijter. “Compositional Kriging: A Spatial Interpolation Method for Compositional Data”. In: *Mathematical Geology* 33.8 (2001).

[65] C. Ward. “Compositions, logratios and geostatsitics: An application to Iron Ore”. MA thesis. Edith Cowan University, 2015.

[66] C. Ward and U. A. Mueller. “Multivariate estimation using logratios: A worked alternative.” In: *Geostatistics Oslo, 2012*. Ed. by P. Abrahamsen, R. Hague, and J. Kolb. Vol. 17. Quantitative Geology and Geostatstics, pp. 333–343.

[67] C. Zacché, J. F. da Silva, and J. F. Ciobra Leite Costa. “Minimum/maximum autocorrelation factors applied to grade estimation”. In: *Revista Escola de Minas* 67.2 (2014).

Appendix A

Data

Table A.1: Raw Data, complete dataset

Y	X	Mn	Fe	Si	Al	Pb	P
2417.308	7008.85	8.780	16.094	57.136	2.570	0.064	0.035
2410.65	6995.311	0.352	1.736	79.094	8.967	0.004	0.026
2419.505	6744.401	0.814	56.308	12.743	1.207	0.013	0.010
2381.066	6698.065	43.890	1.401	24.980	1.359	0.040	0.020
2399.319	6971.338	56.506	0.923	5.019	0.275	0.011	0.018
2366.136	6926.265	58.435	1.335	7.366	0.511	0.055	0.020
2388.05	6973.069	52.364	6.270	7.460	0.794	0.023	0.028
2371.997	6780.021	33.578	23.054	8.514	1.254	0.063	0.020
2362.998	6760.881	0.318	35.373	45.065	1.804	0.014	0.013
2402.054	6775.735	51.811	4.235	5.147	0.500	0.014	0.021
2390.918	6793.372	56.234	1.505	3.443	0.731	0.029	0.023
2392.02	6838.169	55.559	0.615	6.465	0.223	0.008	0.020
2345.119	6785.611	1.669	51.940	21.385	0.311	0.010	0.015
2356.043	6871.161	5.859	41.386	27.493	1.495	0.010	0.040
2414.223	6958.867	33.838	22.403	8.809	0.663	0.039	0.054
2412.204	6935.478	1.496	57.104	12.600	1.133	0.010	0.053
2345.933	6937.286	4.762	22.090	53.071	1.803	0.010	0.043
2343.813	6919.649	0.860	1.203	30.580	1.080	0.002	0.008
2375.013	6743.877	47.836	3.940	11.991	1.390	0.054	0.012
2442.3	6718.929	39.169	19.732	3.730	1.362	0.022	0.020
2365.486	6798.282	20.930	16.011	37.748	0.436	0.023	0.035

Continued on next page

Table A.1 – *Continued from previous page*

Y	X	Mn	Fe	SiO_2	Al_2O_3	Pb	P
2358.114	6742.777	10.199	52.221	5.355	0.282	0.027	0.017
2361.955	6939.681	4.151	28.048	45.740	1.378	0.014	0.109
2415.011	6915.443	9.319	33.759	32.819	0.088	0.016	0.027
2348.648	6858.946	10.517	2.374	34.043	1.268	0.096	0.013
2386.233	6779.482	52.452	0.705	10.757	0.258	0.009	0.025
2360.728	6840.602	40.099	2.493	21.727	4.561	0.034	0.020
2400.75	6863.064	46.098	6.675	11.484	0.172	0.011	0.052
2399.926	6800.094	0.491	63.327	6.130	0.810	0.005	0.011
2409.475	6880.855	40.410	8.185	17.693	0.291	0.013	0.044
2379.522	6916.949	55.296	1.346	4.048	1.731	0.029	0.024
2380.162	6939.652	51.606	1.100	14.299	0.778	0.026	0.017
2356.43	6775.609	55.535	2.520	1.209	0.224	0.629	0.023
2435.193	6737.792	14.721	47.895	1.752	0.785	0.023	0.049
2357.106	6901.682	8.637	27.553	35.133	3.328	0.042	0.089
2360.963	6800.104	49.265	7.811	5.500	0.312	0.099	0.073
2356.125	6765.071	55.597	3.390	3.003	0.254	0.012	0.014
2381.221	6759.145	60.279	0.446	0.695	0.515	0.010	0.017
2420.016	6818.458	2.517	3.819	87.782	0.940	0.009	0.013
2383.075	6803.937	46.858	0.941	20.729	1.095	0.031	0.018
2416.887	6903.895	17.308	27.285	28.932	0.069	0.016	0.029
2420.207	6860.162	9.576	11.578	63.090	0.992	0.030	0.026
2360.027	6960.889	1.900	7.692	37.807	3.738	0.008	0.012
2359.239	6920.115	44.714	10.209	12.193	0.792	0.010	0.067
2359.534	6824.749	7.408	39.098	24.747	2.233	0.016	0.060
2378.948	6818.953	11.425	34.746	25.585	1.141	0.181	0.061
2378.804	6842.849	33.349	1.045	41.602	0.419	0.015	0.018
2379.592	6861.798	46.717	8.856	6.620	0.658	0.018	0.040
2374.138	6875.678	51.276	6.063	8.936	0.690	0.022	0.023
2379.671	6899.929	36.153	12.453	16.134	2.717	0.019	0.062
2383.084	6730.916	39.187	14.619	13.324	0.560	0.034	0.020
2466.915	6691.154	31.017	21.497	15.431	1.545	0.022	0.016
2391.703	6943.298	48.386	4.290	14.562	0.380	0.007	0.046
2378.542	6980.031	1.411	61.145	6.473	0.660	0.007	0.042

Continued on next page

Table A.1 – *Continued from previous page*

Y	X	Mn	Fe	SiO_2	Al_2O_3	Pb	P
2471.044	6750.638	9.317	34.707	29.711	1.509	0.148	0.057
2384.666	6642.159	37.902	7.977	18.871	4.453	0.388	0.021
2436.39	6677.387	52.427	4.091	7.639	1.255	0.035	0.020
2442.088	6666.025	50.596	3.247	10.325	0.907	0.026	0.022
2417.681	6982.476	19.908	32.704	15.417	0.848	0.029	0.103
2433.771	6702.473	45.291	4.154	11.892	4.512	0.104	0.018
2411.278	6638.158	52.577	3.033	4.582	1.981	0.059	0.022
2417.533	6662.891	27.899	22.713	14.964	2.821	0.028	0.025
2398.923	6683.488	47.076	6.060	8.646	2.752	0.095	0.033
2405.721	6702.492	34.995	7.163	30.228	1.875	0.042	0.017
2398.409	6903.61	49.488	3.937	10.449	0.373	0.018	0.053
2365.786	6899.051	29.421	22.112	15.436	1.100	0.013	0.054
2398.352	6984.062	54.659	1.251	9.801	0.976	0.052	0.046
2458.441	6681.053	37.109	19.057	7.516	0.594	0.056	0.016
2379.274	6963.501	51.808	5.178	10.080	0.698	0.009	0.062
2458.776	6779.174	25.724	7.575	35.561	3.293	0.093	0.016
2401.793	6934.536	8.594	31.689	30.379	2.590	0.010	0.102
2478.044	6700.146	15.462	46.753	2.823	0.395	0.018	0.020
2455.85	6700.454	57.308	2.884	0.570	0.349	0.043	0.018
2477.808	6719.316	8.347	45.960	14.330	0.417	0.014	0.016
2456.621	6719.351	56.526	3.148	0.642	0.327	0.212	0.015
2398.801	6888.101	58.770	1.070	1.174	0.227	0.354	0.039
2438.859	6718.597	50.397	1.098	13.619	0.361	0.014	0.017
2442.537	6743.804	39.811	10.250	13.534	1.369	0.043	0.014
2342.924	6876.319	8.339	4.421	40.497	0.927	0.022	0.018
2425.743	6921.554	5.182	4.668	79.814	0.197	0.014	0.020
2395.415	6958.762	55.627	0.879	11.446	0.623	0.011	0.040
2398.51	6920.253	43.816	2.201	22.786	0.119	0.020	0.035
2408.824	6761.539	7.621	39.159	21.121	1.920	0.037	0.115
2368.096	6788.014	35.504	18.559	11.403	0.711	0.165	0.029
2408.52	6778.917	3.463	54.080	9.575	1.373	0.013	0.015
2397.559	6832.288	39.418	6.496	24.642	0.413	0.013	0.028
2355.551	6810.876	7.673	57.071	3.742	0.555	0.019	0.023

Continued on next page

Table A.1 – *Continued from previous page*

Y	X	Mn	Fe	SiO_2	Al_2O_3	Pb	P
2329.006	6779.523	4.070	56.700	10.300	0.510	0.015	0.040
2356.133	6877.771	7.179	5.822	74.193	2.472	0.018	0.035
2423.946	6967.833	5.361	15.040	48.647	2.953	0.026	1.385
2423.67	6959.537	2.725	4.228	75.234	4.224	0.013	0.234
2423.883	6952.313	7.397	19.941	54.742	1.358	0.036	0.271
2369.157	6864.539	56.307	1.650	5.557	0.395	0.016	0.023
2367.67	6856.584	32.293	25.140	6.876	1.333	0.024	0.020
2367.24	6848.788	55.697	0.817	5.124	1.457	0.018	0.014
2367.332	6840.723	56.797	1.069	2.489	0.930	0.018	0.015
2367.308	6832.551	55.757	0.962	3.310	0.605	0.012	0.016
2368.832	6824.921	1.567	55.894	15.745	0.256	0.003	0.017
2375.382	6976.794	8.645	45.417	18.750	0.660	0.015	0.019
2375.609	6966.656	46.131	2.760	23.993	0.306	0.025	0.020
2375.624	6959.855	54.646	4.296	5.672	0.758	0.013	0.045
2375.391	6952.2	43.568	13.551	6.676	1.214	0.021	0.090
2375.473	6944.491	45.020	5.901	16.883	1.317	0.021	0.048
2375.493	6935.891	55.517	0.768	9.135	0.561	0.032	0.016
2375.59	6928.275	54.406	0.862	8.376	0.665	0.036	0.015
2375.325	6918.857	56.615	1.143	6.501	0.360	0.014	0.026
2375.499	6911.589	55.865	1.734	6.184	0.576	0.072	0.026
2375.599	6904.483	44.083	12.122	5.131	1.782	0.074	0.042
2375.545	6895.477	43.295	12.368	9.024	0.356	0.014	0.032
2375.722	6889.343	51.618	6.233	5.714	0.360	0.020	0.028
2375.612	6879.603	48.073	3.680	16.222	0.817	0.010	0.019
2375.804	6871.762	58.392	0.740	1.511	0.232	0.245	0.016
2375.512	6864.24	56.709	2.222	3.405	0.584	0.092	0.021
2375.761	6856.548	47.790	8.088	6.092	0.813	0.018	0.040
2375.212	6849.26	58.103	0.635	1.461	0.660	0.011	0.017
2375.327	6840.449	44.573	0.851	24.399	0.349	0.008	0.011
2375.468	6832.851	57.147	1.751	1.725	0.311	0.570	0.018
2375.662	6825.549	29.224	27.896	10.901	0.314	0.010	0.021
2377.296	6814.702	46.271	3.488	19.219	0.329	0.032	0.017
2376.49	6807.527	30.318	4.099	41.695	0.441	0.007	0.037

Continued on next page

Table A.1 – *Continued from previous page*

Y	X	Mn	Fe	SiO_2	Al_2O_3	Pb	P
2376.444	6799.564	57.721	1.037	1.123	1.082	0.139	0.022
2376.454	6791.758	55.877	1.177	5.397	0.833	0.010	0.020
2375.263	6783.885	41.006	14.124	9.477	1.432	0.097	0.025
2384.078	6983.926	24.869	36.123	5.245	0.380	0.021	0.068
2383.662	6976.286	40.743	19.745	4.521	0.733	0.014	0.047
2383.878	6968.159	43.223	15.678	9.330	0.385	0.014	0.029
2383.812	6960.586	53.729	1.195	14.855	0.392	0.015	0.022
2383.686	6952.954	52.675	0.840	16.603	0.410	0.012	0.026
2384.047	6947.026	59.055	0.701	6.022	0.193	0.009	0.019
2383.44	6936.069	56.118	0.574	5.657	1.131	0.014	0.017
2383.129	6928.146	61.228	0.154	1.733	0.253	0.005	0.013
2383.559	6912.26	59.460	0.650	6.984	0.841	0.010	0.027
2383.518	6897.249	57.713	0.956	3.147	0.253	0.076	0.022
2383.777	6889.217	50.333	2.137	13.763	0.197	0.027	0.021
2383.586	6880.35	56.671	0.952	5.480	0.399	0.009	0.024
2383.194	6872.099	55.760	1.485	10.679	0.869	0.036	0.021
2383.085	6864.167	54.130	2.669	5.302	0.787	0.052	0.024
2383.468	6857.229	49.201	7.450	5.270	0.539	0.031	0.047
2383.422	6850.111	61.512	0.211	0.588	0.200	0.027	0.011
2383.467	6840.381	60.533	0.809	0.588	0.264	0.044	0.012
2383.457	6832.514	53.365	3.184	6.769	0.311	0.015	0.021
2383.601	6824.403	44.583	1.029	25.816	0.204	0.013	0.019
2383.75	6816.79	38.676	0.678	35.410	0.318	0.010	0.012
2384.535	6807.577	49.726	0.784	17.559	0.346	0.007	0.014
2383.78	6799.951	36.722	0.874	37.685	0.483	0.013	0.016
2382.788	6792.388	44.589	0.922	22.922	0.524	0.014	0.019
2383.099	6783.901	37.459	2.261	31.856	1.474	0.054	0.018
2384.674	6905.614	56.968	0.801	7.403	1.331	0.016	0.018
2391.248	6984.029	49.120	9.641	5.161	0.779	0.014	0.056
2392.56	6977.067	58.519	1.572	5.730	0.407	0.065	0.025
2391.476	6967.279	55.097	1.213	10.966	0.543	0.015	0.024
2391.307	6960.238	56.997	0.746	10.118	0.420	0.009	0.026
2390.772	6950.103	53.673	0.769	13.672	0.447	0.010	0.029

Continued on next page

Table A.1 – *Continued from previous page*

Y	X	Mn	Fe	SiO_2	Al_2O_3	Pb	P
2391.751	6936.236	53.716	0.601	10.611	0.265	0.007	0.021
2391.679	6928.593	40.580	0.871	33.095	0.290	0.008	0.014
2391.763	6922.944	47.453	0.697	19.871	0.212	0.009	0.014
2391.913	6912.608	31.061	6.100	38.184	0.270	0.010	0.051
2391.533	6904.717	33.122	5.180	35.807	0.739	0.008	0.040
2390.964	6896.965	48.874	6.439	9.850	0.896	0.019	0.046
2391.978	6888.581	52.398	1.495	10.850	0.335	0.019	0.017
2391.595	6880.28	52.936	0.663	10.672	0.261	0.008	0.016
2391.448	6871.757	45.401	0.995	30.311	0.553	0.015	0.016
2390.662	6864.236	57.471	0.925	10.249	0.466	0.012	0.016
2391.274	6857.376	54.911	2.044	5.577	0.462	0.084	0.023
2391.353	6848.969	59.091	0.661	1.620	0.605	0.011	0.020
2391.067	6832.191	41.953	6.108	19.726	0.701	0.010	0.058
2391.411	6824.588	51.078	0.963	14.383	0.233	0.012	0.018
2391.704	6816.579	15.879	44.729	4.189	0.913	0.017	0.096
2391.501	6808.934	22.413	37.048	1.812	0.760	0.115	0.166
2391.286	6801.055	56.804	1.145	1.364	1.444	0.015	0.022
2391.992	6784.711	55.534	1.504	2.941	1.425	0.038	0.037
2400.391	6984.117	56.947	1.868	5.663	0.402	0.077	0.018
2399.665	6976.404	58.459	0.838	4.949	0.382	0.010	0.024
2399.084	6968.397	58.672	0.740	5.328	0.359	0.009	0.019
2399.84	6959.245	59.121	0.961	5.713	0.529	0.040	0.030
2399.915	6951.591	56.518	0.883	11.722	0.398	0.011	0.021
2400.059	6942.891	59.079	0.832	6.049	0.357	0.010	0.025
2399.781	6928.335	36.592	2.761	34.476	0.268	0.025	0.021
2399.872	6911.639	52.589	4.410	8.546	0.261	0.020	0.039
2399.876	6897.011	56.835	1.022	4.981	0.184	0.013	0.015
2399.544	6879.552	46.208	4.597	13.869	0.812	0.037	0.034
2399.718	6872.078	45.612	0.807	22.789	0.326	0.007	0.008
2399.855	6853.223	46.018	0.623	23.149	0.244	0.008	0.015
2399.966	6849.337	58.625	0.963	1.264	0.495	0.072	0.018
2399.846	6840.409	54.562	1.235	6.564	0.287	0.015	0.017
2399.608	6826.193	22.329	10.411	43.261	2.702	0.052	0.047

Continued on next page

Table A.1 – *Continued from previous page*

Y	X	Mn	Fe	SiO_2	Al_2O_3	Pb	P
2398.385	6808.464	0.869	55.250	16.819	1.617	0.012	0.017
2398.984	6792.032	58.368	1.637	0.346	0.566	0.011	0.029
2400.001	6784.539	59.239	0.395	0.177	0.310	0.023	0.024
2407.163	6904.156	58.645	1.638	1.947	0.206	0.657	0.020
2407.837	6984.295	56.918	3.050	5.391	0.382	0.010	0.022
2407.731	6968.131	59.769	0.448	3.991	0.199	0.036	0.019
2407.622	6960.463	58.595	0.655	7.030	0.262	0.008	0.021
2407.534	6952.607	57.002	2.855	5.438	0.391	0.013	0.029
2407.909	6944.465	58.825	1.431	3.544	0.145	0.014	0.031
2407.878	6936.465	6.204	45.689	22.611	0.247	0.011	0.044
2408.021	6928.519	9.534	45.819	17.996	0.184	0.016	0.017
2407.738	6920.342	32.954	12.817	26.597	0.111	0.016	0.036
2408.137	6912.433	43.260	16.652	3.855	0.236	0.013	0.028
2407.454	6896.702	58.617	1.446	1.070	0.222	0.354	0.025

Table A.2: Calculated oxide data, complete dataset

Y	X	Mn_3O_4	Fe_2O_3	SiO_2	Al_2O_3	PbO	P_2O_5	Service
2417.308	7008.85	12.189	23.010	57.136	2.570	0.069	0.160	4.865
2410.65	6995.311	0.489	2.482	79.094	8.967	0.004	0.240	8.724
2419.505	6744.401	1.130	80.505	12.743	1.207	0.014	0.127	4.273
2381.066	6698.065	60.932	2.003	24.980	1.359	0.043	0.041	10.641
2399.319	6971.338	78.447	1.320	5.019	0.275	0.012	0.073	14.855
2366.136	6926.265	81.125	1.909	7.366	0.511	0.059	0.016	9.014
2388.05	6973.069	72.697	8.964	7.460	0.794	0.024	0.033	10.027
2371.997	6780.021	46.616	32.961	8.514	1.254	0.068	0.024	10.563
2362.998	6760.881	0.441	50.574	45.065	1.804	0.015	0.018	2.083
2402.054	6775.735	71.929	6.055	5.147	0.500	0.015	0.153	16.202
2390.918	6793.372	78.069	2.152	3.443	0.731	0.031	0.019	15.554
2392.02	6838.169	77.132	0.879	6.465	0.223	0.008	0.011	15.281
2345.119	6785.611	2.317	74.260	21.385	0.311	0.011	0.016	1.700
2356.043	6871.161	8.134	59.171	27.493	1.495	0.011	0.138	3.558

Continued on next page

Table A.2 – *Continued from previous page*

Y	X	Mn_3O_4	Fe_2O_3	SiO_2	Al_2O_3	PbO	P_2O_5	Service
2414.223	6958.867	46.977	32.030	8.809	0.663	0.042	0.240	11.238
2412.204	6935.478	2.077	81.644	12.600	1.133	0.011	0.076	2.460
2345.933	6937.286	6.611	31.583	53.071	1.803	0.011	0.088	6.833
2343.813	6919.649	1.194	1.720	30.580	1.080	0.002	0.066	65.358
2375.013	6743.877	66.410	5.633	11.991	1.390	0.058	0.059	14.459
2442.3	6718.929	54.378	28.212	3.730	1.362	0.024	0.039	12.256
2365.486	6798.282	29.057	22.891	37.748	0.436	0.025	0.021	9.821
2358.114	6742.777	14.159	74.662	5.355	0.282	0.029	0.104	5.409
2361.955	6939.681	5.763	40.101	45.740	1.378	0.015	0.095	6.908
2415.011	6915.443	12.937	48.266	32.819	0.088	0.017	0.200	5.672
2348.648	6858.946	14.601	3.394	34.043	1.268	0.104	0.069	46.521
2386.233	6779.482	72.819	1.008	10.757	0.258	0.009	0.137	15.011
2360.728	6840.602	55.669	3.564	21.727	4.561	0.037	0.035	14.407
2400.75	6863.064	63.997	9.543	11.484	0.172	0.012	0.182	14.609
2399.926	6800.094	0.682	90.541	6.130	0.810	0.006	0.021	1.811
2409.475	6880.855	56.101	11.702	17.693	0.291	0.014	0.044	14.155
2379.522	6916.949	76.767	1.924	4.048	1.731	0.031	0.069	15.430
2380.162	6939.652	71.644	1.573	14.299	0.778	0.028	0.011	11.666
2356.43	6775.609	77.099	3.603	1.209	0.224	0.678	0.053	17.135
2435.193	6737.792	20.437	68.477	1.752	0.785	0.025	0.010	8.514
2357.106	6901.682	11.991	39.393	35.133	3.328	0.045	0.025	10.084
2360.963	6800.104	68.394	11.168	5.500	0.312	0.107	0.414	14.105
2356.125	6765.071	77.185	4.847	3.003	0.254	0.013	0.013	14.686
2381.221	6759.145	83.685	0.638	0.695	0.515	0.010	0.008	14.449
2420.016	6818.458	3.494	5.460	87.782	0.940	0.009	0.001	2.313
2383.075	6803.937	65.053	1.345	20.729	1.095	0.034	0.255	11.489
2416.887	6903.895	24.029	39.010	28.932	0.069	0.017	0.098	7.846
2420.207	6860.162	13.294	16.553	63.090	0.992	0.032	0.122	5.917
2360.027	6960.889	2.638	10.998	37.807	3.738	0.008	0.122	44.689
2359.239	6920.115	62.076	14.596	12.193	0.792	0.011	0.409	9.923
2359.534	6824.749	10.284	55.900	24.747	2.233	0.017	0.120	6.699
2378.948	6818.953	15.861	49.678	25.585	1.141	0.195	0.244	7.296
2378.804	6842.849	46.298	1.494	41.602	0.419	0.017	0.075	10.096

Continued on next page

Table A.2 – *Continued from previous page*

Y	X	Mn_3O_4	Fe_2O_3	SiO_2	Al_2O_3	PbO	P_2O_5	Service
2379.592	6861.798	64.857	12.662	6.620	0.658	0.019	0.269	14.915
2374.138	6875.678	71.186	8.668	8.936	0.690	0.023	0.025	10.471
2379.671	6899.929	50.191	17.804	16.134	2.717	0.021	0.090	13.043
2383.084	6730.916	54.403	20.901	13.324	0.560	0.037	0.052	10.722
2466.915	6691.154	43.061	30.735	15.431	1.545	0.023	0.034	9.170
2391.703	6943.298	67.174	6.134	14.562	0.380	0.008	0.115	11.628
2378.542	6980.031	1.959	87.421	6.473	0.660	0.007	0.099	3.381
2471.044	6750.638	12.935	49.622	29.711	1.509	0.159	0.060	6.005
2384.666	6642.159	52.619	11.405	18.871	4.453	0.418	0.101	12.133
2436.39	6677.387	72.784	5.849	7.639	1.255	0.038	0.061	12.374
2442.088	6666.025	70.242	4.642	10.325	0.907	0.028	0.027	13.828
2417.681	6982.476	27.638	46.758	15.417	0.848	0.031	0.172	9.136
2433.771	6702.473	62.877	5.939	11.892	4.512	0.112	0.045	14.623
2411.278	6638.158	72.992	4.336	4.582	1.981	0.063	0.042	16.003
2417.533	6662.891	38.732	32.474	14.964	2.821	0.031	0.019	10.960
2398.923	6683.488	65.355	8.664	8.646	2.752	0.102	0.080	14.401
2405.721	6702.492	48.583	10.241	30.228	1.875	0.046	0.024	9.003
2398.409	6903.61	68.704	5.629	10.449	0.373	0.020	0.259	14.567
2365.786	6899.051	40.845	31.614	15.436	1.100	0.014	0.092	10.898
2398.352	6984.062	75.883	1.789	9.801	0.976	0.056	0.115	11.381
2458.441	6681.053	51.518	27.246	7.516	0.594	0.060	0.025	13.040
2379.274	6963.501	71.925	7.403	10.080	0.698	0.009	0.075	9.810
2458.776	6779.174	35.712	10.830	35.561	3.293	0.100	0.026	14.477
2401.793	6934.536	11.931	45.307	30.379	2.590	0.011	0.586	9.196
2478.044	6700.146	21.466	66.844	2.823	0.395	0.019	0.099	8.354
2455.85	6700.454	79.560	4.123	0.570	0.349	0.046	0.008	15.343
2477.808	6719.316	11.588	65.711	14.330	0.417	0.015	0.001	7.938
2456.621	6719.351	78.475	4.501	0.642	0.327	0.229	0.035	15.792
2398.801	6888.101	81.590	1.530	1.174	0.227	0.381	0.004	15.094
2438.859	6718.597	69.966	1.570	13.619	0.361	0.015	0.003	14.466
2442.537	6743.804	55.269	14.655	13.534	1.369	0.046	0.031	15.096
2342.924	6876.319	11.577	6.321	40.497	0.927	0.024	0.039	40.615
2425.743	6921.554	7.194	6.674	79.814	0.197	0.016	0.131	5.975

Continued on next page

Table A.2 – *Continued from previous page*

Y	X	Mn_3O_4	Fe_2O_3	SiO_2	Al_2O_3	PbO	P_2O_5	Service
2395.415	6958.762	77.227	1.257	11.446	0.623	0.012	0.516	8.920
2398.51	6920.253	60.829	3.147	22.786	0.119	0.022	0.066	13.031
2408.824	6761.539	10.580	55.987	21.121	1.920	0.040	0.423	9.929
2368.096	6788.014	49.290	26.534	11.403	0.711	0.178	0.100	11.784
2408.52	6778.917	4.808	77.320	9.575	1.373	0.014	0.028	6.883
2397.559	6832.288	54.724	9.288	24.642	0.413	0.014	0.043	10.876
2355.551	6810.876	10.652	81.596	3.742	0.555	0.020	0.092	3.342
2329.006	6779.523	5.650	81.066	10.300	0.510	0.016	0.024	2.433
2356.133	6877.771	9.967	8.324	74.193	2.472	0.019	0.058	4.967
2423.946	6967.833	7.443	21.503	48.647	2.953	0.028	16.593	2.833
2423.67	6959.537	3.783	6.045	75.234	4.224	0.014	2.088	8.612
2423.883	6952.313	10.269	28.510	54.742	1.358	0.039	3.328	1.754
2369.157	6864.539	78.171	2.359	5.557	0.395	0.017	0.208	13.293
2367.67	6856.584	44.832	35.944	6.876	1.333	0.026	0.018	10.971
2367.24	6848.788	77.324	1.168	5.124	1.457	0.019	0.016	14.893
2367.332	6840.723	78.851	1.528	2.489	0.930	0.019	0.012	16.170
2367.308	6832.551	77.407	1.375	3.310	0.605	0.013	0.006	17.284
2368.832	6824.921	2.175	79.914	15.745	0.256	0.003	0.009	1.898
2375.382	6976.794	12.002	64.934	18.750	0.660	0.016	0.048	3.590
2375.609	6966.656	64.043	3.946	23.993	0.306	0.027	0.061	7.624
2375.624	6959.855	75.865	6.142	5.672	0.758	0.014	0.174	11.375
2375.391	6952.2	60.485	19.374	6.676	1.214	0.023	0.083	12.144
2375.473	6944.491	62.501	8.437	16.883	1.317	0.023	0.052	10.788
2375.493	6935.891	77.074	1.098	9.135	0.561	0.034	0.044	12.054
2375.59	6928.275	75.531	1.232	8.376	0.665	0.038	0.022	14.135
2375.325	6918.857	78.598	1.634	6.501	0.360	0.015	0.035	12.856
2375.499	6911.589	77.557	2.479	6.184	0.576	0.077	0.027	13.099
2375.599	6904.483	61.200	17.331	5.131	1.782	0.080	0.042	14.434
2375.545	6895.477	60.106	17.683	9.024	0.356	0.015	0.027	12.789
2375.722	6889.343	71.661	8.912	5.714	0.360	0.022	0.041	13.291
2375.612	6879.603	66.739	5.261	16.222	0.817	0.011	0.018	10.932
2375.804	6871.762	81.065	1.058	1.511	0.232	0.263	0.042	15.829
2375.512	6864.24	78.729	3.177	3.405	0.584	0.099	0.005	14.002

Continued on next page

Table A.2 – *Continued from previous page*

Y	X	Mn_3O_4	Fe_2O_3	SiO_2	Al_2O_3	PbO	P_2O_5	Service
2375.761	6856.548	66.346	11.564	6.092	0.813	0.019	0.022	15.143
2375.212	6849.26	80.664	0.908	1.461	0.660	0.012	0.017	16.279
2375.327	6840.449	61.880	1.217	24.399	0.349	0.008	0.003	12.144
2375.468	6832.851	79.337	2.503	1.725	0.311	0.614	0.071	15.439
2375.662	6825.549	40.571	39.884	10.901	0.314	0.011	0.006	8.313
2377.296	6814.702	64.238	4.987	19.219	0.329	0.034	0.030	11.163
2376.49	6807.527	42.090	5.860	41.695	0.441	0.007	0.115	9.791
2376.444	6799.564	80.134	1.483	1.123	1.082	0.150	0.148	15.881
2376.454	6791.758	77.574	1.683	5.397	0.833	0.011	0.004	14.499
2375.263	6783.885	56.928	20.194	9.477	1.432	0.104	0.022	11.843
2384.078	6983.926	34.525	51.646	5.245	0.380	0.023	0.104	8.076
2383.662	6976.286	56.563	28.230	4.521	0.733	0.015	0.040	9.897
2383.878	6968.159	60.006	22.415	9.330	0.385	0.016	0.021	7.827
2383.812	6960.586	74.592	1.709	14.855	0.392	0.016	0.033	8.404
2383.686	6952.954	73.128	1.201	16.603	0.410	0.013	0.062	8.582
2384.047	6947.026	81.986	1.002	6.022	0.193	0.009	0.051	10.737
2383.44	6936.069	77.908	0.821	5.657	1.131	0.015	0.017	14.452
2383.129	6928.146	85.002	0.220	1.733	0.253	0.005	0.012	12.775
2383.559	6912.26	82.548	0.929	6.984	0.841	0.011	0.008	8.679
2383.518	6897.249	80.122	1.367	3.147	0.253	0.082	0.025	15.004
2383.777	6889.217	69.877	3.055	13.763	0.197	0.029	0.011	13.068
2383.586	6880.35	78.676	1.361	5.480	0.399	0.010	0.053	14.021
2383.194	6872.099	77.411	2.123	10.679	0.869	0.038	0.019	8.861
2383.085	6864.167	75.148	3.816	5.302	0.787	0.056	0.041	14.850
2383.468	6857.229	68.305	10.652	5.270	0.539	0.033	0.040	15.160
2383.422	6850.111	85.397	0.302	0.588	0.200	0.029	0.009	13.475
2383.467	6840.381	84.037	1.157	0.588	0.264	0.047	0.001	13.905
2383.457	6832.514	74.086	4.552	6.769	0.311	0.016	0.002	14.264
2383.601	6824.403	61.894	1.471	25.816	0.204	0.014	0.021	10.580
2383.75	6816.79	53.694	0.969	35.410	0.318	0.011	0.050	9.548
2384.535	6807.577	69.034	1.121	17.559	0.346	0.008	0.080	11.852
2383.78	6799.951	50.981	1.250	37.685	0.483	0.014	0.045	9.542
2382.788	6792.388	61.903	1.318	22.922	0.524	0.015	0.116	13.203

Continued on next page

Table A.2 – *Continued from previous page*

Y	X	Mn_3O_4	Fe_2O_3	SiO_2	Al_2O_3	PbO	P_2O_5	Service
2383.099	6783.901	52.004	3.233	31.856	1.474	0.059	0.067	11.308
2384.674	6905.614	79.088	1.145	7.403	1.331	0.017	0.093	10.922
2391.248	6984.029	68.193	13.784	5.161	0.779	0.015	0.067	12.001
2392.56	6977.067	81.241	2.248	5.730	0.407	0.070	0.021	10.283
2391.476	6967.279	76.491	1.734	10.966	0.543	0.016	0.022	10.228
2391.307	6960.238	79.128	1.067	10.118	0.420	0.010	0.046	9.211
2390.772	6950.103	74.514	1.099	13.672	0.447	0.010	0.047	10.210
2391.751	6936.236	74.573	0.859	10.611	0.265	0.008	0.046	13.637
2391.679	6928.593	56.337	1.245	33.095	0.290	0.009	0.024	9.000
2391.763	6922.944	65.879	0.997	19.871	0.212	0.009	0.075	12.958
2391.913	6912.608	43.122	8.721	38.184	0.270	0.011	0.164	9.528
2391.533	6904.717	45.983	7.406	35.807	0.739	0.009	0.247	9.809
2390.964	6896.965	67.851	9.206	9.850	0.896	0.021	0.267	11.909
2391.978	6888.581	72.744	2.137	10.850	0.335	0.020	0.027	13.886
2391.595	6880.28	73.491	0.948	10.672	0.261	0.009	0.028	14.592
2391.448	6871.757	63.030	1.423	30.311	0.553	0.016	0.028	4.640
2390.662	6864.236	79.787	1.323	10.249	0.466	0.012	0.078	8.085
2391.274	6857.376	76.232	2.922	5.577	0.462	0.091	0.038	14.677
2391.353	6848.969	82.036	0.945	1.620	0.605	0.012	0.018	14.764
2391.067	6832.191	58.243	8.733	19.726	0.701	0.011	0.015	12.571
2391.411	6824.588	70.911	1.377	14.383	0.233	0.013	0.057	13.026
2391.704	6816.579	22.045	63.951	4.189	0.913	0.018	0.223	8.661
2391.501	6808.934	31.116	52.969	1.812	0.760	0.124	0.115	13.105
2391.286	6801.055	78.861	1.637	1.364	1.444	0.016	0.007	16.672
2391.992	6784.711	77.097	2.150	2.941	1.425	0.041	0.008	16.337
2400.391	6984.117	79.059	2.671	5.663	0.402	0.083	0.009	12.114
2399.665	6976.404	81.158	1.198	4.949	0.382	0.011	0.022	12.280
2399.084	6968.397	81.454	1.058	5.328	0.359	0.010	0.015	11.776
2399.84	6959.245	82.077	1.374	5.713	0.529	0.043	0.026	10.238
2399.915	6951.591	78.463	1.262	11.722	0.398	0.012	0.019	8.123
2400.059	6942.891	82.019	1.190	6.049	0.357	0.011	0.047	10.327
2399.781	6928.335	50.800	3.947	34.476	0.268	0.027	0.021	10.461
2399.872	6911.639	73.009	6.305	8.546	0.261	0.022	0.217	11.640

Continued on next page

Table A.2 – *Continued from previous page*

Y	X	Mn_3O_4	Fe_2O_3	SiO_2	Al_2O_3	PbO	P_2O_5	Service
2399.876	6897.011	78.904	1.461	4.981	0.184	0.014	0.021	14.436
2399.544	6879.552	64.150	6.572	13.869	0.812	0.040	0.027	14.529
2399.718	6872.078	63.323	1.154	22.789	0.326	0.008	0.018	12.383
2399.855	6853.223	63.886	0.891	23.149	0.244	0.008	0.055	11.766
2399.966	6849.337	81.389	1.377	1.264	0.495	0.078	0.067	15.331
2399.846	6840.409	75.748	1.766	6.564	0.287	0.017	0.004	15.615
2399.608	6826.193	30.999	14.885	43.261	2.702	0.056	0.050	8.047
2398.385	6808.464	1.206	78.993	16.819	1.617	0.013	0.119	1.233
2398.984	6792.032	81.032	2.340	0.346	0.566	0.011	0.079	15.625
2400.001	6784.539	82.241	0.565	0.177	0.310	0.025	0.001	16.681
2407.163	6904.156	81.416	2.342	1.947	0.206	0.708	0.001	13.380
2407.837	6984.295	79.019	4.361	5.391	0.382	0.011	0.007	10.830
2407.731	6968.131	82.977	0.641	3.991	0.199	0.038	0.017	12.138
2407.622	6960.463	81.347	0.936	7.030	0.262	0.009	0.014	10.402
2407.534	6952.607	79.135	4.082	5.438	0.391	0.014	0.033	10.907
2407.909	6944.465	81.666	2.046	3.544	0.145	0.015	0.027	12.556
2407.878	6936.465	8.613	65.323	22.611	0.247	0.012	0.025	3.169
2408.021	6928.519	13.236	65.509	17.996	0.184	0.017	0.062	2.996
2407.738	6920.342	45.750	18.325	26.597	0.111	0.018	0.105	9.095
2408.137	6912.433	60.058	23.808	3.855	0.236	0.015	0.120	11.909
2407.454	6896.702	81.378	2.067	1.070	0.222	0.381	0.016	14.866

Table A.3: Additive Log-ratio transformed data, Complete Dataset

Y	X	alrMn_3O_4	alrFe_2O_3	alrSiO_2	alrAl_2O_3	alrPbO	alrP_2O_5
2417.308	7008.85	0.91847	1.55385	2.46335	-0.63818	-4.25309	-3.41221
2410.65	6995.311	-2.88217	-1.25705	2.20452	0.02743	-7.72416	-3.59293
2419.505	6744.401	-1.33007	2.93598	1.09263	-1.26421	-5.72077	-3.51335
2381.066	6698.065	1.74501	-1.67008	0.85332	-2.05800	-5.50925	-5.55151
2399.319	6971.338	1.66412	-2.42094	-1.08507	-3.98929	-7.08975	-5.32065
2366.136	6926.265	2.19723	-1.55234	-0.20188	-2.87015	-5.02318	-6.31548
2388.05	6973.069	1.98097	-0.11206	-0.29577	-2.53600	-6.02279	-5.70682

Continued on next page

Table A.3 – *Continued from previous page*

Y	X	alrMn_3O_4	alrFe_2O_3	alrSiO_2	alrAl_2O_3	alrPbO	alrP_2O_5
2371.997	6780.021	1.48460	1.13798	-0.21563	-2.13100	-5.04758	-6.08173
2362.998	6760.881	-1.55147	3.18959	3.07426	-0.14384	-4.96206	-4.75751
2402.054	6775.735	1.49057	-0.98423	-1.14669	-3.47825	-6.98765	-4.66378
2390.918	6793.372	1.61326	-1.97806	-1.50800	-3.05768	-6.20614	-6.69008
2392.02	6838.169	1.61890	-2.85527	-0.86022	-4.22721	-7.52407	-7.22376
2345.119	6785.611	0.30960	3.77688	2.53199	-1.69866	-5.06149	-4.68701
2356.043	6871.161	0.82682	2.81120	2.04470	-0.86711	-5.80002	-3.24883
2414.223	6958.867	1.43032	1.04735	-0.24356	-2.83031	-5.58641	-3.84587
2412.204	6935.478	-0.16914	3.50236	1.63369	-0.77514	-5.43080	-3.47455
2345.933	6937.286	-0.03308	1.53079	2.04981	-1.33237	-6.42450	-4.35596
2343.813	6919.649	-4.00263	-3.63758	-0.75954	-4.10292	-10.33631	-6.90366
2375.013	6743.877	1.52456	-0.94262	-0.18713	-2.34198	-5.52489	-5.49664
2442.3	6718.929	1.48996	0.83373	-1.18959	-2.19705	-6.24215	-5.75560
2365.486	6798.282	1.08470	0.84621	1.34637	-3.11467	-5.97057	-6.14011
2358.114	6742.777	0.96234	2.62495	-0.00999	-2.95387	-5.21855	-3.95511
2361.955	6939.681	-0.18125	1.75873	1.89030	-1.61204	-6.12700	-4.28705
2415.011	6915.443	0.82453	2.14114	1.75541	-4.16601	-5.79339	-3.34741
2348.648	6858.946	-1.15885	-2.61785	-0.31229	-3.60247	-6.10677	-6.51299
2386.233	6779.482	1.57916	-2.70088	-0.33325	-4.06361	-7.36968	-4.69296
2360.728	6840.602	1.35173	-1.39672	0.41086	-1.15015	-5.96596	-6.02276
2400.75	6863.064	1.47723	-0.42576	-0.24066	-4.44188	-7.11872	-4.38263
2399.926	6800.094	-0.97724	3.91180	1.21919	-0.80472	-5.73831	-4.48027
2409.475	6880.855	1.37710	-0.19026	0.22312	-3.88448	-6.88813	-5.78278
2379.522	6916.949	1.60446	-2.08168	-1.33809	-2.18761	-6.20924	-5.41556
2380.162	6939.652	1.81500	-2.00392	0.20347	-2.70775	-6.01555	-6.94998
2356.43	6775.609	1.50399	-1.55935	-2.65131	-4.33721	-3.23034	-5.77656
2435.193	6737.792	0.87560	2.08475	-1.58099	-2.38382	-5.83963	-6.77418
2357.106	6901.682	0.17313	1.36260	1.24815	-1.10862	-5.40831	-5.99084
2360.963	6800.104	1.57873	-0.23353	-0.94181	-3.81131	-4.88481	-3.52813
2356.125	6765.071	1.65934	-1.10855	-1.58726	-4.05729	-7.03534	-7.04485
2381.221	6759.145	1.75644	-3.12057	-3.03446	-3.33421	-7.24184	-7.46755
2420.016	6818.458	0.41275	0.85908	3.63646	-0.90027	-5.50018	-7.40281
2383.075	6803.937	1.73378	-2.14474	0.59012	-2.35066	-5.83234	-3.80764

Continued on next page

Table A.3 – *Continued from previous page*

Y	X	alrMn_3O_4	alrFe_2O_3	alrSiO_2	alrAl_2O_3	alrPbO	alrP_2O_5
2416.887	6903.895	1.11930	1.60388	1.30500	-4.73359	-6.12842	-4.38766
2420.207	6860.162	0.80954	1.02880	2.36677	-1.78582	-5.22318	-3.88486
2360.027	6960.889	-2.82981	-1.40206	-0.16724	-2.48118	-8.61257	-5.90095
2359.239	6920.115	1.83355	0.38595	0.20605	-2.52800	-6.82560	-3.18779
2359.534	6824.749	0.42870	2.12162	1.30677	-1.09859	-5.96273	-4.02485
2378.948	6818.953	0.77654	1.91821	1.25467	-1.85543	-3.62222	-3.39729
2378.804	6842.849	1.52301	-1.91059	1.41605	-3.18198	-6.41026	-4.90736
2379.592	6861.798	1.46980	-0.16380	-0.81229	-3.12093	-6.64539	-4.01610
2374.138	6875.678	1.91669	-0.18892	-0.15852	-2.71967	-6.09965	-6.03836
2379.671	6899.929	1.34756	0.31117	0.21265	-1.56875	-6.44337	-4.98139
2383.084	6730.916	1.62408	0.66747	0.21723	-2.95216	-5.66756	-5.32492
2466.915	6691.154	1.54662	1.20941	0.52039	-1.78096	-5.96970	-5.58372
2391.703	6943.298	1.75384	-0.63967	0.22497	-3.42103	-7.33754	-4.61899
2378.542	6980.031	-0.54568	3.25268	0.64958	-1.63357	-6.12712	-3.53028
2471.044	6750.638	0.76739	2.11191	1.59900	-1.38107	-3.63136	-4.60719
2384.666	6642.159	1.46717	-0.06186	0.44171	-1.00233	-3.36731	-4.79052
2436.39	6677.387	1.77190	-0.74932	-0.48233	-2.28846	-5.78786	-5.31156
2442.088	6666.025	1.62524	-1.09149	-0.29214	-2.72432	-6.19261	-6.23066
2417.681	6982.476	1.10700	1.63279	0.52327	-2.37707	-5.67892	-3.97331
2433.771	6702.473	1.45859	-0.90103	-0.20672	-1.17585	-4.87316	-5.78376
2411.278	6638.158	1.51758	-1.30573	-1.25063	-2.08917	-5.53381	-5.93581
2417.533	6662.891	1.26238	1.08614	0.31137	-1.35719	-5.88047	-6.38104
2398.923	6683.488	1.51256	-0.50808	-0.51018	-1.65495	-4.94875	-5.19608
2405.721	6702.492	1.68573	0.12887	1.21122	-1.56894	-5.28159	-5.93502
2398.409	6903.61	1.55104	-0.95086	-0.33226	-3.66494	-6.61179	-4.03084
2365.786	6899.051	1.32116	1.06499	0.34808	-2.29331	-6.63112	-4.77473
2398.352	6984.062	1.89722	-1.85054	-0.14948	-2.45626	-5.32137	-4.59570
2458.441	6681.053	1.37391	0.73689	-0.55099	-3.08890	-5.38295	-6.23973
2379.274	6963.501	1.99225	-0.28146	0.02718	-2.64291	-6.97442	-4.86931
2458.776	6779.174	0.90291	-0.29025	0.89866	-1.48079	-4.97738	-6.31792
2401.793	6934.536	0.26035	1.59467	1.19496	-1.26694	-6.74958	-2.75373
2478.044	6700.146	0.94376	2.07967	-1.08490	-3.05157	-6.06570	-4.43699
2455.85	6700.454	1.64585	-1.31400	-3.29279	-3.78335	-5.81063	-7.52005

Continued on next page

Table A.3 – *Continued from previous page*

Y	X	alrMn_3O_4	alrFe_2O_3	alrSiO_2	alrAl_2O_3	alrPbO	alrP_2O_5
2477.808	6719.316	0.37834	2.11363	0.59072	-2.94630	-6.26595	-8.58680
2456.621	6719.351	1.60325	-1.25527	-3.20269	-3.87732	-4.23566	-6.12054
2398.801	6888.101	1.68739	-2.28917	-2.55390	-4.19712	-3.67962	-8.20399
2438.859	6718.597	1.57617	-2.22085	-0.06037	-3.69071	-6.88966	-8.40825
2442.537	6743.804	1.29780	-0.02965	-0.10921	-2.40034	-5.78659	-6.19526
2342.924	6876.319	-1.25512	-1.86028	-0.00291	-3.77994	-7.44277	-6.93911
2425.743	6921.554	0.18576	0.11071	2.59219	-3.41206	-5.95142	-3.82161
2395.415	6958.762	2.15842	-1.95981	0.24932	-2.66153	-6.62861	-2.85055
2398.51	6920.253	1.54072	-1.42095	0.55880	-4.69598	-6.39815	-5.28796
2408.824	6761.539	0.06357	1.72971	0.75486	-1.64309	-5.51787	-3.15464
2368.096	6788.014	1.43096	0.81168	-0.03289	-2.80785	-4.19419	-4.77267
2408.52	6778.917	-0.35879	2.41895	0.33016	-1.61200	-6.19743	-5.51504
2397.559	6832.288	1.61569	-0.15793	0.81785	-3.27091	-6.65859	-5.52554
2355.551	6810.876	1.15913	3.19514	0.11297	-1.79543	-5.09558	-3.59746
2329.006	6779.523	0.84264	3.50619	1.44307	-1.56242	-4.99599	-4.60229
2356.133	6877.771	0.69644	0.51634	2.70387	-0.69777	-5.54580	-4.44581
2423.946	6967.833	0.96585	2.02682	2.84321	0.04144	-4.61559	1.76760
2423.67	6959.537	-0.82257	-0.35389	2.16749	-0.71233	-6.41698	-1.41676
2423.883	6952.313	1.76724	2.78836	3.44073	-0.25589	-3.81420	0.64040
2369.157	6864.539	1.77168	-1.72895	-0.87216	-3.51609	-6.63507	-4.15652
2367.67	6856.584	1.40765	1.18667	-0.46724	-2.10785	-6.04886	-6.40107
2367.24	6848.788	1.64714	-2.54549	-1.06692	-2.32448	-6.65804	-6.86416
2367.332	6840.723	1.58439	-2.35896	-1.87129	-2.85574	-6.73808	-7.17143
2367.308	6832.551	1.49932	-2.53101	-1.65281	-3.35228	-7.22205	-7.89475
2368.832	6824.921	0.13644	3.74015	2.11573	-2.00337	-6.48149	-5.34131
2375.382	6976.794	1.20700	2.89532	1.65314	-1.69357	-5.41093	-4.30832
2375.609	6966.656	2.12828	-0.65856	1.14648	-3.21545	-5.63577	-4.83478
2375.624	6959.855	1.89753	-0.61625	-0.69588	-2.70850	-6.71944	-4.17745
2375.391	6952.2	1.60552	0.46707	-0.59836	-2.30295	-6.28351	-4.98075
2375.473	6944.491	1.75678	-0.24579	0.44791	-2.10304	-6.16650	-5.33515
2375.493	6935.891	1.85534	-2.39590	-0.27731	-3.06746	-5.86674	-5.62076
2375.59	6928.275	1.67592	-2.43964	-0.52326	-3.05660	-5.91048	-6.45802
2375.325	6918.857	1.81053	-2.06268	-0.68187	-3.57547	-6.73148	-5.90075

Continued on next page

Table A.3 – *Continued from previous page*

Y	X	alrMn_3O_4	alrFe_2O_3	alrSiO_2	alrAl_2O_3	alrPbO	alrP_2O_5
2375.499	6911.589	1.77844	-1.66465	-0.75061	-3.12422	-5.13549	-6.17182
2375.599	6904.483	1.44459	0.18295	-1.03426	-2.09183	-5.19476	-5.83962
2375.545	6895.477	1.54750	0.32399	-0.34872	-3.58143	-6.74514	-6.17576
2375.722	6889.343	1.68484	-0.39976	-0.84419	-3.60876	-6.42475	-5.78529
2375.612	6879.603	1.80911	-0.73128	0.39469	-2.59380	-6.92247	-6.43293
2375.804	6871.762	1.63344	-2.70543	-2.34904	-4.22283	-4.09589	-5.93388
2375.512	6864.24	1.72684	-1.48327	-1.41392	-3.17702	-4.95411	-7.90230
2375.761	6856.548	1.47733	-0.26969	-0.91059	-2.92459	-6.65629	-6.53429
2375.212	6849.26	1.60044	-2.88649	-2.41073	-3.20537	-7.22700	-6.87968
2375.327	6840.449	1.62837	-2.30069	0.69771	-3.54952	-7.27789	-8.44670
2375.468	6832.851	1.63681	-1.81922	-2.19166	-3.90485	-3.22463	-5.38339
2375.662	6825.549	1.58525	1.56815	0.27104	-3.27618	-6.64861	-7.24322
2377.296	6814.702	1.74995	-0.80582	0.54326	-3.52434	-5.79048	-5.92181
2376.49	6807.527	1.45833	-0.51325	1.44890	-3.10019	-7.21113	-4.44550
2376.444	6799.564	1.61858	-2.37129	-2.64911	-2.68630	-4.66401	-4.67404
2376.454	6791.758	1.67715	-2.15362	-0.98824	-2.85680	-7.20487	-8.24235
2375.263	6783.885	1.57007	0.53364	-0.22286	-2.11265	-4.73039	-6.29818
2384.078	6983.926	1.45277	1.85549	-0.43165	-3.05651	-5.86427	-4.35109
2383.662	6976.286	1.74310	1.04813	-0.78352	-2.60287	-6.46868	-5.50838
2383.878	6968.159	2.03691	1.05221	0.17570	-3.01205	-6.22072	-5.90943
2383.812	6960.586	2.18335	-1.59304	0.56966	-3.06517	-6.26185	-5.53495
2383.686	6952.954	2.14255	-1.96653	0.65992	-3.04126	-6.46620	-4.92380
2384.047	6947.026	2.03287	-2.37143	-0.57825	-4.01874	-7.04024	-5.34961
2383.44	6936.069	1.68472	-2.86845	-0.93792	-2.54771	-6.88127	-6.77026
2383.129	6928.146	1.89523	-4.06077	-1.99760	-3.92182	-7.82945	-6.97990
2383.559	6912.26	2.25245	-2.23423	-0.21731	-2.33410	-6.66765	-7.04396
2383.518	6897.249	1.67525	-2.39582	-1.56186	-4.08268	-5.20998	-6.40467
2383.777	6889.217	1.67654	-1.45330	0.05179	-4.19475	-6.12211	-7.10753
2383.586	6880.35	1.72481	-2.33223	-0.93942	-3.55932	-7.23835	-5.57164
2383.194	6872.099	2.16752	-1.42871	0.18666	-2.32203	-5.44034	-6.16356
2383.085	6864.167	1.62148	-1.35879	-1.02990	-2.93751	-5.58687	-5.88241
2383.468	6857.229	1.50530	-0.35298	-1.05666	-3.33673	-6.11807	-5.92879
2383.422	6850.111	1.84646	-3.79925	-3.13187	-4.21028	-6.13446	-7.26932

Continued on next page

Table A.3 – *Continued from previous page*

Y	X	alrMn_3O_4	alrFe_2O_3	alrSiO_2	alrAl_2O_3	alrPbO	alrP_2O_5
2383.467	6840.381	1.79899	-2.48674	-3.16330	-3.96408	-5.68114	-9.40348
2383.457	6832.514	1.64751	-1.14209	-0.74536	-3.82568	-6.80302	-8.87490
2383.601	6824.403	1.76646	-1.97289	0.89203	-3.94860	-6.64170	-6.23351
2383.75	6816.79	1.72693	-2.28748	1.31063	-3.40206	-6.78715	-5.25159
2384.535	6807.577	1.76210	-2.35836	0.39306	-3.53382	-7.33557	-4.99735
2383.78	6799.951	1.67572	-2.03291	1.37353	-2.98347	-6.53259	-5.34721
2382.788	6792.388	1.54512	-2.30416	0.55166	-3.22670	-6.80383	-4.73771
2383.099	6783.901	1.52580	-1.25222	1.03571	-2.03754	-5.26386	-5.13249
2384.674	6905.614	1.97974	-2.25523	-0.38894	-2.10489	-6.43845	-4.76984
2391.248	6984.029	1.73738	0.13855	-0.84383	-2.73471	-6.67693	-5.18419
2392.56	6977.067	2.06692	-1.52067	-0.58479	-3.22945	-4.99151	-6.19676
2391.476	6967.279	2.01209	-1.77450	0.06972	-2.93573	-6.44330	-6.13131
2391.307	6960.238	2.15069	-2.15593	0.09393	-3.08789	-6.82473	-5.29814
2390.772	6950.103	1.98762	-2.22854	0.29199	-3.12856	-6.89735	-5.37139
2391.751	6936.236	1.69902	-2.76444	-0.25088	-3.94079	-7.43325	-5.68297
2391.679	6928.593	1.83410	-1.97787	1.30213	-3.43512	-6.95508	-5.92601
2391.763	6922.944	1.62612	-2.56517	0.42757	-4.11286	-7.23398	-5.15442
2391.913	6912.608	1.50976	-0.08849	1.38815	-3.56360	-6.78637	-4.06313
2391.533	6904.717	1.54499	-0.28099	1.29486	-2.58574	-6.97887	-3.68173
2390.964	6896.965	1.74000	-0.25746	-0.18985	-2.58714	-6.36065	-3.79924
2391.978	6888.581	1.65603	-1.87130	-0.24675	-3.72454	-6.54010	-6.23092
2391.595	6880.28	1.61672	-2.73393	-0.31282	-4.02368	-7.40274	-6.25414
2391.448	6871.757	2.60886	-1.18228	1.87676	-2.12715	-5.68195	-5.12495
2390.662	6864.236	2.28931	-1.81051	0.23714	-2.85361	-6.47932	-4.63703
2391.274	6857.376	1.64750	-1.61389	-0.96764	-3.45848	-5.08473	-5.95202
2391.353	6848.969	1.71493	-2.74874	-2.20980	-3.19475	-7.12786	-6.70657
2391.067	6832.191	1.53322	-0.36432	0.45053	-2.88665	-7.06220	-6.71555
2391.411	6824.588	1.69450	-2.24714	0.09912	-4.02364	-6.91595	-5.42577
2391.704	6816.579	0.93422	1.99926	-0.72639	-2.24987	-6.15901	-3.65832
2391.501	6808.934	0.86473	1.39672	-1.97855	-2.84742	-4.66143	-4.73890
2391.286	6801.055	1.55397	-2.32082	-2.50329	-2.44629	-6.93904	-7.83470
2391.992	6784.711	1.55165	-2.02780	-1.71467	-2.43924	-5.97831	-7.60160
2400.391	6984.117	1.87587	-1.51197	-0.76038	-3.40563	-4.98281	-7.25556

Continued on next page

Table A.3 – *Continued from previous page*

Y	X	alrMn_3O_4	alrFe_2O_3	alrSiO_2	alrAl_2O_3	alrPbO	alrP_2O_5
2399.665	6976.404	1.88845	-2.32720	-0.90877	-3.47029	-7.01825	-6.32680
2399.084	6968.397	1.93395	-2.40970	-0.79311	-3.49051	-7.10075	-6.65214
2399.84	6959.245	2.08153	-2.00842	-0.58339	-2.96290	-5.47926	-5.98228
2399.915	6951.591	2.26796	-1.86162	0.36679	-3.01598	-6.53042	-6.03706
2400.059	6942.891	2.07216	-2.16123	-0.53490	-3.36481	-6.85227	-5.38524
2399.781	6928.335	1.58029	-0.97453	1.19265	-3.66438	-5.95919	-6.23153
2399.872	6911.639	1.83614	-0.61308	-0.30898	-3.79768	-6.27401	-3.98184
2399.876	6897.011	1.69853	-2.29045	-1.06407	-4.36252	-6.95925	-6.53753
2399.544	6879.552	1.48509	-0.79325	-0.04648	-2.88440	-5.89437	-6.27393
2399.718	6872.078	1.63196	-2.37323	0.60999	-3.63715	-7.35044	-6.53786
2399.855	6853.223	1.69187	-2.58096	0.67671	-3.87583	-7.24977	-5.36205
2399.966	6849.337	1.66939	-2.41006	-2.49557	-3.43305	-5.28539	-5.42803
2399.846	6840.409	1.57917	-2.17968	-0.86664	-3.99652	-6.84849	-8.39112
2399.608	6826.193	1.34866	0.61505	1.68195	-1.09131	-4.96744	-5.08480
2398.385	6808.464	-0.02173	4.15997	2.61312	0.27118	-4.54704	-2.33992
2398.984	6792.032	1.64595	-1.89854	-3.81021	-3.31806	-7.22569	-5.28773
2400.001	6784.539	1.59540	-3.38564	-4.54586	-3.98544	-6.50328	-9.34162
2407.163	6904.156	1.80579	-1.74282	-1.92749	-4.17366	-2.93933	-10.05781
2407.837	6984.295	1.98738	-0.90967	-0.69757	-3.34464	-6.91309	-7.35631
2407.731	6968.131	1.92224	-2.94179	-1.11228	-4.11077	-5.75595	-6.59809
2407.622	6960.463	2.05670	-2.40765	-0.39183	-3.68143	-7.07646	-6.64326
2407.534	6952.607	1.98180	-0.98280	-0.69595	-3.32841	-6.64373	-5.80257
2407.909	6944.465	1.87241	-1.81436	-1.26497	-4.46125	-6.72048	-6.13187
2407.878	6936.465	0.99980	3.02588	1.96497	-2.55183	-5.61813	-4.83240
2408.021	6928.519	1.48575	3.08500	1.79296	-2.79001	-5.15855	-3.87655
2407.738	6920.342	1.61547	0.70054	1.07308	-4.40594	-6.24450	-4.46413
2408.137	6912.433	1.61804	0.69276	-1.12789	-3.92119	-6.70845	-4.59414
2407.454	6896.702	1.69999	-1.97282	-2.63145	-4.20419	-3.66442	-6.84990

Table A.4: Raw Data, Reduced Dataset

Y	X	Mn	Fe	SiO_2	Al_2O_3	Pb	P
2423.946	6967.833	5.361	15.040	48.647	2.953	0.026	1.385
2423.883	6952.313	7.397	19.941	54.742	1.358	0.036	0.271
2369.157	6864.539	56.307	1.650	5.557	0.395	0.016	0.023
2367.24	6848.788	55.697	0.817	5.124	1.457	0.018	0.014
2367.308	6832.551	55.757	0.962	3.310	0.605	0.012	0.016
2368.832	6824.921	1.567	55.894	15.745	0.256	0.003	0.017
2375.609	6966.656	46.131	2.760	23.993	0.306	0.025	0.020
2375.391	6952.2	43.568	13.551	6.676	1.214	0.021	0.090
2375.493	6935.891	55.517	0.768	9.135	0.561	0.032	0.016
2375.325	6918.857	56.615	1.143	6.501	0.360	0.014	0.026
2375.599	6904.483	44.083	12.122	5.131	1.782	0.074	0.042
2375.722	6889.343	51.618	6.233	5.714	0.360	0.020	0.028
2375.804	6871.762	58.392	0.740	1.511	0.232	0.245	0.016
2375.761	6856.548	47.790	8.088	6.092	0.813	0.018	0.040
2375.327	6840.449	44.573	0.851	24.399	0.349	0.008	0.011
2375.662	6825.549	29.224	27.896	10.901	0.314	0.010	0.021
2376.49	6807.527	30.318	4.099	41.695	0.441	0.007	0.037
2376.454	6791.758	55.877	1.177	5.397	0.833	0.010	0.020
2383.662	6976.286	40.743	19.745	4.521	0.733	0.014	0.047
2383.812	6960.586	53.729	1.195	14.855	0.392	0.015	0.022
2384.047	6947.026	59.055	0.701	6.022	0.193	0.009	0.019
2383.129	6928.146	61.228	0.154	1.733	0.253	0.005	0.013
2383.559	6912.26	59.460	0.650	6.984	0.841	0.010	0.027
2383.518	6897.249	57.713	0.956	3.147	0.253	0.076	0.022
2383.586	6880.35	56.671	0.952	5.480	0.399	0.009	0.024
2383.085	6864.167	54.130	2.669	5.302	0.787	0.052	0.024
2383.422	6850.111	61.512	0.211	0.588	0.200	0.027	0.011
2383.457	6832.514	53.365	3.184	6.769	0.311	0.015	0.021
2383.75	6816.79	38.676	0.678	35.410	0.318	0.010	0.012
2383.78	6799.951	36.722	0.874	37.685	0.483	0.013	0.016
2383.099	6783.901	37.459	2.261	31.856	1.474	0.054	0.018
2391.248	6984.029	49.120	9.641	5.161	0.779	0.014	0.056

Continued on next page

Table A.4 – *Continued from previous page*

Y	X	Mn	Fe	SiO_2	Al_2O_3	Pb	P
2391.476	6967.279	55.097	1.213	10.966	0.543	0.015	0.024
2390.772	6950.103	53.673	0.769	13.672	0.447	0.010	0.029
2391.751	6936.236	53.716	0.601	10.611	0.265	0.007	0.021
2391.763	6922.944	47.453	0.697	19.871	0.212	0.009	0.014
2391.533	6904.717	33.122	5.180	35.807	0.739	0.008	0.040
2391.978	6888.581	52.398	1.495	10.850	0.335	0.019	0.017
2391.448	6871.757	45.401	0.995	30.311	0.553	0.015	0.016
2391.274	6857.376	54.911	2.044	5.577	0.462	0.084	0.023
2391.067	6832.191	41.953	6.108	19.726	0.701	0.010	0.058
2391.411	6824.588	51.078	0.963	14.383	0.233	0.012	0.018
2391.501	6808.934	22.413	37.048	1.812	0.760	0.115	0.166
2391.992	6784.711	55.534	1.504	2.941	1.425	0.038	0.037
2399.665	6976.404	58.459	0.838	4.949	0.382	0.010	0.024
2399.84	6959.245	59.121	0.961	5.713	0.529	0.040	0.030
2400.059	6942.891	59.079	0.832	6.049	0.357	0.010	0.025
2399.781	6928.335	36.592	2.761	34.476	0.268	0.025	0.021
2399.544	6879.552	46.208	4.597	13.869	0.812	0.037	0.034
2399.966	6849.337	58.625	0.963	1.264	0.495	0.072	0.018
2399.608	6826.193	22.329	10.411	43.261	2.702	0.052	0.047
2398.984	6792.032	58.368	1.637	0.346	0.566	0.011	0.029
2400.001	6784.539	59.239	0.395	0.177	0.310	0.023	0.024
2407.837	6984.295	56.918	3.050	5.391	0.382	0.010	0.022
2407.731	6968.131	59.769	0.448	3.991	0.199	0.036	0.019
2407.878	6936.465	6.204	45.689	22.611	0.247	0.011	0.044
2407.738	6920.342	32.954	12.817	26.597	0.111	0.016	0.036
2407.454	6896.702	58.617	1.446	1.070	0.222	0.354	0.025
2408.057	6872.713	5.807	47.223	21.280	0.463	0.010	0.024
2407.792	6856.414	43.901	1.872	24.641	0.422	0.017	0.014
2407.792	6850.025	5.078	13.136	62.046	5.877	0.010	0.047
2406.285	6843.427	4.078	11.783	70.756	2.646	0.060	0.053
2407.652	6832.305	4.963	4.587	82.633	1.413	0.014	0.024
2408.999	6809.953	0.551	1.033	94.948	2.026	0.003	0.003
2415.581	6944.285	24.952	24.525	19.209	0.270	0.085	0.067

Continued on next page

Table A.4 – *Continued from previous page*

Y	X	Mn	Fe	SiO_2	Al_2O_3	Pb	P
2415.732	6928.147	46.685	13.185	3.405	0.191	0.020	0.038
2415.409	6887.667	0.765	39.951	38.033	1.115	0.008	0.021
2414.84	6880.634	0.832	42.633	34.030	1.333	0.010	0.011
2416.302	6872.881	0.852	18.911	68.741	1.178	0.020	0.010
2416.977	6865.051	9.617	5.947	71.107	1.877	0.018	0.024
2415.478	6848.18	3.868	5.443	81.117	2.467	0.012	0.018
2415.467	6792.862	1.470	30.000	46.200	4.370	0.020	0.016
2386.39	6839.868	54.152	5.142	2.892	0.489	0.025	0.030
2381.696	6973.955	47.509	7.527	12.640	0.767	0.027	0.034
2375.878	6949.893	38.505	16.005	9.358	1.417	0.030	0.108
2407.532	6949.918	55.006	4.313	4.905	0.391	0.025	0.046
2415.35	6941.762	33.925	23.180	6.724	0.694	0.021	0.054
2363.876	6934.111	30.162	24.373	10.812	1.093	0.034	0.052
2375.13	6933.885	55.665	0.658	6.450	0.385	0.008	0.015
2407.353	6933.803	5.385	47.410	22.077	0.159	0.009	0.029
2367.095	6909.846	49.669	8.449	4.955	0.496	0.029	0.063
2383.463	6910.002	56.380	0.705	9.093	1.801	0.015	0.021
2399.671	6909.963	51.642	3.594	7.682	0.233	0.017	0.032
2415.611	6909.848	46.096	12.336	6.460	0.265	0.010	0.023
2365.392	6893.821	32.513	18.572	17.910	0.535	0.020	0.031
2381.269	6893.991	40.019	13.658	13.295	0.352	0.017	0.023
2376.101	6869.926	56.467	1.883	3.220	0.397	0.622	0.023
2391.969	6869.954	45.694	1.902	28.245	0.606	0.017	0.018
2423.918	6869.835	7.970	6.468	70.949	3.578	0.020	0.027
2359.662	6862.472	57.685	0.821	3.454	0.656	0.010	0.015
2368.065	6862.018	56.988	1.454	5.267	0.741	0.060	0.020
2352.092	6854.373	18.527	23.691	24.709	3.764	0.093	0.056
2352.091	6846.201	1.371	8.525	77.644	3.031	0.009	0.102
2367.793	6845.839	55.910	0.756	3.526	1.320	0.022	0.015
2383.787	6846.099	41.684	0.366	30.790	0.268	0.003	0.012
2399.825	6846.147	36.879	0.780	38.302	0.264	0.007	0.013
2352.256	6838.216	12.153	3.575	36.247	0.444	0.005	0.019
2375.918	6838.074	40.710	17.843	2.508	0.422	0.045	0.167

Continued on next page

Table A.4 – *Continued from previous page*

Y	X	Mn	Fe	SiO_2	Al_2O_3	Pb	P
2360.126	6830.17	5.550	30.300	36.900	5.440	0.010	0.026
2383.972	6830.018	46.574	8.767	10.523	0.331	0.010	0.048
2391.445	6829.331	54.792	1.131	6.521	0.377	0.090	0.017
2503.627	6797.582	11.168	7.776	67.849	1.196	0.074	0.015
2496.716	6717.443	3.292	3.269	83.984	2.212	0.007	0.022
2474.209	6700.106	3.564	43.759	20.225	6.014	0.010	0.012
2488.167	6701.753	1.800	5.220	80.200	5.480	0.014	0.007
2476.675	6693.745	45.831	14.432	2.044	1.375	0.019	0.034
2466.645	6684.517	36.000	17.500	13.400	1.150	0.035	0.031
2459.975	6678.687	0.909	30.907	44.503	5.373	0.018	0.010
2452.027	6670.445	42.925	1.802	23.287	1.657	0.051	0.014
2460.44	6669.989	1.220	32.886	44.644	2.925	0.010	0.023
2435.466	6661.795	47.354	3.133	14.302	3.259	0.075	0.018
2439.818	6662.37	47.995	2.308	13.303	2.998	0.010	0.017
2447.937	6662.579	36.750	16.788	11.085	1.425	0.082	0.024
2456.911	6661.773	1.457	11.324	71.745	5.201	0.014	0.009
2410.023	6653.005	22.300	10.400	44.500	1.490	0.340	0.034
2415.97	6653.736	34.500	7.560	25.300	3.720	0.430	0.035
2423.795	6653.876	50.943	7.384	3.867	1.953	0.056	0.031
2432.385	6653.919	30.800	9.513	28.255	4.447	0.205	0.040
2440.644	6653.822	47.321	0.816	19.234	2.329	0.136	0.011
2448.413	6653.42	33.748	23.326	6.344	1.437	0.020	0.079
2456.083	6653.483	2.171	4.604	87.777	1.182	0.006	0.002
2424.033	6645.857	47.281	5.472	11.047	1.890	0.142	0.028
2439.549	6646.255	50.162	1.415	15.832	1.069	0.034	0.014
2432.01	6637.622	36.619	6.948	21.950	4.061	0.055	0.045
2424.13	6630.048	3.551	21.843	58.308	1.838	0.009	0.019
2389.528	6985.378	2.175	39.791	36.069	1.642	0.007	0.021
2408.83	6985.826	57.487	1.211	5.307	0.244	0.015	0.020
2418.611	6975.982	14.361	37.155	21.129	0.663	0.027	0.044
2389.041	6965.995	54.756	1.269	10.591	1.131	0.030	0.021
2409.172	6965.62	59.210	0.810	6.689	0.502	0.008	0.030
2374.583	6955.767	15.772	32.195	19.267	2.303	0.077	0.146

Continued on next page

Table A.4 – *Continued from previous page*

Y	X	Mn	Fe	SiO_2	Al_2O_3	Pb	P
2384.656	6955.56	50.905	0.701	18.159	0.281	0.009	0.024
2404.938	6955.511	56.809	2.029	7.199	0.697	0.084	0.030
2370.855	6945.866	11.405	36.233	24.274	2.059	0.181	0.053
2381.044	6946.139	52.484	2.625	11.661	0.655	0.062	0.040
2400.708	6946.409	57.802	1.790	6.333	0.451	0.018	0.032
2410.788	6945.881	50.725	9.733	2.547	0.160	0.043	0.045
2388.877	6935.626	55.611	0.582	9.600	0.335	0.007	0.018
2387.226	6925.825	44.209	9.082	11.191	0.525	0.010	0.089
2397.167	6926.228	43.433	4.641	19.168	0.319	0.008	0.037
2417.351	6925.859	6.142	37.236	35.050	0.375	0.011	0.026
2369.451	6916.05	52.496	6.724	5.271	0.709	0.031	0.059
2389.889	6915.902	57.229	1.354	4.513	0.509	0.056	0.023
2379.133	6905.78	52.009	5.573	3.061	1.312	0.018	0.033
2389.467	6905.886	54.671	4.728	7.555	0.629	0.016	0.043
2408.877	6906.22	58.477	1.899	2.020	0.154	0.627	0.019
2400.664	6896.032	57.948	1.108	1.954	0.163	0.366	0.014
2410.691	6896.04	52.428	2.530	10.566	0.238	0.032	0.031
2356.895	6885.965	35.503	15.701	15.479	1.086	0.013	0.054
2378.463	6886.275	49.986	6.873	6.078	0.552	0.010	0.052
2388.829	6886.218	55.234	1.124	5.792	0.285	0.014	0.021
2366.537	6876.494	55.724	1.425	4.700	0.378	0.113	0.019
2385.696	6876.49	55.404	0.682	12.021	0.499	0.008	0.019
2395.863	6876.432	46.487	2.296	17.697	0.473	0.029	0.024
2405.653	6876.498	50.791	4.331	8.530	0.396	0.020	0.027
2360.486	6866.217	54.451	2.067	4.131	0.992	0.040	0.019
2369.803	6866.391	57.297	0.763	2.515	0.573	0.009	0.020
2380.367	6856.242	36.172	24.234	3.155	0.714	0.011	0.044
2389.728	6856.189	58.119	0.569	2.103	0.268	0.188	0.014
2410.314	6856.035	53.168	5.078	3.515	0.499	0.060	0.045
2429.609	6676.444	32.548	16.515	19.995	1.735	0.021	0.015
2458.452	6719.395	57.999	2.651	0.570	0.744	0.013	0.016
2467.968	6704.717	3.474	34.714	35.166	5.095	0.010	0.009
2466.976	6726.027	7.227	41.588	25.875	1.258	0.013	0.010

Continued on next page

Table A.4 – *Continued from previous page*

Y	X	Mn	Fe	SiO_2	Al_2O_3	Pb	P
2444.472	6725.992	28.959	21.556	15.200	2.914	0.024	0.020
2455.086	6716.435	58.113	2.068	1.057	0.555	0.009	0.012
2467.148	6706.215	2.977	46.956	21.722	2.923	0.006	0.040
2376.835	6655.633	26.655	9.241	34.900	4.783	0.113	0.021
2436.972	6646.078	10.733	1.823	68.563	7.578	0.273	0.010
2426.976	6646.082	30.877	3.726	39.111	3.017	0.151	0.027
2373.232	6645.282	14.999	22.298	40.228	1.094	0.238	0.031
2436.981	6636.052	4.468	42.646	28.422	1.162	0.008	0.020
2416.93	6636.531	34.070	15.206	14.221	4.324	0.022	0.038
2395.72	6636.761	48.199	3.461	13.997	1.571	0.047	0.023
2406.328	6626.279	9.433	17.612	50.537	4.633	0.069	0.034
2384.63	6626.099	27.455	9.777	36.039	2.597	0.058	0.022
2351.477	6806.151	58.709	1.102	1.699	0.342	0.364	0.015
2343.865	6806.086	2.233	29.470	45.201	4.956	0.010	0.025
2359.706	6797.765	25.376	26.942	12.943	0.332	0.246	0.125
2351.555	6790.371	42.368	20.038	1.088	0.218	0.602	0.011
2363.893	6782.254	52.462	1.365	11.472	0.301	0.017	0.019
2336.767	6781.91	0.514	44.920	34.260	0.225	0.004	0.009
2394.67	6774.256	46.102	1.323	19.261	1.443	0.035	0.024
2374.226	6774.037	35.323	18.847	10.082	2.536	0.032	0.037
2347.47	6774.168	57.534	0.610	4.142	0.277	0.049	0.015
2361.125	6765.413	59.062	1.035	1.634	0.339	0.342	0.017
2367.391	6755.876	57.758	1.745	0.855	0.581	0.064	0.017
2376.496	6746.145	58.554	0.750	2.857	0.456	0.009	0.018
2356.768	6745.869	6.968	58.853	2.330	0.201	0.012	0.031
2377.455	6735.992	59.775	0.391	0.582	0.312	0.029	0.013
2367.086	6735.986	60.017	0.968	0.858	0.349	0.016	0.018
2372.387	6726.083	37.872	9.005	23.339	0.975	0.038	0.016
2386.741	6716.124	2.601	13.115	72.769	2.385	0.007	0.008
2366.384	6716.069	13.085	30.344	32.981	0.746	0.024	0.018
2376.835	6706.001	4.344	3.782	85.851	1.136	0.010	0.005
2357.29	6706.406	1.079	1.011	96.663	0.105	0.002	0.004
2386.762	6695.962	40.860	1.332	29.786	1.645	0.040	0.015

Continued on next page

Table A.4 – *Continued from previous page*

Y	X	Mn	Fe	SiO_2	Al_2O_3	Pb	P
2368.064	6695.374	43.390	5.335	19.454	0.888	0.019	0.037
2446.518	6685.805	52.835	3.119	7.297	2.199	0.032	0.023
2426.866	6685.051	41.604	18.360	3.718	1.014	0.013	0.018

Oxide Data, Reduced Dataset

Y	X	Mn_3O_4	Fe_2O_3	SiO_2	Al_2O_3	PbO	P_2O_5	Service
2423.946	6967.833	7.443	21.503	48.647	2.953	0.028	16.593	2.833
2423.883	6952.313	10.269	28.510	54.742	1.358	0.039	3.328	1.754
2369.157	6864.539	78.171	2.359	5.557	0.395	0.017	0.208	13.293
2367.24	6848.788	77.324	1.168	5.124	1.457	0.019	0.016	14.893
2367.308	6832.551	77.407	1.375	3.310	0.605	0.013	0.006	17.284
2368.832	6824.921	2.175	79.914	15.745	0.256	0.003	0.009	1.898
2375.609	6966.656	64.043	3.946	23.993	0.306	0.027	0.061	7.624
2375.391	6952.2	60.485	19.374	6.676	1.214	0.023	0.083	12.144
2375.493	6935.891	77.074	1.098	9.135	0.561	0.034	0.044	12.054
2375.325	6918.857	78.598	1.634	6.501	0.360	0.015	0.035	12.856
2375.599	6904.483	61.200	17.331	5.131	1.782	0.080	0.042	14.434
2375.722	6889.343	71.661	8.912	5.714	0.360	0.022	0.041	13.291
2375.804	6871.762	81.065	1.058	1.511	0.232	0.263	0.042	15.829
2375.761	6856.548	66.346	11.564	6.092	0.813	0.019	0.022	15.143
2375.327	6840.449	61.880	1.217	24.399	0.349	0.008	0.003	12.144
2375.662	6825.549	40.571	39.884	10.901	0.314	0.011	0.006	8.313
2376.49	6807.527	42.090	5.860	41.695	0.441	0.007	0.115	9.791
2376.454	6791.758	77.574	1.683	5.397	0.833	0.011	0.004	14.499
2383.662	6976.286	56.563	28.230	4.521	0.733	0.015	0.040	9.897
2383.812	6960.586	74.592	1.709	14.855	0.392	0.016	0.033	8.404
2384.047	6947.026	81.986	1.002	6.022	0.193	0.009	0.051	10.737
2383.129	6928.146	85.002	0.220	1.733	0.253	0.005	0.012	12.775
2383.559	6912.26	82.548	0.929	6.984	0.841	0.011	0.008	8.679
2383.518	6897.249	80.122	1.367	3.147	0.253	0.082	0.025	15.004
2383.586	6880.35	78.676	1.361	5.480	0.399	0.010	0.053	14.021

Continued on next page

Table A.5 – *Continued from previous page*

Y	X	Mn_3O_4	Fe_2O_3	SiO_2	Al_2O_3	PbO	P_2O_5	Service
2383.085	6864.167	75.148	3.816	5.302	0.787	0.056	0.041	14.850
2383.422	6850.111	85.397	0.302	0.588	0.200	0.029	0.009	13.475
2383.457	6832.514	74.086	4.552	6.769	0.311	0.016	0.002	14.264
2383.75	6816.79	53.694	0.969	35.410	0.318	0.011	0.050	9.548
2383.78	6799.951	50.981	1.250	37.685	0.483	0.014	0.045	9.542
2383.099	6783.901	52.004	3.233	31.856	1.474	0.059	0.067	11.308
2391.248	6984.029	68.193	13.784	5.161	0.779	0.015	0.067	12.001
2391.476	6967.279	76.491	1.734	10.966	0.543	0.016	0.022	10.228
2390.772	6950.103	74.514	1.099	13.672	0.447	0.010	0.047	10.210
2391.751	6936.236	74.573	0.859	10.611	0.265	0.008	0.046	13.637
2391.763	6922.944	65.879	0.997	19.871	0.212	0.009	0.075	12.958
2391.533	6904.717	45.983	7.406	35.807	0.739	0.009	0.247	9.809
2391.978	6888.581	72.744	2.137	10.850	0.335	0.020	0.027	13.886
2391.448	6871.757	63.030	1.423	30.311	0.553	0.016	0.028	4.640
2391.274	6857.376	76.232	2.922	5.577	0.462	0.091	0.038	14.677
2391.067	6832.191	58.243	8.733	19.726	0.701	0.011	0.015	12.571
2391.411	6824.588	70.911	1.377	14.383	0.233	0.013	0.057	13.026
2391.501	6808.934	31.116	52.969	1.812	0.760	0.124	0.115	13.105
2391.992	6784.711	77.097	2.150	2.941	1.425	0.041	0.008	16.337
2399.665	6976.404	81.158	1.198	4.949	0.382	0.011	0.022	12.280
2399.84	6959.245	82.077	1.374	5.713	0.529	0.043	0.026	10.238
2400.059	6942.891	82.019	1.190	6.049	0.357	0.011	0.047	10.327
2399.781	6928.335	50.800	3.947	34.476	0.268	0.027	0.021	10.461
2399.544	6879.552	64.150	6.572	13.869	0.812	0.040	0.027	14.529
2399.966	6849.337	81.389	1.377	1.264	0.495	0.078	0.067	15.331
2399.608	6826.193	30.999	14.885	43.261	2.702	0.056	0.050	8.047
2398.984	6792.032	81.032	2.340	0.346	0.566	0.011	0.079	15.625
2400.001	6784.539	82.241	0.565	0.177	0.310	0.025	0.001	16.681
2407.837	6984.295	79.019	4.361	5.391	0.382	0.011	0.007	10.830
2407.731	6968.131	82.977	0.641	3.991	0.199	0.038	0.017	12.138
2407.878	6936.465	8.613	65.323	22.611	0.247	0.012	0.025	3.169
2407.738	6920.342	45.750	18.325	26.597	0.111	0.018	0.105	9.095
2407.454	6896.702	81.378	2.067	1.070	0.222	0.381	0.016	14.866

Continued on next page

Table A.5 – *Continued from previous page*

Y	X	Mn_3O_4	Fe_2O_3	SiO_2	Al_2O_3	PbO	P_2O_5	Service
2408.057	6872.713	8.062	67.516	21.280	0.463	0.011	0.094	2.574
2407.792	6856.414	60.947	2.676	24.641	0.422	0.018	0.053	11.241
2407.792	6850.025	7.050	18.781	62.046	5.877	0.011	0.187	6.048
2406.285	6843.427	5.661	16.847	70.756	2.646	0.065	0.531	3.494
2407.652	6832.305	6.890	6.558	82.633	1.413	0.015	0.275	2.215
2408.999	6809.953	0.765	1.477	94.948	2.026	0.003	0.029	0.752
2415.581	6944.285	34.641	35.064	19.209	0.270	0.092	0.043	10.681
2415.732	6928.147	64.812	18.851	3.405	0.191	0.022	0.141	12.578
2415.409	6887.667	1.062	57.119	38.033	1.115	0.009	0.234	2.428
2414.84	6880.634	1.155	60.954	34.030	1.333	0.011	0.068	2.450
2416.302	6872.881	1.183	27.038	68.741	1.178	0.022	0.055	1.784
2416.977	6865.051	13.351	8.503	71.107	1.877	0.020	0.266	4.876
2415.478	6848.18	5.370	7.782	81.117	2.467	0.013	0.212	3.039
2415.467	6792.862	2.041	42.892	46.200	4.370	0.022	0.206	4.269
2386.39	6839.868	75.179	7.352	2.892	0.489	0.027	0.224	13.837
2381.696	6973.955	65.956	10.762	12.640	0.767	0.029	0.032	9.814
2375.878	6949.893	53.456	22.883	9.358	1.417	0.032	0.221	12.634
2407.532	6949.918	76.364	6.166	4.905	0.391	0.027	0.071	12.074
2415.35	6941.762	47.098	33.141	6.724	0.694	0.023	0.054	12.266
2363.876	6934.111	41.874	34.847	10.812	1.093	0.037	0.057	11.281
2375.13	6933.885	77.279	0.941	6.450	0.385	0.009	0.026	14.910
2407.353	6933.803	7.476	67.784	22.077	0.159	0.010	0.012	2.482
2367.095	6909.846	68.955	12.080	4.955	0.496	0.031	0.046	13.437
2383.463	6910.002	78.272	1.008	9.093	1.801	0.016	0.033	9.777
2399.671	6909.963	71.694	5.138	7.682	0.233	0.018	0.172	15.062
2415.611	6909.848	63.995	17.637	6.460	0.265	0.011	0.029	11.604
2365.392	6893.821	45.138	26.553	17.910	0.535	0.022	0.008	9.835
2381.269	6893.991	55.558	19.527	13.295	0.352	0.018	0.067	11.183
2376.101	6869.926	78.393	2.692	3.220	0.397	0.670	0.049	14.578
2391.969	6869.954	63.437	2.719	28.245	0.606	0.019	0.058	4.916
2423.918	6869.835	11.065	9.248	70.949	3.578	0.022	0.170	4.969
2359.662	6862.472	80.084	1.174	3.454	0.656	0.011	0.172	14.450
2368.065	6862.018	79.116	2.079	5.267	0.741	0.065	0.011	12.721

Continued on next page

Table A.5 – *Continued from previous page*

Y	X	Mn_3O_4	Fe_2O_3	SiO_2	Al_2O_3	PbO	P_2O_5	Service
2352.092	6854.373	25.721	33.872	24.709	3.764	0.100	0.798	11.036
2352.091	6846.201	1.903	12.188	77.644	3.031	0.010	0.412	4.811
2367.793	6845.839	77.619	1.081	3.526	1.320	0.024	0.188	16.242
2383.787	6846.099	57.870	0.523	30.790	0.268	0.004	0.007	10.539
2399.825	6846.147	51.199	1.115	38.302	0.264	0.008	0.005	9.107
2352.256	6838.216	16.872	5.111	36.247	0.444	0.006	0.258	41.062
2375.918	6838.074	56.517	25.511	2.508	0.422	0.049	0.054	14.939
2360.126	6830.17	7.705	43.321	36.900	5.440	0.011	0.314	6.309
2383.972	6830.018	64.658	12.534	10.523	0.331	0.011	0.070	11.873
2391.445	6829.331	76.067	1.617	6.521	0.377	0.097	0.029	15.292
2503.627	6797.582	15.504	11.118	67.849	1.196	0.080	0.187	4.066
2496.716	6717.443	4.570	4.674	83.984	2.212	0.007	0.241	4.311
2474.209	6700.106	4.948	62.564	20.225	6.014	0.011	0.067	6.172
2488.167	6701.753	2.499	7.463	80.200	5.480	0.015	0.023	4.320
2476.675	6693.745	63.627	20.634	2.044	1.375	0.020	0.440	11.860
2466.645	6684.517	49.979	25.020	13.400	1.150	0.037	0.354	10.060
2459.975	6678.687	1.262	44.189	44.503	5.373	0.020	0.001	4.652
2452.027	6670.445	59.592	2.576	23.287	1.657	0.055	0.018	12.813
2460.44	6669.989	1.694	47.018	44.644	2.925	0.011	0.086	3.622
2435.466	6661.795	65.741	4.479	14.302	3.259	0.081	0.130	12.008
2439.818	6662.37	66.631	3.300	13.303	2.998	0.011	0.039	13.718
2447.937	6662.579	51.020	24.002	11.085	1.425	0.088	0.052	12.328
2456.911	6661.773	2.023	16.190	71.745	5.201	0.015	0.016	4.810
2410.023	6653.005	30.959	14.869	44.500	1.490	0.366	0.394	7.422
2415.97	6653.736	47.896	10.809	25.300	3.720	0.463	0.252	11.560
2423.795	6653.876	70.724	10.557	3.867	1.953	0.060	0.127	12.712
2432.385	6653.919	42.759	13.601	28.255	4.447	0.221	0.025	10.691
2440.644	6653.822	65.695	1.167	19.234	2.329	0.147	0.050	11.378
2448.413	6653.42	46.852	33.350	6.344	1.437	0.022	0.246	11.750
2456.083	6653.483	3.014	6.582	87.777	1.182	0.006	0.002	1.436
2424.033	6645.857	65.640	7.824	11.047	1.890	0.153	0.130	13.317
2439.549	6646.255	69.640	2.023	15.832	1.069	0.037	0.097	11.302
2432.01	6637.622	50.838	9.934	21.950	4.061	0.059	0.256	12.902

Continued on next page

Table A.5 – *Continued from previous page*

Y	X	Mn_3O_4	Fe_2O_3	SiO_2	Al_2O_3	PbO	P_2O_5	Service
2424.13	6630.048	4.930	31.230	58.308	1.838	0.010	0.094	3.591
2389.528	6985.378	3.020	56.891	36.069	1.642	0.008	0.198	2.173
2408.83	6985.826	79.809	1.731	5.307	0.244	0.016	0.117	12.776
2418.611	6975.982	19.937	53.122	21.129	0.663	0.029	0.085	5.035
2389.041	6965.995	76.017	1.814	10.591	1.131	0.033	0.072	10.342
2409.172	6965.62	82.201	1.158	6.689	0.502	0.009	0.062	9.379
2374.583	6955.767	21.896	46.030	19.267	2.303	0.082	0.734	9.687
2384.656	6955.56	70.671	1.002	18.159	0.281	0.009	0.076	9.802
2404.938	6955.511	78.867	2.901	7.199	0.697	0.090	0.088	10.157
2370.855	6945.866	15.833	51.804	24.274	2.059	0.195	0.062	5.773
2381.044	6946.139	72.863	3.753	11.661	0.655	0.067	0.157	10.844
2400.708	6946.409	80.246	2.559	6.333	0.451	0.019	0.061	10.331
2410.788	6945.881	70.421	13.916	2.547	0.160	0.047	0.046	12.863
2388.877	6935.626	77.204	0.832	9.600	0.335	0.008	0.023	11.998
2387.226	6925.825	61.375	12.985	11.191	0.525	0.011	0.060	13.853
2397.167	6926.228	60.298	6.635	19.168	0.319	0.008	0.067	13.505
2417.351	6925.859	8.527	53.238	35.050	0.375	0.011	0.197	2.602
2369.451	6916.05	72.880	9.614	5.271	0.709	0.033	0.335	11.159
2389.889	6915.902	79.451	1.936	4.513	0.509	0.060	0.020	13.511
2379.133	6905.78	72.204	7.968	3.061	1.312	0.020	0.159	15.277
2389.467	6905.886	75.899	6.760	7.555	0.629	0.017	0.022	9.119
2408.877	6906.22	81.183	2.715	2.020	0.154	0.676	0.023	13.229
2400.664	6896.032	80.449	1.584	1.954	0.163	0.394	0.013	15.443
2410.691	6896.04	72.785	3.617	10.566	0.238	0.034	0.010	12.750
2356.895	6885.965	49.289	22.448	15.479	1.086	0.014	0.092	11.592
2378.463	6886.275	69.395	9.827	6.078	0.552	0.011	0.067	14.071
2388.829	6886.218	76.681	1.607	5.792	0.285	0.015	0.021	15.599
2366.537	6876.494	77.361	2.037	4.700	0.378	0.122	0.100	15.302
2385.696	6876.49	76.917	0.975	12.021	0.499	0.009	0.015	9.564
2395.863	6876.432	64.538	3.283	17.697	0.473	0.031	0.047	13.932
2405.653	6876.498	70.513	6.192	8.530	0.396	0.022	0.077	14.270
2360.486	6866.217	75.594	2.955	4.131	0.992	0.043	0.163	16.122
2369.803	6866.391	79.545	1.091	2.515	0.573	0.010	0.014	16.253

Continued on next page

Table A.5 – *Continued from previous page*

Y	X	Mn_3O_4	Fe_2O_3	SiO_2	Al_2O_3	PbO	P_2O_5	Service
2380.367	6856.242	50.217	34.648	3.155	0.714	0.012	0.207	11.047
2389.728	6856.189	80.686	0.814	2.103	0.268	0.203	0.007	15.919
2410.314	6856.035	73.813	7.260	3.515	0.499	0.065	0.162	14.686
2429.609	6676.444	45.186	23.612	19.995	1.735	0.023	0.004	9.445
2458.452	6719.395	80.520	3.790	0.570	0.744	0.014	0.052	14.311
2467.968	6704.717	4.823	49.632	35.166	5.095	0.011	0.001	5.273
2466.976	6726.027	10.033	59.460	25.875	1.258	0.014	0.057	3.303
2444.472	6725.992	40.204	30.819	15.200	2.914	0.025	0.040	10.798
2455.086	6716.435	80.678	2.957	1.057	0.555	0.010	0.014	14.729
2467.148	6706.215	4.133	67.135	21.722	2.923	0.007	0.007	4.074
2376.835	6655.633	37.005	13.212	34.900	4.783	0.122	0.036	9.942
2436.972	6646.078	14.901	2.606	68.563	7.578	0.294	0.056	6.002
2426.976	6646.082	42.866	5.327	39.111	3.017	0.163	0.299	9.217
2373.232	6645.282	20.823	31.880	40.228	1.094	0.256	0.211	5.508
2436.981	6636.052	6.203	60.972	28.422	1.162	0.009	0.130	3.102
2416.93	6636.531	47.299	21.741	14.221	4.324	0.024	0.175	12.217
2395.72	6636.761	66.914	4.948	13.997	1.571	0.051	0.040	12.479
2406.328	6626.279	13.096	25.180	50.537	4.633	0.074	0.199	6.281
2384.63	6626.099	38.116	13.979	36.039	2.597	0.062	0.053	9.154
2351.477	6806.151	81.505	1.576	1.699	0.342	0.392	0.036	14.450
2343.865	6806.086	3.100	42.134	45.201	4.956	0.011	0.007	4.591
2359.706	6797.765	35.229	38.520	12.943	0.332	0.265	0.912	11.799
2351.555	6790.371	58.819	28.649	1.088	0.218	0.648	0.010	10.568
2363.893	6782.254	72.833	1.952	11.472	0.301	0.018	0.046	13.379
2336.767	6781.91	0.714	64.224	34.260	0.225	0.004	0.003	0.571
2394.67	6774.256	64.003	1.892	19.261	1.443	0.037	0.133	13.231
2374.226	6774.037	49.039	26.946	10.082	2.536	0.034	0.031	11.331
2347.47	6774.168	79.874	0.872	4.142	0.277	0.052	0.002	14.781
2361.125	6765.413	81.995	1.480	1.634	0.339	0.368	0.011	14.172
2367.391	6755.876	80.185	2.495	0.855	0.581	0.069	0.051	15.764
2376.496	6746.145	81.290	1.072	2.857	0.456	0.010	0.072	14.243
2356.768	6745.869	9.674	84.144	2.330	0.201	0.013	0.001	3.637
2377.455	6735.992	82.985	0.559	0.582	0.312	0.032	0.005	15.525

Continued on next page

Table A.5 – *Continued from previous page*

Y	X	Mn_3O_4	Fe_2O_3	SiO_2	Al_2O_3	PbO	P_2O_5	Service
2367.086	6735.986	83.321	1.384	0.858	0.349	0.017	0.002	14.069
2372.387	6726.083	52.577	12.875	23.339	0.975	0.041	0.023	10.170
2386.741	6716.124	3.611	18.751	72.769	2.385	0.007	0.055	2.422
2366.384	6716.069	18.166	43.384	32.981	0.746	0.026	0.027	4.671
2376.835	6706.001	6.031	5.407	85.851	1.136	0.011	0.066	1.499
2357.29	6706.406	1.498	1.445	96.663	0.105	0.002	0.010	0.277
2386.762	6695.962	56.726	1.904	29.786	1.645	0.043	0.234	9.662
2368.064	6695.374	60.238	7.628	19.454	0.888	0.020	0.178	11.593
2446.518	6685.805	73.350	4.459	7.297	2.199	0.035	0.072	12.587
2426.866	6685.051	57.758	26.250	3.718	1.014	0.014	0.003	11.242

Table A.6: Additive Log-ratio transformed data, Reduced Dataset

Y	X	alrMn_3O_4	alrFe_2O_3	alrSiO_2	alrAl_2O_3	alrPbO	alrP_2O_5
2423.946	6967.833	0.96585	2.02682	2.84321	0.04144	-4.61559	1.76760
2423.883	6952.313	1.76724	2.78836	3.44073	-0.25589	-3.81420	0.64040
2369.157	6864.539	1.77168	-1.72895	-0.87216	-3.51609	-6.63507	-4.15652
2367.24	6848.788	1.64714	-2.54549	-1.06692	-2.32448	-6.65804	-6.86416
2367.308	6832.551	1.49932	-2.53101	-1.65281	-3.35228	-7.22205	-7.89475
2368.832	6824.921	0.13644	3.74015	2.11573	-2.00337	-6.48149	-5.34131
2375.609	6966.656	2.12828	-0.65856	1.14648	-3.21545	-5.63577	-4.83478
2375.391	6952.2	1.60552	0.46707	-0.59836	-2.30295	-6.28351	-4.98075
2375.493	6935.891	1.85534	-2.39590	-0.27731	-3.06746	-5.86674	-5.62076
2375.325	6918.857	1.81053	-2.06268	-0.68187	-3.57547	-6.73148	-5.90075
2375.599	6904.483	1.44459	0.18295	-1.03426	-2.09183	-5.19476	-5.83962
2375.722	6889.343	1.68484	-0.39976	-0.84419	-3.60876	-6.42475	-5.78529
2375.804	6871.762	1.63344	-2.70543	-2.34904	-4.22283	-4.09589	-5.93388
2375.761	6856.548	1.47733	-0.26969	-0.91059	-2.92459	-6.65629	-6.53429
2375.327	6840.449	1.62837	-2.30069	0.69771	-3.54952	-7.27789	-8.44670
2375.662	6825.549	1.58525	1.56815	0.27104	-3.27618	-6.64861	-7.24322
2376.49	6807.527	1.45833	-0.51325	1.44890	-3.10019	-7.21113	-4.44550
2376.454	6791.758	1.67715	-2.15362	-0.98824	-2.85680	-7.20487	-8.24235

Continued on next page

Table A.6 – *Continued from previous page*

Y	X	alrMn_3O_4	alrFe_2O_3	alrSiO_2	alrAl_2O_3	alrPbO	alrP_2O_5
2383.662	6976.286	1.74310	1.04813	-0.78352	-2.60287	-6.46868	-5.50838
2383.812	6960.586	2.18335	-1.59304	0.56966	-3.06517	-6.26185	-5.53495
2384.047	6947.026	2.03287	-2.37143	-0.57825	-4.01874	-7.04024	-5.34961
2383.129	6928.146	1.89523	-4.06077	-1.99760	-3.92182	-7.82945	-6.97990
2383.559	6912.26	2.25245	-2.23423	-0.21731	-2.33410	-6.66765	-7.04396
2383.518	6897.249	1.67525	-2.39582	-1.56186	-4.08268	-5.20998	-6.40467
2383.586	6880.35	1.72481	-2.33223	-0.93942	-3.55932	-7.23835	-5.57164
2383.085	6864.167	1.62148	-1.35879	-1.02990	-2.93751	-5.58687	-5.88241
2383.422	6850.111	1.84646	-3.79925	-3.13187	-4.21028	-6.13446	-7.26932
2383.457	6832.514	1.64751	-1.14209	-0.74536	-3.82568	-6.80302	-8.87490
2383.75	6816.79	1.72693	-2.28748	1.31063	-3.40206	-6.78715	-5.25159
2383.78	6799.951	1.67572	-2.03291	1.37353	-2.98347	-6.53259	-5.34721
2383.099	6783.901	1.52580	-1.25222	1.03571	-2.03754	-5.26386	-5.13249
2391.248	6984.029	1.73738	0.13855	-0.84383	-2.73471	-6.67693	-5.18419
2391.476	6967.279	2.01209	-1.77450	0.06972	-2.93573	-6.44330	-6.13131
2390.772	6950.103	1.98762	-2.22854	0.29199	-3.12856	-6.89735	-5.37139
2391.751	6936.236	1.69902	-2.76444	-0.25088	-3.94079	-7.43325	-5.68297
2391.763	6922.944	1.62612	-2.56517	0.42757	-4.11286	-7.23398	-5.15442
2391.533	6904.717	1.54499	-0.28099	1.29486	-2.58574	-6.97887	-3.68173
2391.978	6888.581	1.65603	-1.87130	-0.24675	-3.72454	-6.54010	-6.23092
2391.448	6871.757	2.60886	-1.18228	1.87676	-2.12715	-5.68195	-5.12495
2391.274	6857.376	1.64750	-1.61389	-0.96764	-3.45848	-5.08473	-5.95202
2391.067	6832.191	1.53322	-0.36432	0.45053	-2.88665	-7.06220	-6.71555
2391.411	6824.588	1.69450	-2.24714	0.09912	-4.02364	-6.91595	-5.42577
2391.501	6808.934	0.86473	1.39672	-1.97855	-2.84742	-4.66143	-4.73890
2391.992	6784.711	1.55165	-2.02780	-1.71467	-2.43924	-5.97831	-7.60160
2399.665	6976.404	1.88845	-2.32720	-0.90877	-3.47029	-7.01825	-6.32680
2399.84	6959.245	2.08153	-2.00842	-0.58339	-2.96290	-5.47926	-5.98228
2400.059	6942.891	2.07216	-2.16123	-0.53490	-3.36481	-6.85227	-5.38524
2399.781	6928.335	1.58029	-0.97453	1.19265	-3.66438	-5.95919	-6.23153
2399.544	6879.552	1.48509	-0.79325	-0.04648	-2.88440	-5.89437	-6.27393
2399.966	6849.337	1.66939	-2.41006	-2.49557	-3.43305	-5.28539	-5.42803
2399.608	6826.193	1.34866	0.61505	1.68195	-1.09131	-4.96744	-5.08480

Continued on next page

Table A.6 – *Continued from previous page*

Y	X	alrMn_3O_4	alrFe_2O_3	alrSiO_2	alrAl_2O_3	alrPbO	alrP_2O_5
2398.984	6792.032	1.64595	-1.89854	-3.81021	-3.31806	-7.22569	-5.28773
2400.001	6784.539	1.59540	-3.38564	-4.54586	-3.98544	-6.50328	-9.34162
2407.837	6984.295	1.98738	-0.90967	-0.69757	-3.34464	-6.91309	-7.35631
2407.731	6968.131	1.92224	-2.94179	-1.11228	-4.11077	-5.75595	-6.59809
2407.878	6936.465	0.99980	3.02588	1.96497	-2.55183	-5.61813	-4.83240
2407.738	6920.342	1.61547	0.70054	1.07308	-4.40594	-6.24450	-4.46413
2407.454	6896.702	1.69999	-1.97282	-2.63145	-4.20419	-3.66442	-6.84990
2408.057	6872.713	1.14154	3.26677	2.11217	-1.71562	-5.47639	-3.31285
2407.792	6856.414	1.69041	-1.43510	0.78481	-3.28235	-6.41976	-5.34821
2407.792	6850.025	0.15320	1.13305	2.32809	-0.02874	-6.33058	-3.47582
2406.285	6843.427	0.48267	1.57314	3.00823	-0.27796	-3.99004	-1.88310
2407.652	6832.305	1.13461	1.08524	3.61894	-0.44976	-4.97690	-2.08664
2408.999	6809.953	0.01711	0.67501	4.83838	0.99112	-5.54851	-3.24739
2415.581	6944.285	1.17653	1.18869	0.58688	-3.67783	-4.75596	-5.51612
2415.732	6928.147	1.63956	0.40463	-1.30670	-4.18742	-6.36812	-4.49046
2415.409	6887.667	-0.82671	3.15824	2.75155	-0.77805	-5.59628	-2.33920
2414.84	6880.634	-0.75178	3.21419	2.63131	-0.60850	-5.42672	-3.58858
2416.302	6872.881	-0.41093	2.71840	3.65151	-0.41501	-4.41648	-3.47967
2416.977	6865.051	1.00729	0.55606	2.67987	-0.95464	-5.50608	-2.90705
2415.478	6848.18	0.56934	0.94034	3.28442	-0.20847	-5.46339	-2.66114
2415.467	6792.862	-0.73813	2.30722	2.38152	0.02330	-5.28911	-3.02994
2386.39	6839.868	1.69249	-0.63245	-1.56543	-3.34277	-6.24188	-4.12288
2381.696	6973.955	1.90521	0.09220	0.25308	-2.54905	-5.82851	-5.71341
2375.878	6949.893	1.44251	0.59403	-0.30012	-2.18781	-5.98528	-4.04779
2407.532	6949.918	1.84443	-0.67197	-0.90083	-3.43014	-6.09087	-5.13004
2415.35	6941.762	1.34536	0.99391	-0.60118	-2.87215	-6.28633	-5.43099
2363.876	6934.111	1.31153	1.12784	-0.04247	-2.33420	-5.72762	-5.29447
2375.13	6933.885	1.64539	-2.76310	-0.83796	-3.65655	-7.45415	-6.34270
2407.353	6933.803	1.10244	3.30707	2.18529	-2.74810	-5.51548	-5.33931
2367.095	6909.846	1.63547	-0.10645	-0.99759	-3.29916	-6.05901	-5.67503
2383.463	6910.002	2.08016	-2.27210	-0.07253	-1.69169	-6.38545	-5.70131
2399.671	6909.963	1.56023	-1.07542	-0.67329	-4.16889	-6.73635	-4.46958
2415.611	6909.848	1.70749	0.41870	-0.58568	-3.77934	-6.98210	-5.99945

Continued on next page

Table A.6 – *Continued from previous page*

Y	X	alrMn_3O_4	alrFe_2O_3	alrSiO_2	alrAl_2O_3	alrPbO	alrP_2O_5
2365.392	6893.821	1.52375	0.99318	0.59939	-2.91146	-6.12361	-7.15310
2381.269	6893.991	1.60305	0.55744	0.17301	-3.45850	-6.41454	-5.12481
2376.101	6869.926	1.68219	-1.68919	-1.51016	-3.60336	-3.07964	-5.68612
2391.969	6869.954	2.55759	-0.59206	1.74846	-2.09333	-5.56926	-4.43125
2423.918	6869.835	0.80046	0.62106	2.65867	-0.32849	-5.44108	-3.37599
2359.662	6862.472	1.71239	-2.51043	-1.43115	-3.09228	-7.20147	-4.43117
2368.065	6862.018	1.82765	-1.81146	-0.88181	-2.84302	-5.28230	-7.01974
2352.092	6854.373	0.84611	1.12139	0.80598	-1.07571	-4.70696	-2.62645
2352.091	6846.201	-0.92728	0.92959	2.78124	-0.46201	-6.16665	-2.45738
2367.793	6845.839	1.56424	-2.70980	-1.52741	-2.50995	-6.53158	-4.45673
2383.787	6846.099	1.70315	-3.00268	1.07215	-3.67181	-7.97988	-7.32028
2399.825	6846.147	1.72666	-2.10003	1.43645	-3.54086	-7.07723	-7.46459
2352.256	6838.216	-0.88943	-2.08363	-0.12473	-4.52701	-8.90041	-5.06906
2375.918	6838.074	1.33057	0.53512	-1.78450	-3.56673	-5.72750	-5.62003
2360.126	6830.17	0.19990	1.92666	1.76624	-0.14819	-6.37276	-2.99942
2383.972	6830.018	1.69487	0.05423	-0.12068	-3.57989	-7.00504	-5.13837
2391.445	6829.331	1.60430	-2.24672	-0.85229	-3.70283	-5.06088	-6.26935
2503.627	6797.582	1.33849	1.00590	2.81465	-1.22365	-3.93357	-3.07678
2496.716	6717.443	0.05829	0.08070	2.96935	-0.66738	-6.38641	-2.88330
2474.209	6700.106	-0.22100	2.31623	1.18696	-0.02587	-6.35075	-4.52263
2488.167	6701.753	-0.54744	0.54669	2.92123	0.23781	-5.67683	-5.24060
2476.675	6693.745	1.67990	0.55380	-1.75823	-2.15468	-6.36207	-3.29360
2466.645	6684.517	1.60302	0.91112	0.28669	-2.16881	-5.59810	-3.34744
2459.975	6678.687	-1.30463	2.25117	2.25826	0.14409	-5.46000	-8.06324
2452.027	6670.445	1.53704	-1.60410	0.59741	-2.04548	-5.44327	-6.54415
2460.44	6669.989	-0.76004	2.56357	2.51175	-0.21367	-5.81776	-3.73472
2435.466	6661.795	1.70016	-0.98608	0.17484	-1.30414	-5.00145	-4.52715
2439.818	6662.37	1.58047	-1.42483	-0.03071	-1.52076	-7.14950	-5.85293
2447.937	6662.579	1.42034	0.66628	-0.10628	-2.15770	-4.93823	-5.47610
2456.911	6661.773	-0.86626	1.21370	2.70241	0.07814	-5.78789	-5.69749
2410.023	6653.005	1.42824	0.69487	1.79107	-1.60564	-3.00885	-2.93631
2415.97	6653.736	1.42152	-0.06716	0.78329	-1.13379	-3.21711	-3.82461
2423.795	6653.876	1.71626	-0.18571	-1.19004	-1.87315	-5.35054	-4.60520

Continued on next page

Table A.6 – *Continued from previous page*

Y	X	alrMn_3O_4	alrFe_2O_3	alrSiO_2	alrAl_2O_3	alrPbO	alrP_2O_5
2432.385	6653.919	1.38615	0.24071	0.97183	-0.87721	-3.87981	-6.04648
2440.644	6653.822	1.75332	-2.27756	0.52497	-1.58627	-4.35243	-5.42364
2448.413	6653.42	1.38315	1.04322	-0.61633	-2.10128	-6.30149	-3.86813
2456.083	6653.483	0.74120	1.52235	4.11274	-0.19486	-5.45291	-6.53750
2424.033	6645.857	1.59513	-0.53192	-0.18689	-1.95247	-4.46660	-4.63259
2439.549	6646.255	1.81833	-1.72039	0.33703	-2.35828	-5.73202	-4.75292
2432.01	6637.622	1.37126	-0.26143	0.53139	-1.15595	-5.38342	-3.91930
2424.13	6630.048	0.31699	2.16306	2.78743	-0.66963	-5.88134	-3.64378
2389.528	6985.378	0.32894	3.26497	2.80927	-0.28025	-5.60322	-2.39671
2408.83	6985.826	1.83207	-1.99863	-0.87853	-3.95815	-6.66743	-4.69566
2418.611	6975.982	1.37620	2.35620	1.43426	-2.02737	-5.15407	-4.08126
2389.041	6965.995	1.99477	-1.74047	0.02381	-2.21309	-5.75211	-4.97087
2409.172	6965.62	2.17064	-2.09176	-0.33806	-2.92768	-6.99788	-5.01762
2374.583	6955.767	0.81552	1.55851	0.68761	-1.43658	-4.76592	-2.57997
2384.656	6955.56	1.97549	-2.28030	0.61662	-3.55194	-6.94911	-4.86243
2404.938	6955.511	2.04958	-1.25316	-0.34425	-2.67916	-4.72400	-4.74762
2370.855	6945.866	1.00886	2.19419	1.43614	-1.03105	-3.38990	-4.53561
2381.044	6946.139	1.90496	-1.06106	0.07262	-2.80675	-5.08982	-4.23578
2400.708	6946.409	2.04993	-1.39547	-0.48940	-3.13146	-6.30159	-5.13928
2410.788	6945.881	1.70012	0.07863	-1.61946	-4.38696	-5.61553	-5.62958
2388.877	6935.626	1.86171	-2.66854	-0.22298	-3.57837	-7.33735	-6.26975
2387.226	6925.825	1.48852	-0.06470	-0.21337	-3.27284	-7.12397	-5.43752
2397.167	6926.228	1.49625	-0.71062	0.35020	-3.74561	-7.40850	-5.30632
2417.351	6925.859	1.18680	3.01834	2.60035	-1.93725	-5.43113	-2.58218
2369.451	6916.05	1.87659	-0.14905	-0.75000	-2.75612	-5.81142	-3.50712
2389.889	6915.902	1.77161	-1.94298	-1.09657	-3.27884	-5.41381	-6.51220
2379.133	6905.78	1.55314	-0.65093	-1.60761	-2.45480	-6.66017	-4.56677
2389.467	6905.886	2.11910	-0.29932	-0.18810	-2.67393	-6.30274	-6.04129
2408.877	6906.22	1.81432	-1.58357	-1.87929	-4.45319	-2.97402	-6.34605
2400.664	6896.032	1.65048	-2.27710	-2.06726	-4.55115	-3.66755	-7.08598
2410.691	6896.04	1.74201	-1.25980	-0.18786	-3.98099	-5.92860	-7.17045
2356.895	6885.965	1.44737	0.66089	0.28916	-2.36782	-6.71875	-4.83478
2378.463	6886.275	1.59573	-0.35899	-0.83941	-3.23829	-7.17487	-5.34747

Continued on next page

Table A.6 – *Continued from previous page*

Y	X	alrMn_3O_4	alrFe_2O_3	alrSiO_2	alrAl_2O_3	alrPbO	alrP_2O_5
2388.829	6886.218	1.59243	-2.27284	-0.99075	-4.00249	-6.94165	-6.62509
2366.537	6876.494	1.62053	-2.01630	-1.18040	-3.70082	-4.83046	-5.03383
2385.696	6876.49	2.08469	-2.28328	0.22862	-2.95319	-6.95208	-6.48905
2395.863	6876.432	1.53303	-1.44556	0.23918	-3.38288	-6.11437	-5.70048
2405.653	6876.498	1.59761	-0.83490	-0.51459	-3.58452	-6.49583	-5.21936
2360.486	6866.217	1.54518	-1.69661	-1.36167	-2.78822	-5.92469	-4.59636
2369.803	6866.391	1.58807	-2.70126	-1.86598	-3.34512	-7.39231	-7.08983
2380.367	6856.242	1.51421	1.14309	-1.25317	-2.73903	-6.83478	-3.97863
2389.728	6856.189	1.62302	-2.97393	-2.02418	-4.08431	-4.36439	-7.68509
2410.314	6856.035	1.61461	-0.70451	-1.42988	-3.38207	-5.42595	-4.50623
2429.609	6676.444	1.56528	0.91624	0.74997	-1.69451	-6.03437	-7.78668
2458.452	6719.395	1.72749	-1.32858	-3.22313	-2.95672	-6.94100	-5.62432
2467.968	6704.717	-0.08915	2.24210	1.89755	-0.03427	-6.19332	-8.72328
2466.976	6726.027	1.11103	2.89043	2.05841	-0.96534	-5.45277	-4.06365
2444.472	6725.992	1.31458	1.04877	0.34192	-1.30985	-6.05513	-5.60761
2455.086	6716.435	1.70063	-1.60576	-2.63440	-3.27862	-7.31361	-6.92713
2467.148	6706.215	0.01445	2.80215	1.67378	-0.33193	-6.37698	-6.38624
2376.835	6655.633	1.31431	0.28440	1.25575	-0.73167	-4.40273	-5.60742
2436.972	6646.078	0.90937	-0.83406	2.43572	0.23322	-3.01593	-4.66800
2426.976	6646.082	1.53704	-0.54822	1.44536	-1.11678	-4.03714	-3.42858
2373.232	6645.282	1.32983	1.75575	1.98833	-1.61639	-3.06893	-3.26374
2436.981	6636.052	0.69304	2.97845	2.21519	-0.98183	-5.87076	-3.17104
2416.93	6636.531	1.35366	0.57635	0.15189	-1.03865	-6.24516	-4.24771
2395.72	6636.761	1.67940	-0.92497	0.11483	-2.07230	-5.50724	-5.73793
2406.328	6626.279	0.73478	1.38856	2.08520	-0.30430	-4.43678	-3.45404
2384.63	6626.099	1.42638	0.42328	1.37036	-1.25989	-4.98717	-5.15191
2351.477	6806.151	1.72997	-2.21608	-2.14066	-3.74364	-3.60654	-5.99742
2343.865	6806.086	-0.39268	2.21676	2.28702	0.07650	-6.05489	-6.49822
2359.706	6797.765	1.09389	1.18319	0.09257	-3.57061	-3.79603	-2.55995
2351.555	6790.371	1.71666	0.99732	-2.27346	-3.88106	-2.79092	-6.99954
2363.893	6782.254	1.69451	-1.92501	-0.15375	-3.79430	-6.59382	-5.67467
2336.767	6781.91	0.22373	4.72356	4.09517	-0.93046	-4.92256	-5.22144
2394.67	6774.256	1.57634	-1.94520	0.37549	-2.21586	-5.87001	-4.60198

Continued on next page

Table A.6 – *Continued from previous page*

Y	X	alrMn_3O_4	alrFe_2O_3	alrSiO_2	alrAl_2O_3	alrPbO	alrP_2O_5
2374.226	6774.037	1.46504	0.86627	-0.11682	-1.49698	-5.79521	-5.88914
2347.47	6774.168	1.68711	-2.83015	-1.27216	-3.97708	-5.64430	-9.10120
2361.125	6765.413	1.75538	-2.25939	-2.16025	-3.73303	-3.64984	-7.12819
2367.391	6755.876	1.62660	-1.84349	-2.91439	-3.30074	-5.43223	-5.73114
2376.496	6746.145	1.74179	-2.58643	-1.60646	-3.44150	-7.27748	-5.28380
2356.768	6745.869	0.97813	3.14126	-0.44540	-2.89572	-5.65396	-8.11294
2377.455	6735.992	1.67618	-3.32404	-3.28376	-3.90723	-6.19936	-8.06293
2367.086	6735.986	1.77873	-2.31901	-2.79712	-3.69665	-6.70476	-9.02299
2372.387	6726.083	1.64284	0.23582	0.83068	-2.34477	-5.52112	-6.08858
2386.741	6716.124	0.39947	2.04674	3.40279	-0.01530	-5.79886	-3.78546
2366.384	6716.069	1.35819	2.22874	1.95458	-1.83438	-5.20562	-5.15972
2376.835	6706.001	1.39222	1.28309	4.04796	-0.27714	-4.94043	-3.13033
2357.29	6706.406	1.68858	1.65290	5.85571	-0.96932	-4.81421	-3.36882
2386.762	6695.962	1.76999	-1.62407	1.12580	-1.77050	-5.42464	-3.72037
2368.064	6695.374	1.64786	-0.41866	0.51761	-2.56922	-6.33938	-4.17380
2446.518	6685.805	1.76258	-1.03766	-0.54520	-1.74466	-5.89185	-5.15691
2426.866	6685.051	1.63660	0.84799	-1.10648	-2.40577	-6.68810	-8.09570

Continued on next page

Table A.7: Raw data summary statistics. RD Dataset

VARIABLE	Count	Minimum	Maximum	Mean	Std. Dev.	Variance	Variat.Coef.	Skewness	Kurtosis
Al_2O_3	234	0.1	10.55	1.32	1.48	2.2	1.12	2.42	10.81
Fe	234	0.15	58.85	10.09	12.67	160.42	1.25	1.76	5.41
Mn	234	0.51	61.51	36.11	20.67	427.28	0.57	-0.56	1.77
P	234	0	1.38	0.04	0.09	0.01	2.59	13.24	191.2
Pb	234	0	0.63	0.06	0.11	0.01	1.82	3.47	15.82
SiO_2	234	0.18	96.66	22.13	23.09	533.18	1.04	1.43	4.2

Table A.8: Raw data correlation matrix. RD Dataset

VARIABLE	Al_2O_3	Fe	Mn	P	Pb	SiO_2
Al_2O_3	1	0.2	-0.44	0.06	0.19	0.41
Fe	0.2	1	-0.62	0.11	-0.07	0.11
Mn	-0.44	-0.62	1	-0.12	0.11	-0.79
P	0.06	0.11	-0.12	1	-0.02	0.05
Pb	0.19	-0.07	0.11	-0.02	1	-0.1
SiO_2	0.41	0.11	-0.79	0.05	-0.1	1

Appendix B

Input Data Summary Figures

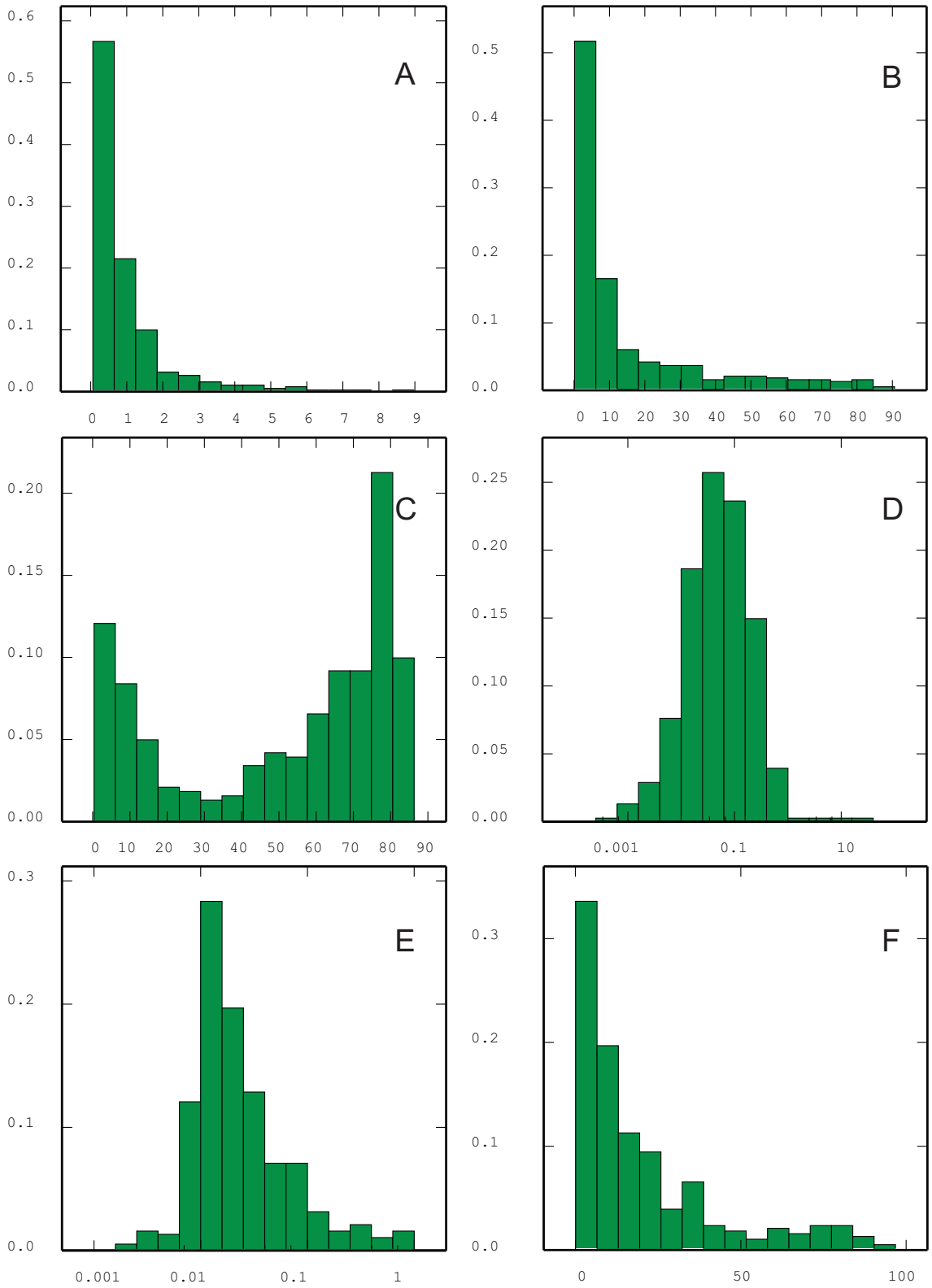

Figure B.1: Histograms of input data distributions Domain 1 (Complete Dataset). A - Al_2O_3, B - Fe_2O_3, C - Mn_3O_4, D - P_2O_5, E - PbO, F - SiO_2,

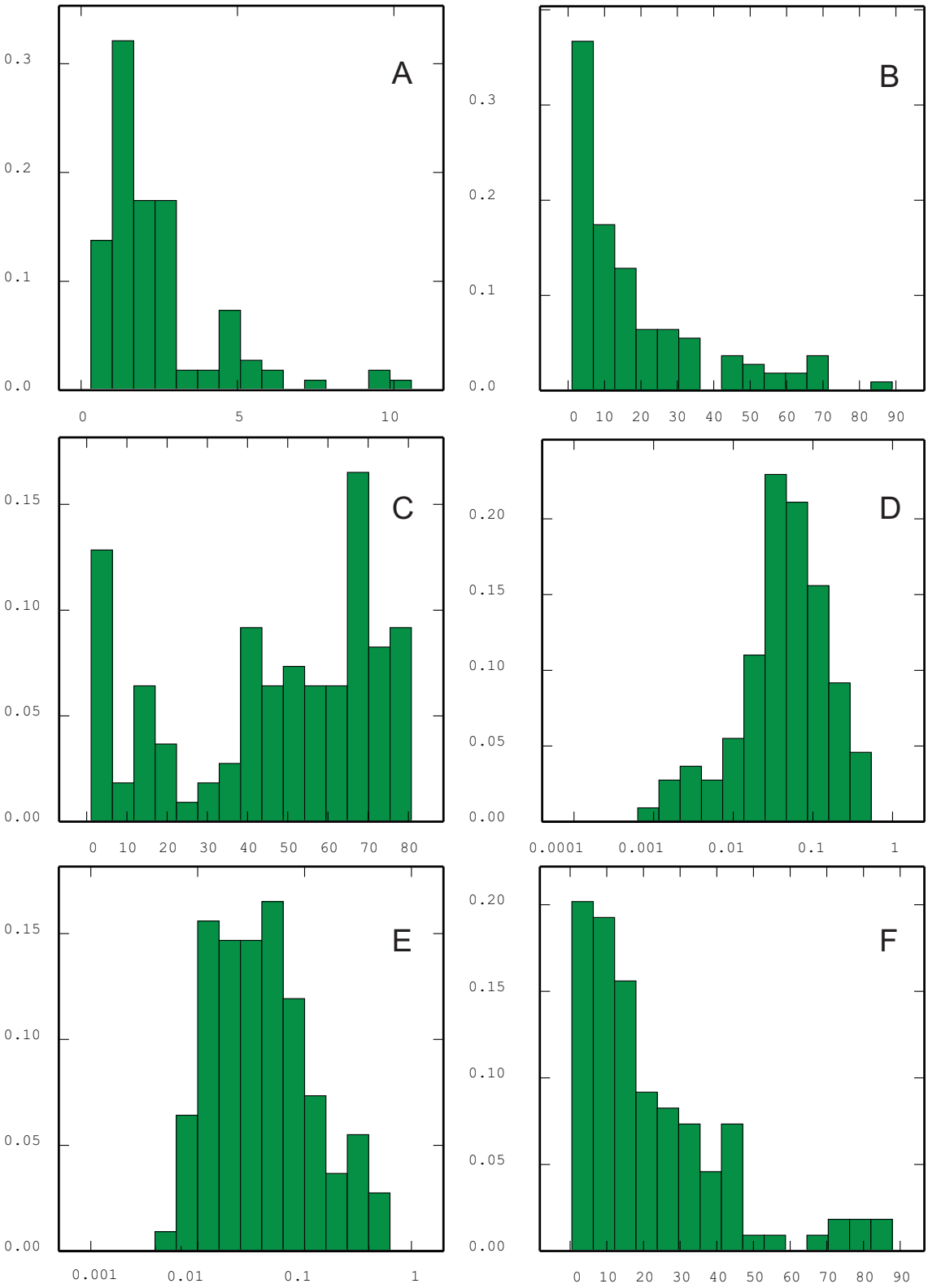

Figure B.2: Histograms of input data distributions Domain 2 (Complete Dataset). A - Al_2O_3, B - Fe_2O_3, C - Mn_3O_4, D - P_2O_5, E - PbO, F - SiO_2,

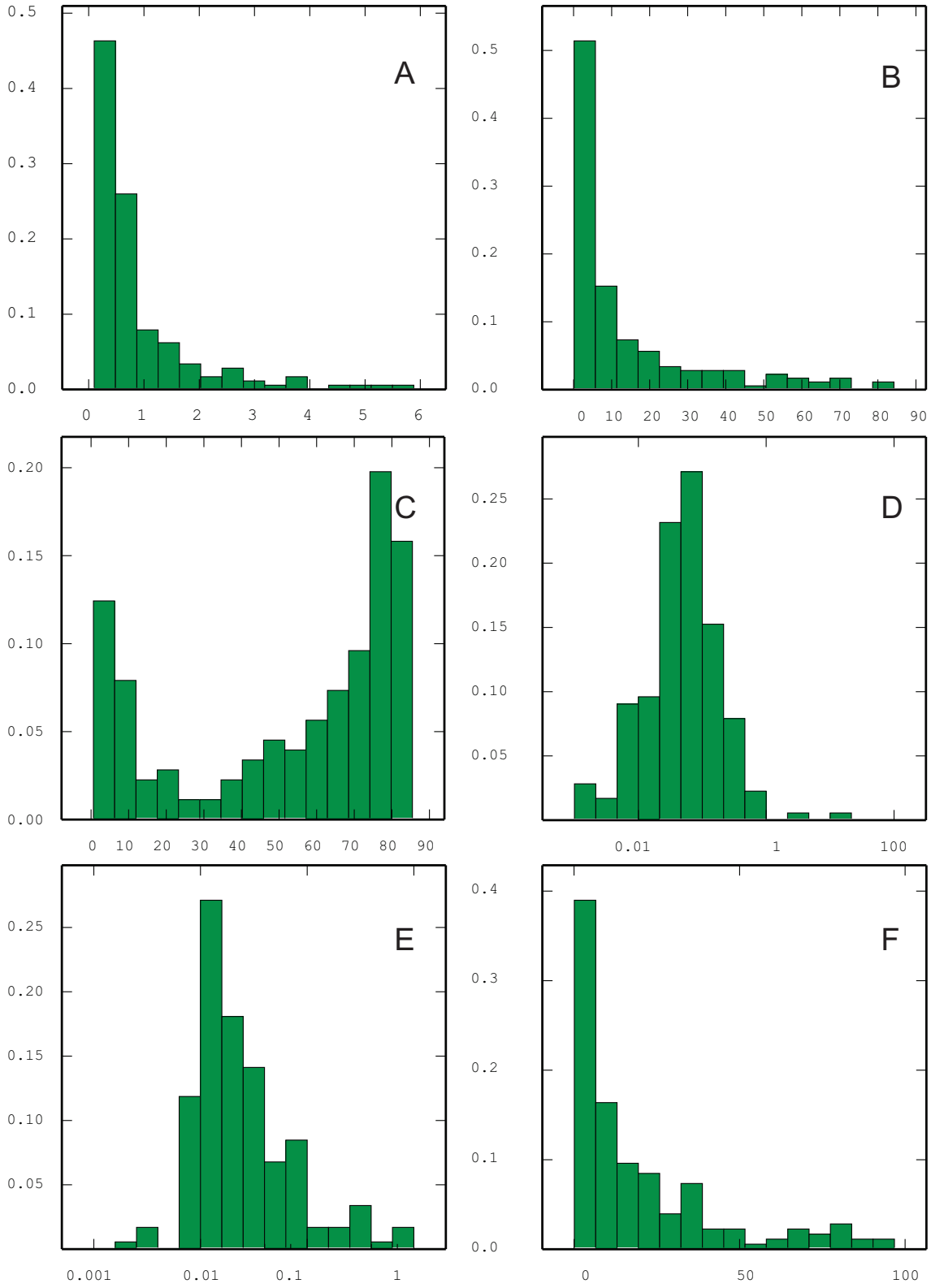

Figure B.3: Histograms of input data distributions Domain 1 (Reduced Dataset). A - Al_2O_3, B - Fe_2O_3, C - Mn_3O_4, D - P_2O_5, E - PbO, F - SiO_2,

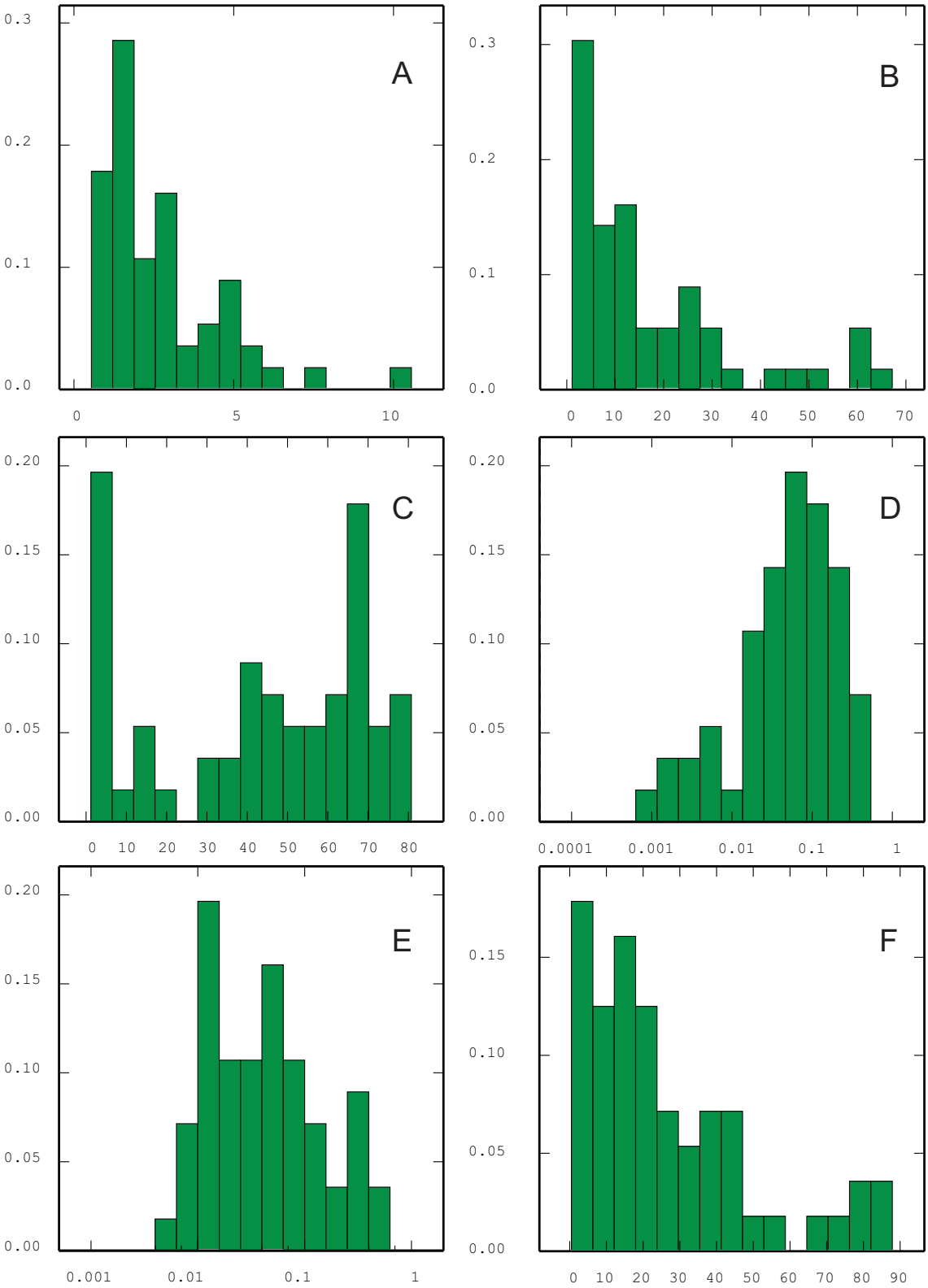

Figure B.4: Histograms of input data distributions Domain 2 (Reduced Dataset). A - Al_2O_3, B - Fe_2O_3, C - Mn_3O_4, D - P_2O_5, E - PbO, F - SiO_2,

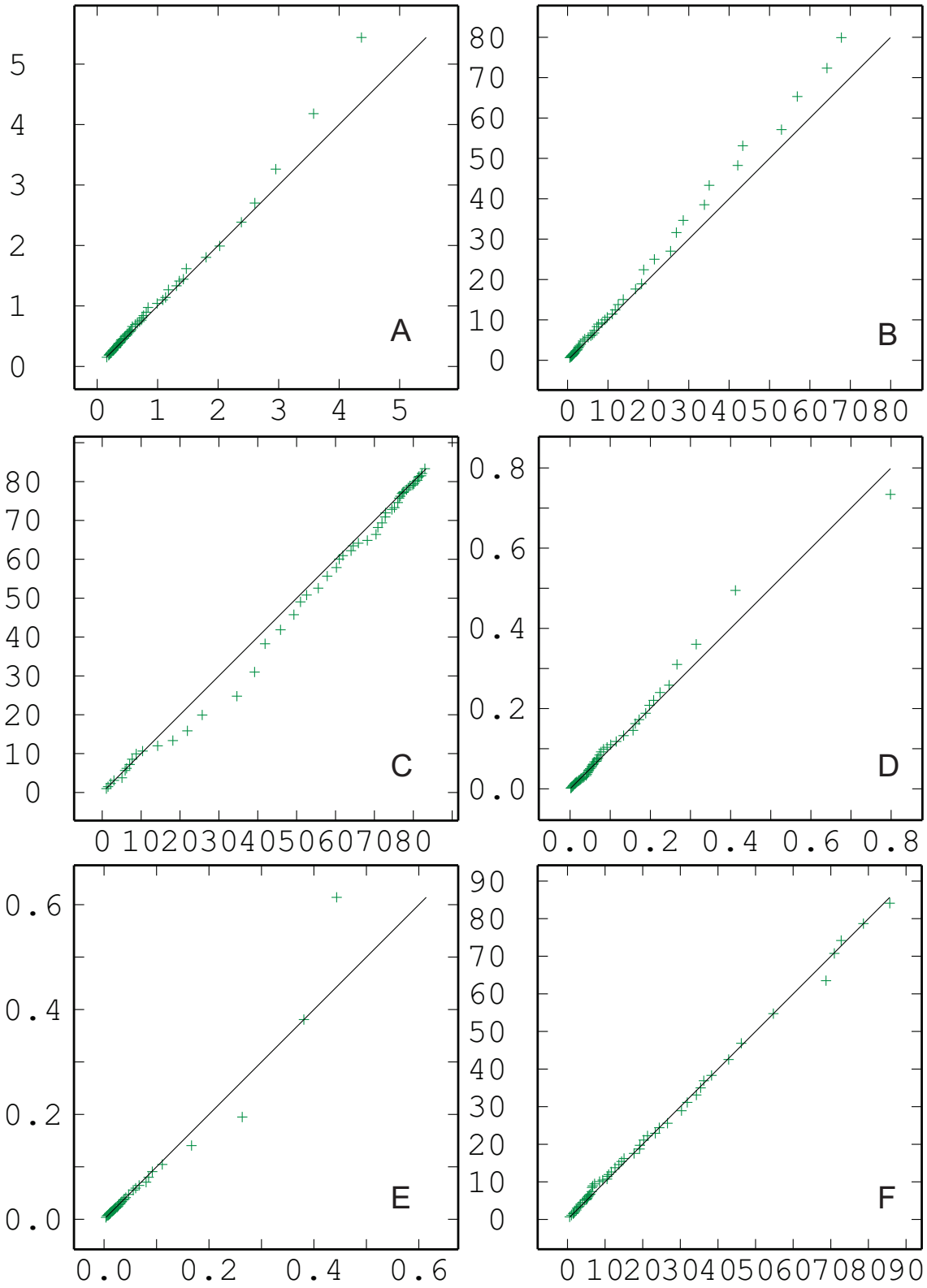

Figure B.5: Comparative Q-Q plot of input datasets Domain 1: Reduced Data Ordinate, All Data Abcissa. A - Al_2O_3, B - Fe_2O_3, C - Mn_3O_4, D - P_2O_5, E - PbO, F - SiO_2,

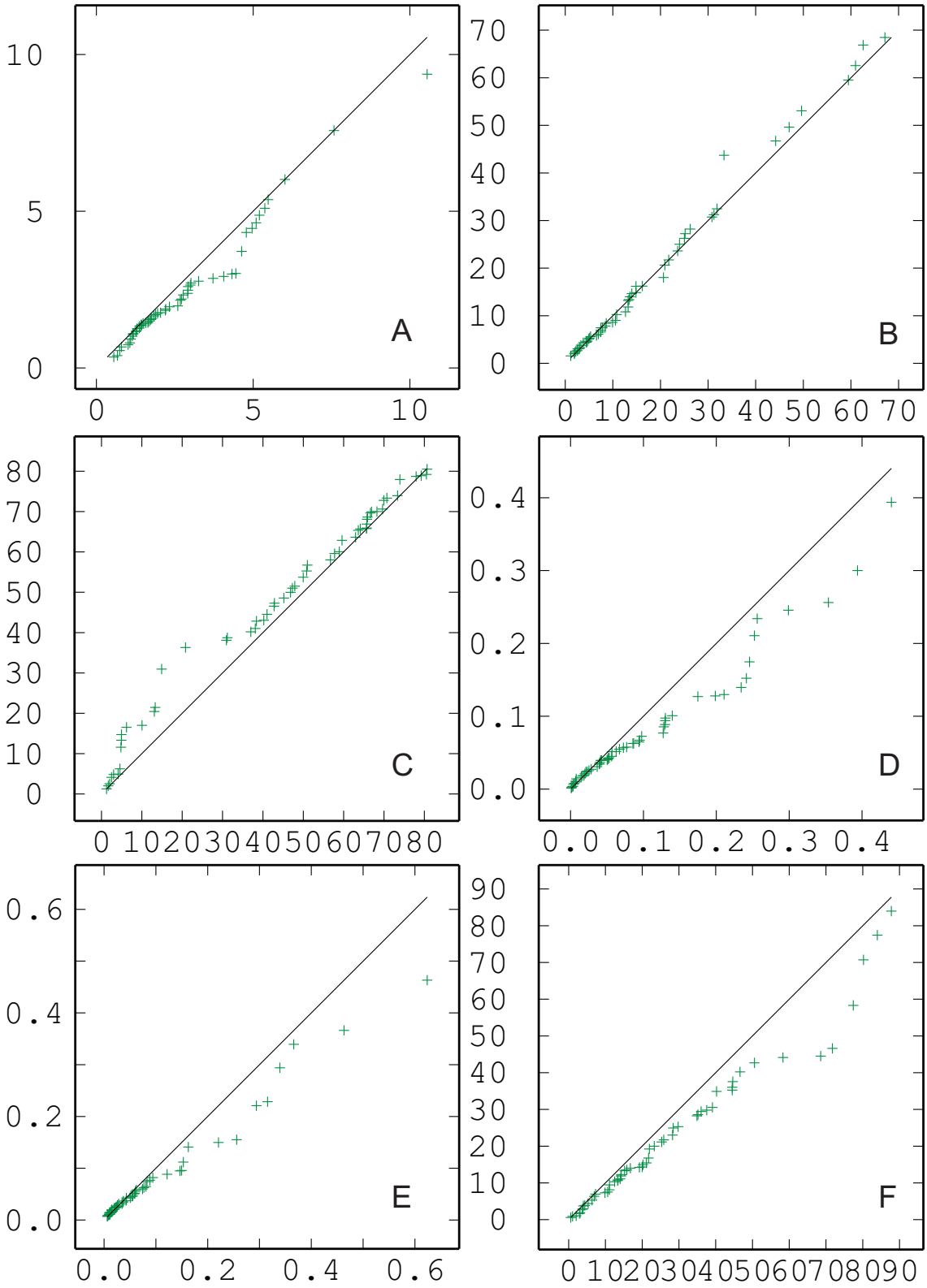

Figure B.6: Comparative Q-Q plot of input datasets Domain 2: Reduced Data Ordinate, All Data Abcissa. A - Al_2O_3, B - Fe_2O_3, C - Mn_3O_4, D - P_2O_5, E - PbO, F - SiO_2,

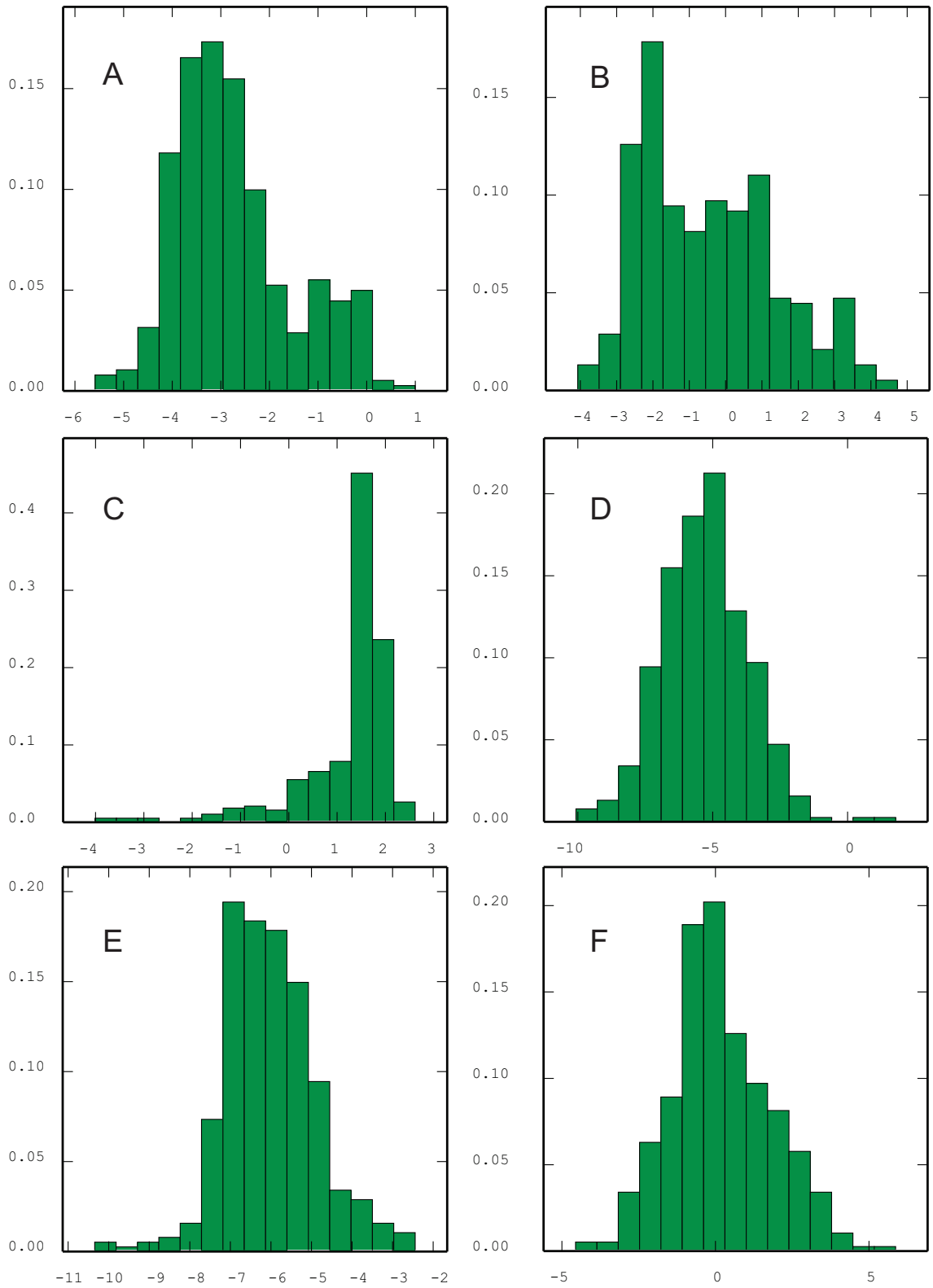

Figure B.7: Distributions of log-ratio transformed input data; Complete dataset Domain 1. A - alrAl_2O_3, B - alrFe_2O_3, C - alrMn_3O_4, D - alrP_2O_5, E - alrPbO, F - alrSiO_2

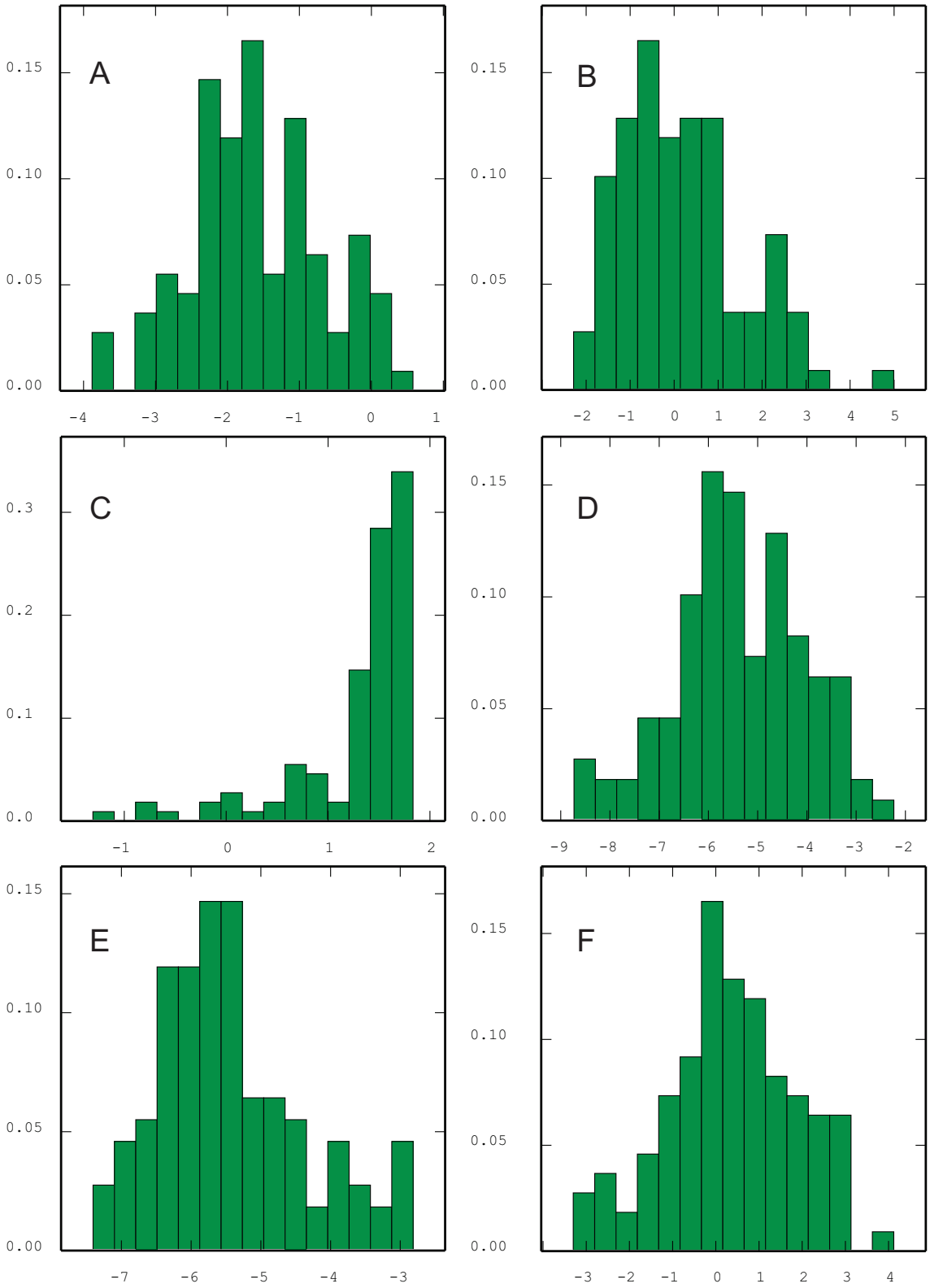

Figure B.8: Distributions of log-ratio transformed input data; Complete dataset Domain 2. A - alrAl_2O_3, B - alrFe_2O_3, C - alrMn_3O_4, D - alrP_2O_5, E - alrPbO, F - alrSiO_2

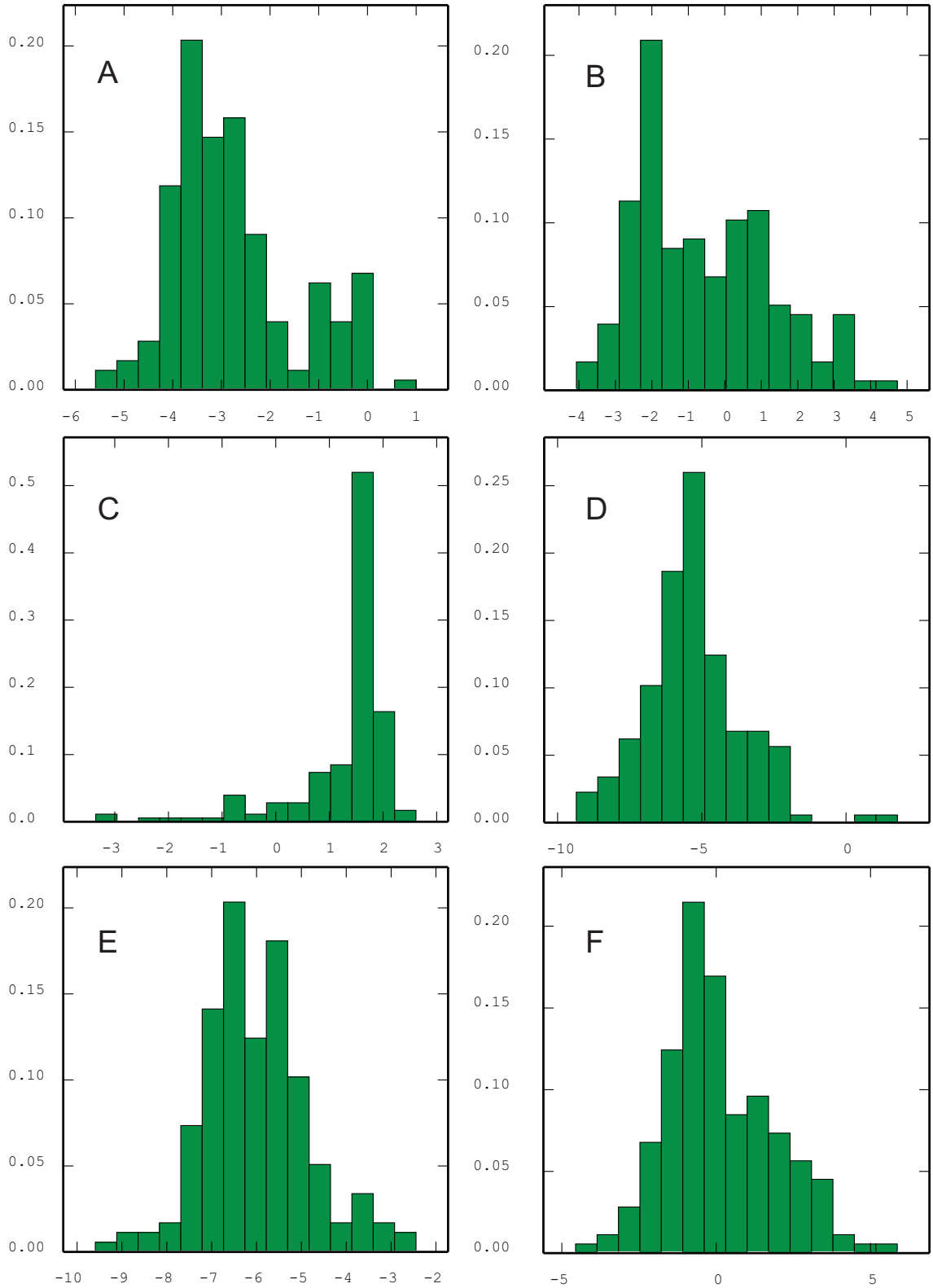

Figure B.9: Distributions of log-ratio transformed input data; RD dataset Domain 1. A - alrAl_2O_3, B - alrFe_2O_3, C - alrMn_3O_4, D - alrP_2O_5, E - alrPbO, F - alrSiO_2

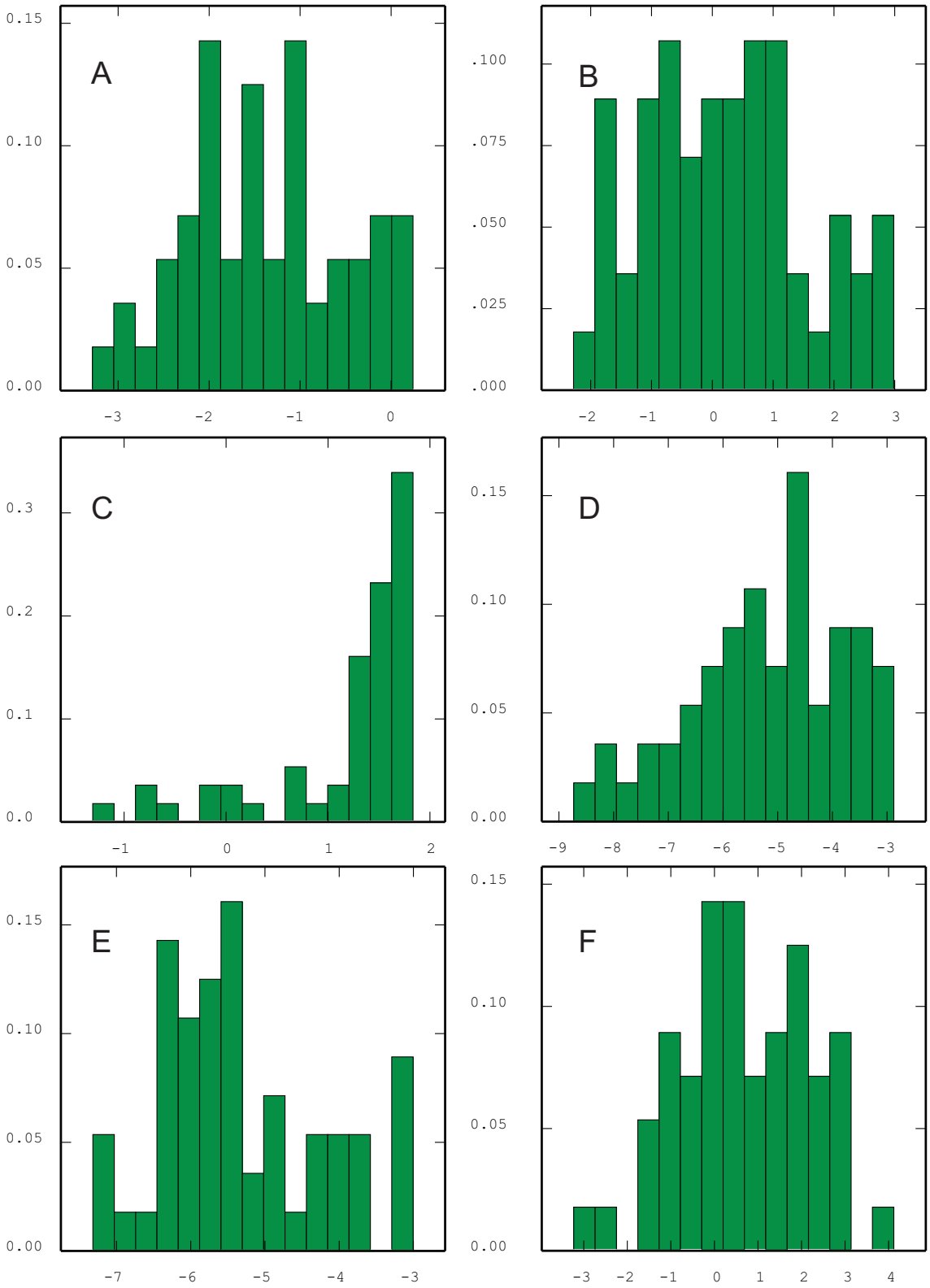

Figure B.10: Distributions of log-ratio transformed input data; RD dataset Domain 2. A - alrAl_2O_3, B - alrFe_2O_3, C - alrMn_3O_4, D - alrP_2O_5, E - alrPbO, F - alrSiO_2

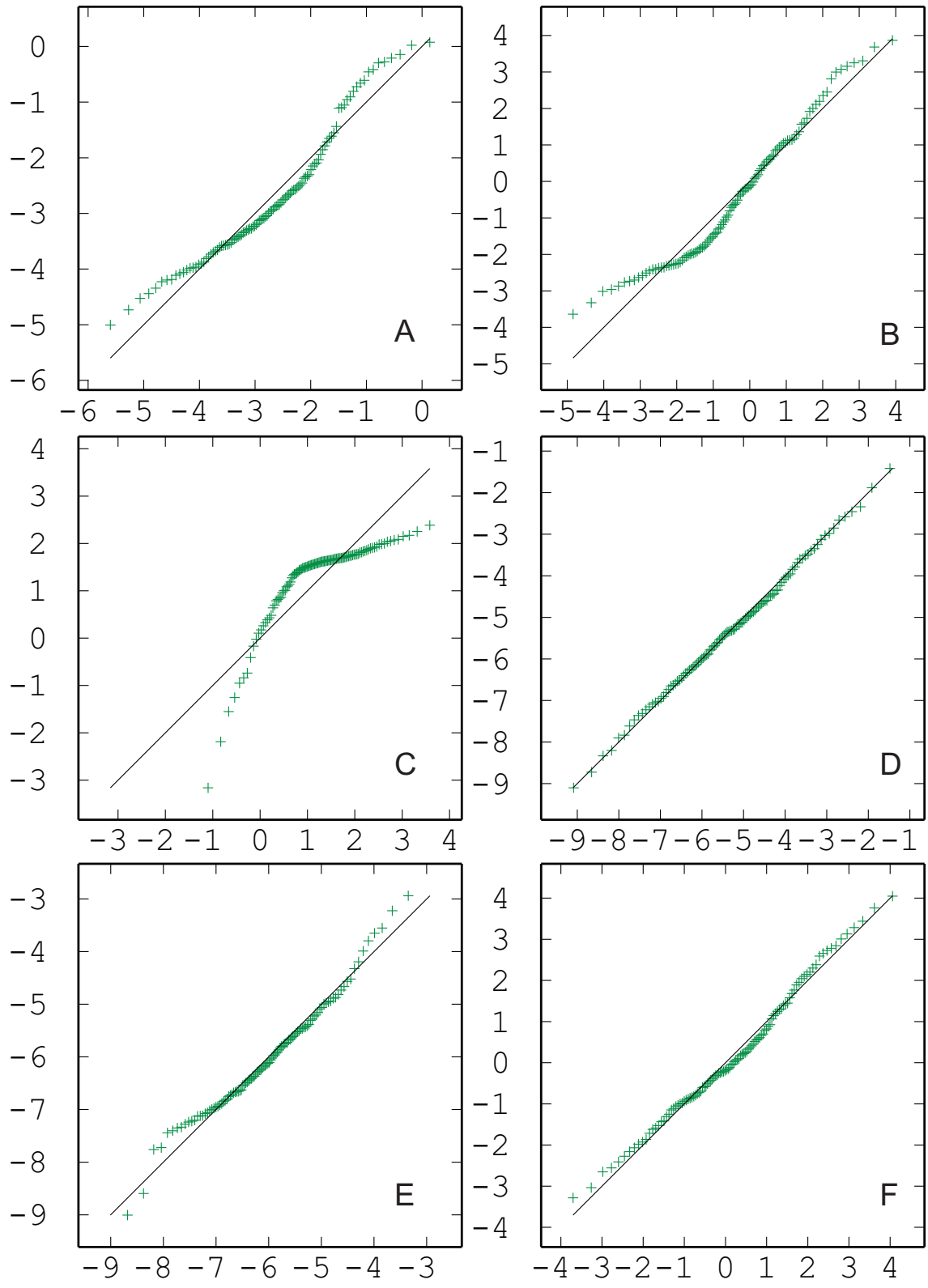

Figure B.11: Q-Q plot comparison of ALR transformed data against a Gaussian distribution; Complete dataset Domain 1. A - alrAl_2O_3, B - alrFe_2O_3, C - alrMn_3O_4, D - alrP_2O_5, E - alrPbO, F - alrSiO_2

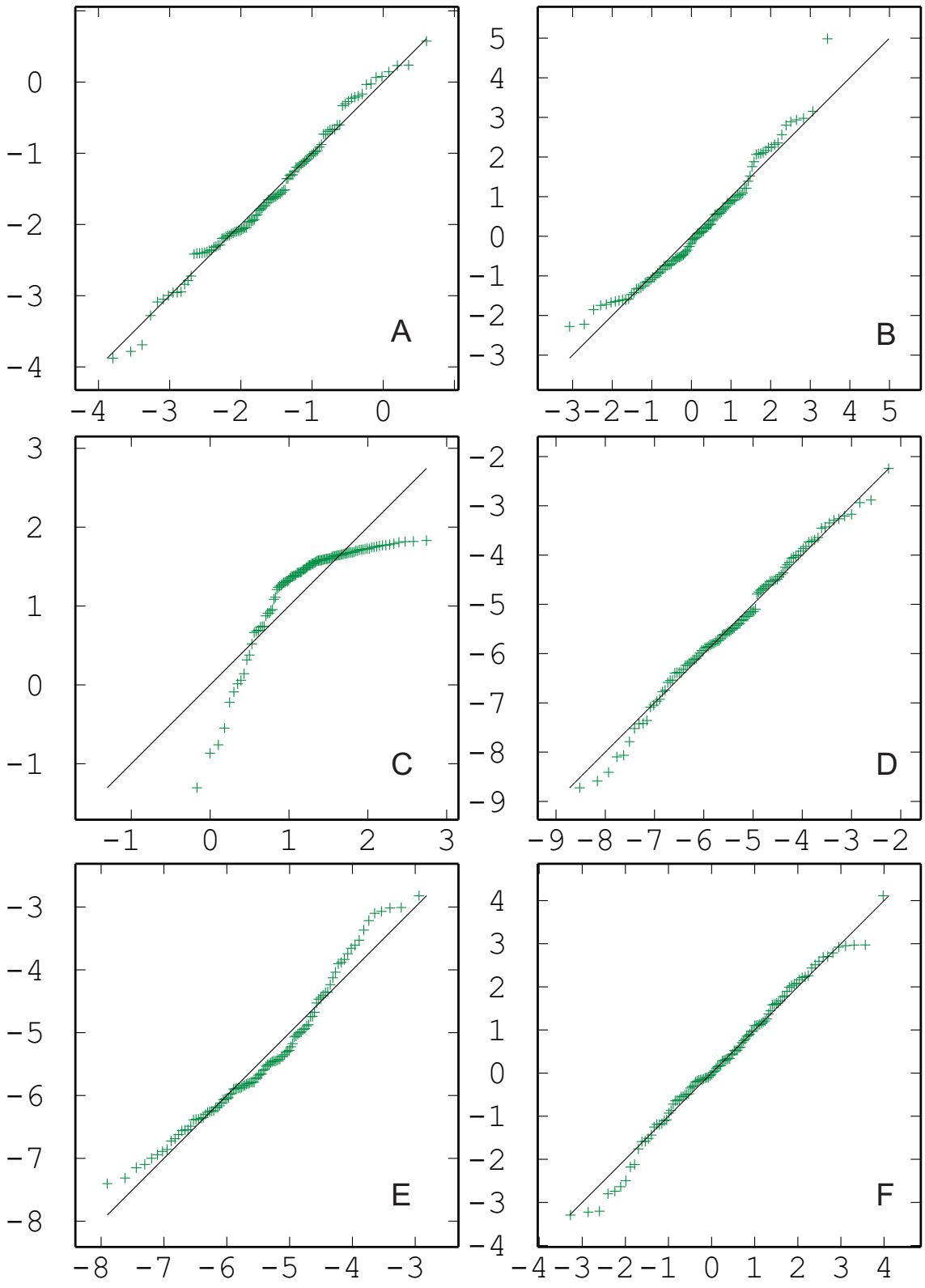

Figure B.12: Q-Q plot comparison of ALR transformed data against a Gaussian distribution; Complete dataset Domain 2. A - alrAl_2O_3, B - alrFe_2O_3, C - alrMn_3O_4, D - alrP_2O_5, E - alrPbO, F - alrSiO_2

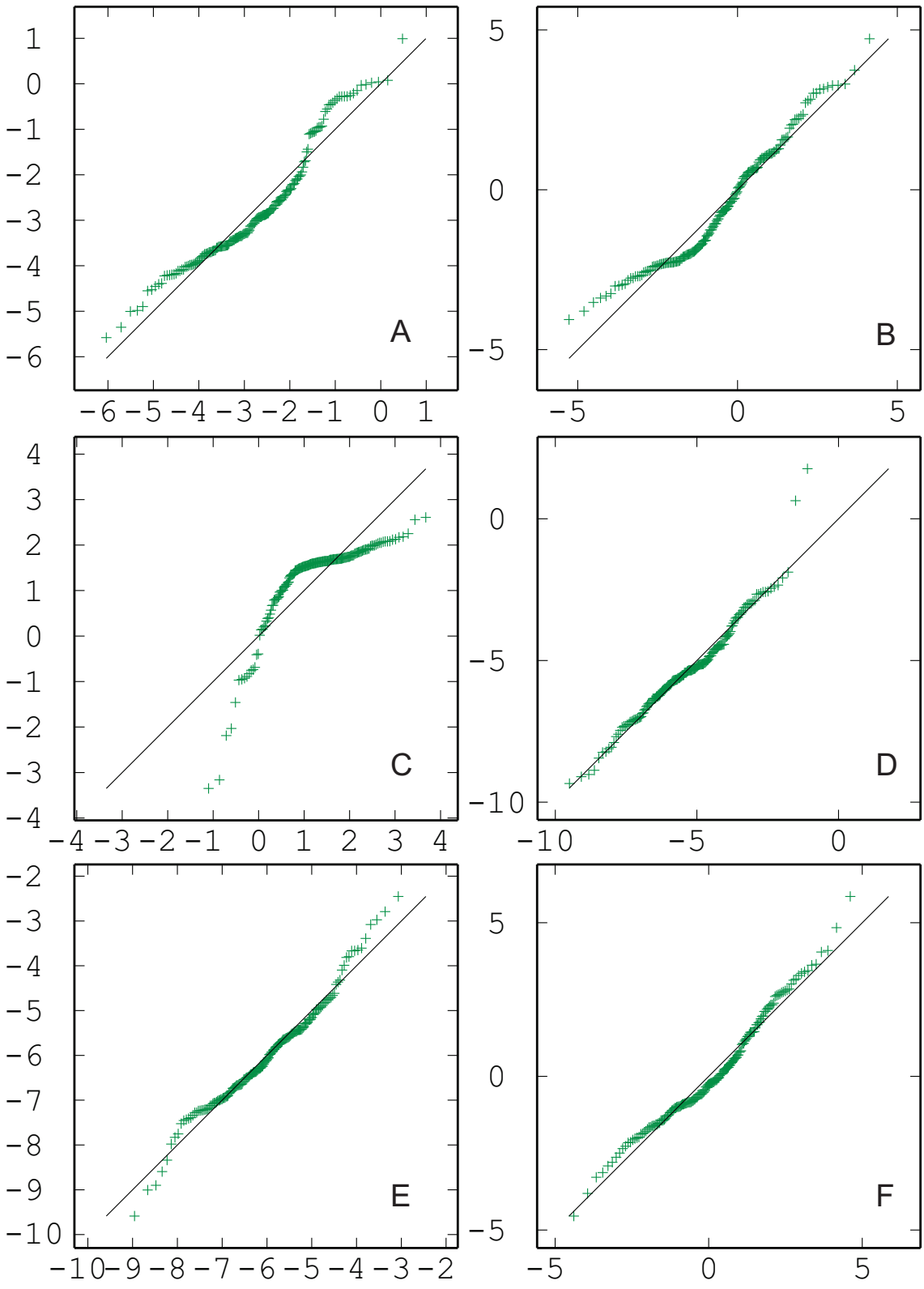

Figure B.13: Q-Q plot comparison of ALR transformed data against a Gaussian distribution; Reduced dataset Domain 1. A - alrAl_2O_3, B - alrFe_2O_3, C - alrMn_3O_4, D - alrP_2O_5, E - alrPbO, F - alrSiO_2

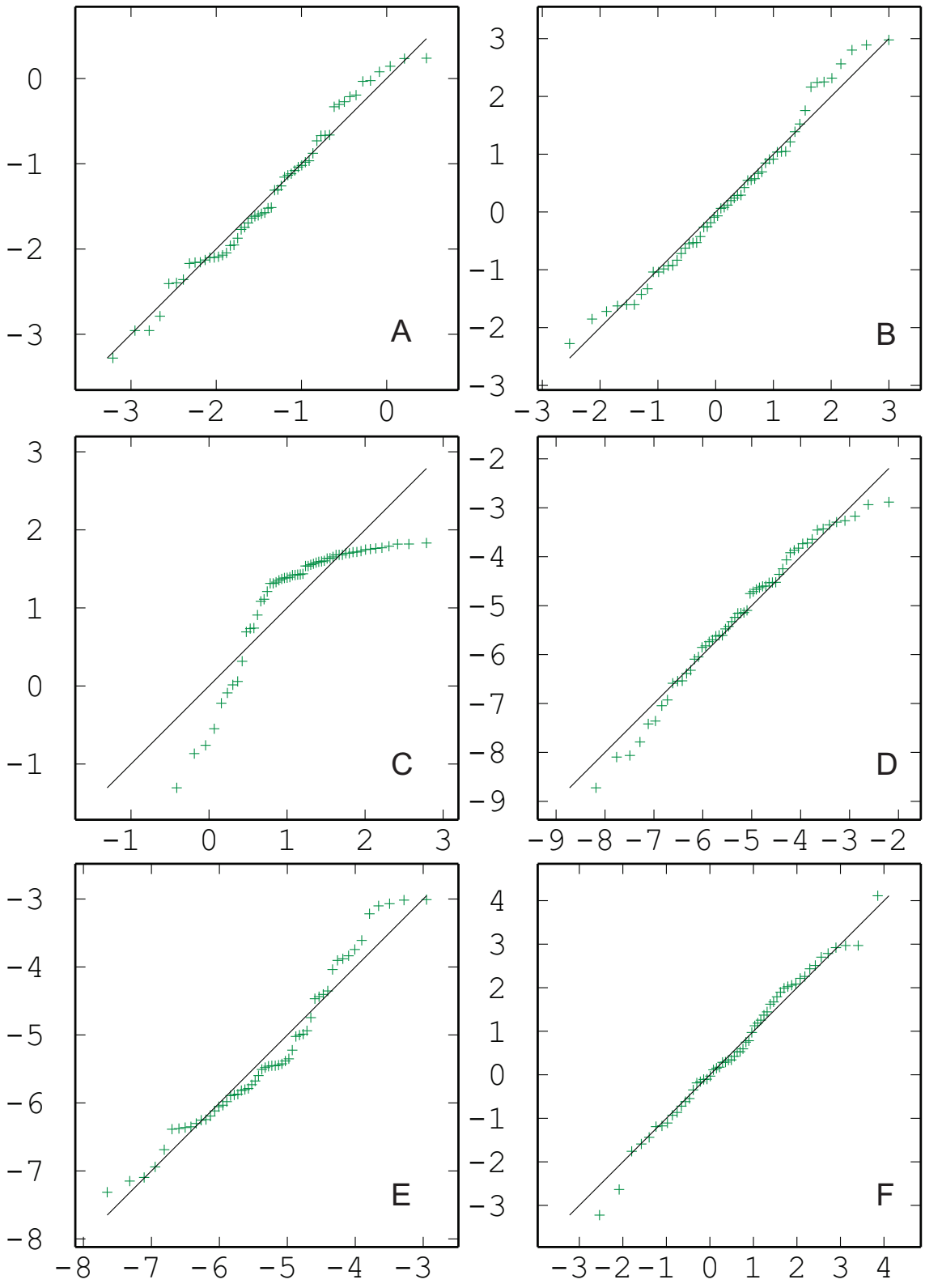

Figure B.14: Q-Q plot comparison of ALR transformed data against a Gaussian distribution; Reduced dataset Domain 2. A - alrAl_2O_3, B - alrFe_2O_3, C - alrMn_3O_4, D - alrP_2O_5, E - alrPbO, F - alrSiO_2

Appendix C

Experimental Variography

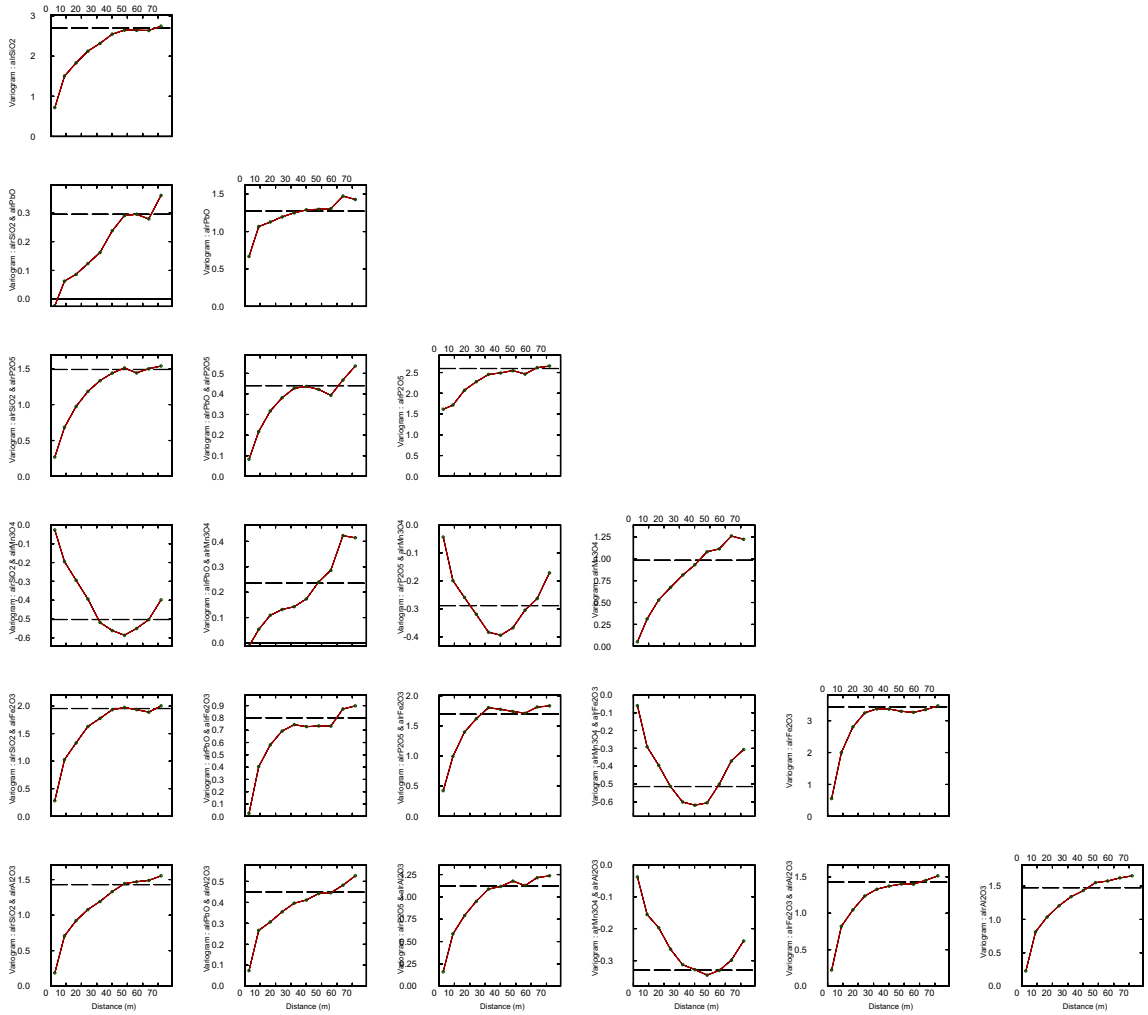

Figure C.1: Omnidirectional experimental (cross-)semivariograms log-ratio data Domain 1. Complete Dataset.

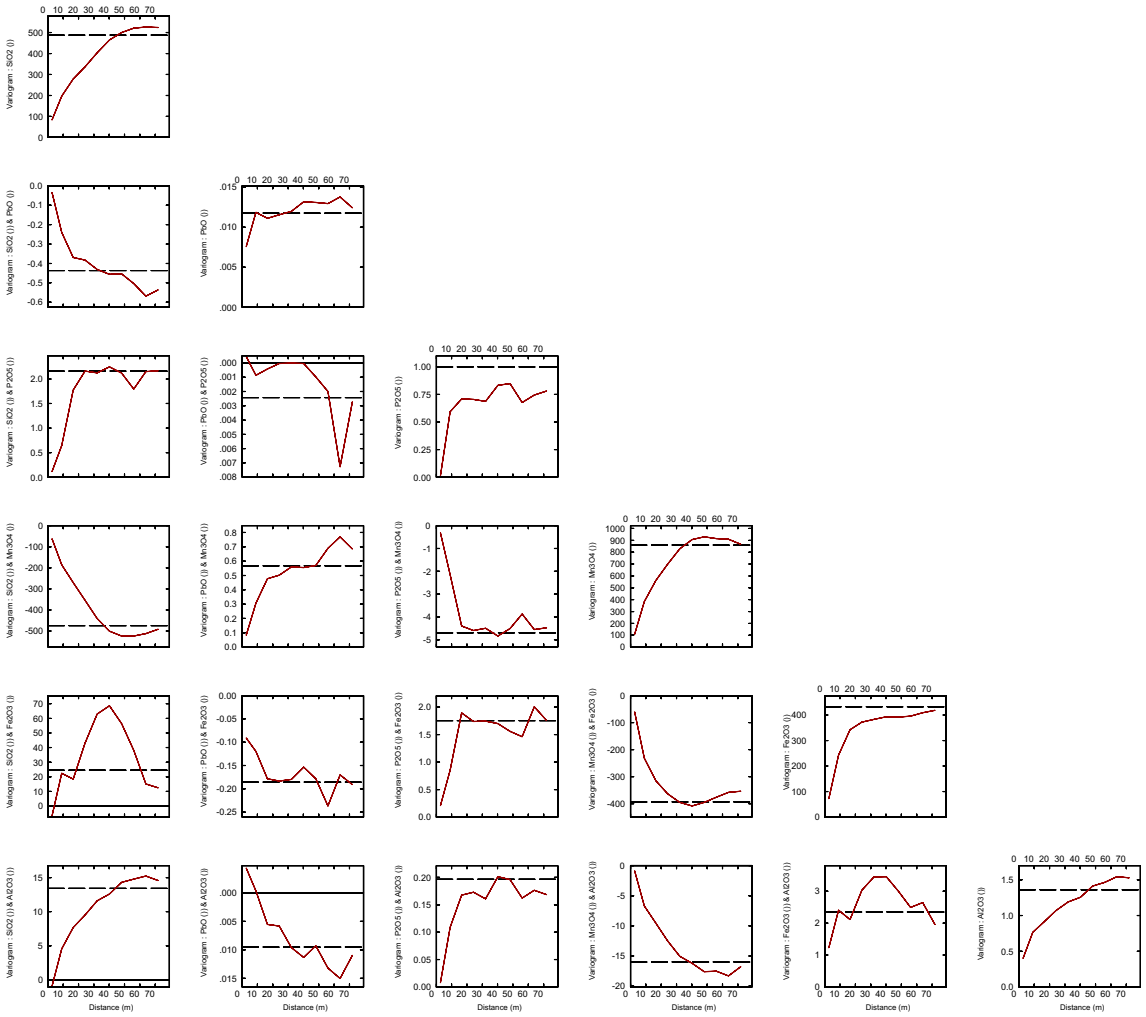

Figure C.2: Omnidirectional experimental (cross-)semivariograms oxide data Domain 1. Complete Dataset.

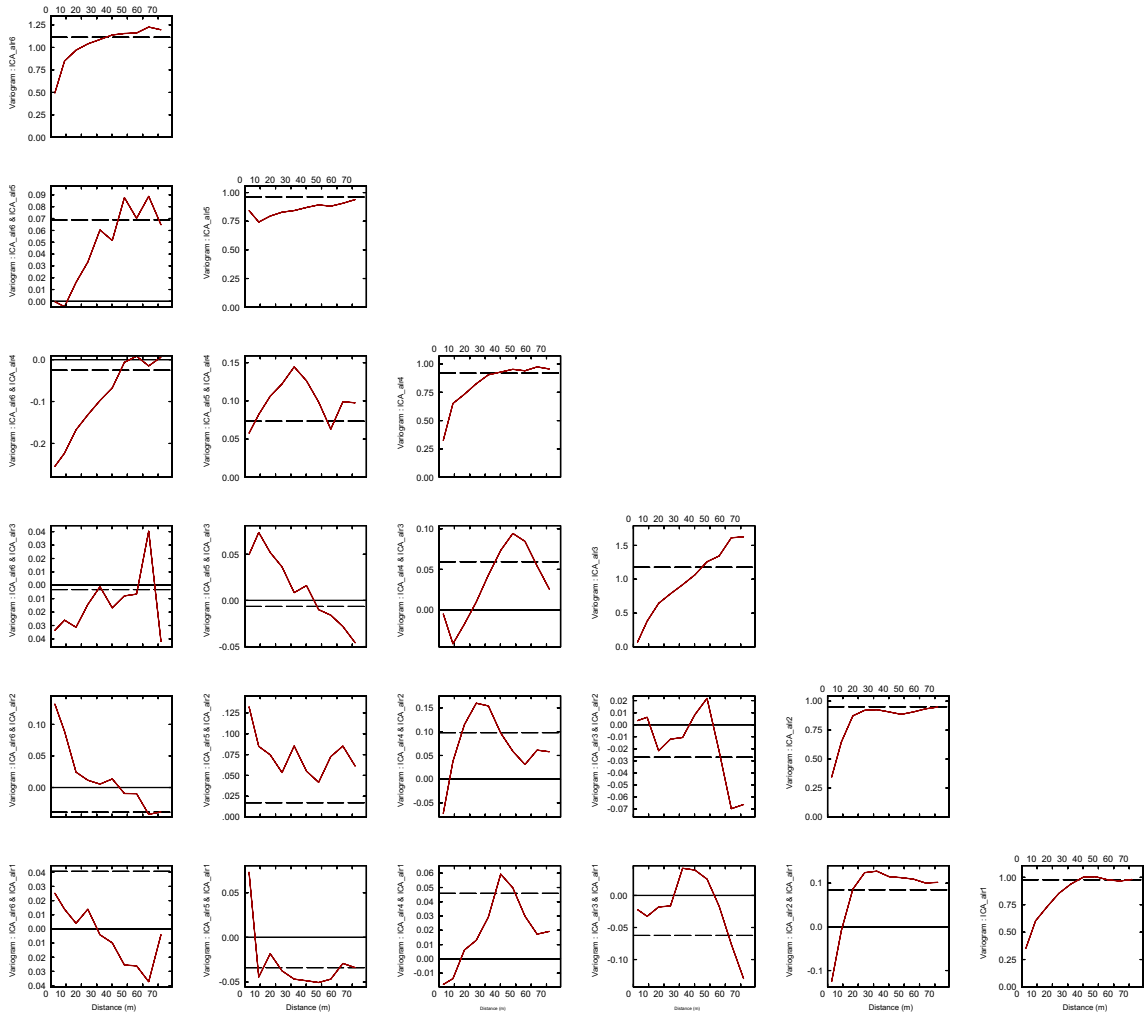

Figure C.3: Omnidirectional experimental (cross-)semivariograms ICA decorrelated log-ratio data Domain 1. Complete Dataset.

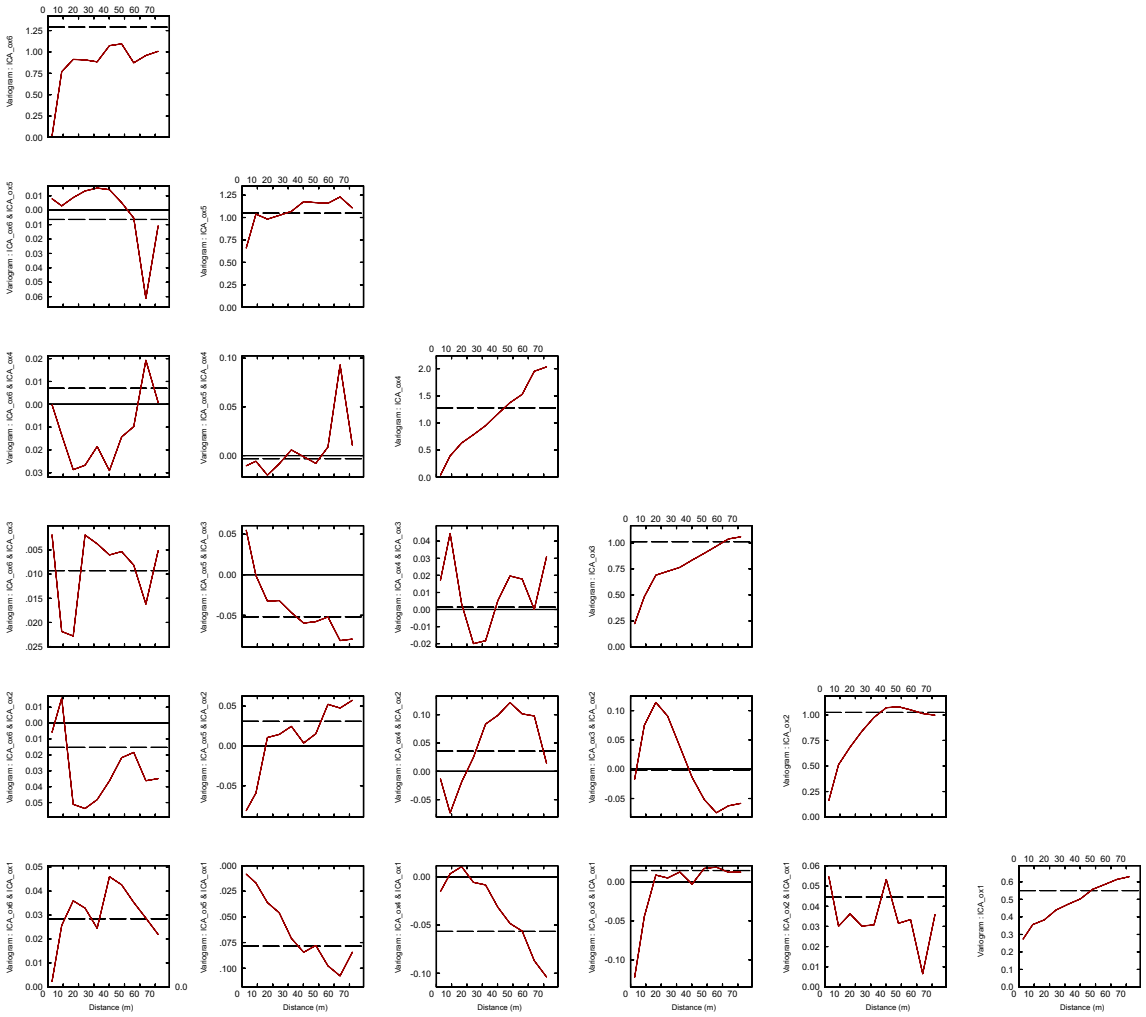

Figure C.4: Omnidirectional experimental (cross-)semivariograms ICA decorrelated oxide data Domain 1. Complete Dataset.

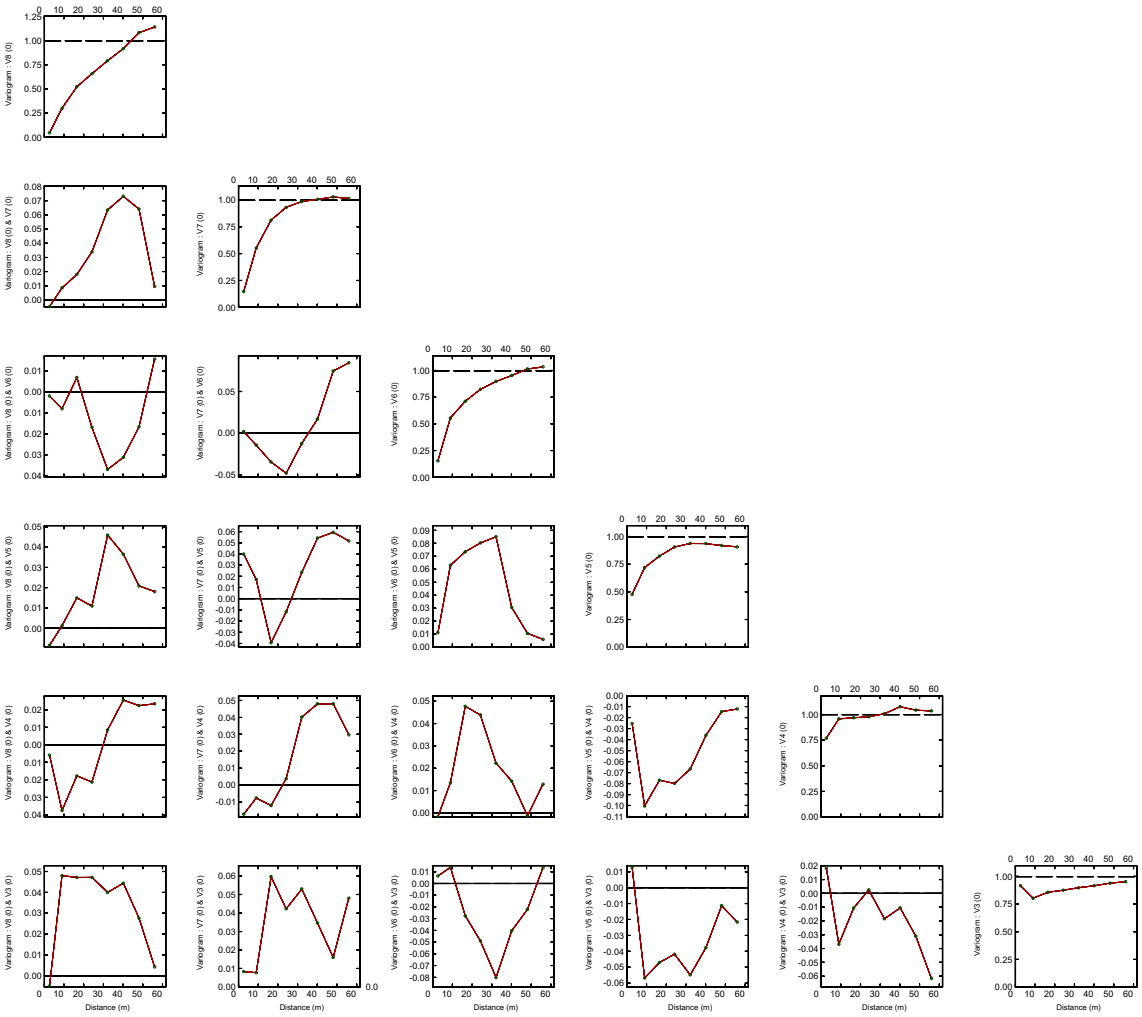

Figure C.5: Omnidirectional experimental (cross-)semivariograms MAF decorrelated log-ratio data Domain 1. Complete Dataset.

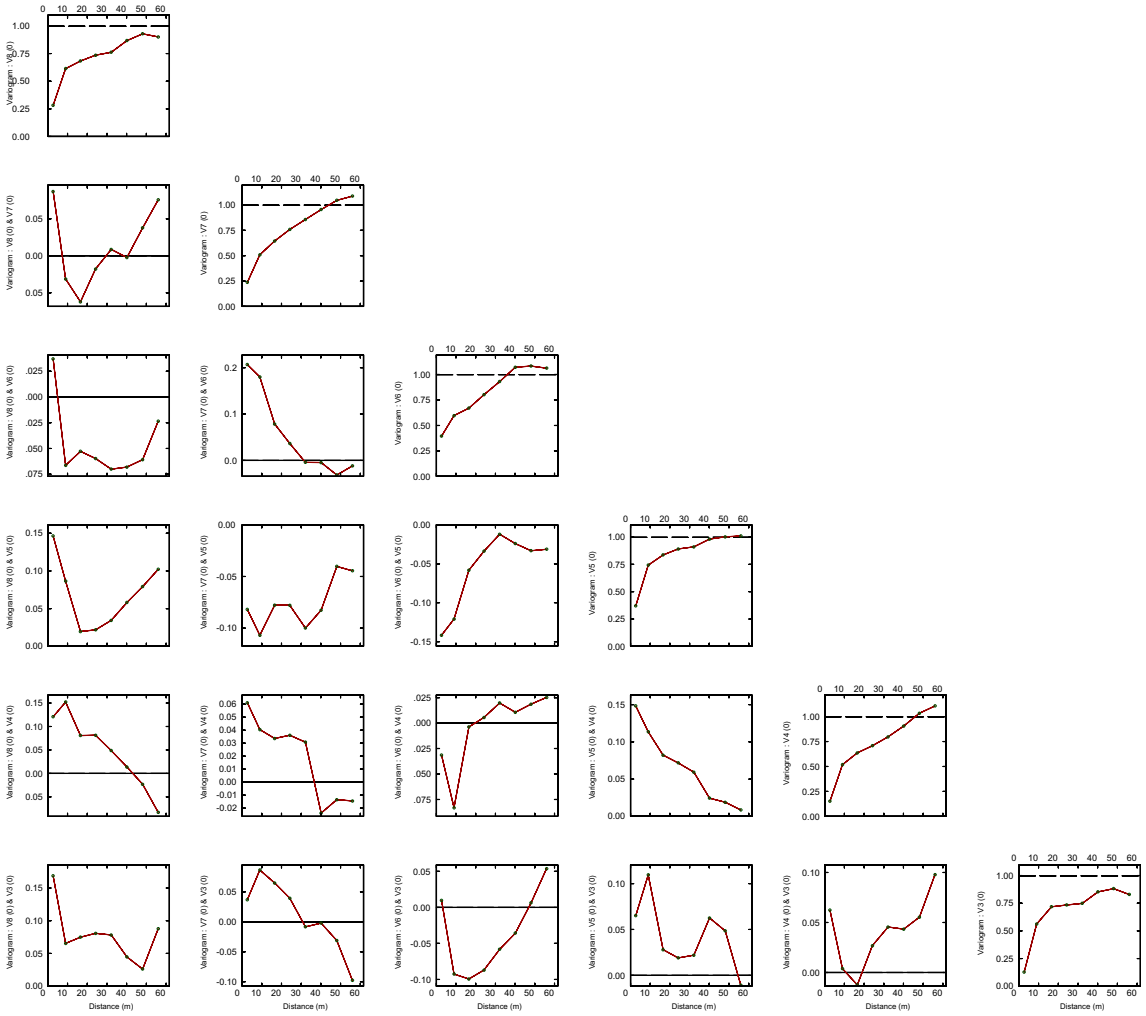

Figure C.6: Omnidirectional experimental (cross-)semivariograms MAF decorrelated oxide data Domain 1. Complete Dataset.

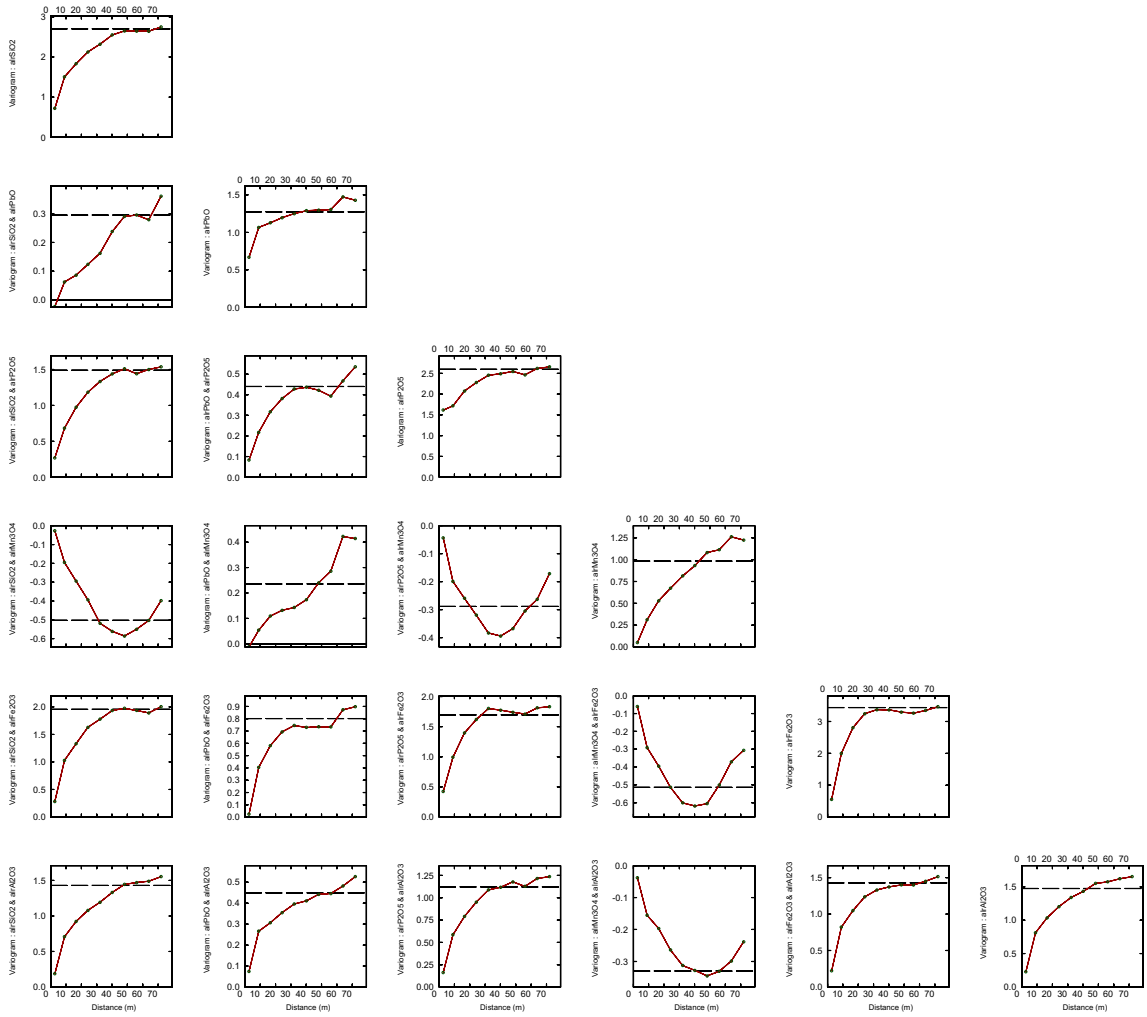

Figure C.7: Omnidirectional experimental (cross-)semivariograms log-ratio data Domain 2. Complete Dataset.

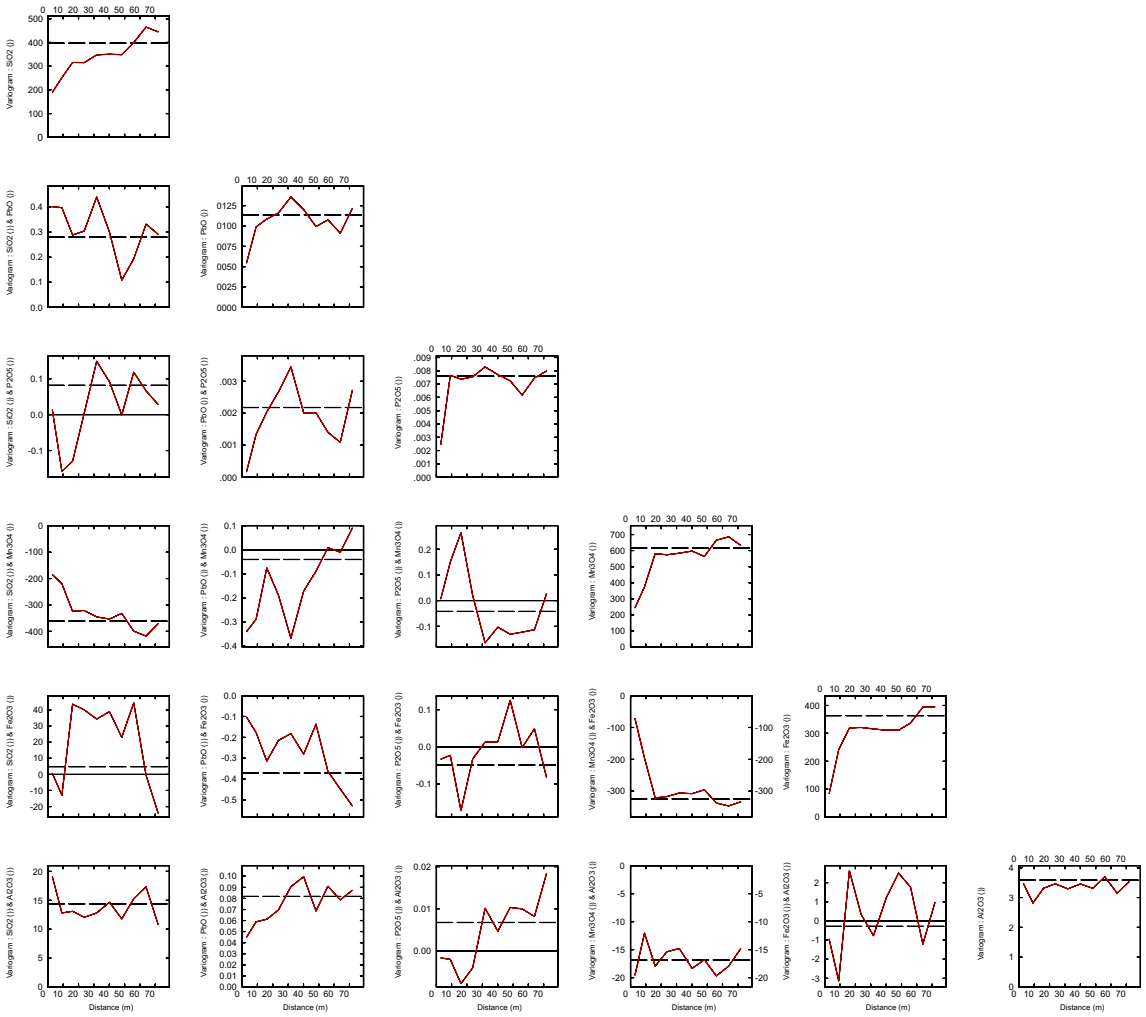

Figure C.8: Omnidirectional experimental (cross-)semivariograms oxide data Domain 2. Complete Dataset.

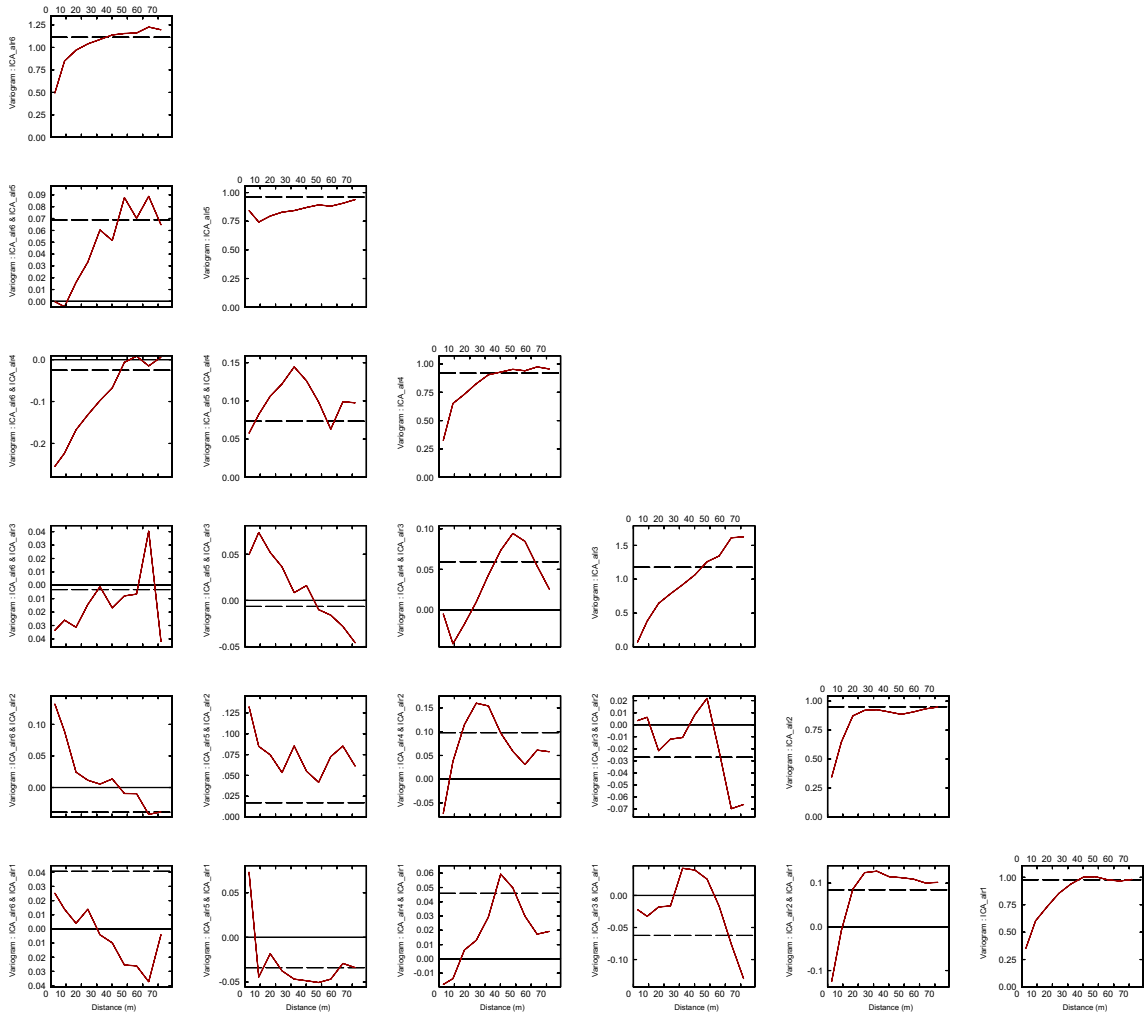

Figure C.9: Omnidirectional experimental (cross-)semivariograms ICA decorrelated log-ratio data Domain 2. Complete Dataset.

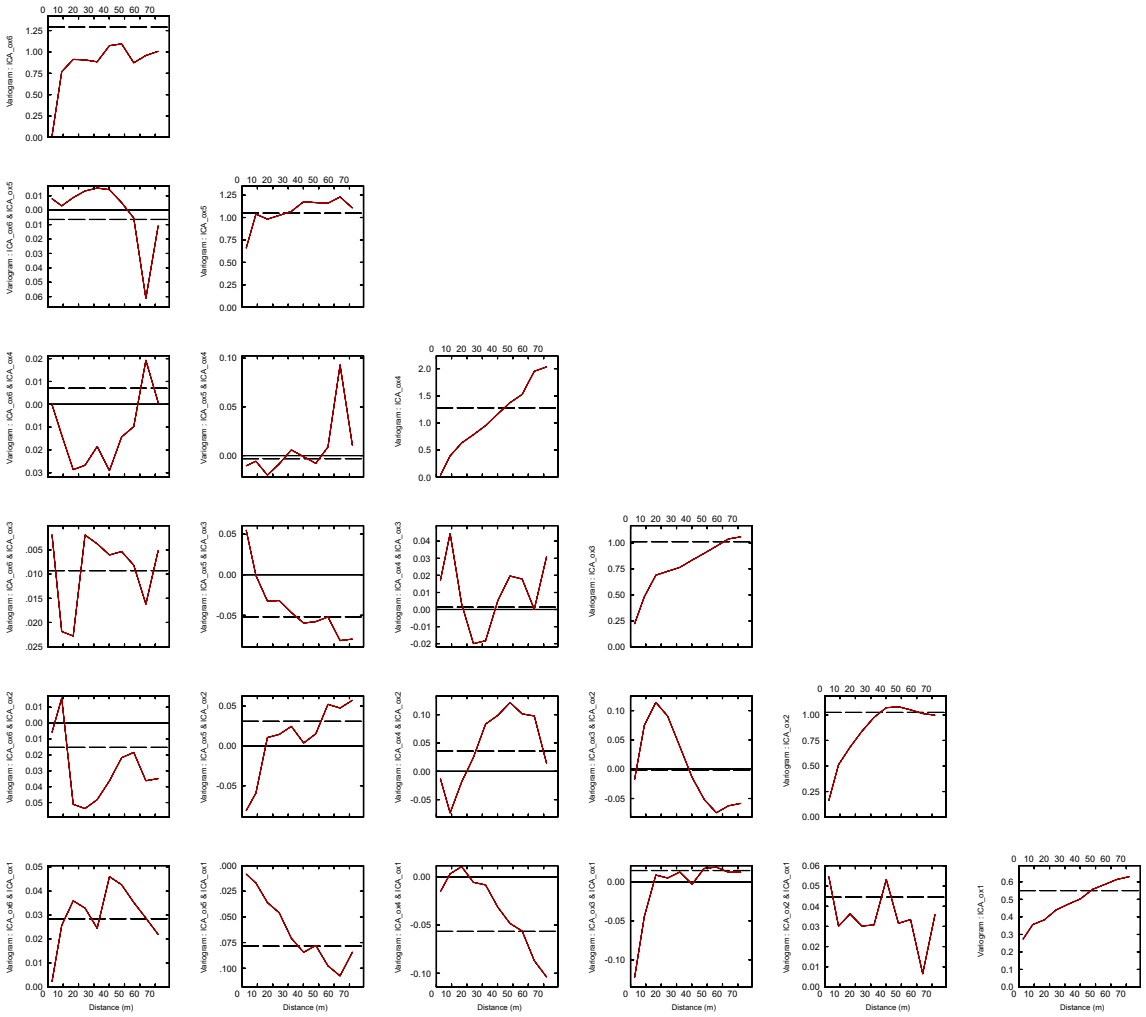

Figure C.10: Omnidirectional experimental (cross-)semivariograms ICA decorrelated oxide data Domain 2. Complete Dataset.

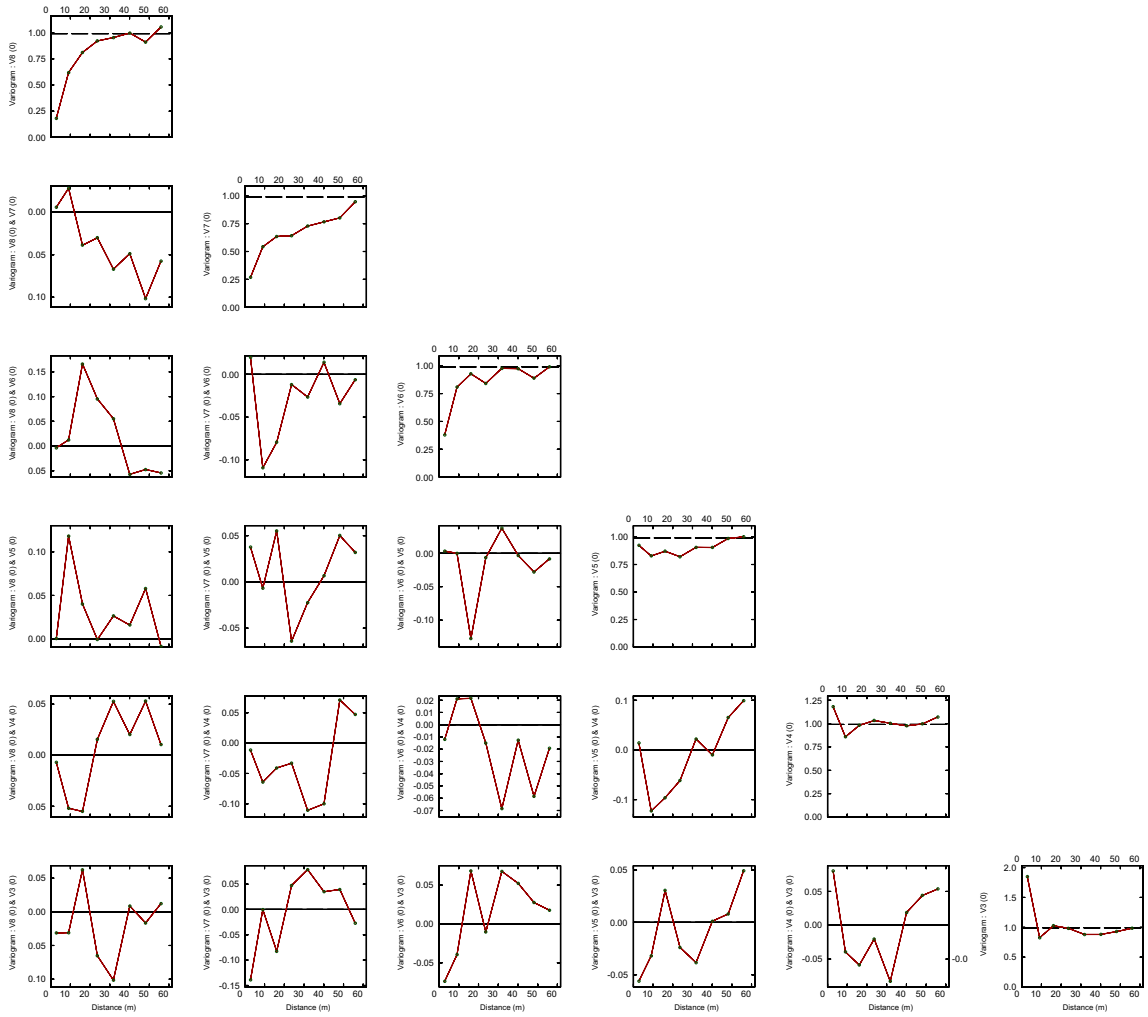

Figure C.11: Omnidirectional experimental (cross-)semivariograms MAF decorrelated log-ratio data Domain 2. Complete Dataset.

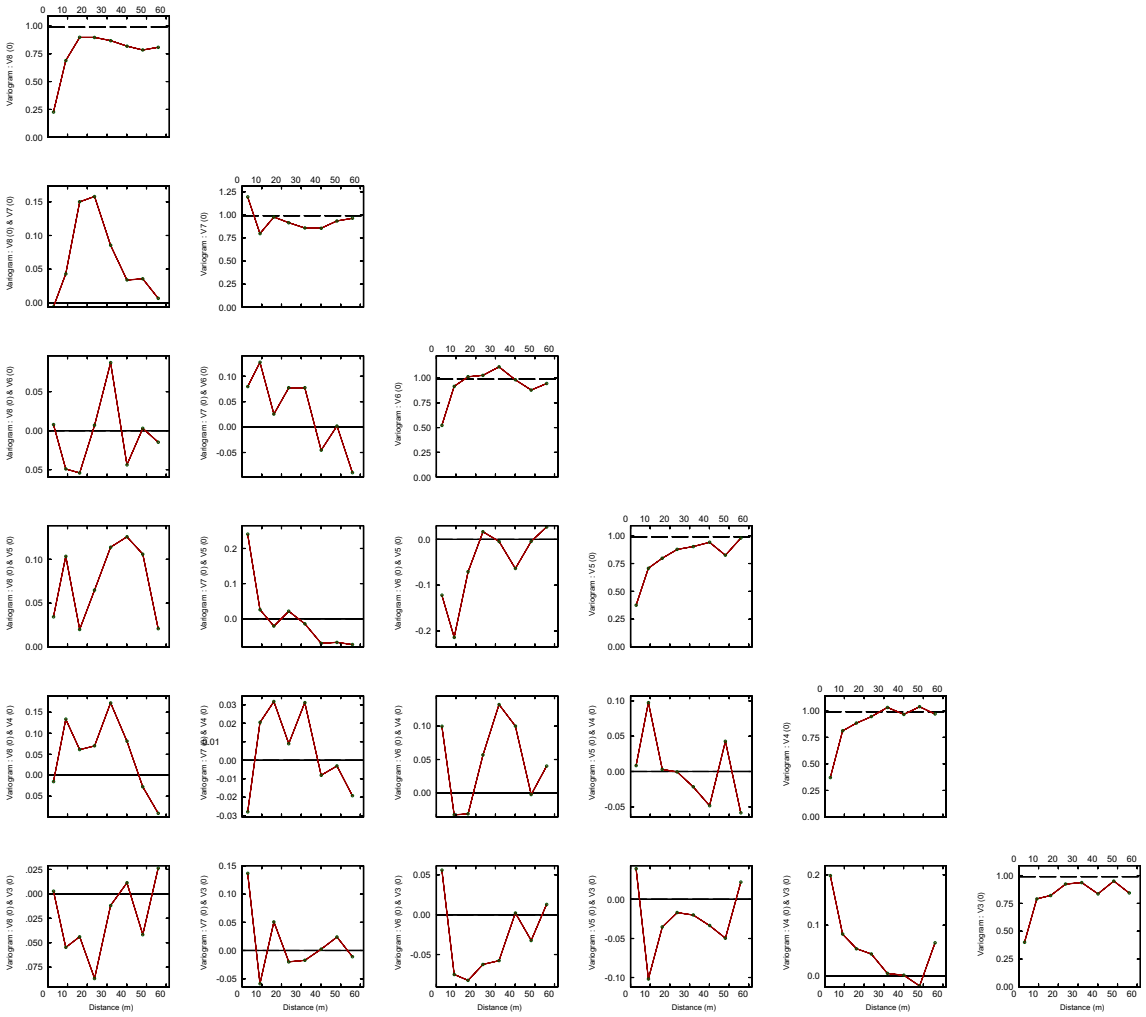

Figure C.12: Omnidirectional experimental (cross-)semivariograms MAF decorrelated oxide data Domain 2. Complete Dataset.

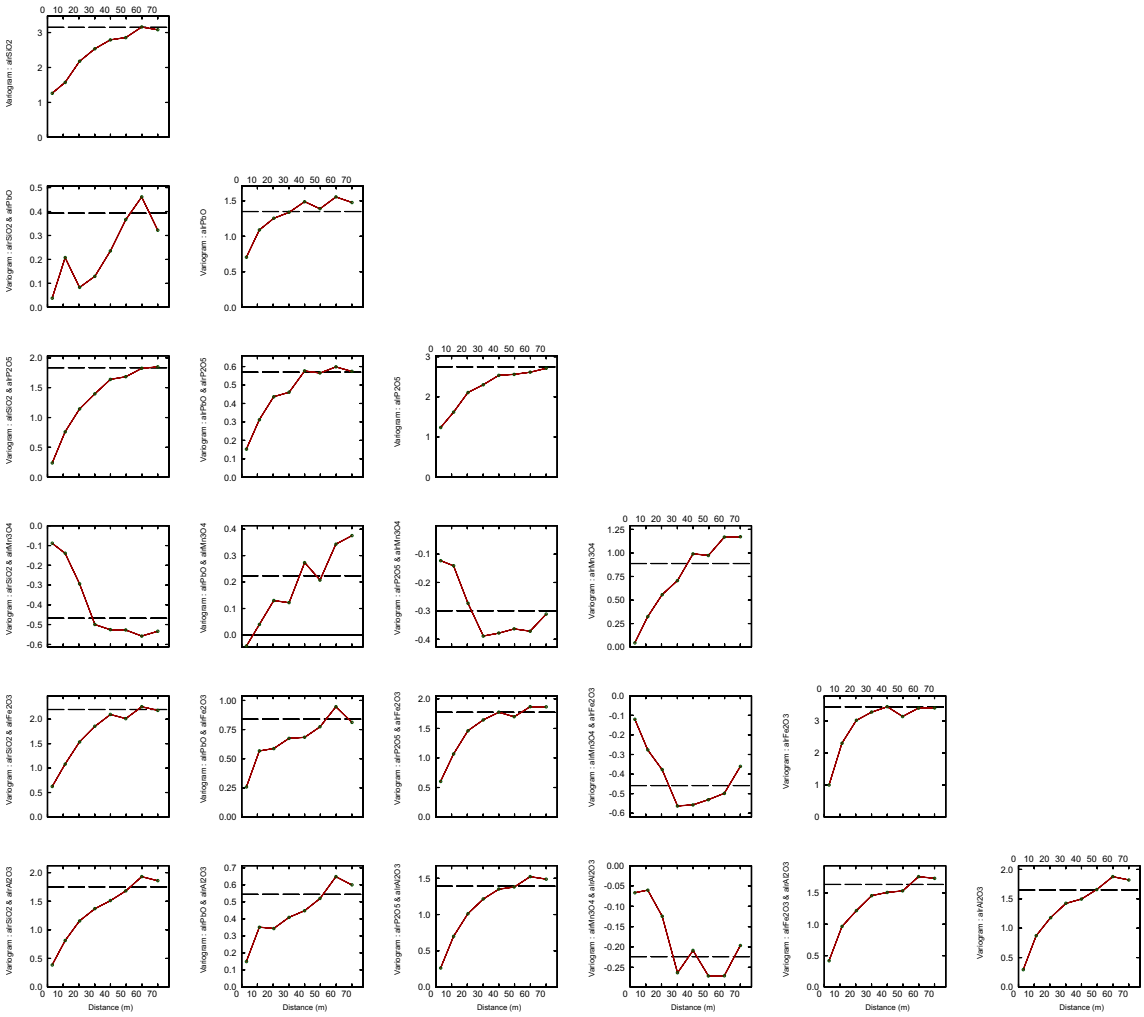

Figure C.13: Omnidirectional experimental semivariograms log-ratio data Domain 1. Reduced (RD) Dataset.

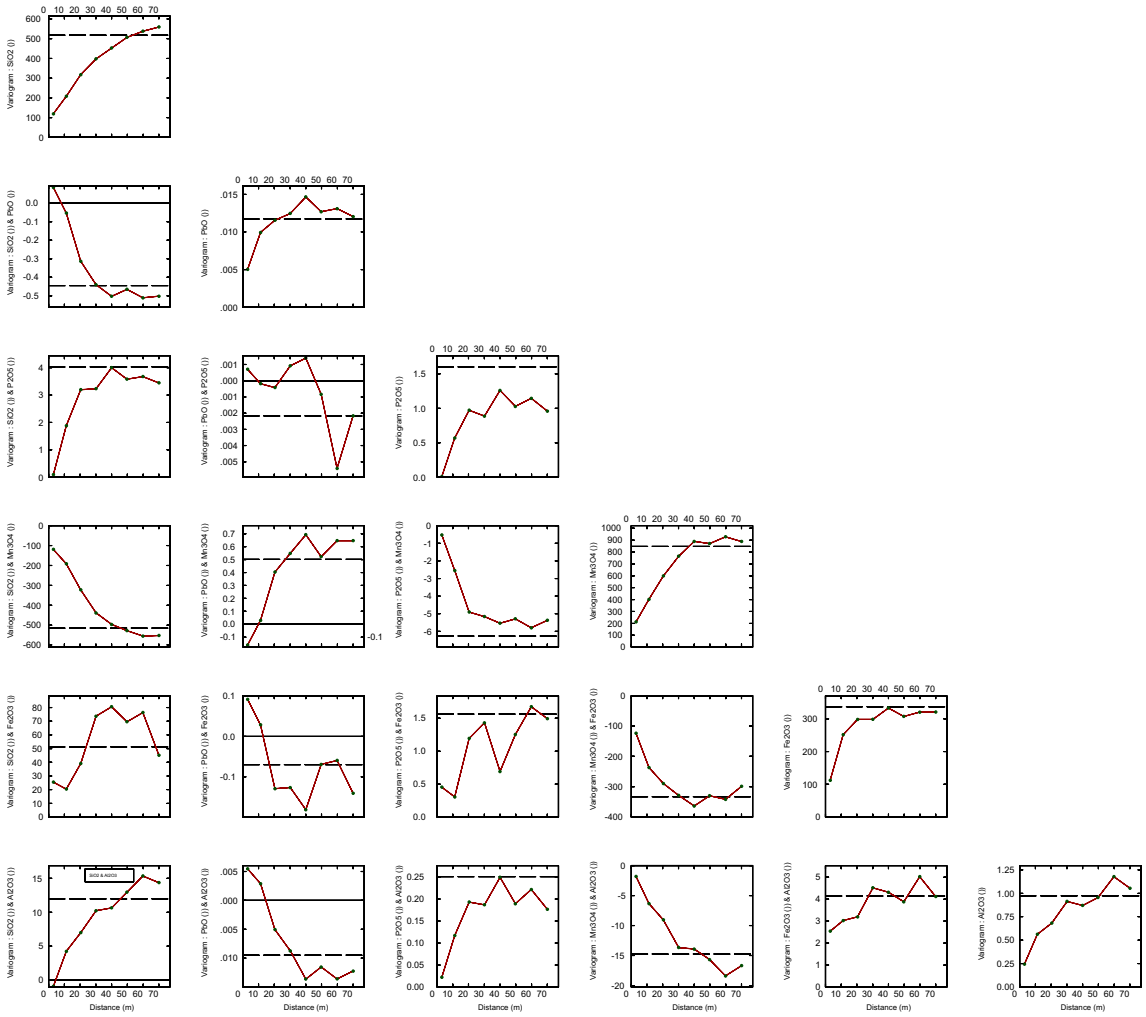

Figure C.14: Omnidirectional experimental semivariograms oxide data Domain 1. Reduced (RD) Dataset.

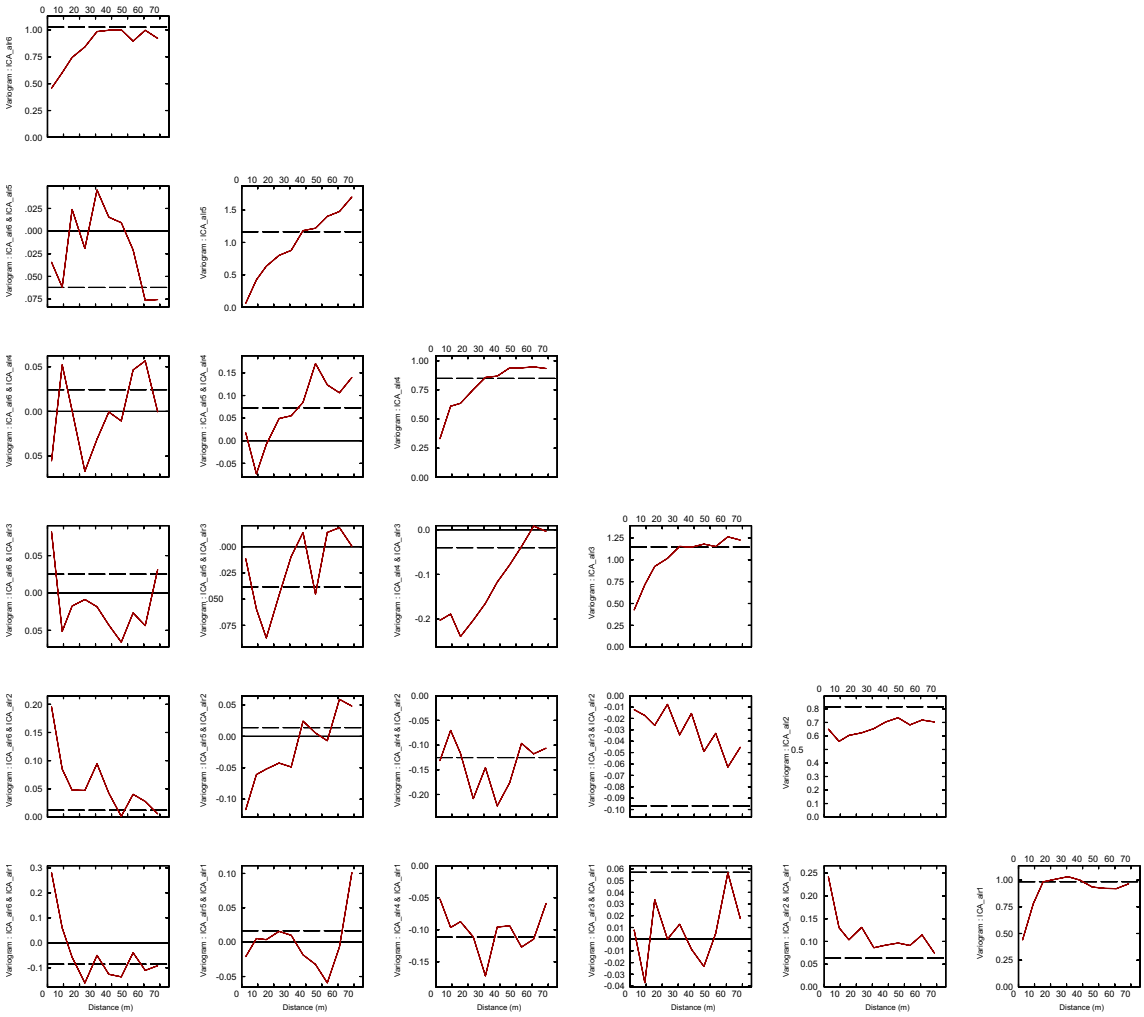

Figure C.15: Omnidirectional experimental semivariograms ICA decorrelated log-ratio data Domain 1. Reduced (RD) Dataset.

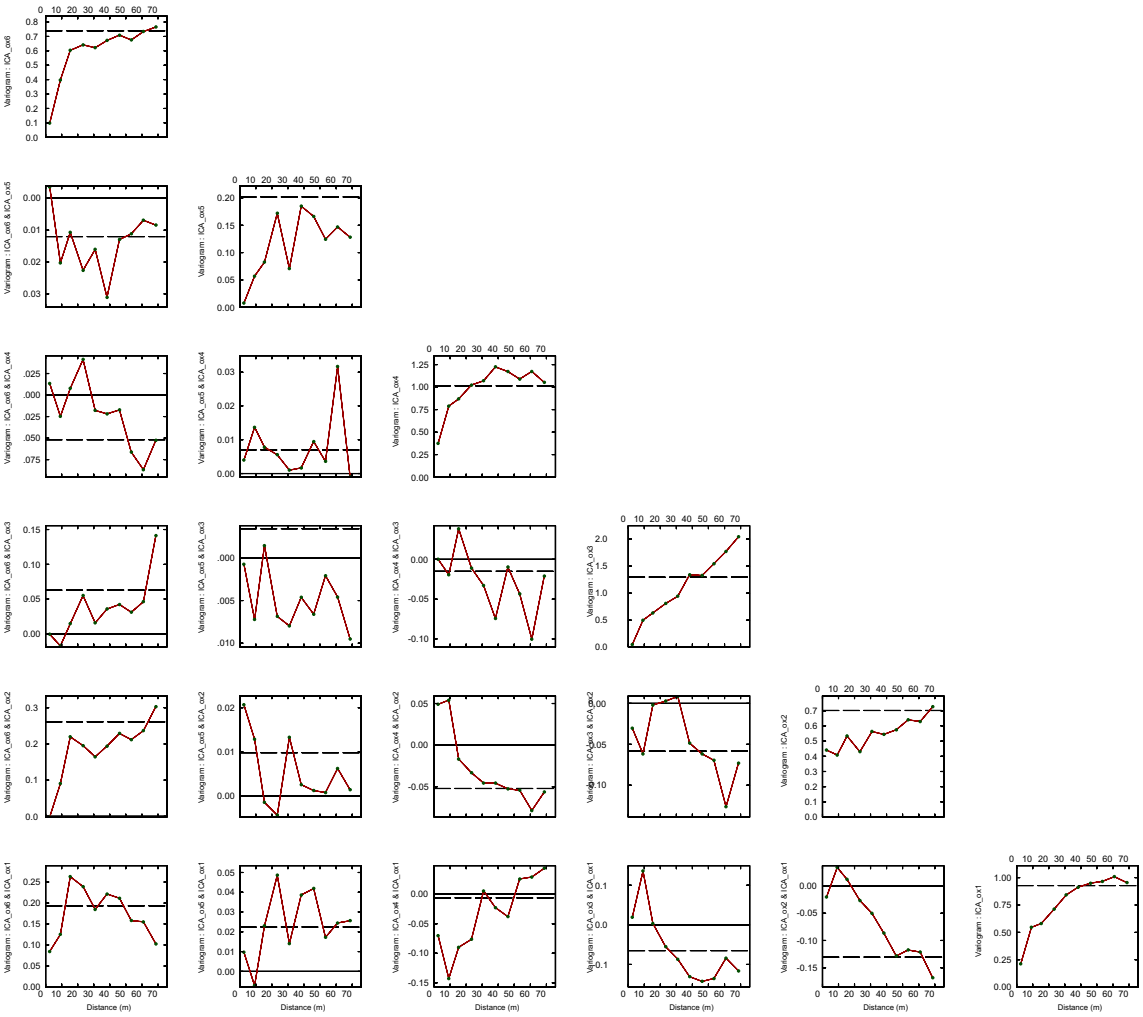

Figure C.16: Omnidirectional experimental semivariograms ICA decorrelated oxide data Domain 1. Reduced (RD) Dataset.

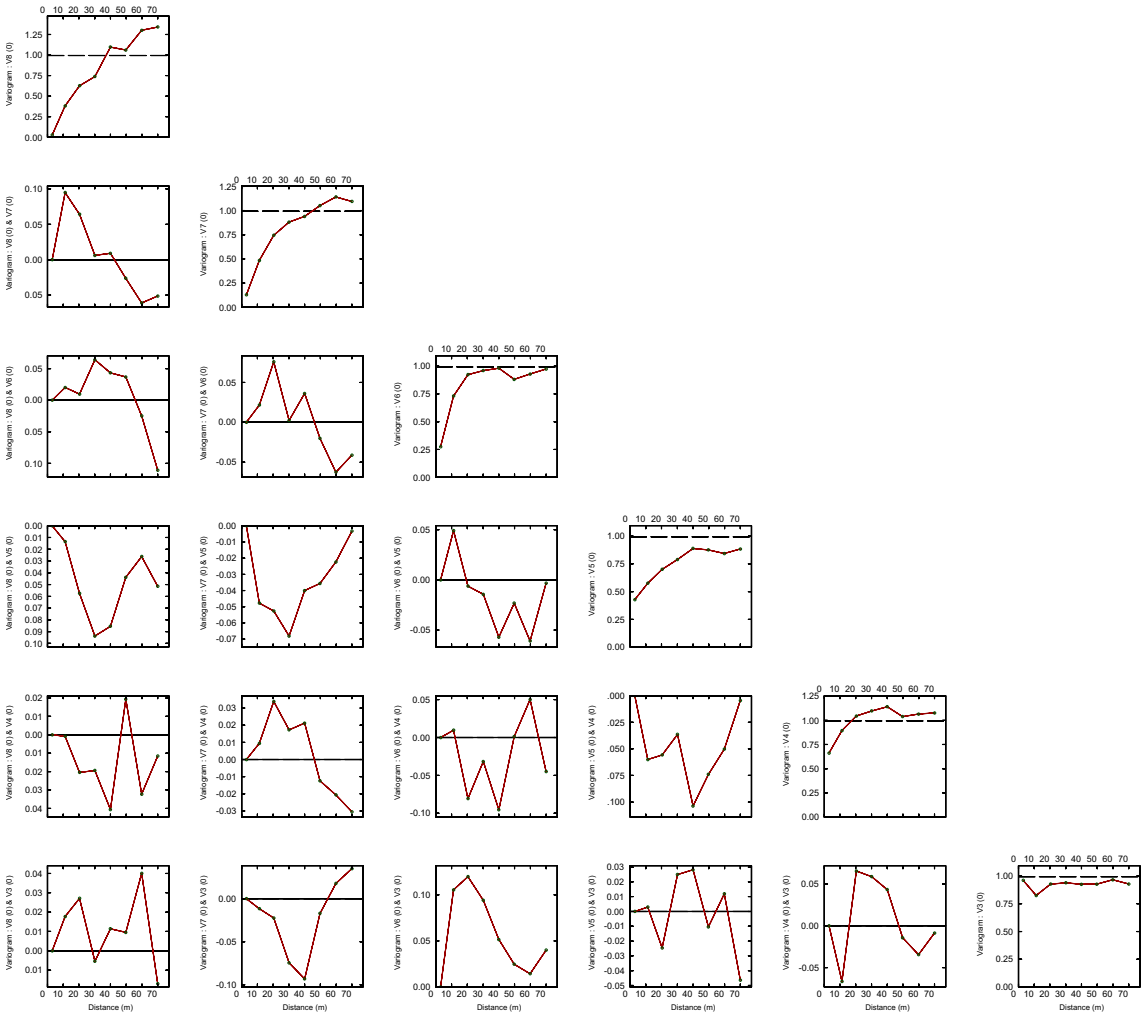

Figure C.17: Omnidirectional experimental semivariograms MAF decorrelated log-ratio data Domain 1. Reduced (RD) Dataset.

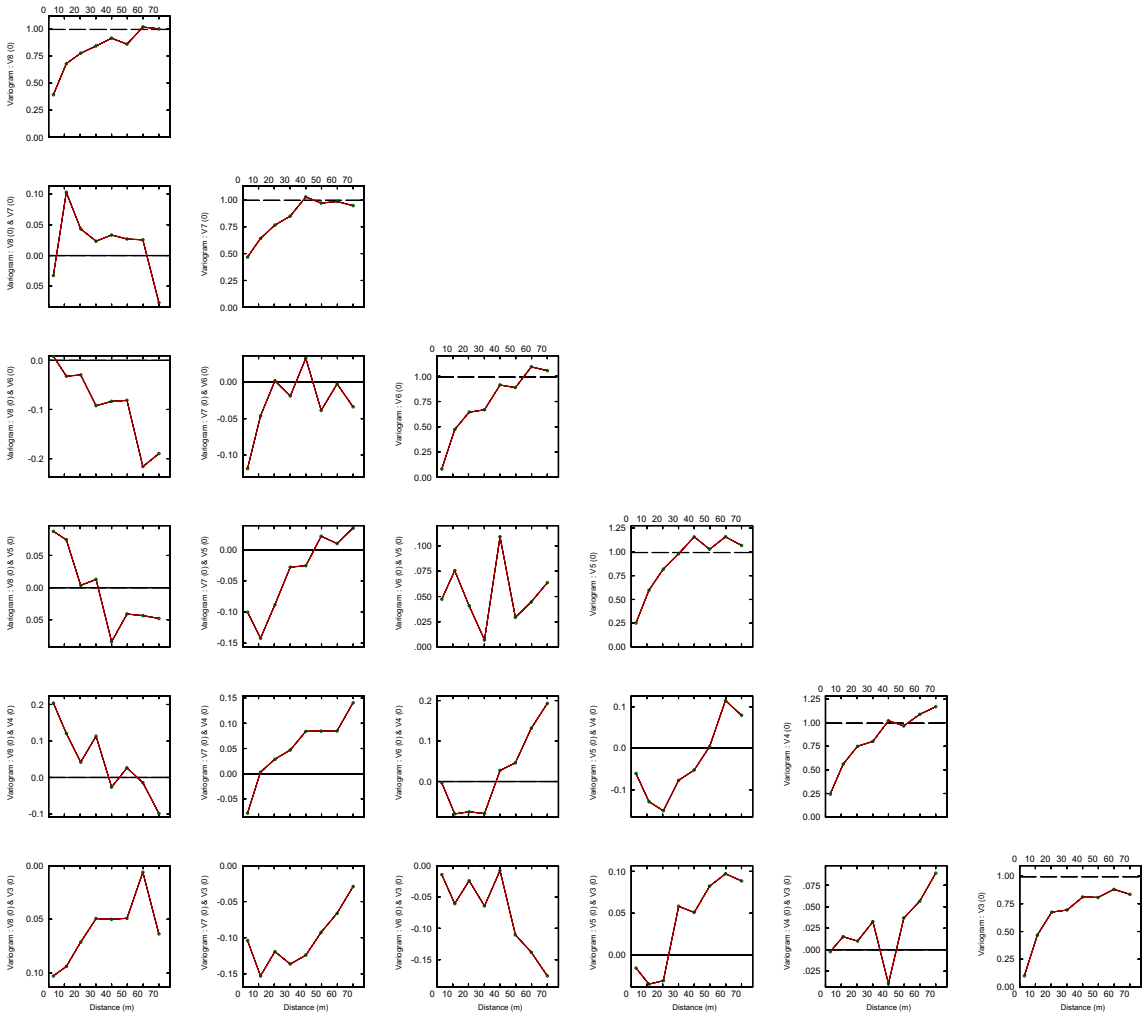

Figure C.18: Omnidirectional experimental semivariograms MAF decorrelated oxide data Domain 1. Reduced (RD) Dataset.

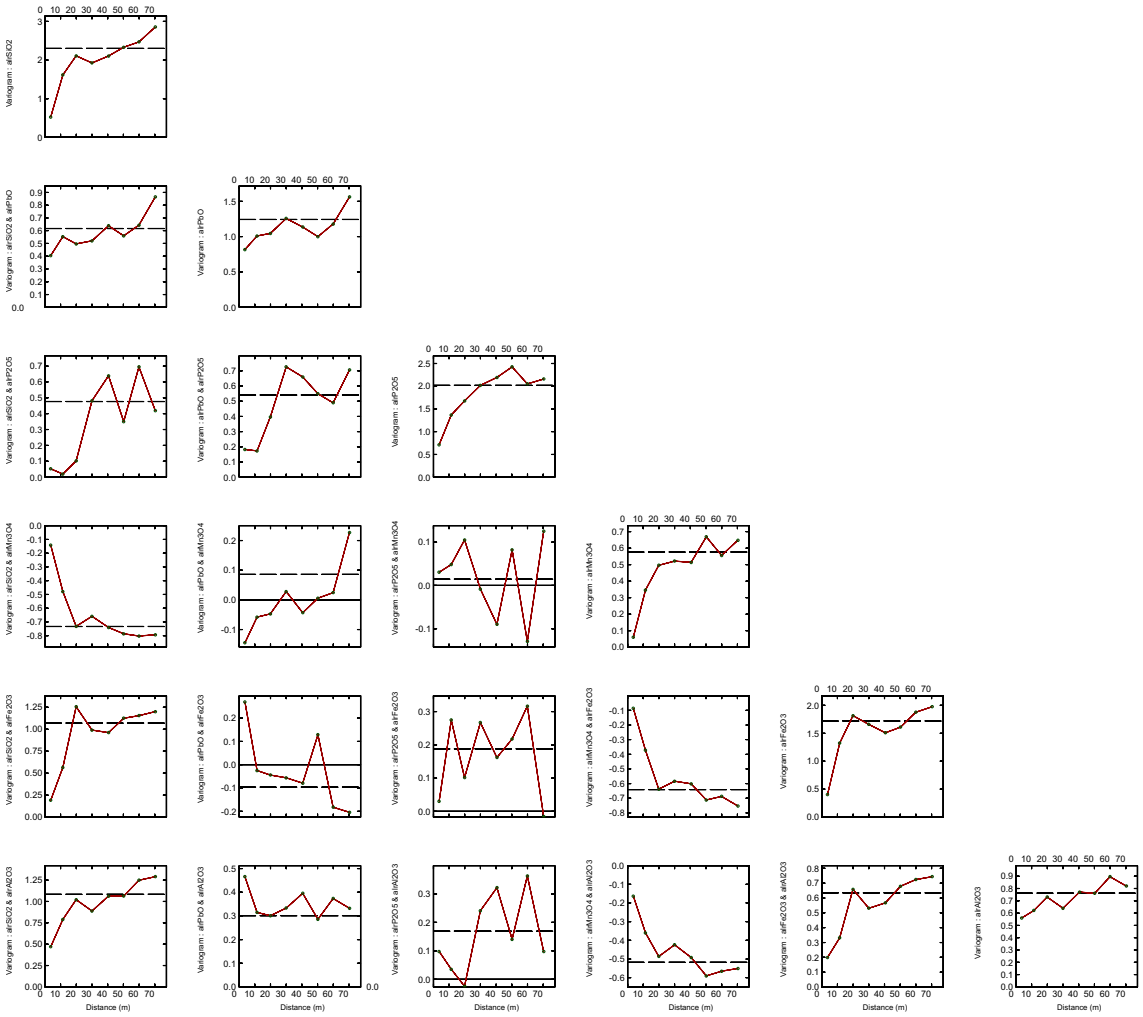

Figure C.19: Omnidirectional experimental semivariograms log-ratio data Domain 2. Reduced (RD) Dataset.

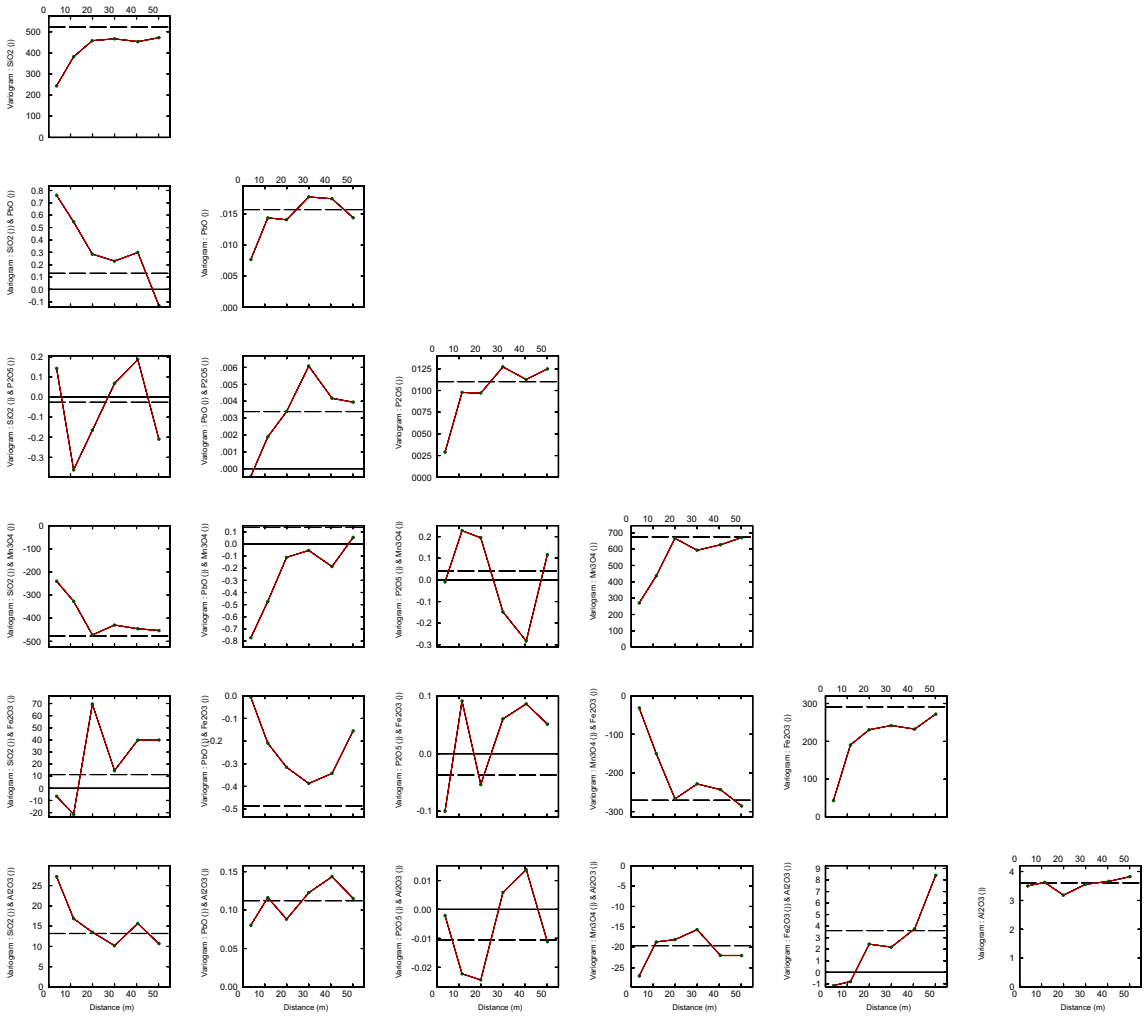

Figure C.20: Omnidirectional experimental semivariograms oxide data Domain 2. Reduced (RD) Dataset.

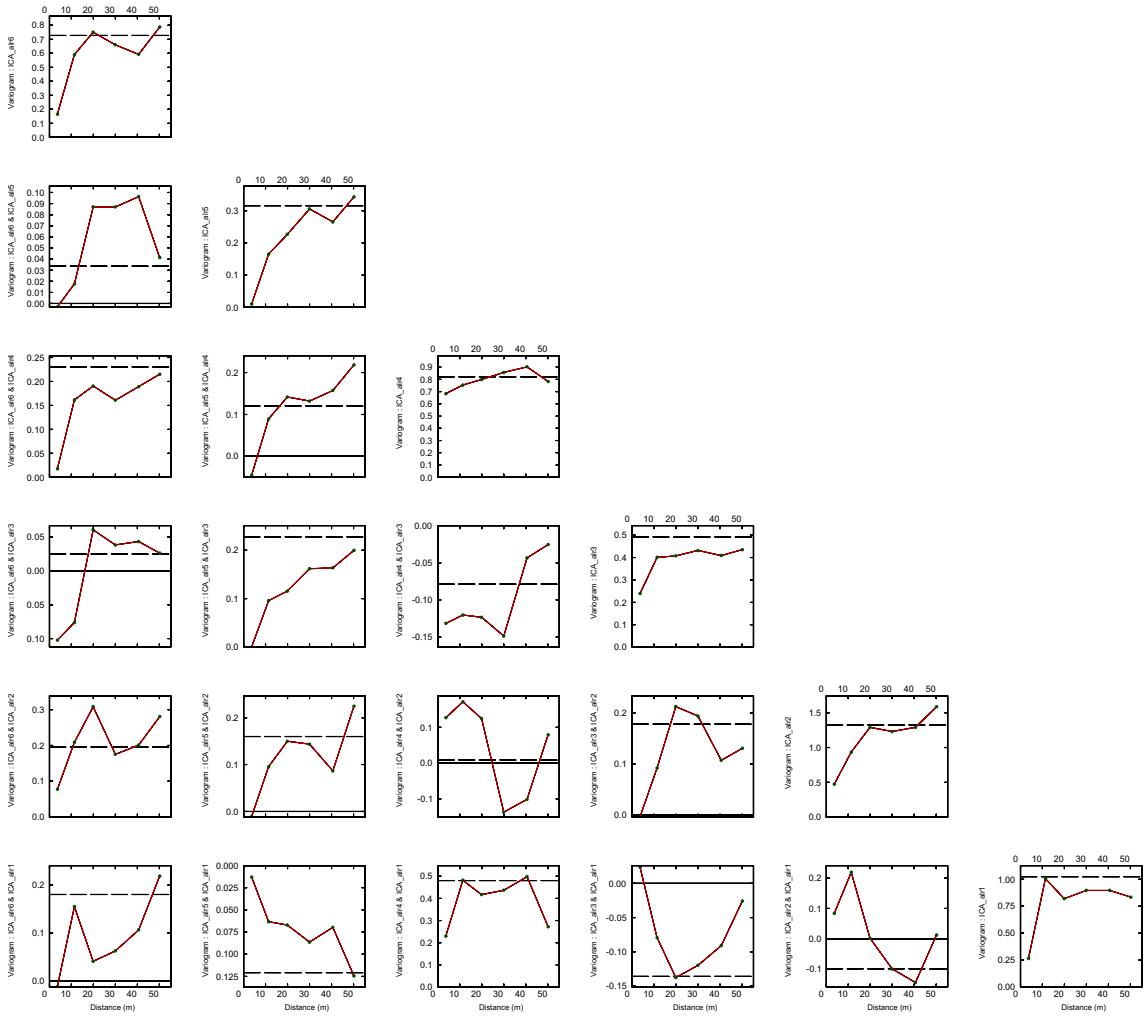

Figure C.21: Omnidirectional experimental semivariograms ICA decorrelated log-ratio data Domain 2. Reduced (RD) Dataset.

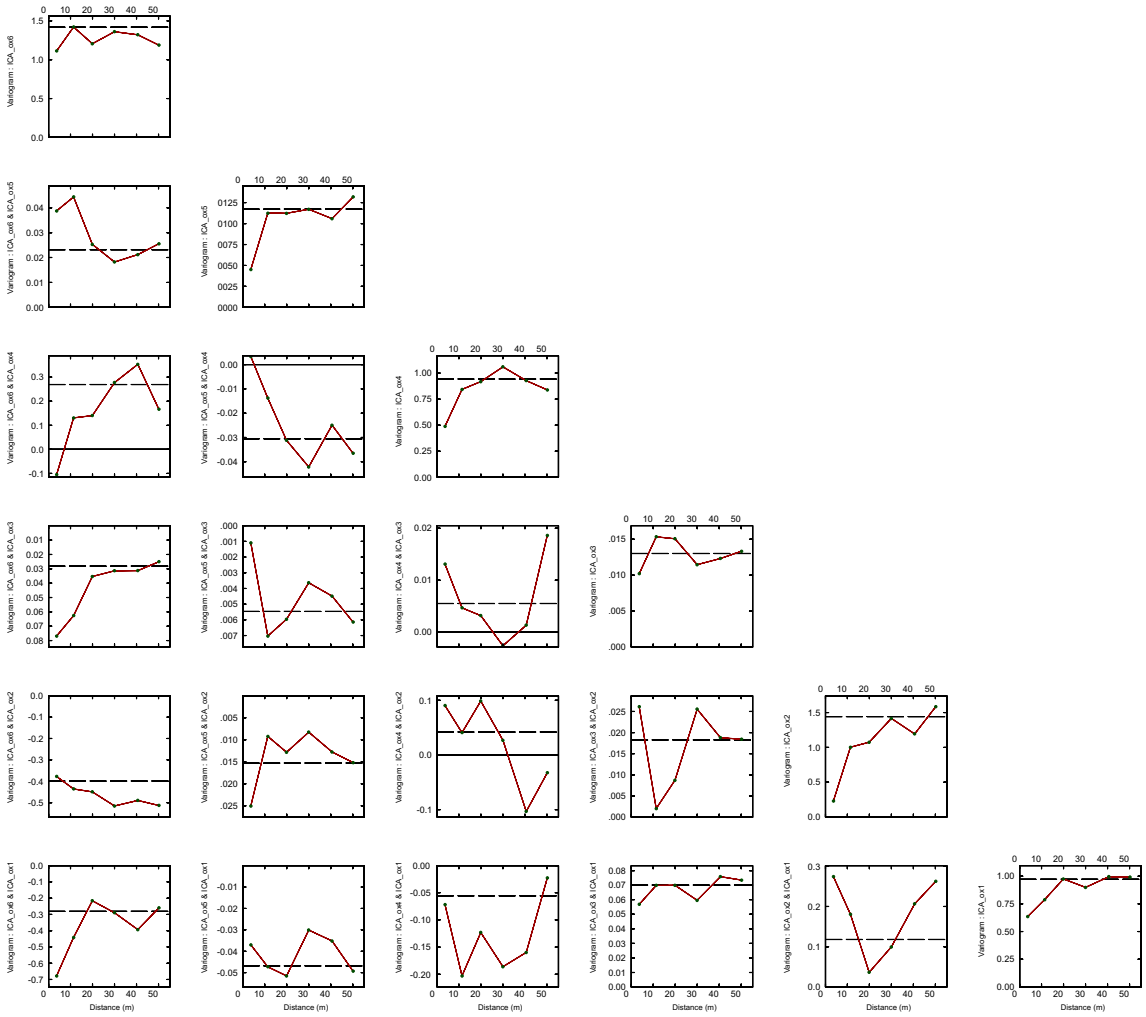

Figure C.22: Omnidirectional experimental semivariograms ICA decorrelated oxide data Domain 2. Reduced (RD) Dataset.

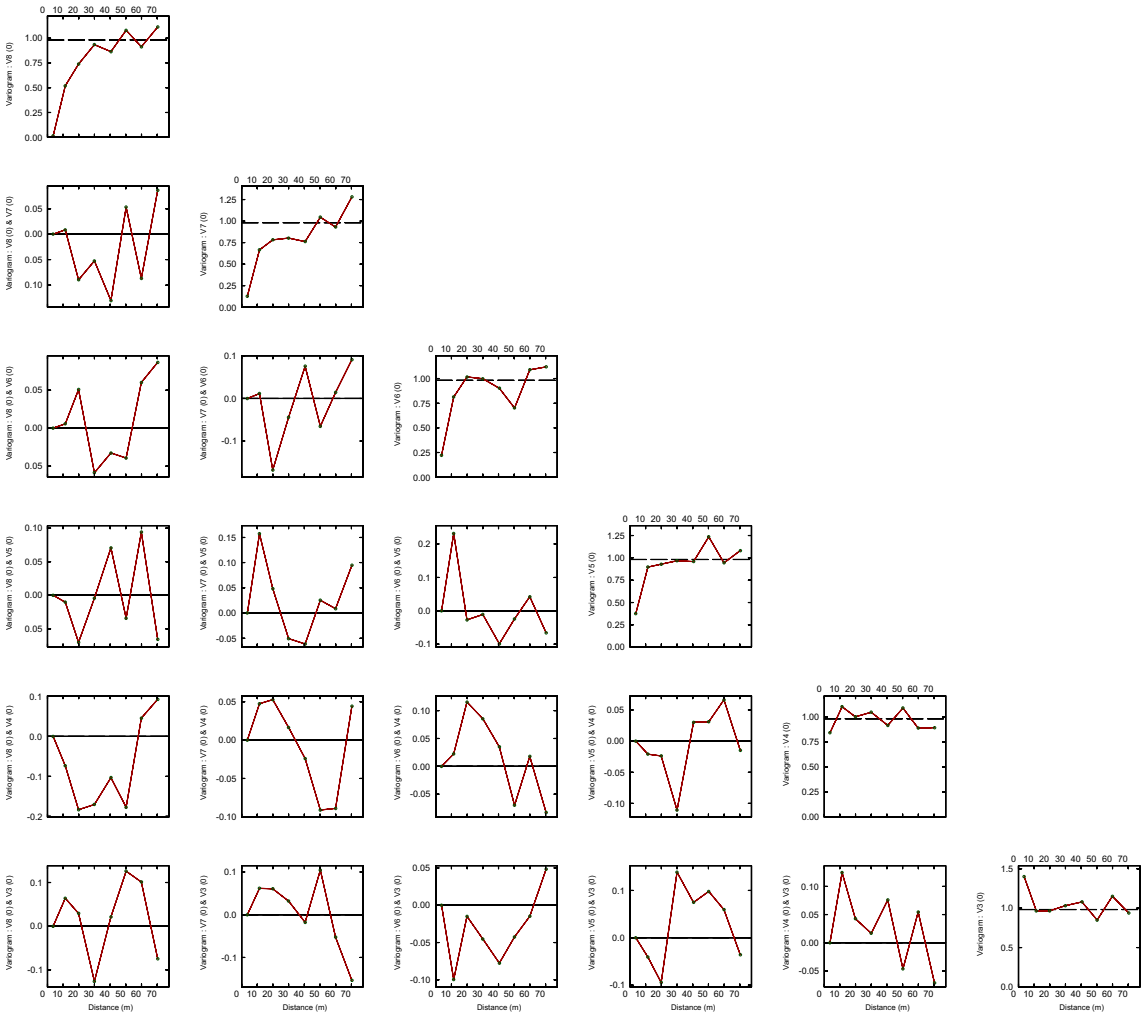

Figure C.23: Omnidirectional experimental semivariograms MAF decorrelated log-ratio data Domain 2. Reduced (RD) Dataset.

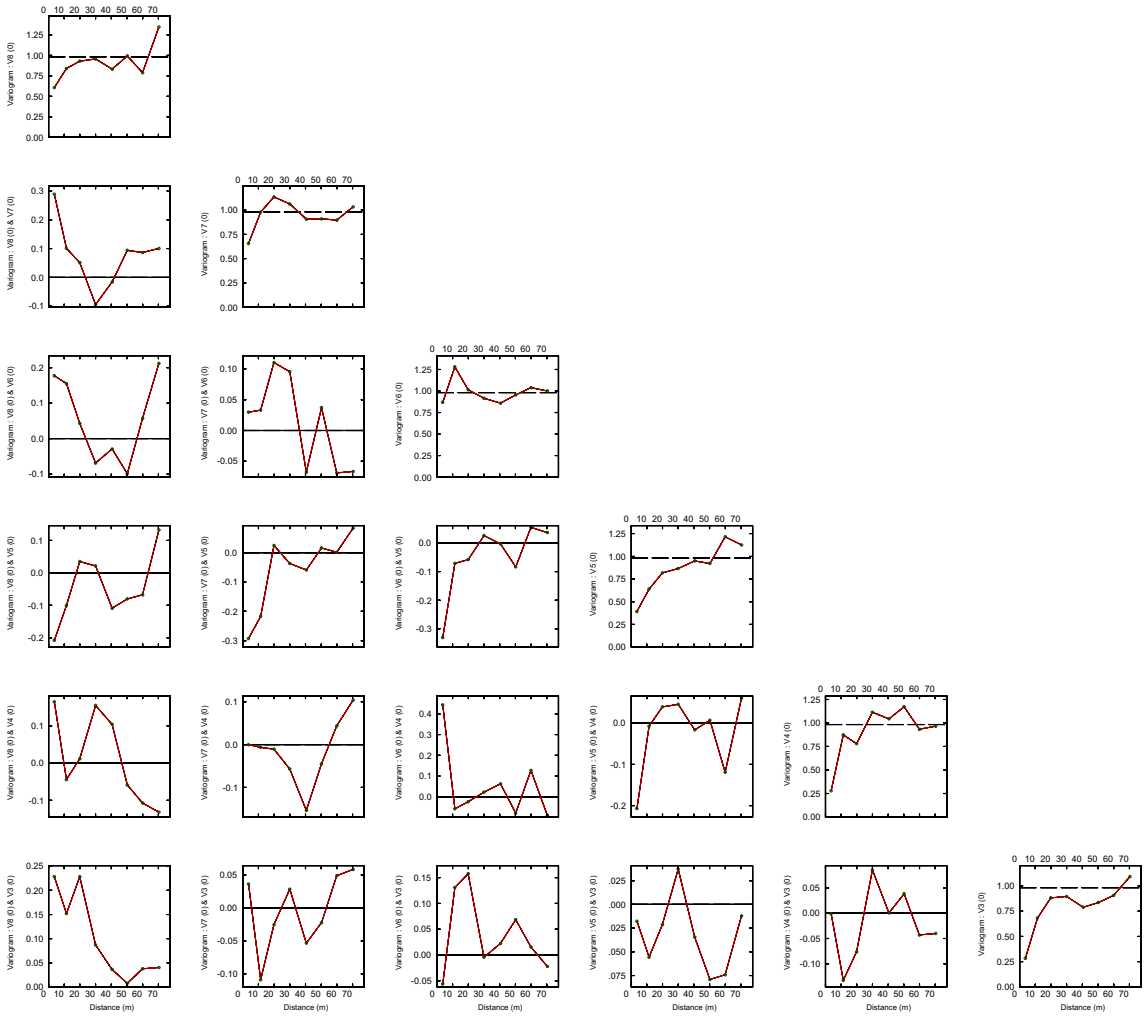

Figure C.24: Omnidirectional experimental semivariograms MAF decorrelated oxide data Domain 2. Reduced (RD) Dataset.

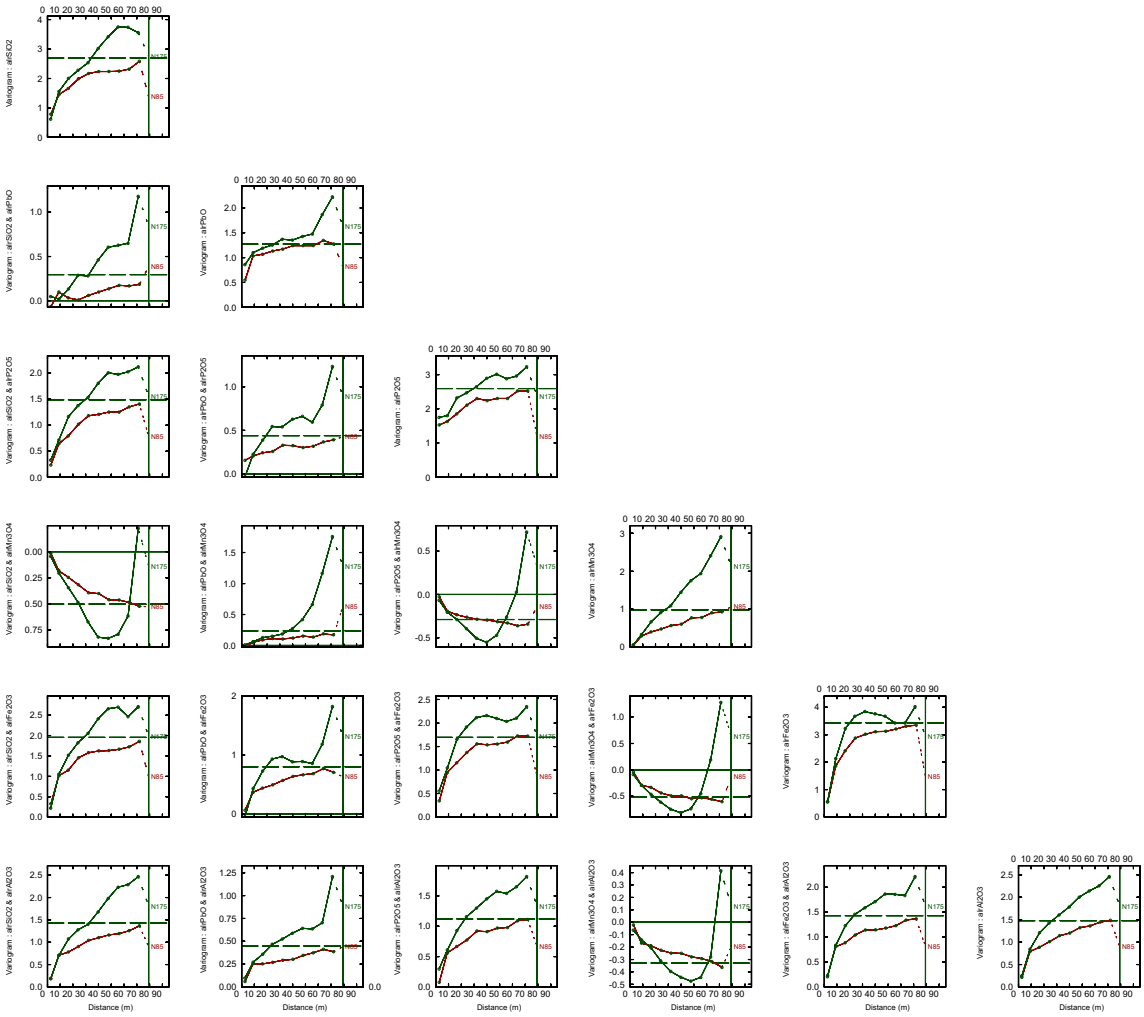

Figure C.25: Directional experimental semivariograms log-ratio data Domain 1. Complete Dataset.

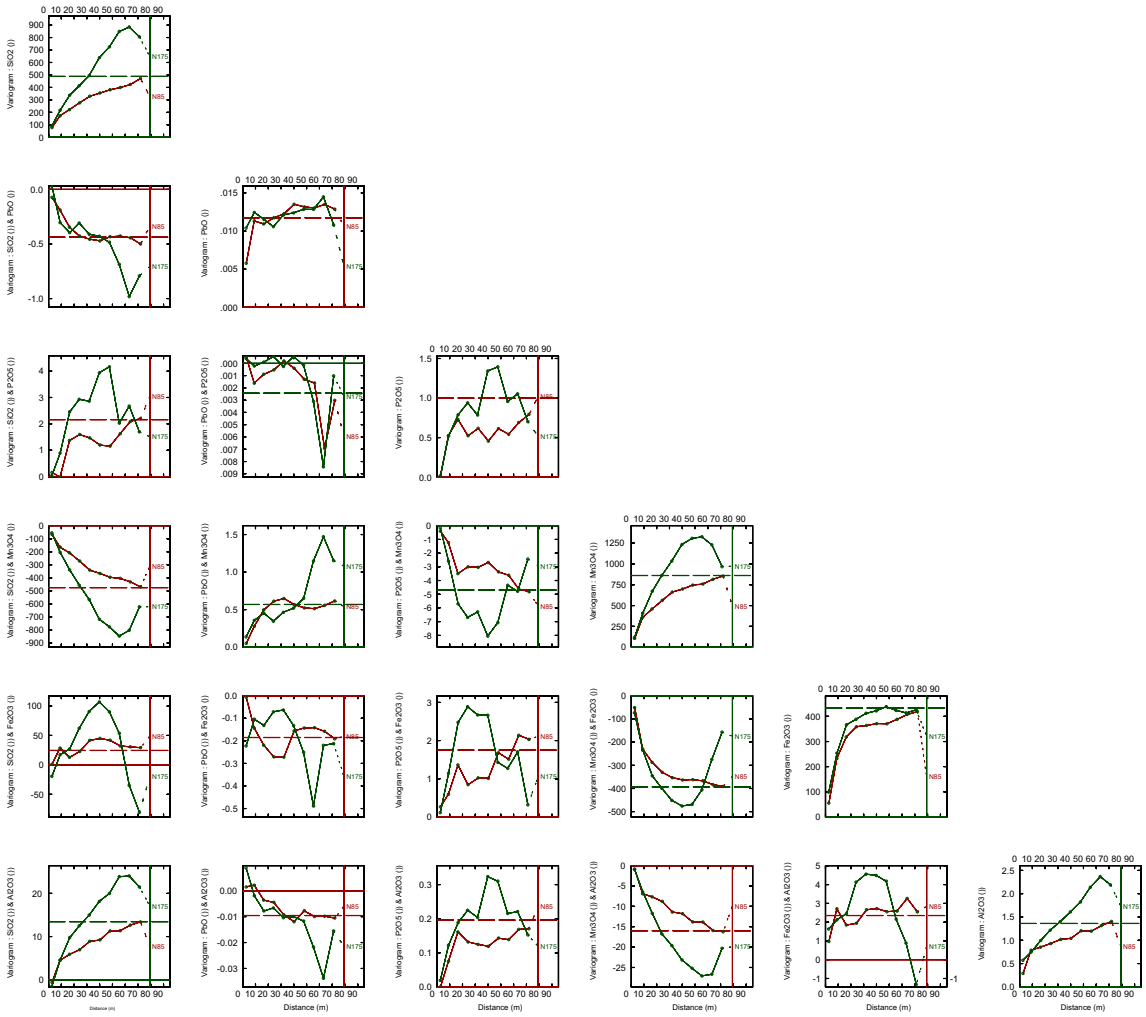

Figure C.26: Directional experimental semivariograms oxide data Domain 1. Complete Dataset.

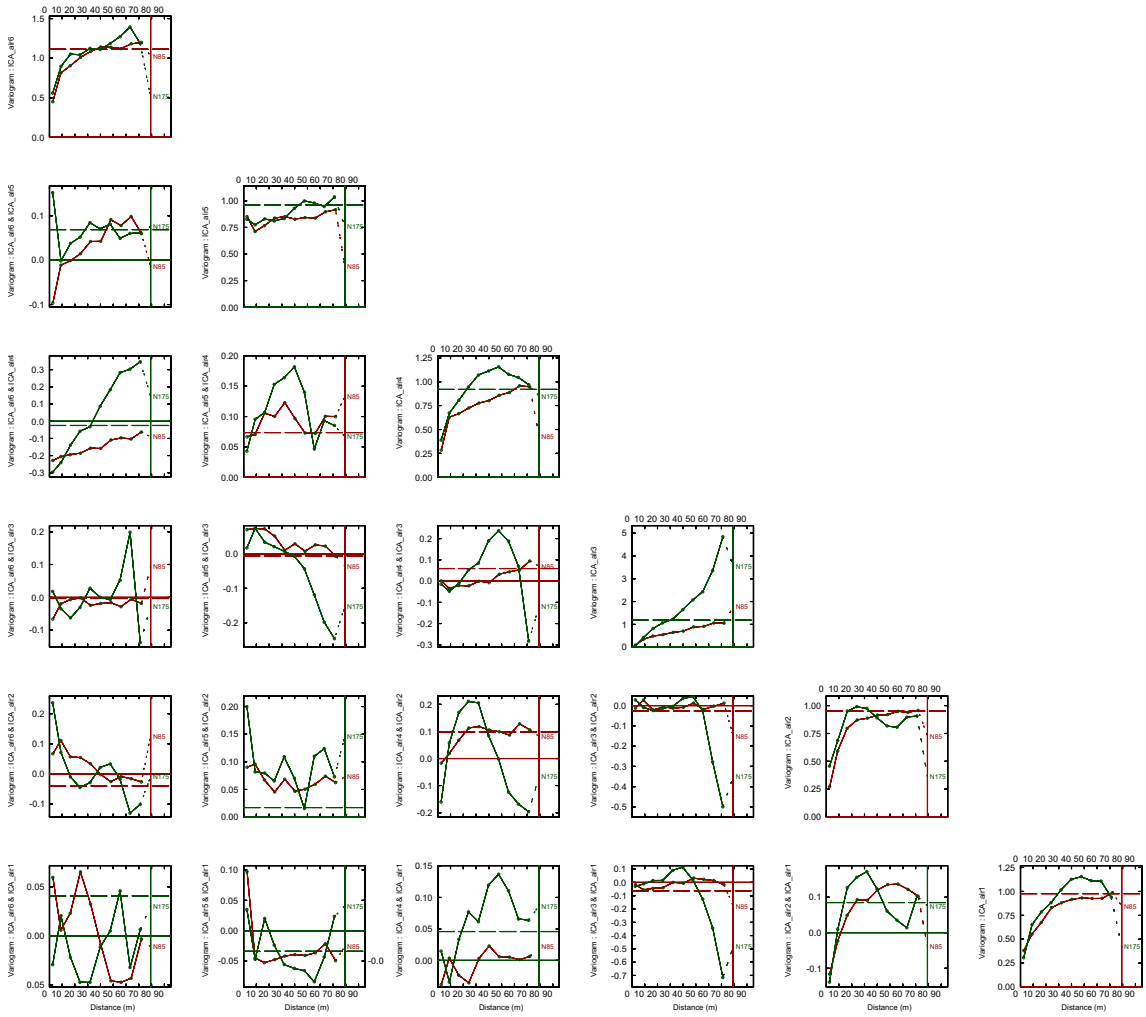

Figure C.27: Directional experimental semivariograms ICA decorrelated log-ratio data Domain 1. Complete Dataset.

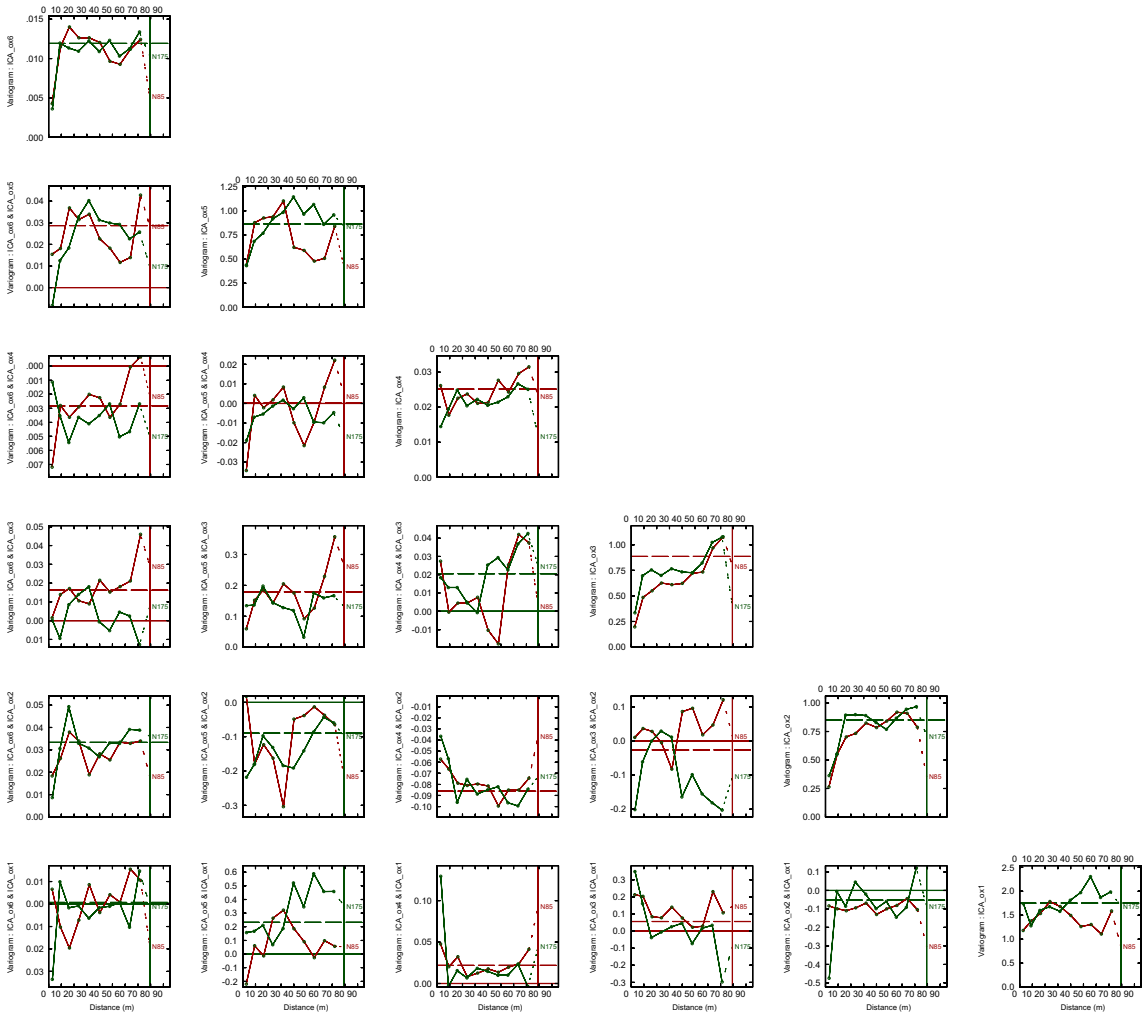

Figure C.28: Directional experimental semivariograms ICA decorrelated oxide data Domain 1. Complete Dataset.

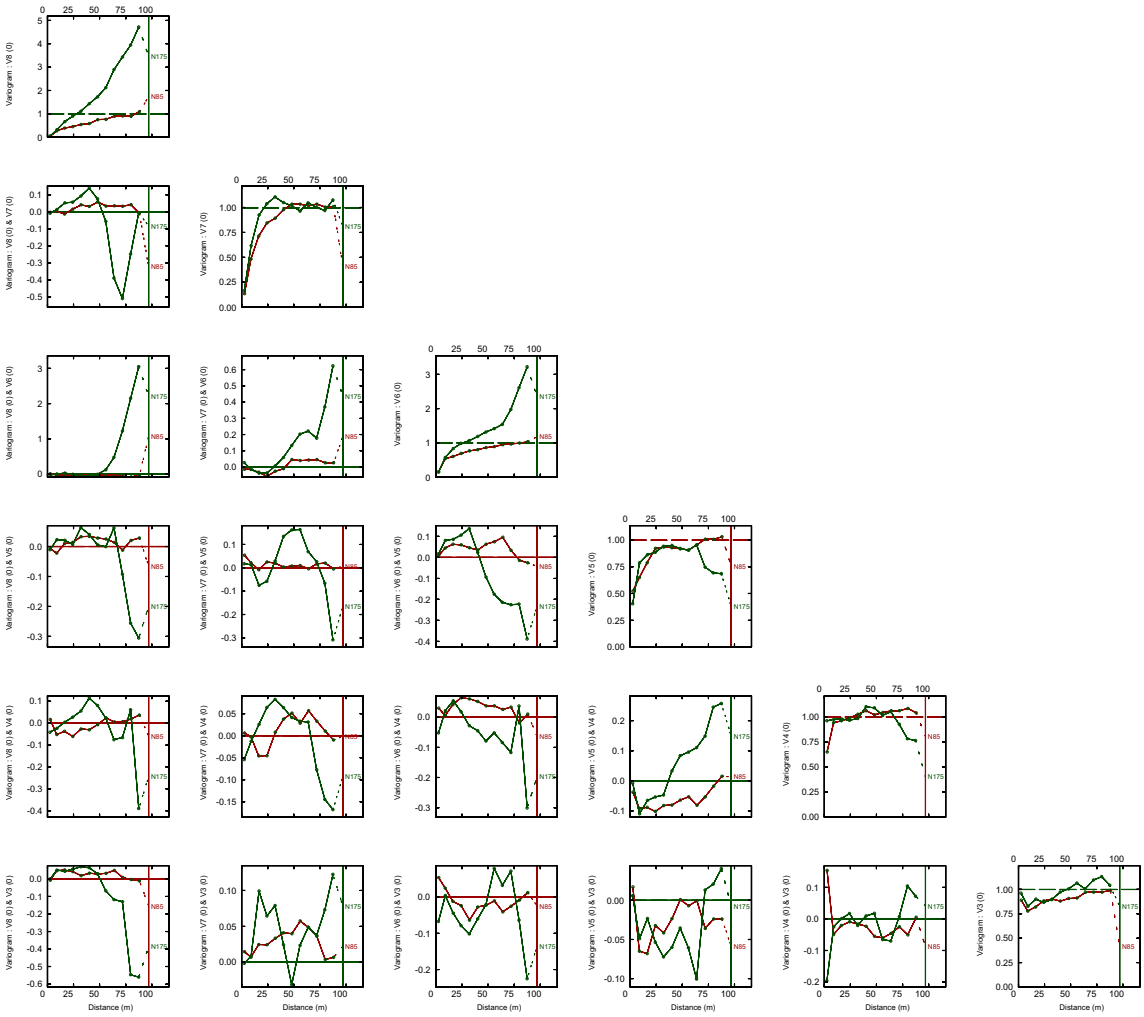

Figure C.29: Directional experimental semivariograms MAF decorrelated log-ratio data Domain 1. Complete Dataset.

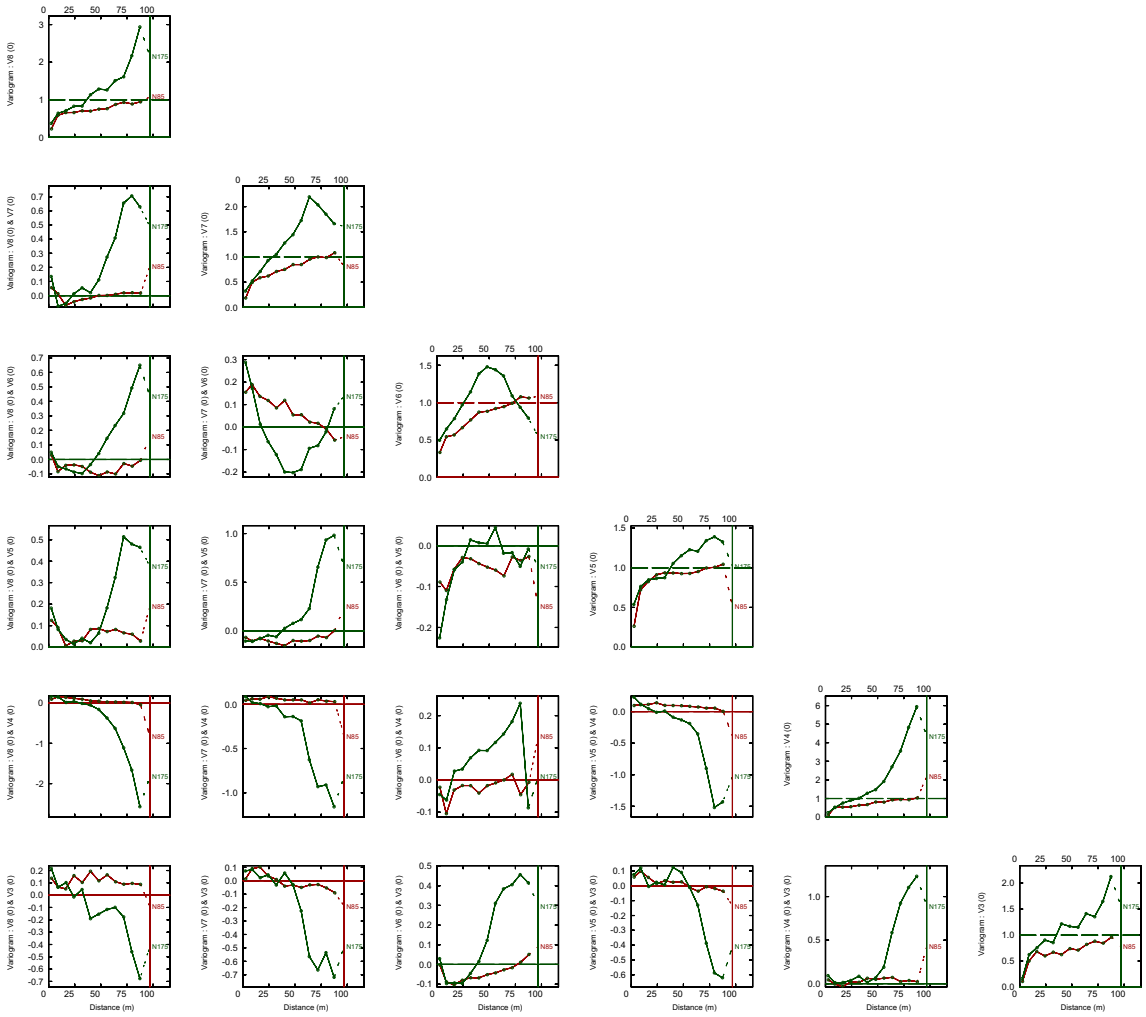

Figure C.30: Directional experimental semivariograms MAF decorrelated oxide data Domain 1. Complete Dataset.

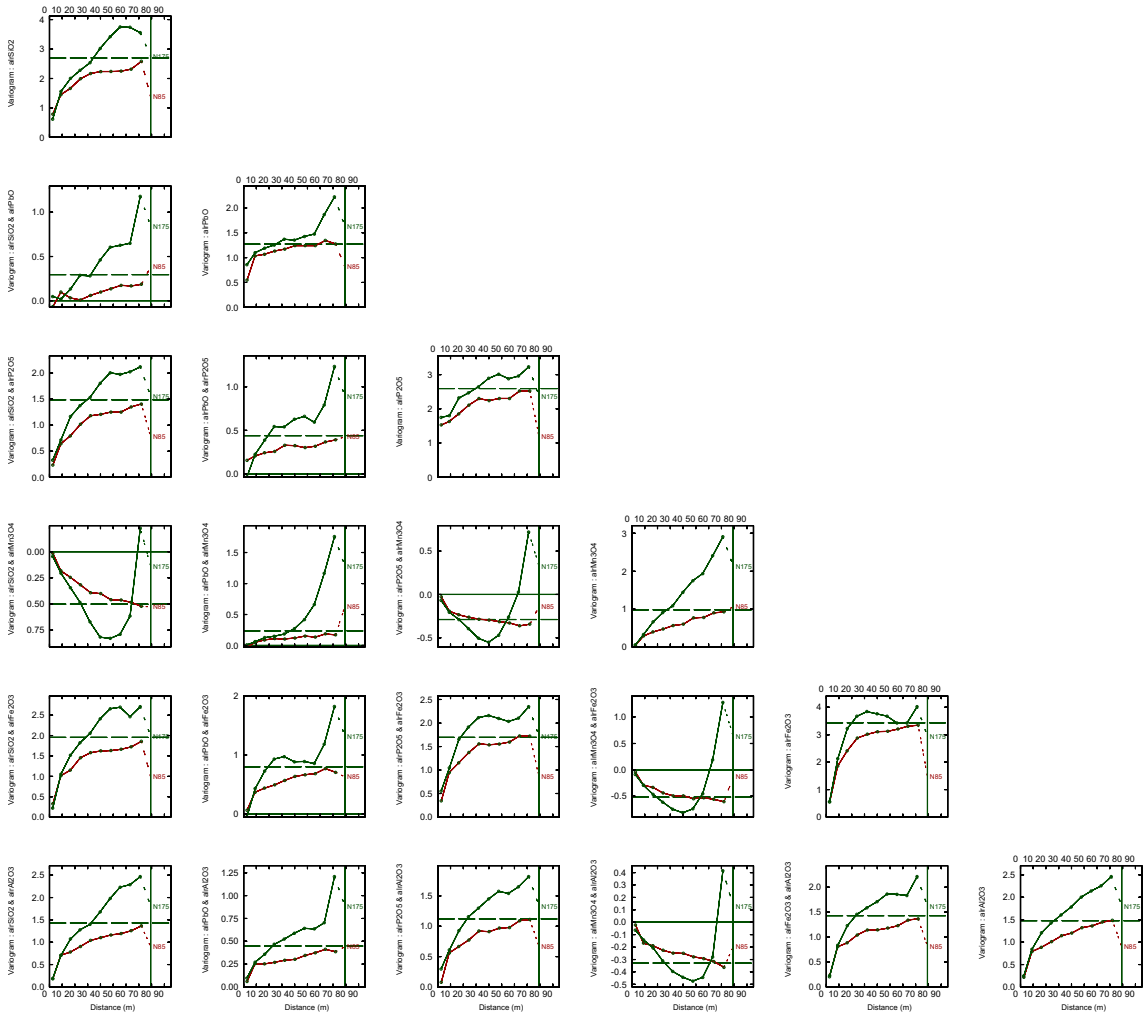

Figure C.31: Directional experimental semivariograms log-ratio data Domain 2. Complete Dataset.

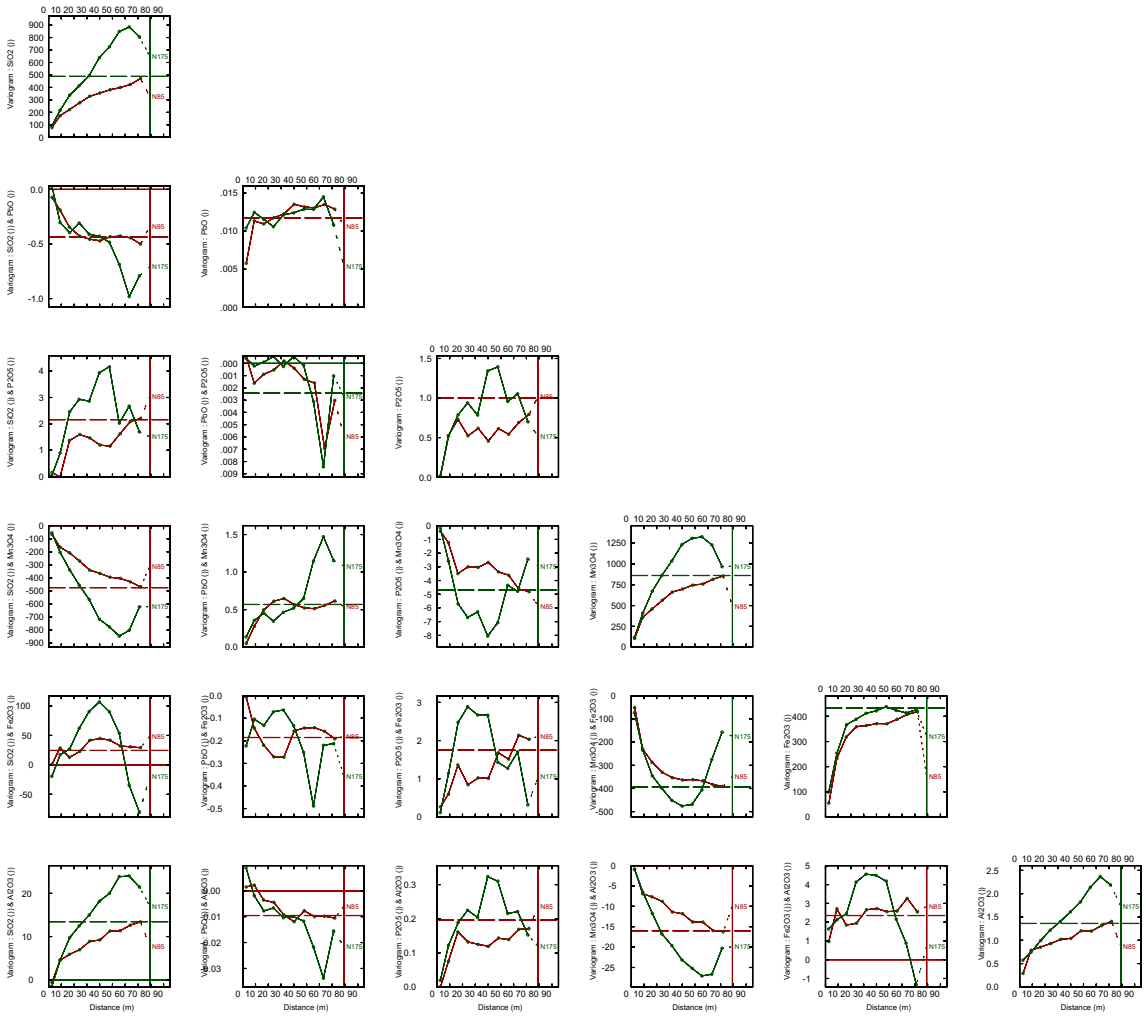

Figure C.32: Directional experimental semivariograms oxide data Domain 2. Complete Dataset.

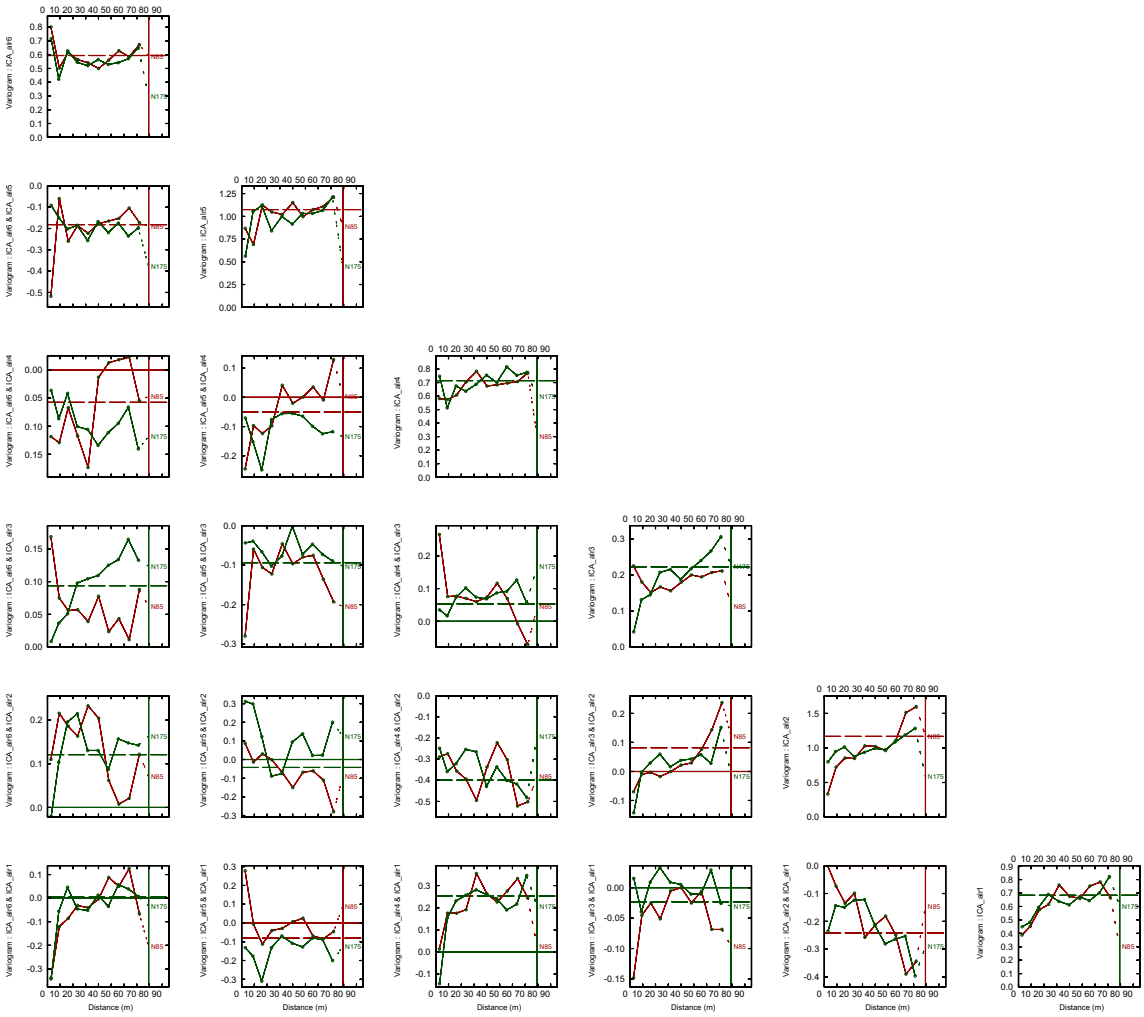

Figure C.33: Directional experimental semivariograms ICA decorrelated log-ratio data Domain 2. Complete Dataset.

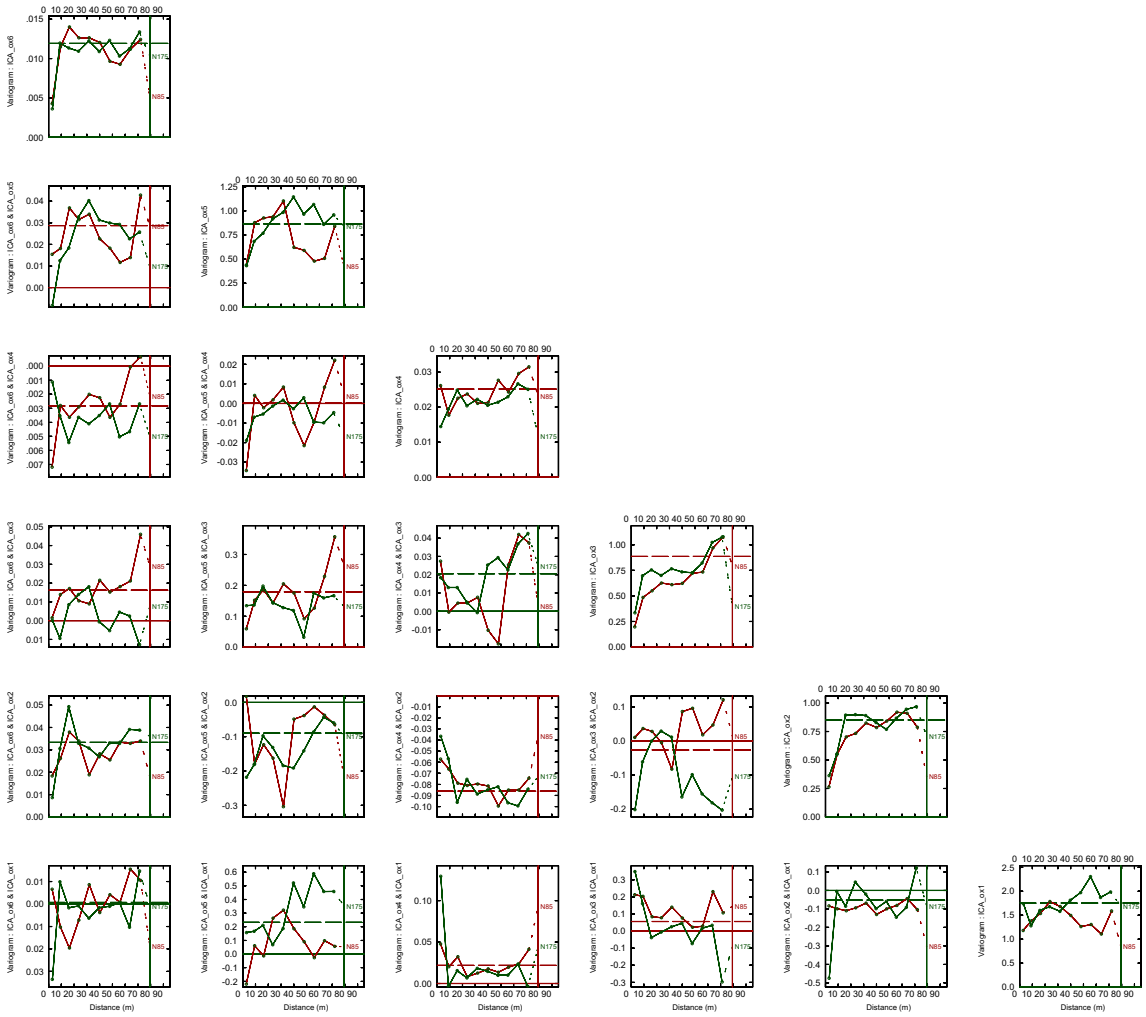

Figure C.34: Directional experimental semivariograms ICA decorrelated oxide data Domain 2. Complete Dataset.

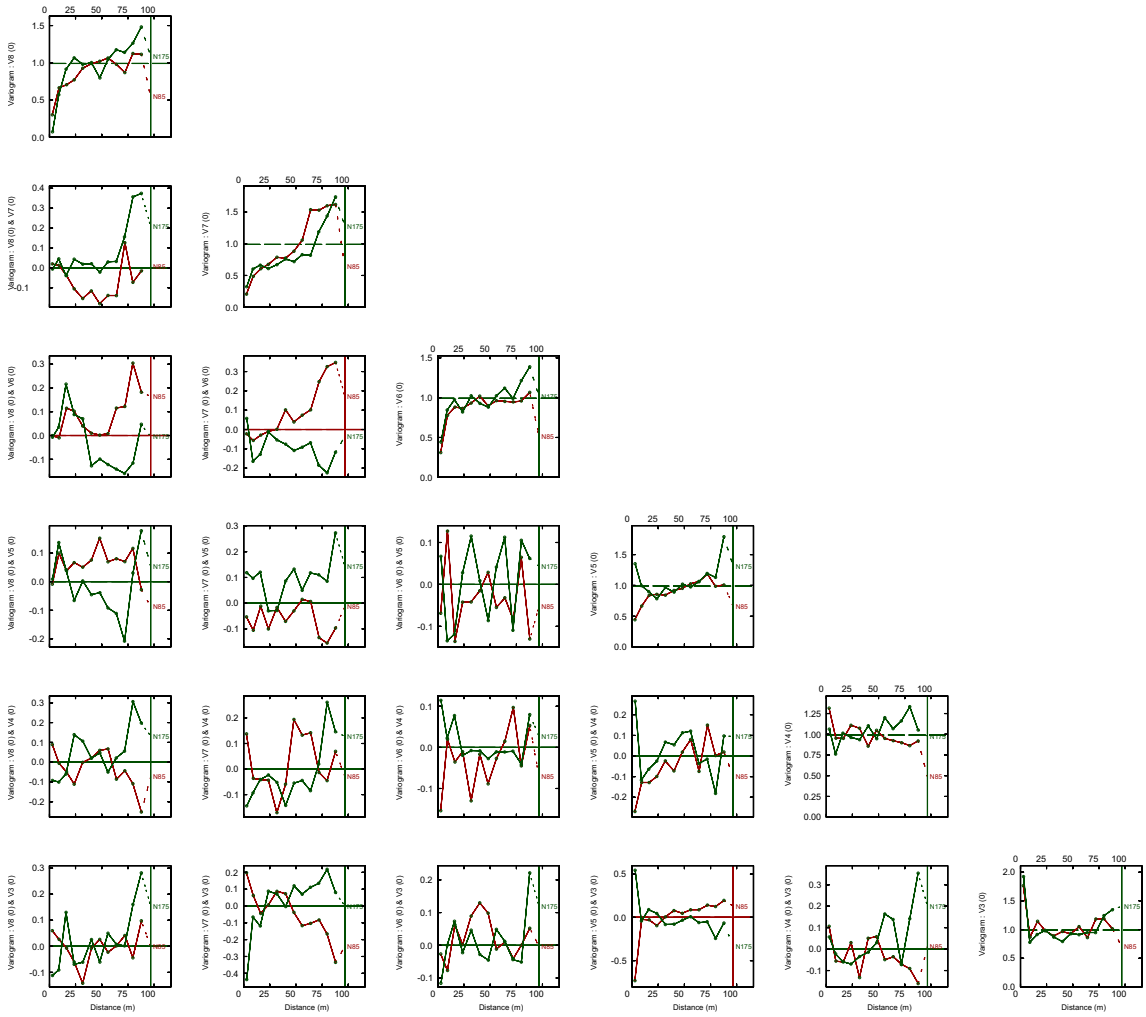

Figure C.35: Directional experimental semivariograms MAF decorrelated log-ratio data Domain 2. Complete Dataset.

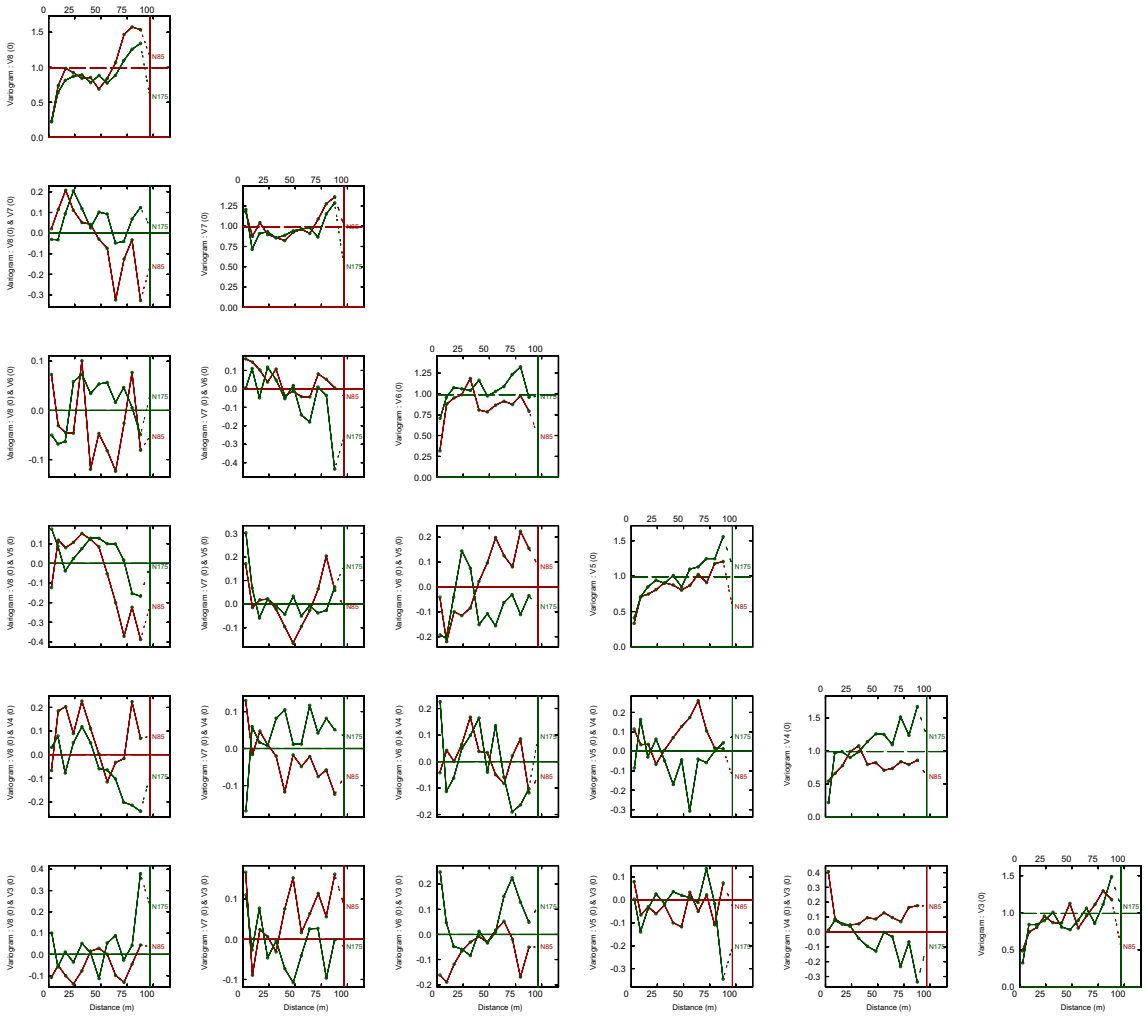

Figure C.36: Directional experimental semivariograms MAF decorrelated oxide data Domain 2. Complete Dataset.

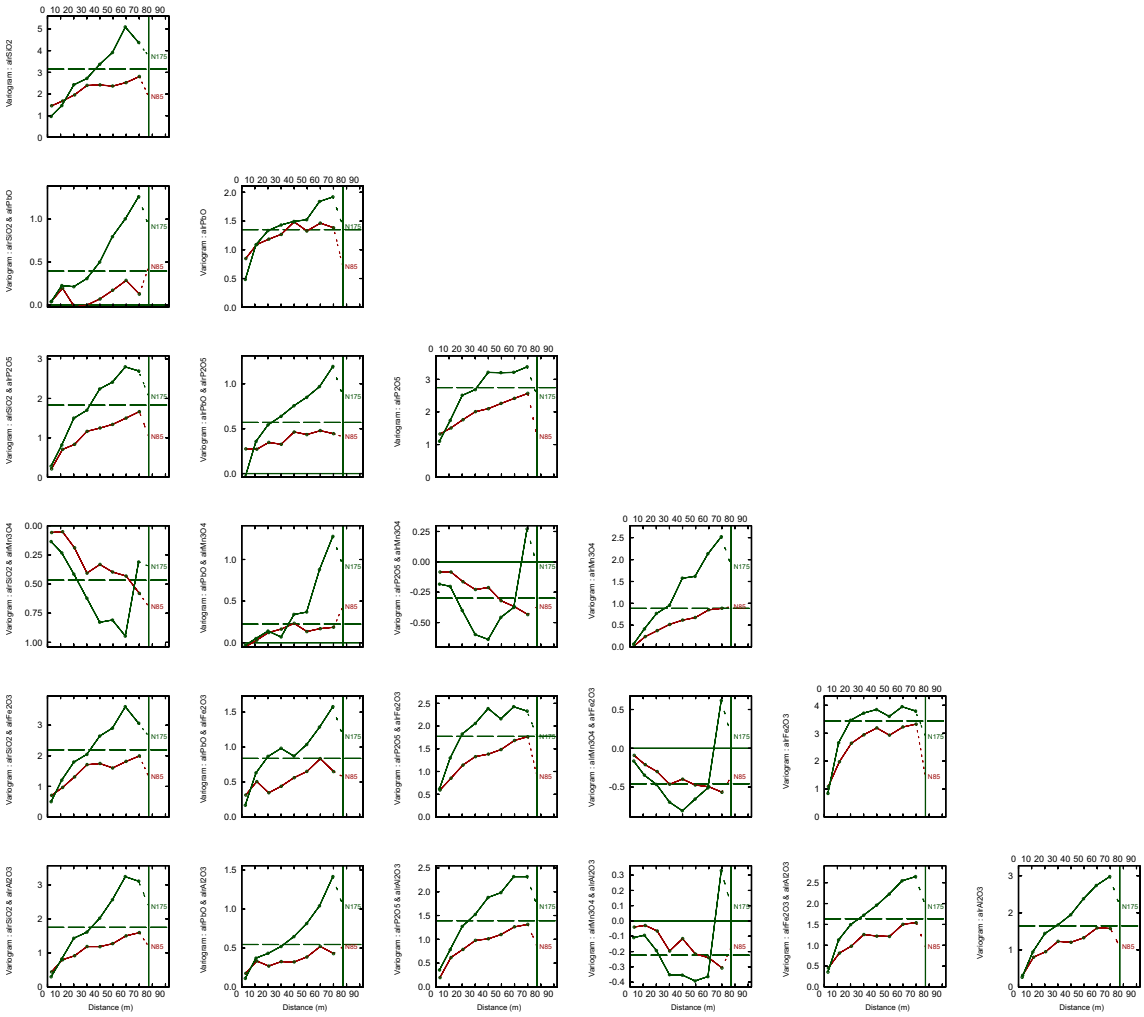

Figure C.37: Directional experimental semivariograms log-ratio data Domain 1. Reduced (RD) Dataset.

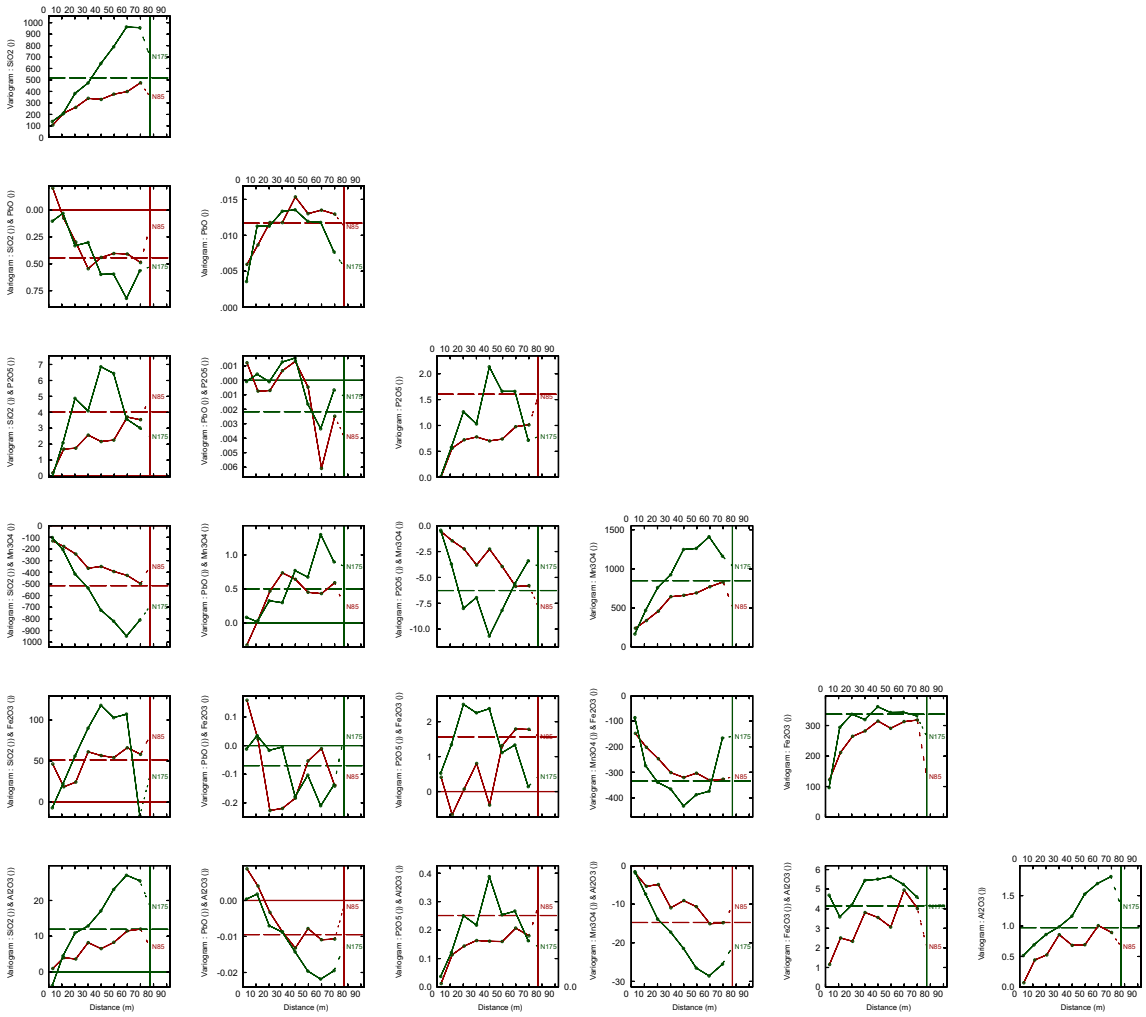

Figure C.38: Directional experimental semivariograms oxide data Domain 1. Reduced (RD) Dataset.

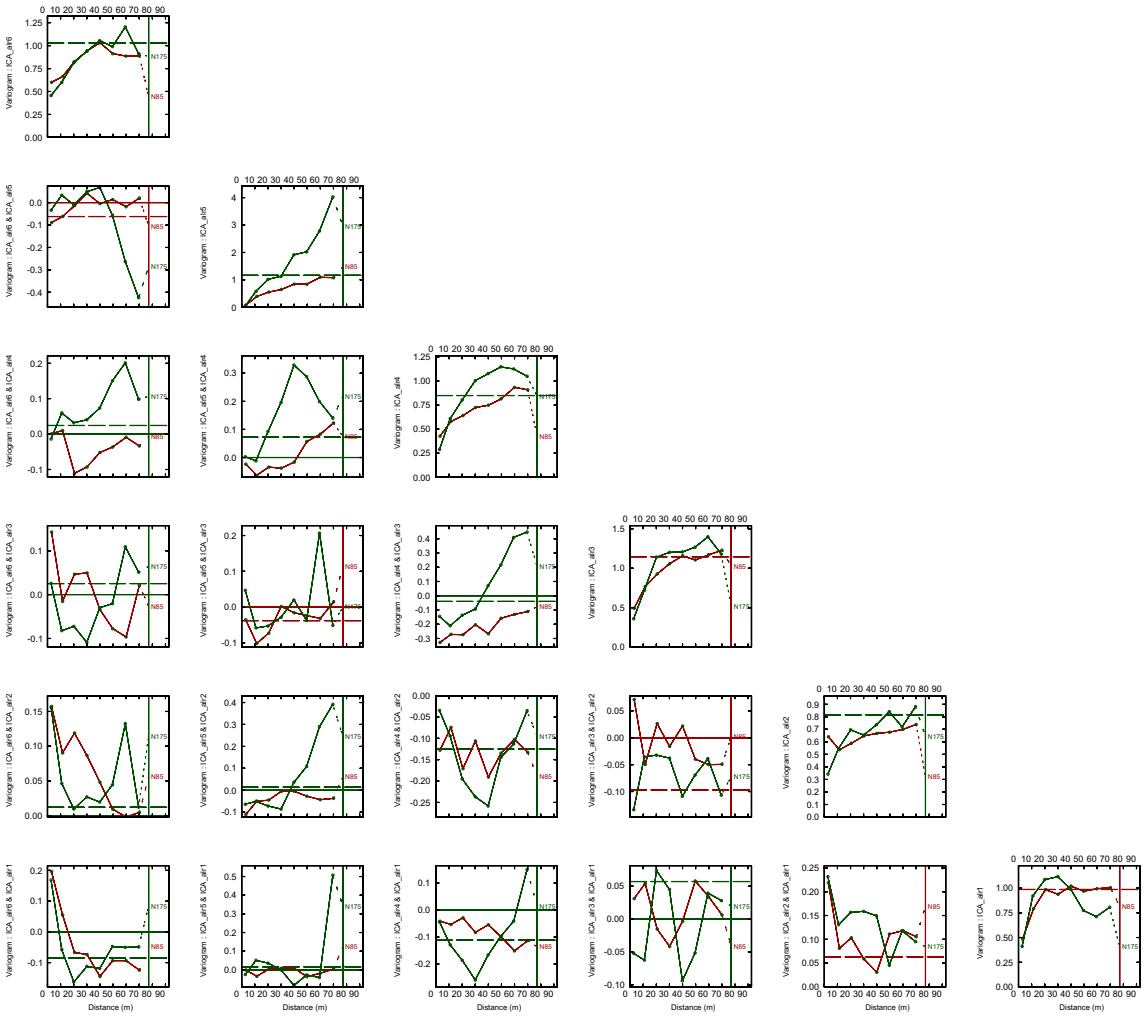

Figure C.39: Directional experimental semivariograms ICA decorrelated log-ratio data Domain 1. Reduced (RD) Dataset.

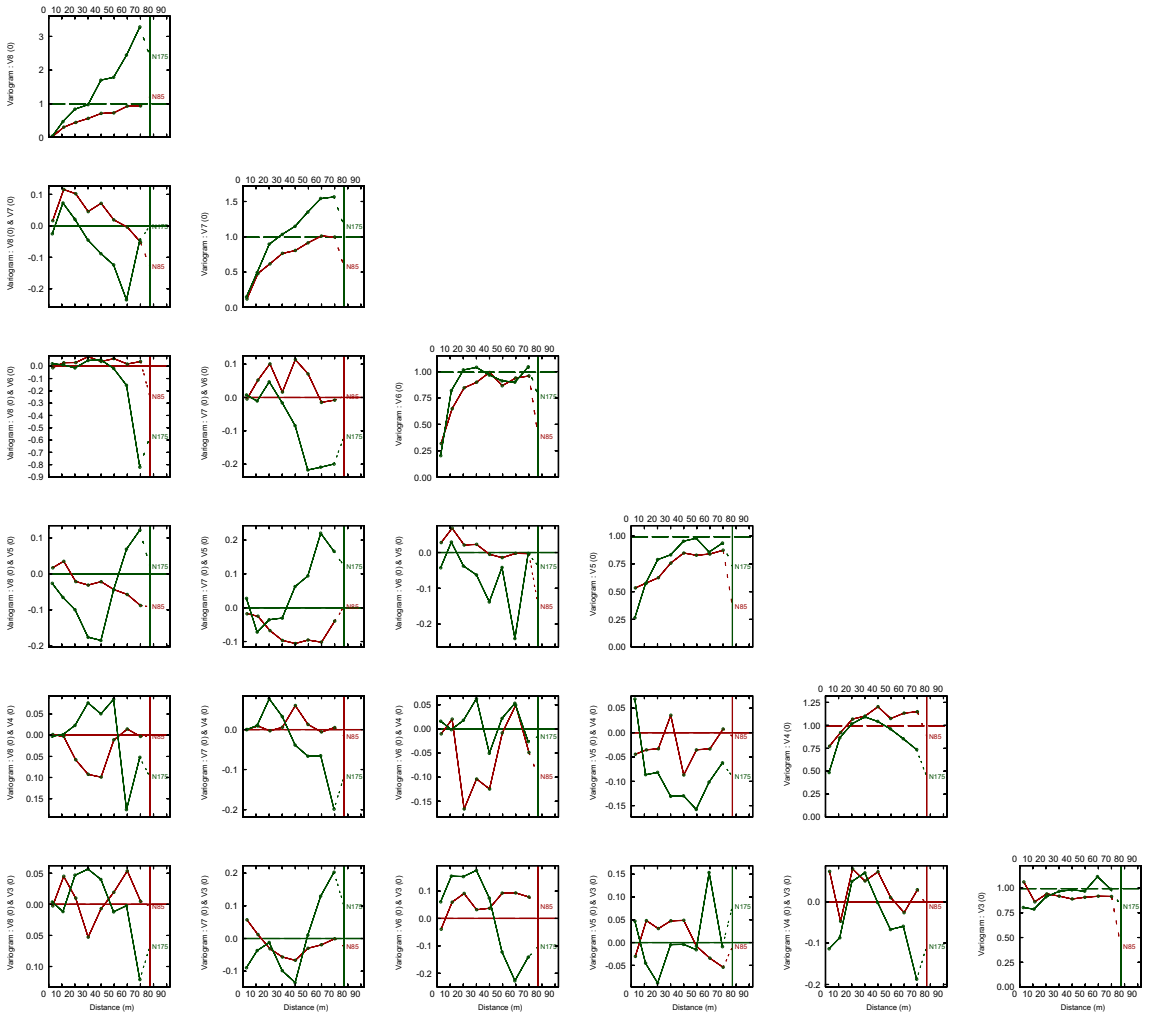

Figure C.40: Directional experimental semivariograms ICA decorrelated oxide data Domain 1. Reduced (RD) Dataset.

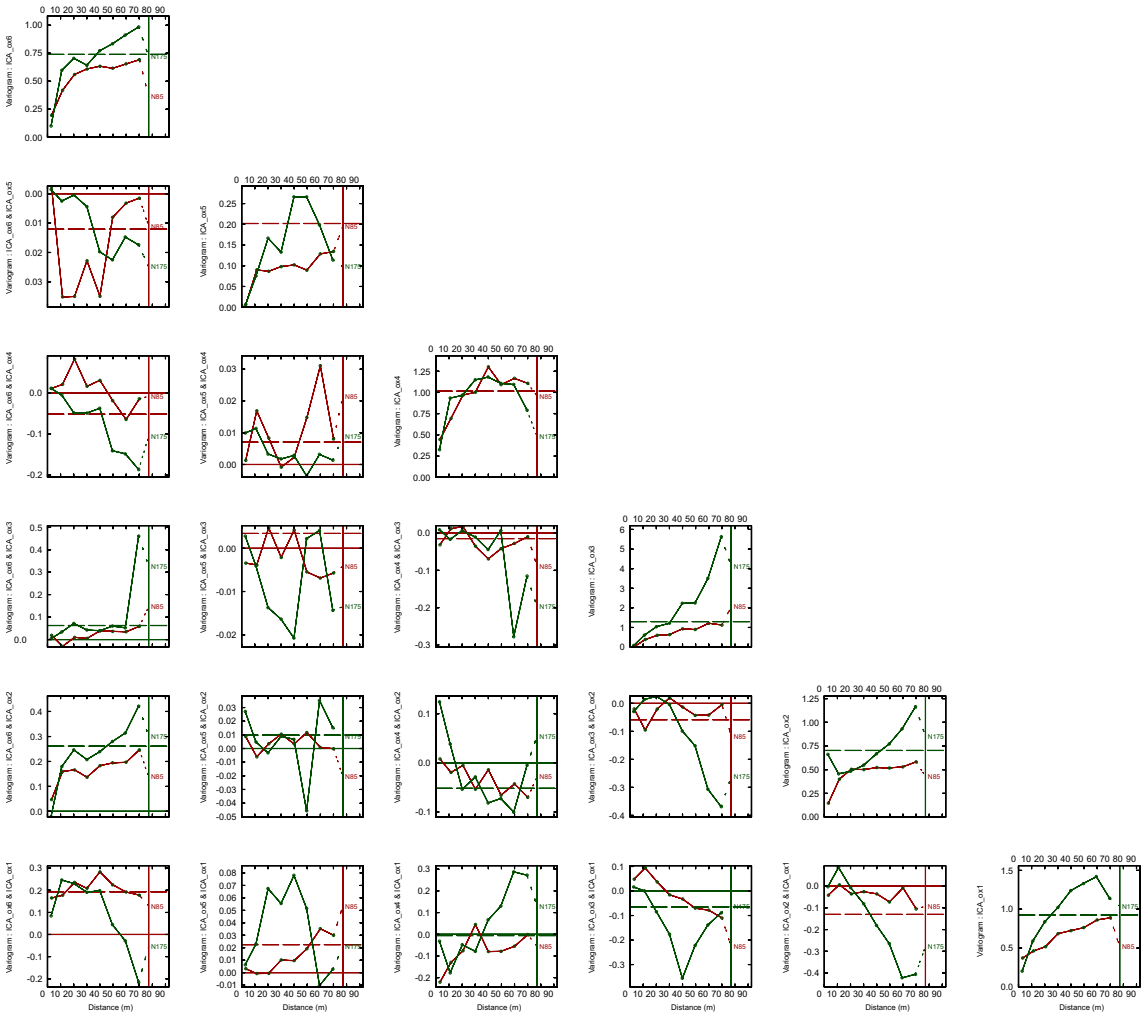

Figure C.41: Directional experimental semivariograms MAF decorrelated log-ratio data Domain 1. Reduced (RD) Dataset.

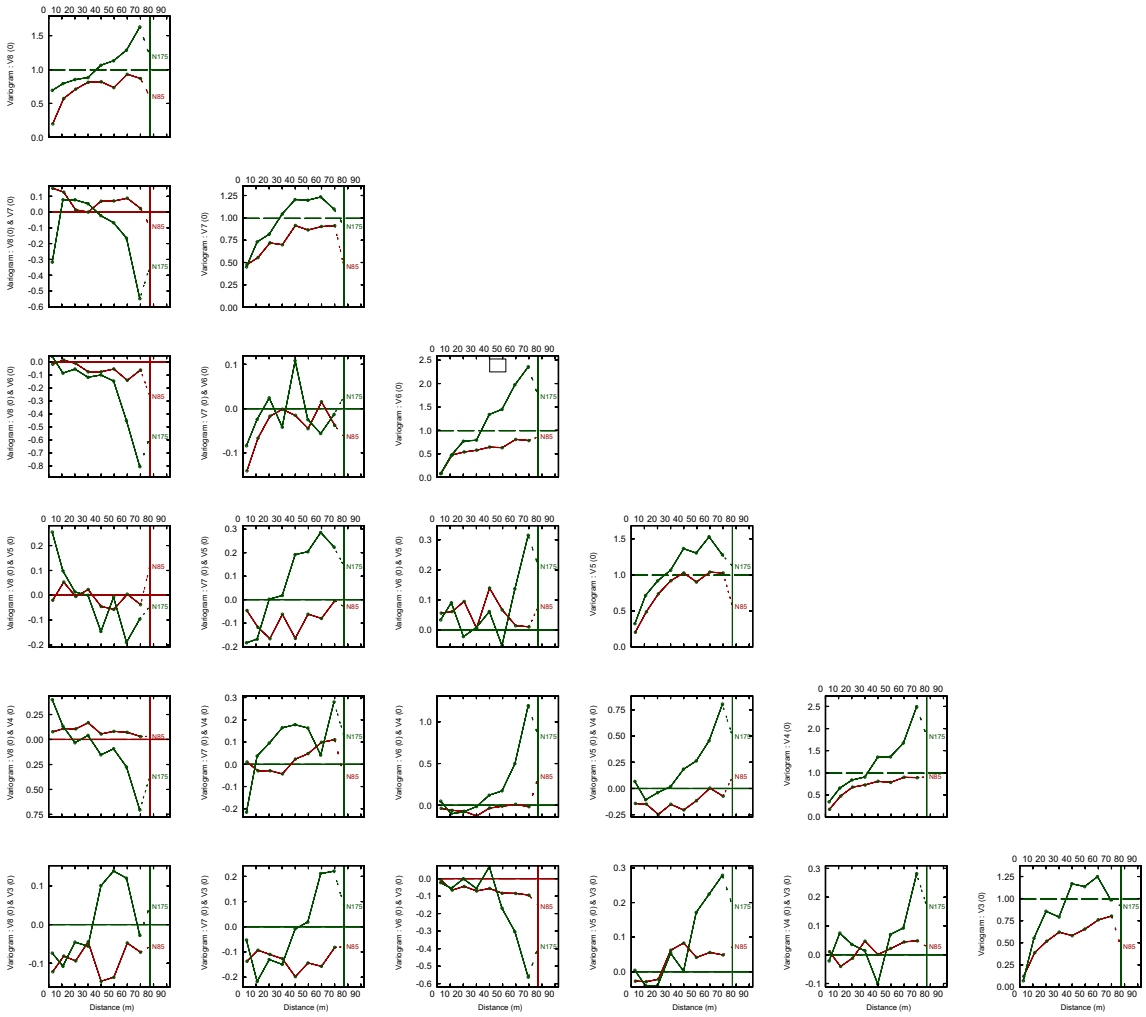

Figure C.42: Directional experimental semivariograms MAF decorrelated oxide data Domain 1. Reduced (RD) Dataset.

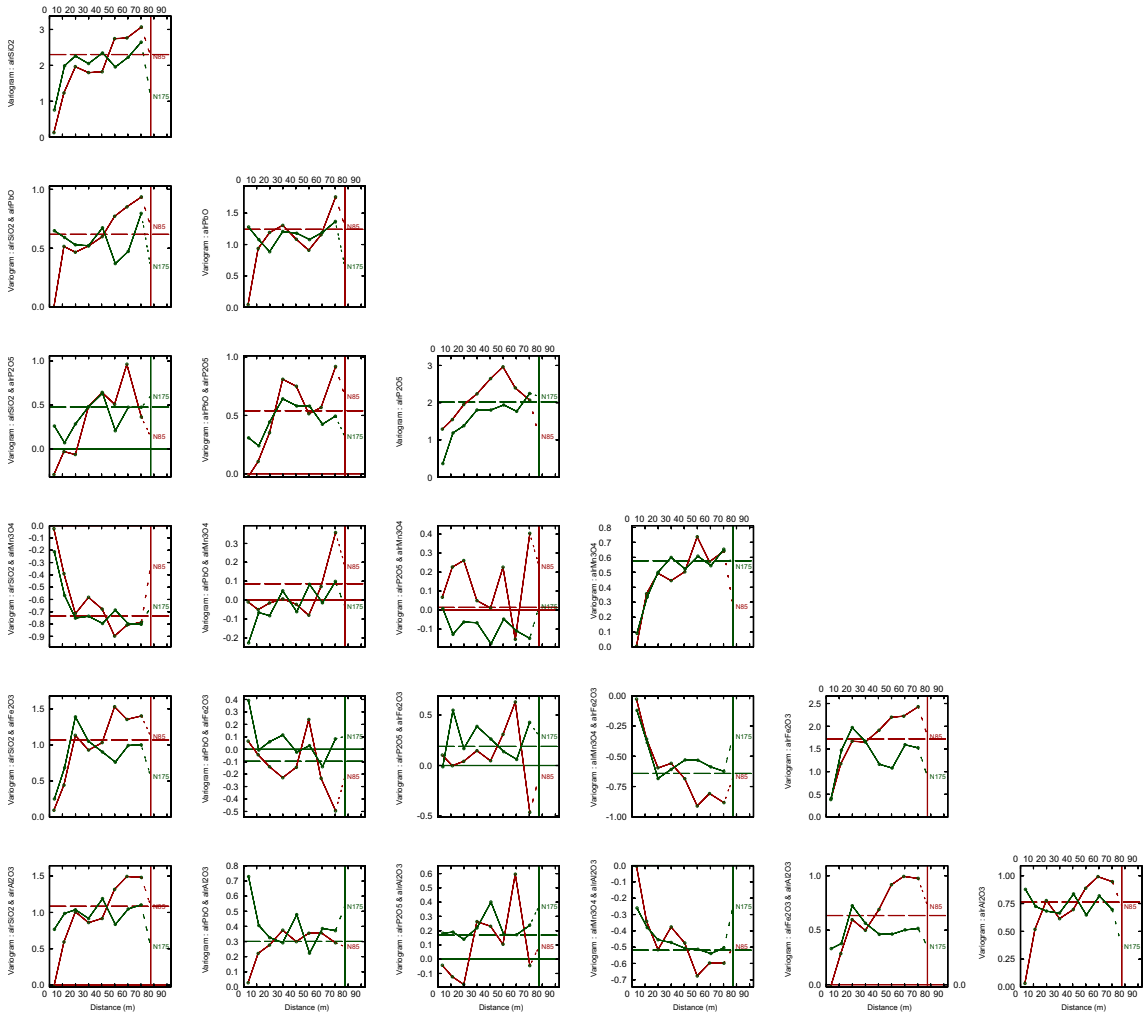

Figure C.43: Directional experimental semivariograms log-ratio data Domain 2. Reduced (RD) Dataset.

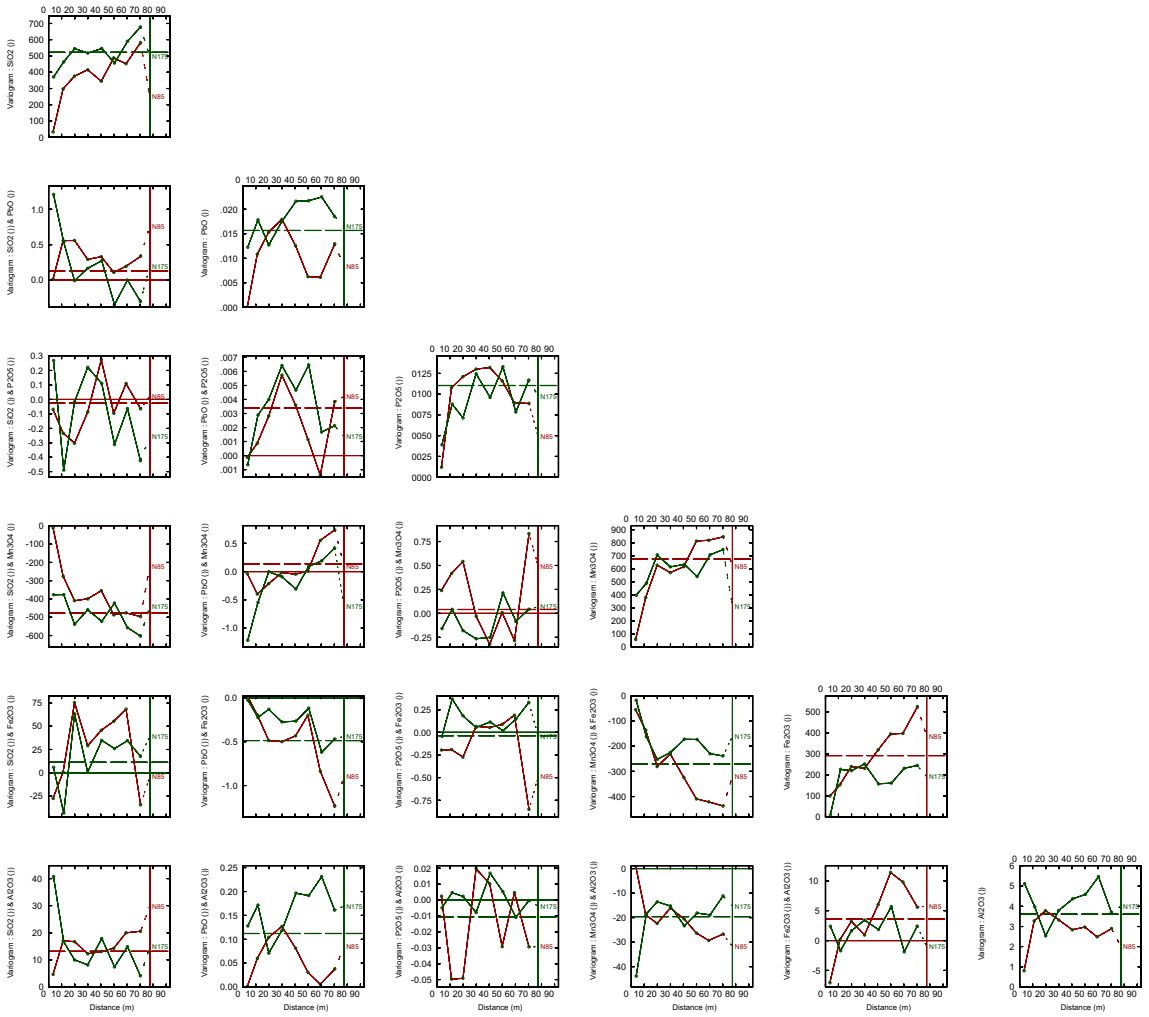

Figure C.44: Directional experimental semivariograms oxide data Domain 2. Reduced (RD) Dataset.

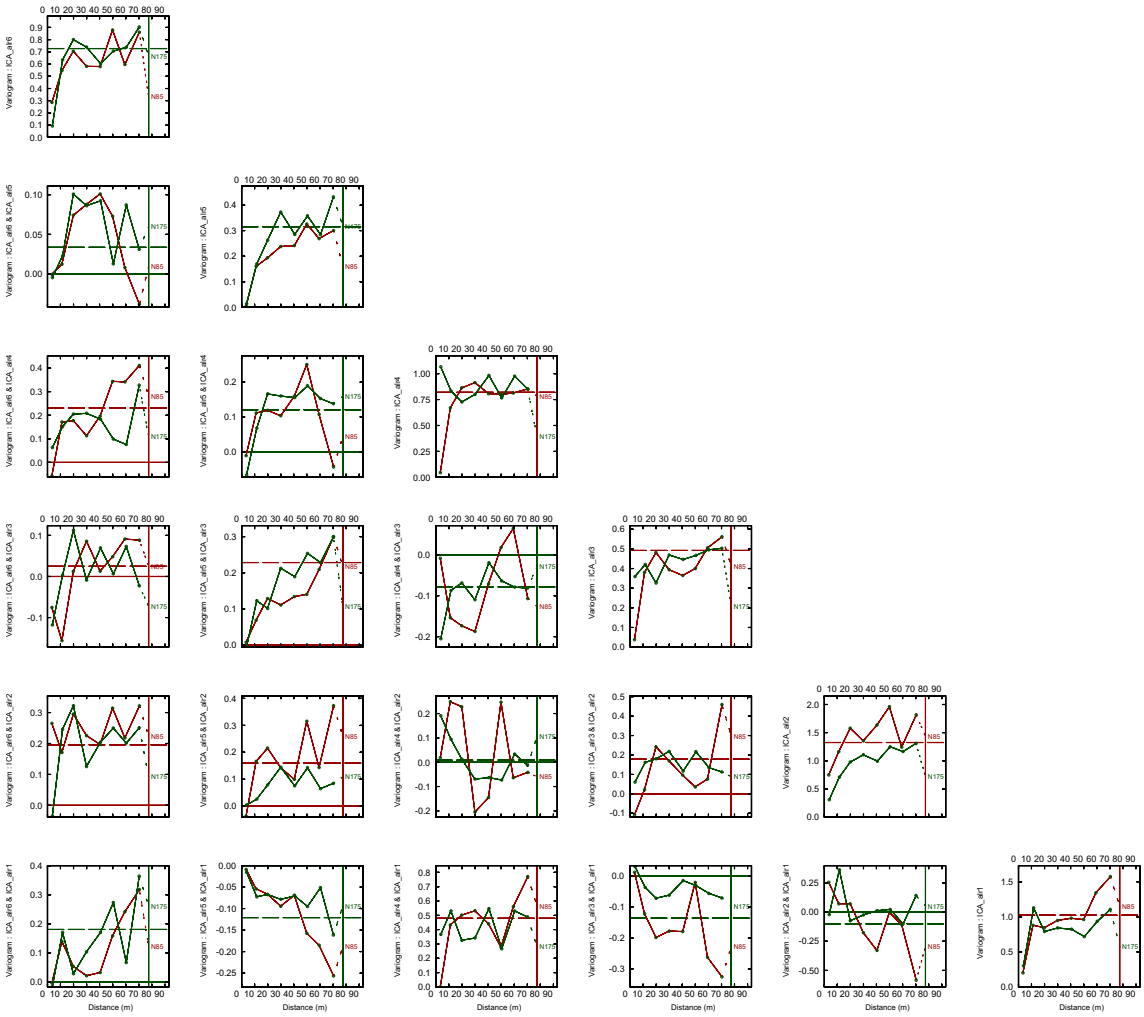

Figure C.45: Directional experimental semivariograms ICA decorrelated log-ratio data Domain 2. Reduced (RD) Dataset.

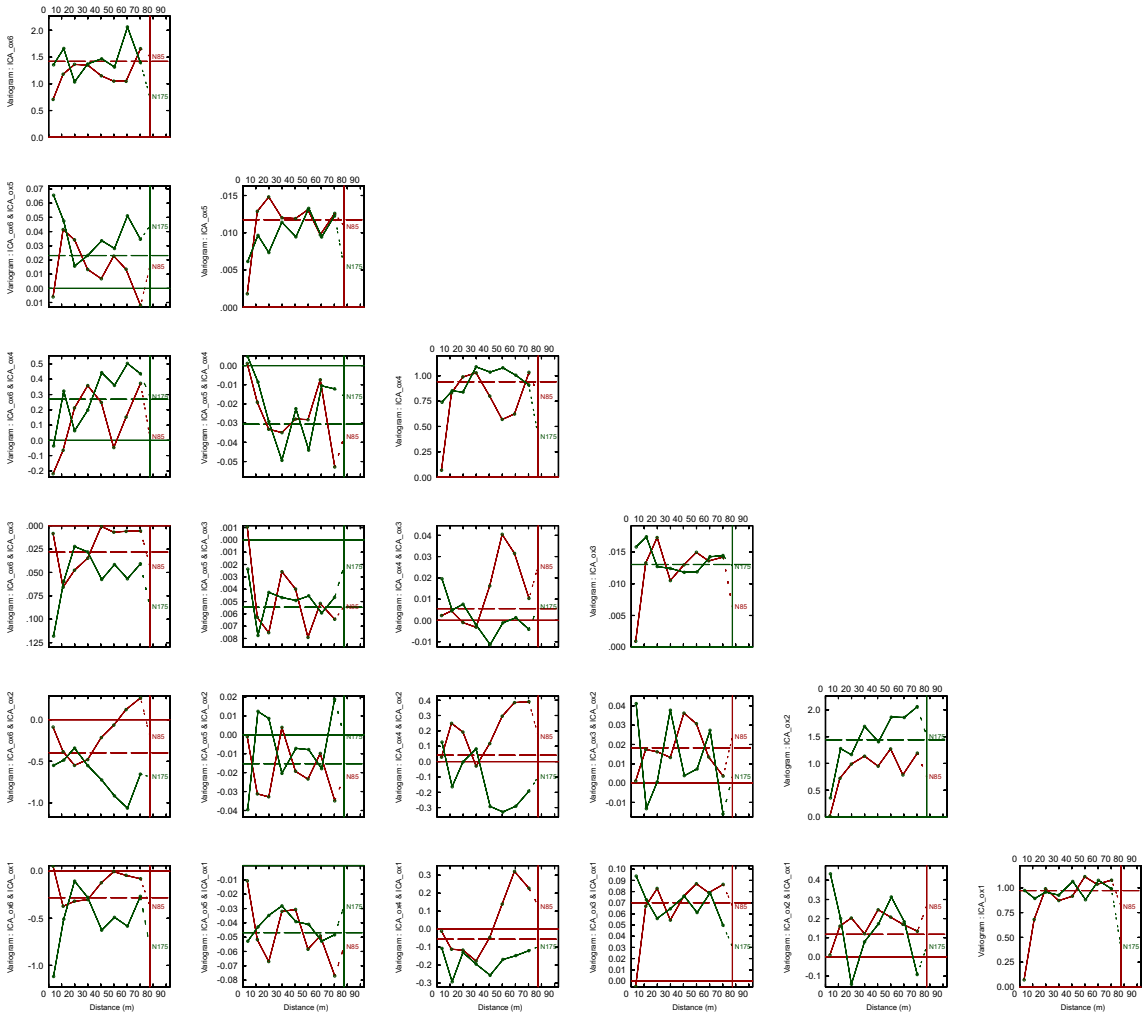

Figure C.46: Directional experimental semivariograms ICA decorrelated oxide data Domain 2. Reduced (RD) Dataset.

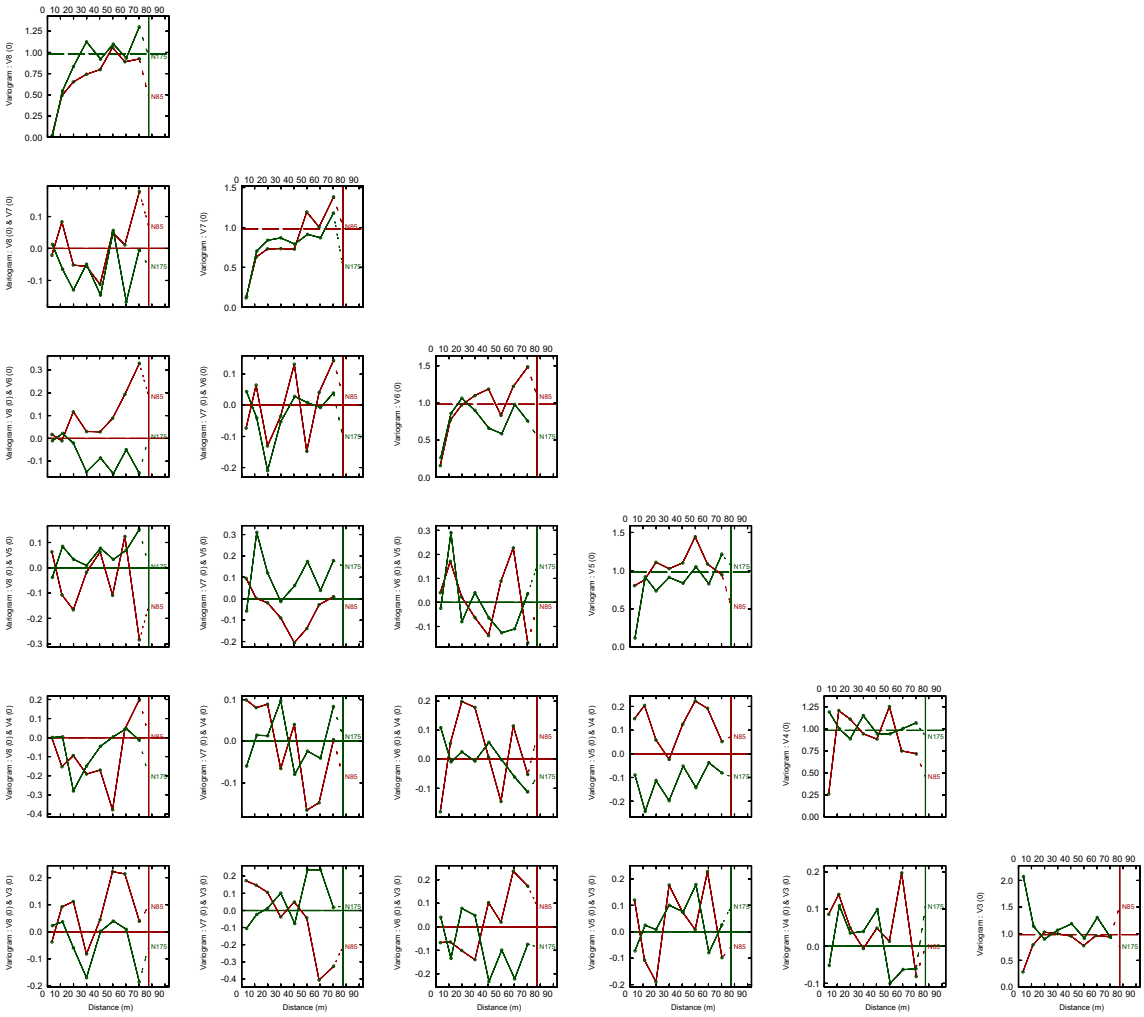

Figure C.47: Directional experimental semivariograms MAF decorrelated log-ratio data Domain 2. Reduced (RD) Dataset.

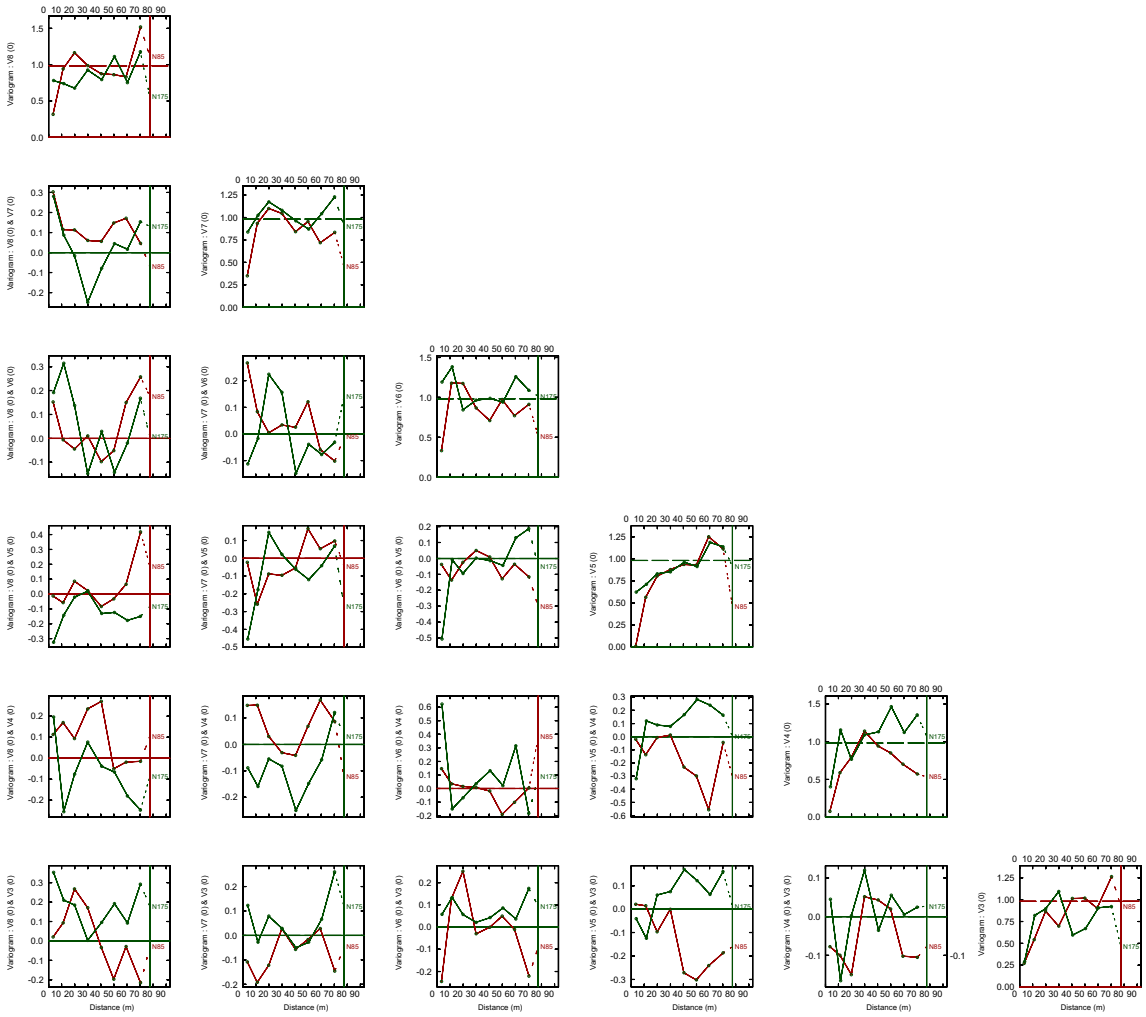

Figure C.48: Directional experimental semivariograms MAF decorrelated oxide data Domain 2. Reduced (RD) Dataset.

Appendix D

Semivariogram Models for Estimation / Simulation

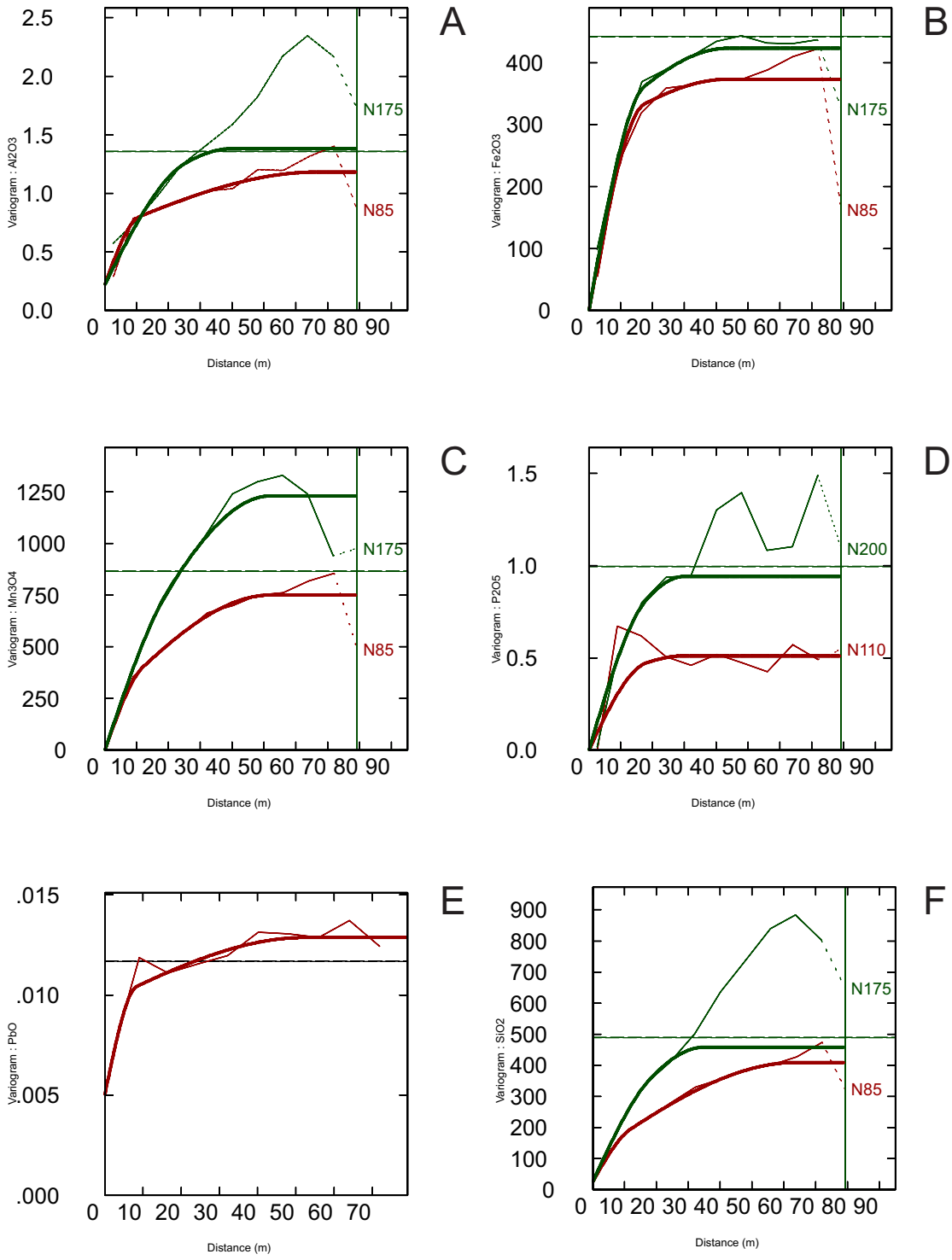

Figure D.1: All Data Domain 1 oxide model semivariograms. A - Al_2O_3, B - Fe_2O_3, C - Mn_3O_4, D - P_2O_5, E - PbO, F - SiO_2

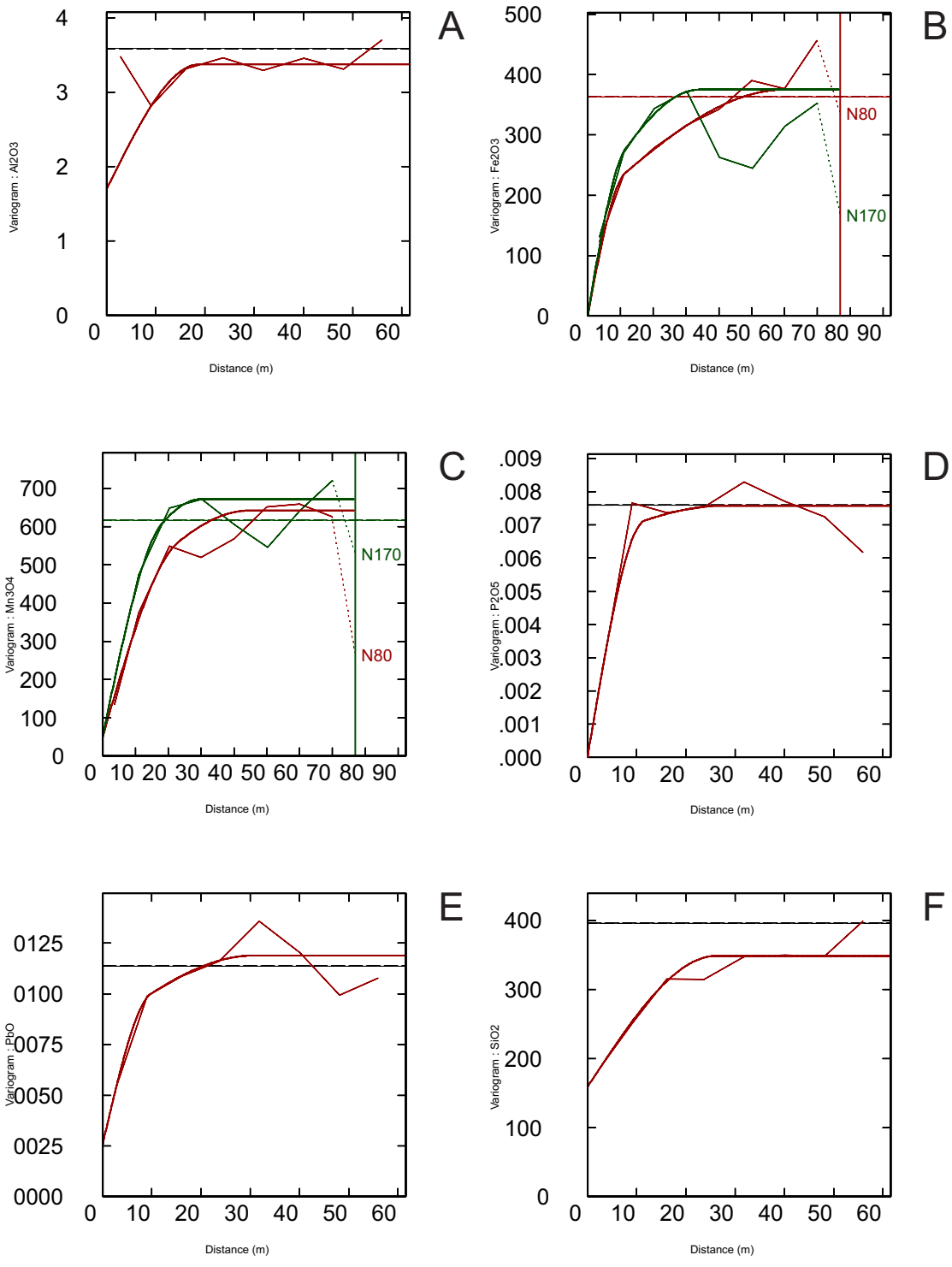

Figure D.2: All Data Domain 2 oxide model semivariograms. A - Al_2O_3, B - Fe_2O_3, C - Mn_3O_4, D - P_2O_5, E - PbO, F - SiO_2

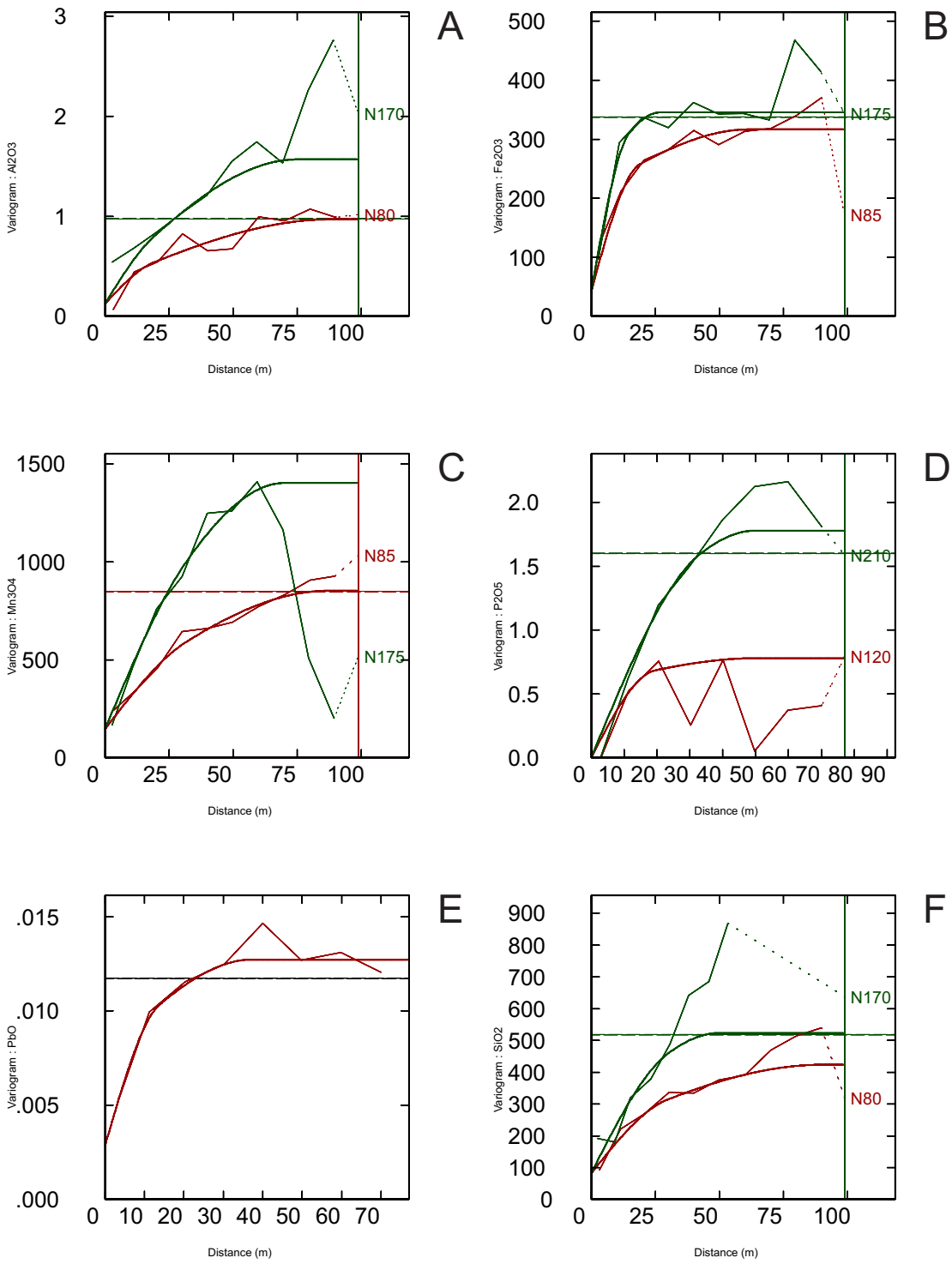

Figure D.3: RD Data Domain 1 oxide model semivariograms. A - Al_2O_3, B - Fe_2O_3, C - Mn_3O_4, D - P_2O_5, E - PbO, F - SiO_2

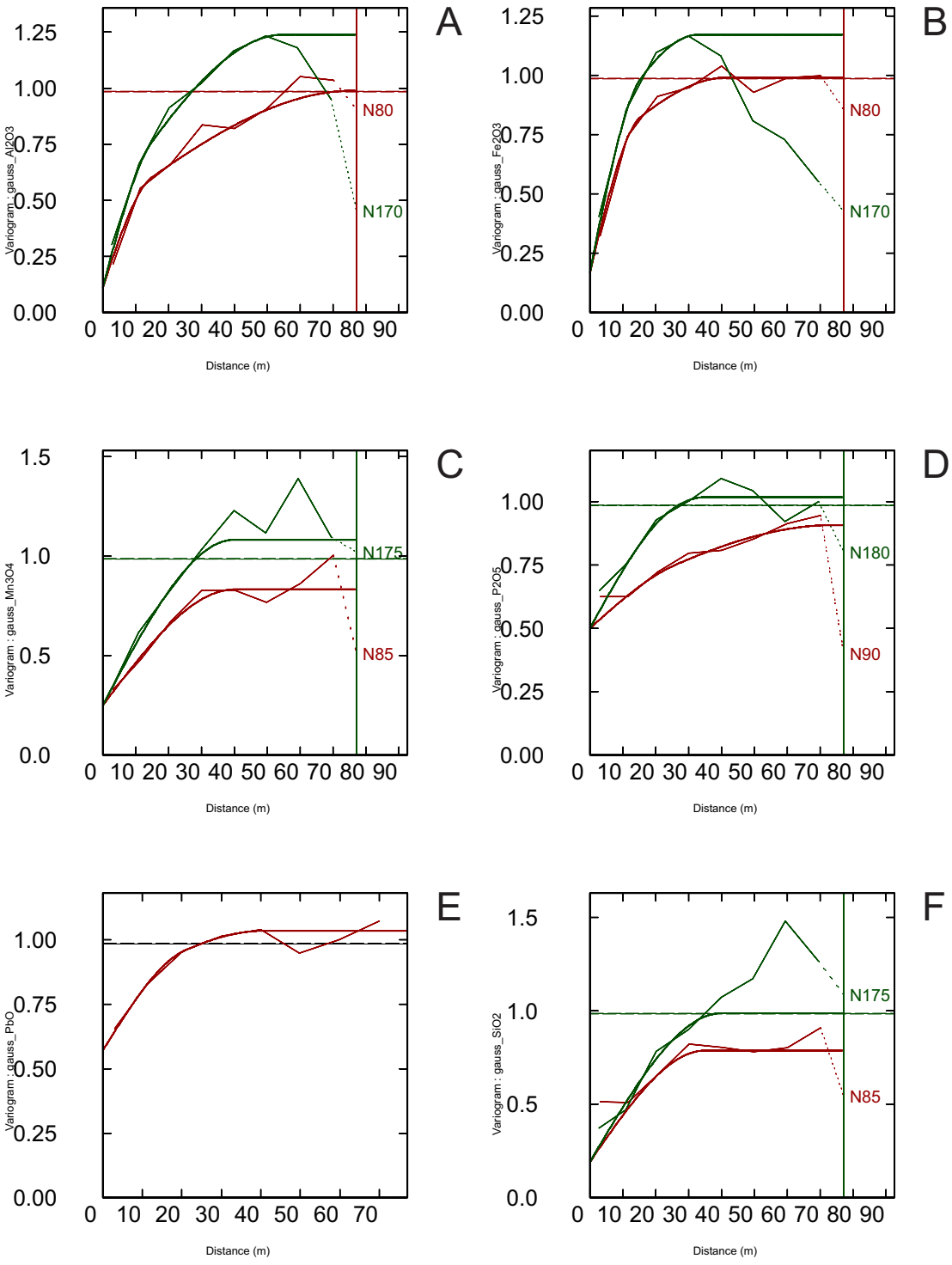

Figure D.4: RD Data Domain 2 oxide model semivariograms. A - Al_2O_3, B - Fe_2O_3, C - Mn_3O_4, D - P_2O_5, E - PbO, F - SiO_2

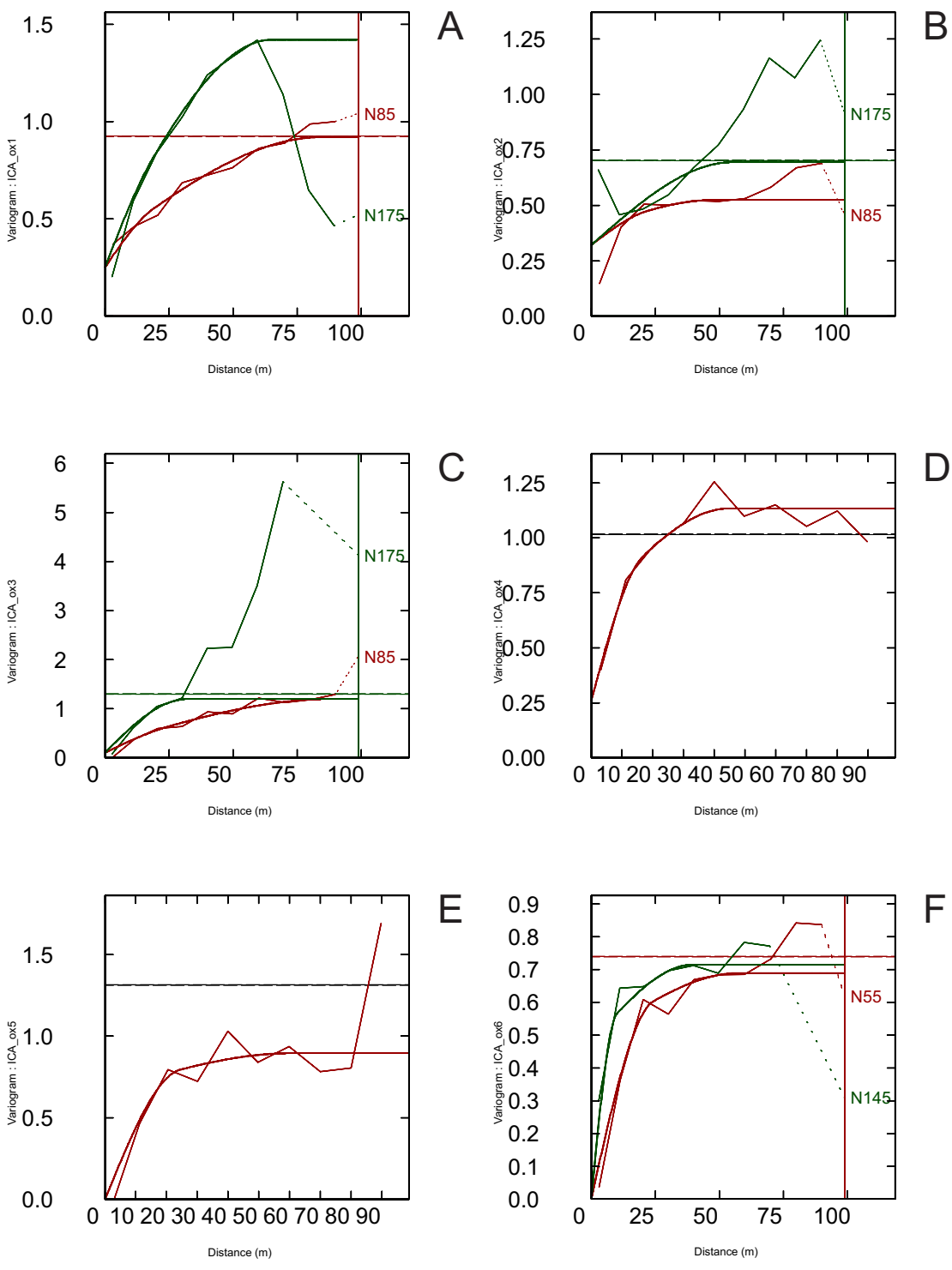

Figure D.5: RD Data Domain 1 gaussian transformed oxide model semivariograms. A - Al_2O_3, B - Fe_2O_3, C - Mn_3O_4, D - P_2O_5, E - PbO, F - SiO_2

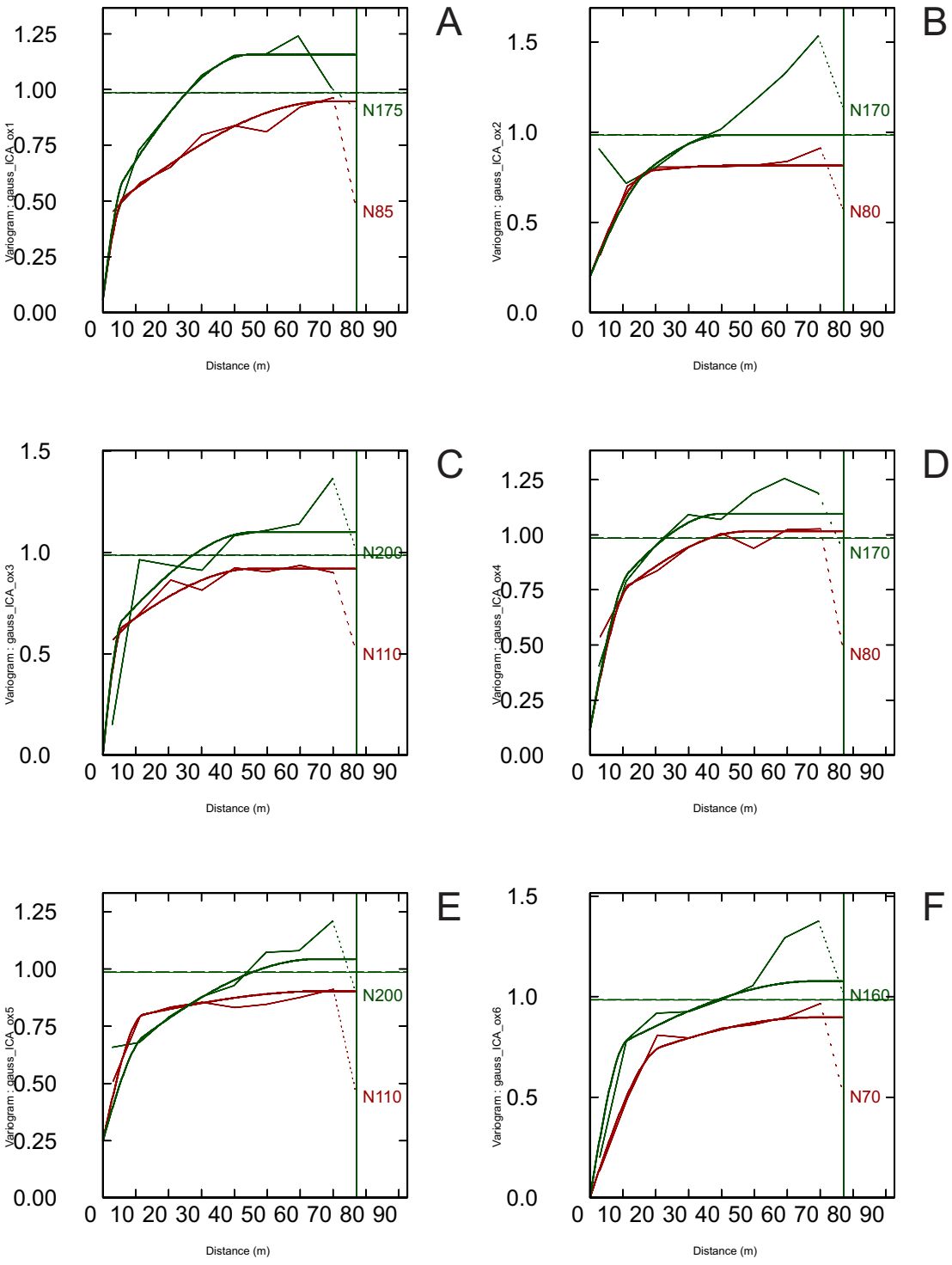

Figure D.6: RD Data Domain 2 gaussian transformed oxide model semivariograms. A - Al_2O_3, B - Fe_2O_3, C - Mn_3O_4, D - P_2O_5, E - PbO, F - SiO_2

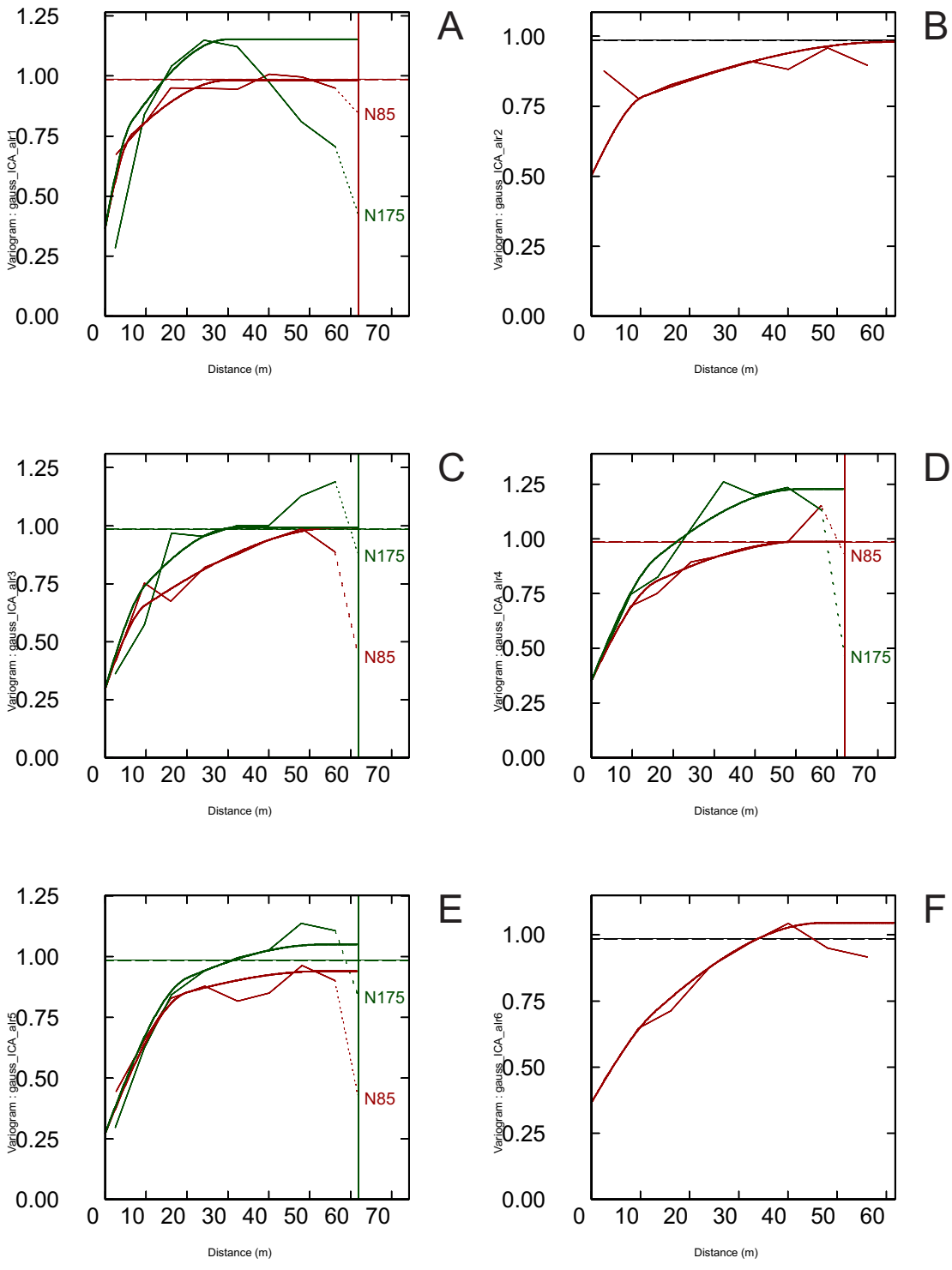

Figure D.7: RD Data Domain 1 ICA decorrelated oxide model semivariograms. A - Factor 1, B - Factor 2, C - Factor 3, D - Factor 4, E - Factor 5, F - Factor 6

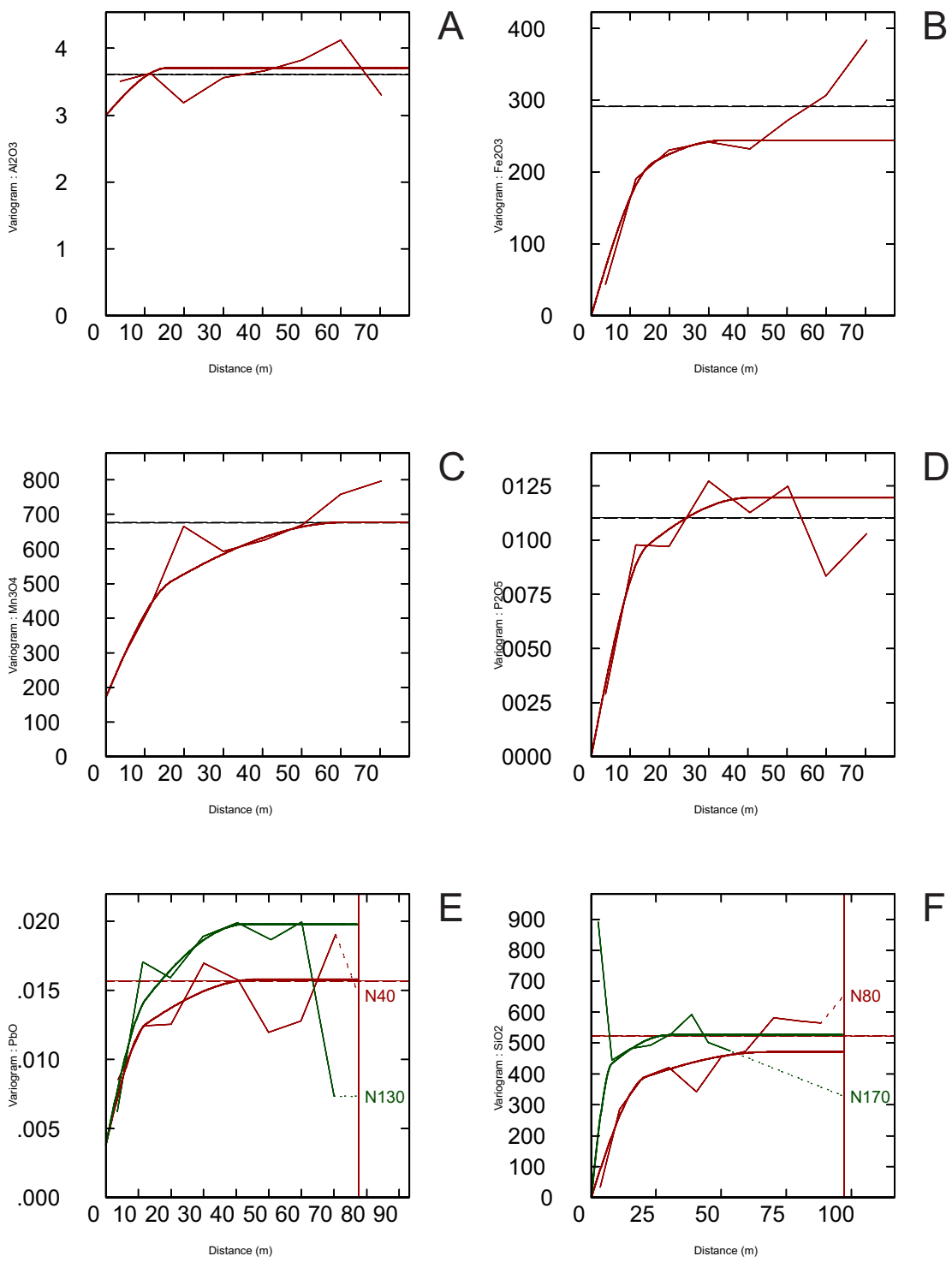

Figure D.8: RD Data Domain 2 ICA decorrelated oxide model semivariograms. A - Factor 1, B - Factor 2, C - Factor 3, D - Factor 4, E - Factor 5, F - Factor 6

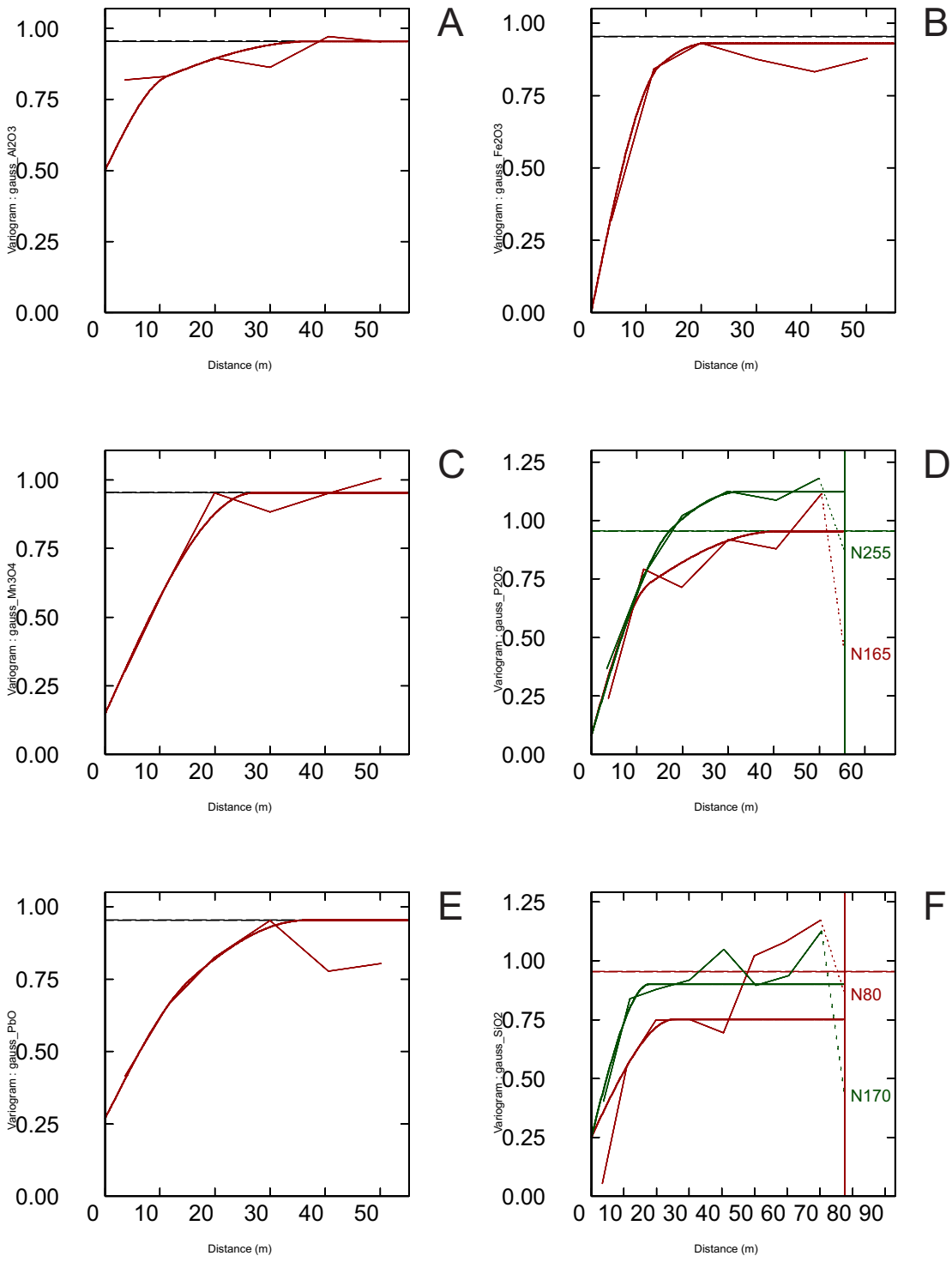

Figure D.9: RD Data Domain 1 gaussian transformed ICA decorrelated oxide model semi-variograms. A - Factor 1, B - Factor 2, C - Factor 3, D - Factor 4, E - Factor 5, F - Factor 6

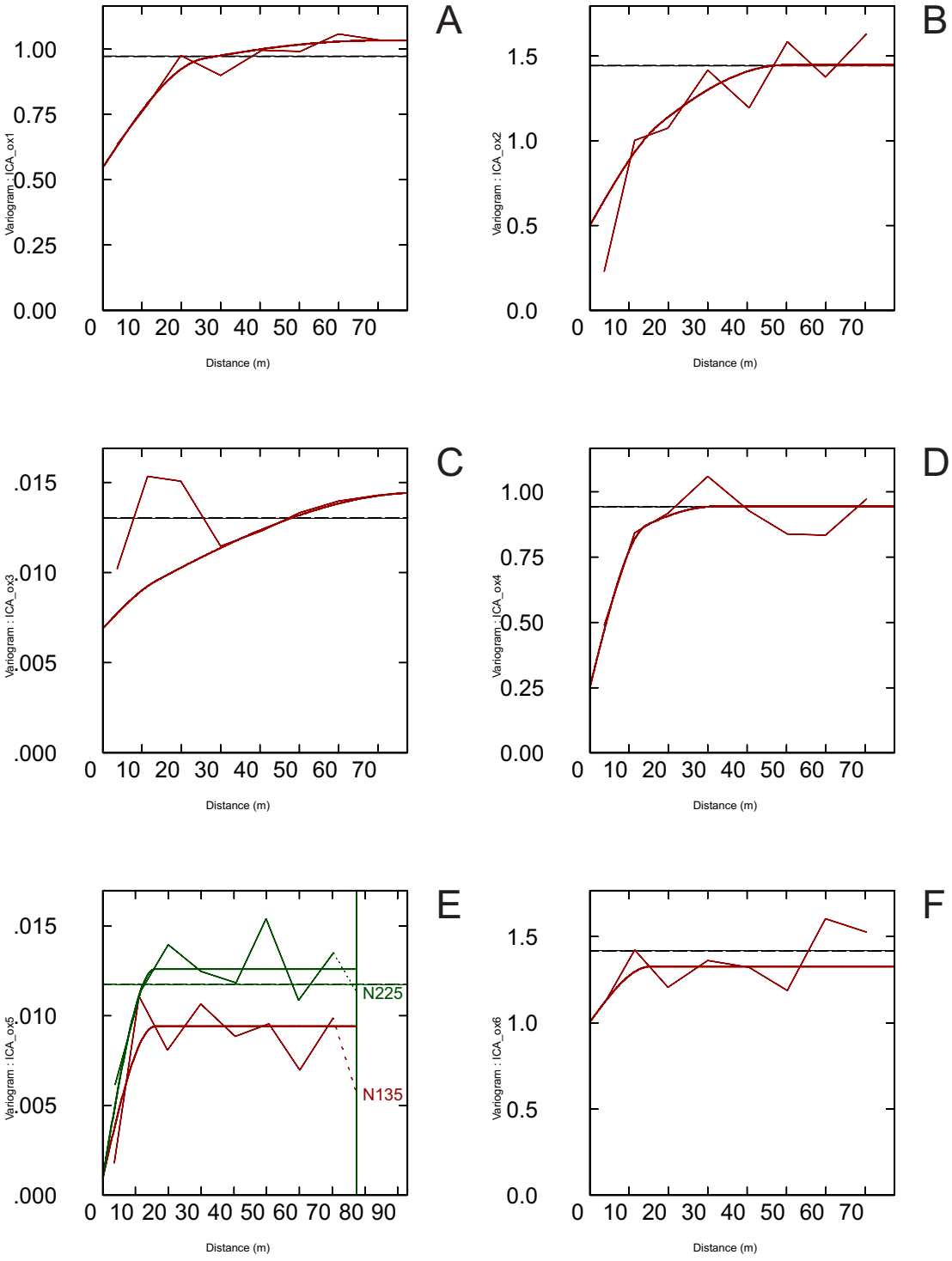

Figure D.10: RD Data Domain 2 gaussian transformed ICA decorrelated oxide model semi-variograms. A - Factor 1, B - Factor 2, C - Factor 3, D - Factor 4, E - Factor 5, F - Factor 6

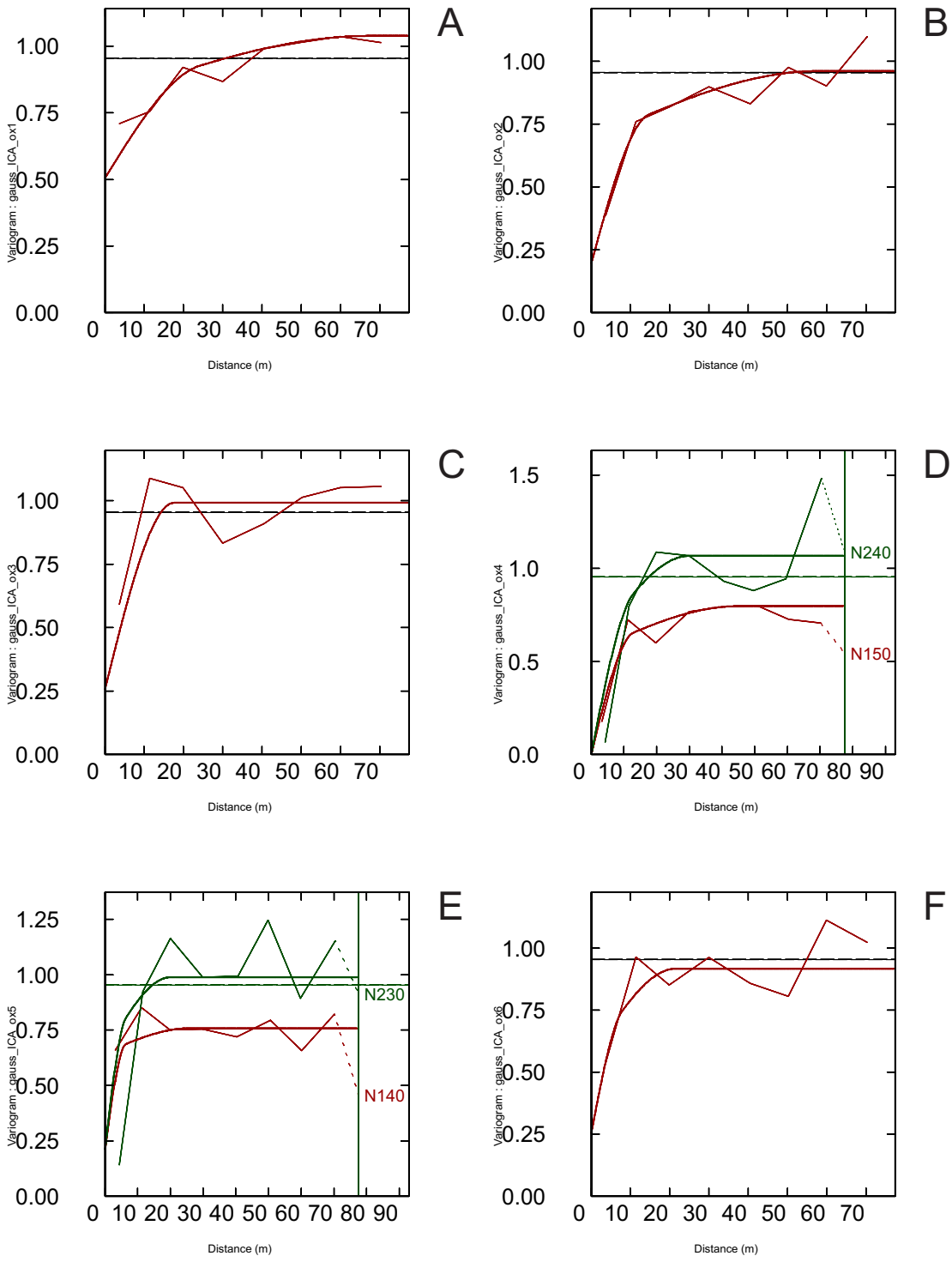

Figure D.11: RD Data Domain 1 gaussian transformed ICA decorrelated log-ratio model semivariograms. A - Factor 1, B - Factor 2, C - Factor 3, D - Factor 4, E - Factor 5, F - Factor 6

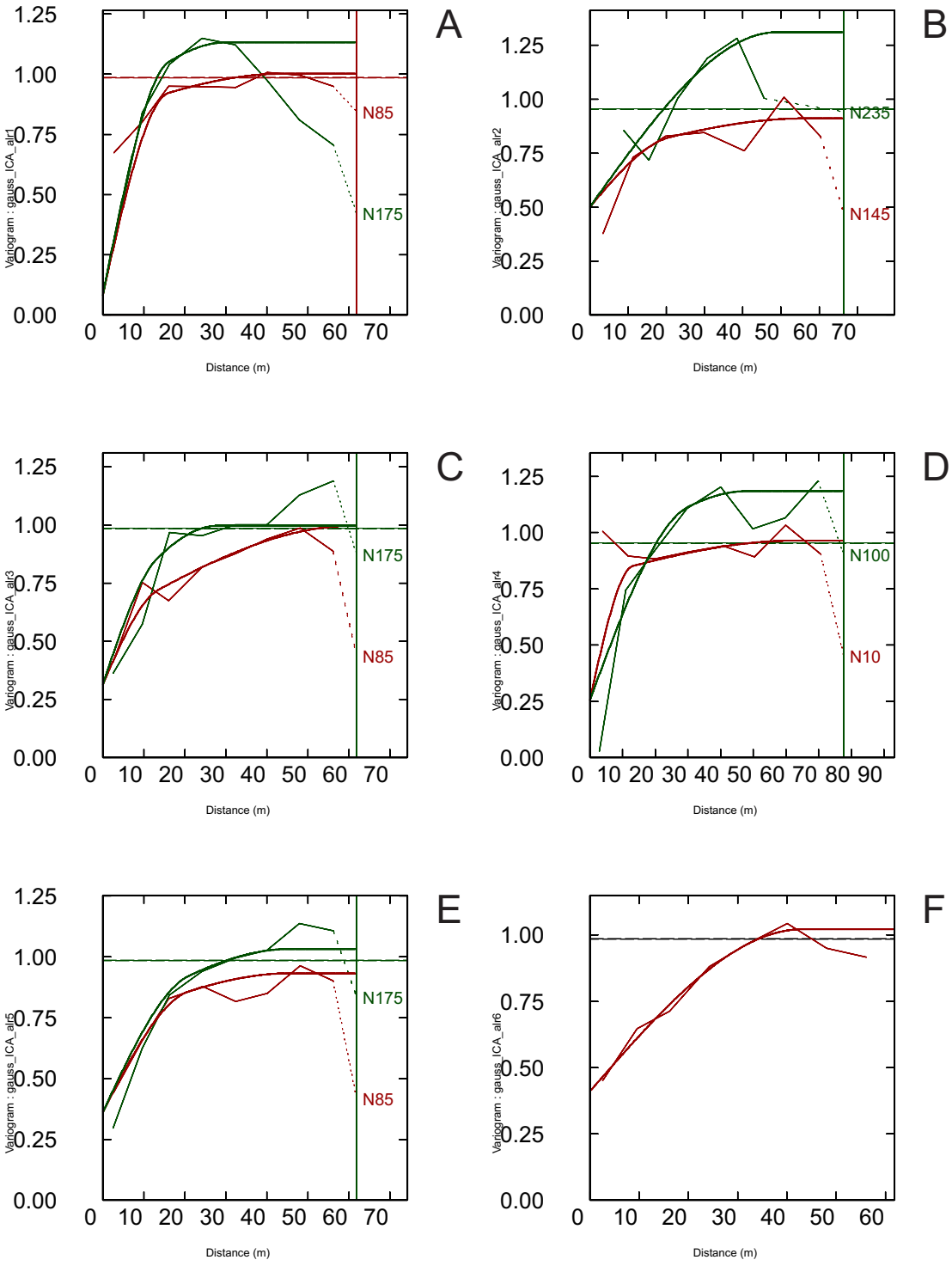

Figure D.12: RD Data Domain 2 gaussian transformed ICA decorrelated log-ratio model semivariograms. A - Factor 1, B - Factor 2, C - Factor 3, D - Factor 4, E - Factor 5, F - Factor 6

Appendix E

Isatis Journal Files and Parameters Files

Data relating to Anamorphoses, Semivariogram Models, Search Ellipses and Journal Files for the execution of the work presented in this thesis are available digitally. DVD accompanies this thesis.

Appendix F

Decorrelation and Back Transform Script (R Code)

```
%\begin{verbatim}
# Script Generated and Finalised 20 March
# Author
# M. Cobb
# NOTE: This script tests decorrelation BY DOMAIN
# This Script takes Raw input data of major oxides and alr transformed
# decorrelates via ICA and MAF, and produces Zeta / Tau / Kappa plots for
#
# It also compiles CSV files
#
# START OF SECTION
# Creates objects to decorrelate via ICA from alr data and raw oxide data
# uses both full dataset and RD dataset
# Decorrelates
# Creates RGeostats DBs and variograms for later use in Zet / Tau / Kappa including non-decorrelated oxide and alr data variograms
##Extract Coordinate data
alr_all_Dom1<-read.csv("GSC158_AllData_Dom1.csv")
all_coords_Dom1<-cbind(alr_all_Dom1[,3],alr_all_Dom1[,2])
##Extract Oxide data, ALR Data
#alr
all_alr_data_Dom1<-alr_all_Dom1[,18:23]
#oxides
all_ox_data_Dom1<-alr_all_Dom1[,11:16]
##Adds back coords for MAF calculation
```

```
#alr
all_alr_data_Dom1_xy<-cbind(all_coords_Dom1,all_alr_data_Dom1)
#oxides
all_ox_data_Dom1_xy<-cbind(all_coords_Dom1,all_ox_data_Dom1)

##ICA
library(fastICA)
#alr
ICA_all_alr_data_Dom1<-fastICA(all_alr_data_Dom1,6,alg.typ="parallel", fun="exp", method = "R", row.norm = FALSE,maxit = 300, tol =
    1e-05, verbose=TRUE,w.init=NULL)
#oxides
ICA_all_ox_data_Dom1<-fastICA(all_ox_data_Dom1,6,alg.typ="parallel", fun="exp", method = "R", row.norm = FALSE,maxit = 300, tol = 1e-05,
    verbose=TRUE,w.init=NULL)
## Adds ICA factors to coords for decorrelation assessment
#alr
ICA_all_alr_data_Dom1_xy<-cbind(all_coords_Dom1,ICA_all_alr_data_Dom1$S)
#oxides
ICA_all_ox_data_Dom1_xy<-cbind(all_coords_Dom1,ICA_all_ox_data_Dom1$S)

## This part generates RGeostats databases for the experimental variography required for zet / tau / kappa
library(RGeostats)
#alr
RAW_all_alr_Dom1_db<-db.create(all_alr_data_Dom1_xy,flag.grid=FALSE,ndim=2,nvar=6, autoname=FALSE)
ICA_all_alr_Dom1_db<-db.create(ICA_all_alr_data_Dom1_xy,flag.grid=FALSE,ndim=2,nvar=6, autoname=FALSE)
#oxides
```

```
RAW_all_ox_Dom1_db<-db.create(all_ox_data_xy,flag.grid=FALSE,ndim=2,nvar=6, autoname=FALSE)
ICA_all_ox_Dom1_db<-db.create(ICA_all_ox_data_xy,flag.grid=FALSE,ndim=2,nvar=6, autoname=FALSE)

## Creates omnidirectional experimental variograms of non-decorrelated data
#alr
RAW_all_alr_Dom1_omnivar<-vario.calc(RAW_all_alr_Dom1_db,lag=7.5,nlag=16)
#oxides
RAW_all_ox_Dom1_omnivar<-vario.calc(RAW_all_ox_Dom1_db,lag=7.5,nlag=16)

## Creates directional experimental variograms of non-decorrelated data
#alr
RAW_all_alr_Dom1_dirvar<-vario.calc(RAW_all_alr_Dom1_db,dirvect=c(085,175), toldis =0.5, tolang=c(45,45), lag =7.5, nlag=16)
#oxides
RAW_all_ox_Dom1_dirvar<-vario.calc(RAW_all_ox_Dom1_db,dirvect=c(085,175),toldis=0.5, tolang=c(45,45), lag =7.5, nlag=16)

## Creates omnidirectional experimental variograms of decorrelated data via ICA
#alr
ICA_all_alr_Dom1_omnivar<-vario.calc(ICA_all_alr_Dom1_db,lag=7.5,nlag=16)
#oxides
ICA_all_ox_Dom1_omnivar<-vario.calc(ICA_all_ox_Dom1_db,lag=7.5,nlag=16)

## Creates directional experimental variograms of decorrelated data via ICA
#alr
ICA_all_alr_Dom1_dirvar<-vario.calc(ICA_all_alr_Dom1_db,dirvect=c(085,175), toldis =0.5, tolang=c(45,45), lag =7.5, nlag=16)
#oxides
```

```
ICA_all_ox_Dom1_dirvar<-vario.calc(ICA_all_ox_Dom1_db,dirvect=c(085,175), toldis =0.5,  tolang=c(45,45),  lag =7.5, nlag=16)

#End of  Section
#-----------------

# START OF SECTION
# Creates  objects  to  decorrelate  via  PCA using previously  created  objects
# uses  both  full  dataset  and RD dataset
#  Decorrelates
# Creates  RGeostats  DBs and variograms  for  later  use  in  Zeta  /  Tau  /  Kappa


## General  variance  covariance  matrix
#alr
all_alr_data_Dom1_B<-cov(all_alr_data_Dom1)
#oxides
all_ox_data_Dom1_B<-cov(all_ox_data_Dom1)

##PCA ( _W denotes  rotation  matrix  )
#alr
all_alr_data_Dom1_rootlambda<-diag((eigen(all_alr_data_Dom1_B)$values)^0.5)
all_alr_data_Dom1_invroot<- solve(all_alr_data_Dom1_rootlambda)
all_alr_Dom1_Q<-eigen(all_alr_data_Dom1_B)$vectors
PCA_all_alr_Dom1_W<-(all_alr_data_Dom1_invroot)%*%t(all_alr_Dom1_Q)
t_PCA_all_alr_data_Dom1<-PCA_all_alr_Dom1_W%*%t(as.matrix(all_alr_data_Dom1))
```

```
PCA_all_alr_data_Dom1<-t(t_PCA_all_alr_data_Dom1)
#oxides
all_ox_data_Dom1_rootlambda<-diag((eigen(all_ox_data_Dom1_B)$values)^0.5)
all_ox_data_Dom1_invroot<- solve(all_ox_data_Dom1_rootlambda)
all_ox_Dom1_Q<-eigen(all_ox_data_Dom1_B)$vectors
PCA_all_ox_Dom1_W<-(all_ox_data_Dom1_invroot)%*%t(all_ox_Dom1_Q)
t_PCA_all_ox_data_Dom1<-PCA_all_ox_Dom1_W%*%t(as.matrix(all_ox_data_Dom1))
PCA_all_ox_data_Dom1<-t(t_PCA_all_ox_data_Dom1)

## Adds PCA factors to coords for decorrelation assessment
#alr
PCA_all_alr_data_Dom1_xy<-cbind(all_coords_Dom1,PCA_all_alr_data_Dom1)
#oxides
PCA_all_ox_data_Dom1_xy<-cbind(all_coords_Dom1,PCA_all_ox_data_Dom1)

## This part generates RGeostats databases for the experimental variography required for zet / tau / kappa
library (RGeostats)
#alr
PCA_all_alr_Dom1_db<-db.create(PCA_all_alr_data_Dom1_xy,flag.grid=FALSE,ndim=2,nvar=6, autoname=FALSE)
#oxides
PCA_all_ox_Dom1_db<-db.create(PCA_rd_alr_data_xy,flag.grid=FALSE,ndim=2,nvar=6, autoname=FALSE)

## Creates omnidirectional experimental variograms of decorrelated data via PCA
#alr
PCA_all_alr_Dom1_omnivar<-vario.calc(PCA_all_alr_Dom1_db,lag=7.5,nlag=16)
```

```
#oxides
PCA_all_ox_Dom1_omnivar<-vario.calc(PCA_all_ox_Dom1_db,lag=7.5,nlag=16)

## Creates directional experimental variograms of decorrelated data via PCA
#alr
PCA_all_alr_Dom1_dirvar<-vario.calc(PCA_all_alr_Dom1_db,dirvect=c(085,175), toldis =0.5, tolang=c(45,45), lag =7.5,nlag=16)
#oxides
PCA_all_ox_Dom1_dirvar<-vario.calc(PCA_all_ox_Dom1_db,dirvect=c(085,175),toldis =0.5, tolang=c(45,45), lag =7.5,nlag=16)

#End of Section
#----------------

# START OF SECTION
# Creates objects to decorrelate via MAF using previously created objects
# uses both full dataset and RD dataset
# Decorrelates
# Creates RGeostats DBs and variograms for later use in Zeta / Tau / Kappa

## creates the array in which to store the semivariances from the 1s lag of the PCA factors omnidirectional semivariogram
#alr
PCA_all_alr_data_Dom1_Bh<-array(rep(NA,36),dim=c(6,6))
for (r in 1:6){
    for (column in 1:6){
    PCA_all_alr_data_Dom1_Bh[r,column]<-PCA_all_alr_Dom1_omnivar[1,r,column,1]$gg
    }
```

```
}
Eigen_PCA_all_alr_data_Dom1_Bh<-eigen(PCA_all_alr_data_Dom1_Bh)
PCA_all_alr_Dom1_Q<-t(Eigen_PCA_all_alr_data_Dom1_Bh$vectors)
MAF_all_alr_Dom1_W<-PCA_all_alr_Dom1_Q%*%PCA_all_alr_Dom1_W
t_MAF_all_alr_data_Dom1<-MAF_all_alr_Dom1_W%*%t(as.matrix(all_alr_data_Dom1))
MAF_all_alr_data_Dom1<-t(t_MAF_all_alr_data_Dom1)

#oxides
PCA_all_ox_data_Dom1_Bh<-array(rep(NA,36),dim=c(6,6))
for (r in 1:6){
    for (column in 1:6){
    PCA_all_ox_data_Dom1_Bh[r,column]<-PCA_all_ox_Dom1_omnivar[1,r,column,1]$gg
    }
}
Eigen_PCA_all_ox_data_Dom1_Bh<-eigen(PCA_all_ox_data_Dom1_Bh)
PCA_all_ox_Dom1_Q<-t(Eigen_PCA_all_ox_data_Dom1_Bh$vectors)
MAF_all_ox_Dom1_W<-PCA_all_ox_Dom1_Q%*%PCA_all_ox_Dom1_W
t_MAF_all_ox_data_Dom1<-MAF_all_ox_Dom1_W%*%t(as.matrix(all_ox_data_Dom1))
MAF_all_ox_data_Dom1<-t(t_MAF_all_ox_data_Dom1)

## Creates directional MAF rotated data:
#alr
PCA_all_alr_data_Dom1_B1h<-array(rep(NA,36),dim=c(6,6))
for (r in 1:6){
    for (column in 1:6){
```

```
    PCA_all_alr_data_Dom1_B1h[r,column]<-PCA_all_alr_Dom1_dirvar[1,r,column,1]$gg
    }
}
Eigen_PCA_all_alr_data_Dom1_B1h<-eigen(PCA_all_alr_data_Dom1_B1h)
PCA_all_alr_Dom1_Q1<-t(Eigen_PCA_all_alr_data_Dom1_B1h$vectors)
MAF_all_alr_Dom1_W1<-PCA_all_alr_Dom1_Q1%*%PCA_all_alr_Dom1_W
t_DMAF_all_alr_data_Dom1<-MAF_all_alr_Dom1_W1%*%t(as.matrix(all_alr_data_Dom1))
DMAF_all_alr_data_Dom1<-t(t_DMAF_all_alr_data_Dom1)

#oxides
PCA_all_ox_data_Dom1_B1h<-array(rep(NA,36),dim=c(6,6))
for (r in 1:6){
    for (column in 1:6){
    PCA_all_ox_data_Dom1_B1h[r,column]<-PCA_all_ox_Dom1_dirvar[1,r,column,1]$gg
    }
}
Eigen_PCA_all_ox_data_Dom1_B1h<-eigen(PCA_all_ox_data_Dom1_B1h)
PCA_all_ox_Dom1_Q1<-t(Eigen_PCA_all_ox_data_Dom1_B1h$vectors)
MAF_all_ox_Dom1_W1<-PCA_all_ox_Dom1_Q1%*%PCA_all_ox_Dom1_W
t_DMAF_all_ox_data_Dom1<-MAF_all_ox_Dom1_W1%*%t(as.matrix(all_ox_data_Dom1))
DMAF_all_ox_data_Dom1<-t(t_DMAF_all_ox_data_Dom1)


## Adds Omni MAF factors to coords for decorrelation assessment
#alr
```

```
MAF_all_alr_data_Dom1_xy<-cbind(all_coords_Dom1,MAF_all_alr_data_Dom1)
#oxides
MAF_all_ox_data_Dom1_xy<-cbind(all_coords_Dom1,MAF_all_ox_data_Dom1)

## Adds Directional MAF factors to coords for decorrelation assessment
#alr
DMAF_all_alr_data_Dom1_xy<-cbind(all_coords_Dom1,DMAF_all_alr_data_Dom1)
#oxides
DMAF_all_ox_data_Dom1_xy<-cbind(all_coords_Dom1,DMAF_all_ox_data_Dom1)

## This part generates RGeostats databases for the experimental variography required for zet / tau / kappa
 library (RGeostats)
#OmniMAF
#alr
MAF_all_alr_Dom1_db<-db.create(MAF_all_alr_data_Dom1_xy,flag.grid=FALSE,ndim=2,nvar=6, autoname=FALSE)
#oxides
MAF_all_ox_Dom1_db<-db.create(MAF_all_ox_data_Dom1_xy,flag.grid=FALSE,ndim=2,nvar=6, autoname=FALSE)
#DirMAF
#alr
DMAF_all_alr_Dom1_db<-db.create(DMAF_all_alr_data_Dom1_xy,flag.grid=FALSE,ndim=2,nvar=6, autoname=FALSE)
#oxides
DMAF_all_ox_Dom1_db<-db.create(DMAF_all_ox_data_Dom1_xy,flag.grid=FALSE,ndim=2,nvar=6, autoname=FALSE)

## Creates omnidirectional experimental variograms of decorrelated data via MAF
#alr
```

```
MAF_all_alr_Dom1_omnivar<-vario.calc(MAF_all_alr_Dom1_db,lag=7.5,nlag=16)
#oxides
MAF_all_ox_Dom1_omnivar<-vario.calc(MAF_all_ox_Dom1_db,lag=7.5,nlag=16)

## Creates directional experimental variograms of decorrelated data via MAF
#alr
MAF_all_alr_Dom1_dirvar<-vario.calc(MAF_all_alr_Dom1_db,dirvect=c(085,175), toldis =0.5, tolang=c(45,45), lag =7.5, nlag=16)
#oxides
MAF_all_ox_Dom1_dirvar<-vario.calc(MAF_all_ox_Dom1_db,dirvect=c(085,175),toldis=0.5, tolang=c(45,45), lag =7.5, nlag=16)

## Creates omnidirectional experimental variograms of decorrelated data via DirMAF
#alr
DMAF_all_alr_Dom1_omnivar<-vario.calc(DMAF_all_alr_Dom1_db,lag=7.5,nlag=16)
#oxides
DMAF_all_ox_Dom1_omnivar<-vario.calc(DMAF_all_ox_Dom1_db,lag=7.5,nlag=16)

## Creates directional experimental variograms of decorrelated data via DirMAF
#alr
DMAF_all_alr_Dom1_dirvar<-vario.calc(DMAF_all_alr_Dom1_db,dirvect=c(085,175),toldis=0.5, tolang=c(45,45), lag =7.5, nlag=16)
#oxides
DMAF_all_ox_Dom1_dirvar<-vario.calc(DMAF_all_ox_Dom1_db,dirvect=c(085,175),toldis=0.5, tolang=c(45,45), lag =7.5, nlag=16)

#End of Section
#---------------
```

```
# START OF SECTION
# Gneerates Zeta Tau and Kappa values for alr / oxide data, ICA_alr / ICA_ox data, MAF_alr / MAF_ox data
# Plots values for each decorrelation method

## Zeta values for non-decorrelated alr data
RAW_all_alr_Dom1_omnizeta<-c(rep(NA, 16))
for (h in 1:16){
RAW_all_alr_Dom1_omnizeta[h]<-((2*RAW_all_alr_Dom1_omnivar[1,1,2,h]$gg^2)
+(2*RAW_all_alr_Dom1_omnivar[1,1,3,h]$gg^2)+(2*RAW_all_alr_Dom1_omnivar[1,1,4,h]$gg^2)
+(2*RAW_all_alr_Dom1_omnivar[1,1,5,h]$gg^2)+(2*RAW_all_alr_Dom1_omnivar[1,1,6,h]$gg^2)
+(2*RAW_all_alr_Dom1_omnivar[1,3,2,h]$gg^2)+(2*RAW_all_alr_Dom1_omnivar[1,4,2,h]$gg^2)
+(2*RAW_all_alr_Dom1_omnivar[1,5,2,h]$gg^2)+(2*RAW_all_alr_Dom1_omnivar[1,6,2,h]$gg^2)
+(2*RAW_all_alr_Dom1_omnivar[1,3,4,h]$gg^2)+(2*RAW_all_alr_Dom1_omnivar[1,3,5,h]$gg^2)
+(2*RAW_all_alr_Dom1_omnivar[1,3,6,h]$gg^2)+(2*RAW_all_alr_Dom1_omnivar[1,4,5,h]$gg^2)
+(2*RAW_all_alr_Dom1_omnivar[1,4,6,h]$gg^2)+(2*RAW_all_alr_Dom1_omnivar[1,5,6,h]$gg^2))
}

RAW_all_alr_Dom1_dirzeta<-array(rep(NA, (2*16)),dim = c(2,16) )
for (d in 1:2){
for (h in 1:16){
RAW_all_alr_Dom1_dirzeta[d,h]<-((2*RAW_all_alr_Dom1_dirvar[d,1,2,h]$gg^2)
+(2*RAW_all_alr_Dom1_dirvar[d,1,3,h]$gg^2)+(2*RAW_all_alr_Dom1_dirvar[d,1,4,h]$gg^2)
+(2*RAW_all_alr_Dom1_dirvar[d,1,5,h]$gg^2)+(2*RAW_all_alr_Dom1_dirvar[d,1,6,h]$gg^2)
+(2*RAW_all_alr_Dom1_dirvar[d,3,2,h]$gg^2)+(2*RAW_all_alr_Dom1_dirvar[d,4,2,h]$gg^2)
+(2*RAW_all_alr_Dom1_dirvar[d,5,2,h]$gg^2)+(2*RAW_all_alr_Dom1_dirvar[d,6,2,h]$gg^2)
```

```
+(2*RAW_all_alr_Dom1_dirvar[d,3,4,h]$gg^2)+(2*RAW_all_alr_Dom1_dirvar[d,3,5,h]$gg^2)
+(2*RAW_all_alr_Dom1_dirvar[d,3,6,h]$gg^2)+(2*RAW_all_alr_Dom1_dirvar[d,4,5,h]$gg^2)
+(2*RAW_all_alr_Dom1_dirvar[d,4,6,h]$gg^2)+(2*RAW_all_alr_Dom1_dirvar[d,5,6,h]$gg^2))
}
}

## Zeta values for non-decorrelated ox data
RAW_all_ox_Dom1_omnizeta<-c(rep(NA, 16))
for (h in 1:16){
RAW_all_ox_Dom1_omnizeta[h]<-((2*RAW_all_ox_Dom1_omnivar[1,1,2,h]$gg^2)
+(2*RAW_all_ox_Dom1_omnivar[1,1,3,h]$gg^2)+(2*RAW_all_ox_Dom1_omnivar[1,1,4,h]$gg^2)
+(2*RAW_all_ox_Dom1_omnivar[1,1,5,h]$gg^2)+(2*RAW_all_ox_Dom1_omnivar[1,1,6,h]$gg^2)
+(2*RAW_all_ox_Dom1_omnivar[1,3,2,h]$gg^2)+(2*RAW_all_ox_Dom1_omnivar[1,4,2,h]$gg^2)
+(2*RAW_all_ox_Dom1_omnivar[1,5,2,h]$gg^2)+(2*RAW_all_ox_Dom1_omnivar[1,6,2,h]$gg^2)
+(2*RAW_all_ox_Dom1_omnivar[1,3,4,h]$gg^2)+(2*RAW_all_ox_Dom1_omnivar[1,3,5,h]$gg^2)
+(2*RAW_all_ox_Dom1_omnivar[1,3,6,h]$gg^2)+(2*RAW_all_ox_Dom1_omnivar[1,4,5,h]$gg^2)
+(2*RAW_all_ox_Dom1_omnivar[1,4,6,h]$gg^2)+(2*RAW_all_ox_Dom1_omnivar[1,5,6,h]$gg^2))
}

RAW_all_ox_Dom1_dirzeta<-array(rep(NA, (2*16)),dim = c(2,16))
for (d in 1:2){
for (h in 1:16){
RAW_all_ox_Dom1_dirzeta[d,h]<-((2*RAW_all_ox_Dom1_dirvar[d,1,2,h]$gg^2)
+(2*RAW_all_ox_Dom1_dirvar[d,1,3,h]$gg^2)+(2*RAW_all_ox_Dom1_dirvar[d,1,4,h]$gg^2)
+(2*RAW_all_ox_Dom1_dirvar[d,1,5,h]$gg^2)+(2*RAW_all_ox_Dom1_dirvar[d,1,6,h]$gg^2)
```

```
+(2*RAW_all_ox_Dom1_dirvar[d,3,2,h]$gg^2)+(2*RAW_all_ox_Dom1_dirvar[d,4,2,h]$gg^2)
+(2*RAW_all_ox_Dom1_dirvar[d,5,2,h]$gg^2)+(2*RAW_all_ox_Dom1_dirvar[d,6,2,h]$gg^2)
+(2*RAW_all_ox_Dom1_dirvar[d,3,4,h]$gg^2)+(2*RAW_all_ox_Dom1_dirvar[d,3,5,h]$gg^2)
+(2*RAW_all_ox_Dom1_dirvar[d,3,6,h]$gg^2)+(2*RAW_all_ox_Dom1_dirvar[d,4,5,h]$gg^2)
+(2*RAW_all_ox_Dom1_dirvar[d,4,6,h]$gg^2)+(2*RAW_all_ox_Dom1_dirvar[d,5,6,h]$gg^2))
}
}

## Zeta Values for alr data MAF
MAF_all_alr_Dom1_omnizeta<-c(rep(NA, 16))
for (h in 1:16){
MAF_all_alr_Dom1_omnizeta[h]<-((2*MAF_all_alr_Dom1_omnivar[1,1,2,h]$gg^2)
+(2*MAF_all_alr_Dom1_omnivar[1,1,3,h]$gg^2)+(2*MAF_all_alr_Dom1_omnivar[1,1,4,h]$gg^2)
+(2*MAF_all_alr_Dom1_omnivar[1,1,5,h]$gg^2)+(2*MAF_all_alr_Dom1_omnivar[1,1,6,h]$gg^2)
+(2*MAF_all_alr_Dom1_omnivar[1,3,2,h]$gg^2)+(2*MAF_all_alr_Dom1_omnivar[1,4,2,h]$gg^2)
+(2*MAF_all_alr_Dom1_omnivar[1,5,2,h]$gg^2)+(2*MAF_all_alr_Dom1_omnivar[1,6,2,h]$gg^2)
+(2*MAF_all_alr_Dom1_omnivar[1,3,4,h]$gg^2)+(2*MAF_all_alr_Dom1_omnivar[1,3,5,h]$gg^2)
+(2*MAF_all_alr_Dom1_omnivar[1,3,6,h]$gg^2)+(2*MAF_all_alr_Dom1_omnivar[1,4,5,h]$gg^2)
+(2*MAF_all_alr_Dom1_omnivar[1,4,6,h]$gg^2)+(2*MAF_all_alr_Dom1_omnivar[1,5,6,h]$gg^2))
}

MAF_all_alr_Dom1_dirzeta<-array(rep(NA, (2*16)),dim = c(2,16) )
for (d in 1:2){
for (h in 1:16){
MAF_all_alr_Dom1_dirzeta[d,h]<-((2*MAF_all_alr_Dom1_dirvar[d,1,2,h]$gg^2)
```

```
+(2*MAF_all_alr_Dom1_dirvar[d,1,3,h]$gg^2)+(2*MAF_all_alr_Dom1_dirvar[d,1,4,h]$gg^2)
+(2*MAF_all_alr_Dom1_dirvar[d,1,5,h]$gg^2)+(2*MAF_all_alr_Dom1_dirvar[d,1,6,h]$gg^2)
+(2*MAF_all_alr_Dom1_dirvar[d,3,2,h]$gg^2)+(2*MAF_all_alr_Dom1_dirvar[d,4,2,h]$gg^2)
+(2*MAF_all_alr_Dom1_dirvar[d,5,2,h]$gg^2)+(2*MAF_all_alr_Dom1_dirvar[d,6,2,h]$gg^2)
+(2*MAF_all_alr_Dom1_dirvar[d,3,4,h]$gg^2)+(2*MAF_all_alr_Dom1_dirvar[d,3,5,h]$gg^2)
+(2*MAF_all_alr_Dom1_dirvar[d,3,6,h]$gg^2)+(2*MAF_all_alr_Dom1_dirvar[d,4,5,h]$gg^2)
+(2*MAF_all_alr_Dom1_dirvar[d,4,6,h]$gg^2)+(2*MAF_all_alr_Dom1_dirvar[d,5,6,h]$gg^2))
}
}

## Zeta Values for ox data MAF
MAF_all_ox_Dom1_omnizeta<-c(rep(NA, 16))
for (h in 1:16){
MAF_all_ox_Dom1_omnizeta[h]<-((2*MAF_all_ox_Dom1_omnivar[1,1,2,h]$gg^2)
+(2*MAF_all_ox_Dom1_omnivar[1,1,3,h]$gg^2)+(2*MAF_all_ox_Dom1_omnivar[1,1,4,h]$gg^2)
+(2*MAF_all_ox_Dom1_omnivar[1,1,5,h]$gg^2)+(2*MAF_all_ox_Dom1_omnivar[1,1,6,h]$gg^2)
+(2*MAF_all_ox_Dom1_omnivar[1,3,2,h]$gg^2)+(2*MAF_all_ox_Dom1_omnivar[1,4,2,h]$gg^2)
+(2*MAF_all_ox_Dom1_omnivar[1,5,2,h]$gg^2)+(2*MAF_all_ox_Dom1_omnivar[1,6,2,h]$gg^2)
+(2*MAF_all_ox_Dom1_omnivar[1,3,4,h]$gg^2)+(2*MAF_all_ox_Dom1_omnivar[1,3,5,h]$gg^2)
+(2*MAF_all_ox_Dom1_omnivar[1,3,6,h]$gg^2)+(2*MAF_all_ox_Dom1_omnivar[1,4,5,h]$gg^2)
+(2*MAF_all_ox_Dom1_omnivar[1,4,6,h]$gg^2)+(2*MAF_all_ox_Dom1_omnivar[1,5,6,h]$gg^2))
}

MAF_all_ox_Dom1_dirzeta<-array(rep(NA, (2*16)),dim = c(2,16))
for (d in 1:2){
```

```
for (h in 1:16){
MAF_all_ox_Dom1_dirzeta[d,h]<-((2*MAF_all_ox_Dom1_dirvar[d,1,2,h]$gg^2)
+(2*MAF_all_ox_Dom1_dirvar[d,1,3,h]$gg^2)+(2*MAF_all_ox_Dom1_dirvar[d,1,4,h]$gg^2)
+(2*MAF_all_ox_Dom1_dirvar[d,1,5,h]$gg^2)+(2*MAF_all_ox_Dom1_dirvar[d,1,6,h]$gg^2)
+(2*MAF_all_ox_Dom1_dirvar[d,3,2,h]$gg^2)+(2*MAF_all_ox_Dom1_dirvar[d,4,2,h]$gg^2)
+(2*MAF_all_ox_Dom1_dirvar[d,5,2,h]$gg^2)+(2*MAF_all_ox_Dom1_dirvar[d,6,2,h]$gg^2)
+(2*MAF_all_ox_Dom1_dirvar[d,3,4,h]$gg^2)+(2*MAF_all_ox_Dom1_dirvar[d,3,5,h]$gg^2)
+(2*MAF_all_ox_Dom1_dirvar[d,3,6,h]$gg^2)+(2*MAF_all_ox_Dom1_dirvar[d,4,5,h]$gg^2)
+(2*MAF_all_ox_Dom1_dirvar[d,4,6,h]$gg^2)+(2*MAF_all_ox_Dom1_dirvar[d,5,6,h]$gg^2))
}
}

## Zeta Values for alr data ICA
ICA_all_alr_Dom1_omnizeta<-c(rep(NA, 16))
for (h in 1:16){
ICA_all_alr_Dom1_omnizeta[h]<-((2*ICA_all_alr_Dom1_omnivar[1,1,2,h]$gg^2)
+(2*ICA_all_alr_Dom1_omnivar[1,1,3,h]$gg^2)+(2*ICA_all_alr_Dom1_omnivar[1,1,4,h]$gg^2)
+(2*ICA_all_alr_Dom1_omnivar[1,1,5,h]$gg^2)+(2*ICA_all_alr_Dom1_omnivar[1,1,6,h]$gg^2)
+(2*ICA_all_alr_Dom1_omnivar[1,3,2,h]$gg^2)+(2*ICA_all_alr_Dom1_omnivar[1,4,2,h]$gg^2)
+(2*ICA_all_alr_Dom1_omnivar[1,5,2,h]$gg^2)+(2*ICA_all_alr_Dom1_omnivar[1,6,2,h]$gg^2)
+(2*ICA_all_alr_Dom1_omnivar[1,3,4,h]$gg^2)+(2*ICA_all_alr_Dom1_omnivar[1,3,5,h]$gg^2)
+(2*ICA_all_alr_Dom1_omnivar[1,3,6,h]$gg^2)+(2*ICA_all_alr_Dom1_omnivar[1,4,5,h]$gg^2)
+(2*ICA_all_alr_Dom1_omnivar[1,4,6,h]$gg^2)+(2*ICA_all_alr_Dom1_omnivar[1,5,6,h]$gg^2))
}
```

```
ICA_all_alr_Dom1_dirzeta<-array(rep(NA, (2*16)),dim = c(2,16))
for (d in 1:2){
for (h in 1:16){
ICA_all_alr_Dom1_dirzeta[d,h]<-((2*ICA_all_alr_Dom1_dirvar[d,1,2,h]$gg^2)
+(2*ICA_all_alr_Dom1_dirvar[d,1,3,h]$gg^2)+(2*ICA_all_alr_Dom1_dirvar[d,1,4,h]$gg^2)
+(2*ICA_all_alr_Dom1_dirvar[d,1,5,h]$gg^2)+(2*ICA_all_alr_Dom1_dirvar[d,1,6,h]$gg^2)
+(2*ICA_all_alr_Dom1_dirvar[d,3,2,h]$gg^2)+(2*ICA_all_alr_Dom1_dirvar[d,4,2,h]$gg^2)
+(2*ICA_all_alr_Dom1_dirvar[d,5,2,h]$gg^2)+(2*ICA_all_alr_Dom1_dirvar[d,6,2,h]$gg^2)
+(2*ICA_all_alr_Dom1_dirvar[d,3,4,h]$gg^2)+(2*ICA_all_alr_Dom1_dirvar[d,3,5,h]$gg^2)
+(2*ICA_all_alr_Dom1_dirvar[d,3,6,h]$gg^2)+(2*ICA_all_alr_Dom1_dirvar[d,4,5,h]$gg^2)
+(2*ICA_all_alr_Dom1_dirvar[d,4,6,h]$gg^2)+(2*ICA_all_alr_Dom1_dirvar[d,5,6,h]$gg^2))
}
}

## Zeta Values for ox data ICA
ICA_all_ox_Dom1_omnizeta<-c(rep(NA, 16))
for (h in 1:16){
ICA_all_ox_Dom1_omnizeta[h]<-((2*ICA_all_ox_Dom1_omnivar[1,1,2,h]$gg^2)
+(2*ICA_all_ox_Dom1_omnivar[1,1,3,h]$gg^2)+(2*ICA_all_ox_Dom1_omnivar[1,1,4,h]$gg^2)
+(2*ICA_all_ox_Dom1_omnivar[1,1,5,h]$gg^2)+(2*ICA_all_ox_Dom1_omnivar[1,1,6,h]$gg^2)
+(2*ICA_all_ox_Dom1_omnivar[1,3,2,h]$gg^2)+(2*ICA_all_ox_Dom1_omnivar[1,4,2,h]$gg^2)
+(2*ICA_all_ox_Dom1_omnivar[1,5,2,h]$gg^2)+(2*ICA_all_ox_Dom1_omnivar[1,6,2,h]$gg^2)
+(2*ICA_all_ox_Dom1_omnivar[1,3,4,h]$gg^2)+(2*ICA_all_ox_Dom1_omnivar[1,3,5,h]$gg^2)
+(2*ICA_all_ox_Dom1_omnivar[1,3,6,h]$gg^2)+(2*ICA_all_ox_Dom1_omnivar[1,4,5,h]$gg^2)
+(2*ICA_all_ox_Dom1_omnivar[1,4,6,h]$gg^2)+(2*ICA_all_ox_Dom1_omnivar[1,5,6,h]$gg^2))
```

```
}

ICA_all_ox_Dom1_dirzeta<-array(rep(NA, (2*16)),dim = c(2,16) )
for (d in 1:2){
for (h in 1:16){
ICA_all_ox_Dom1_dirzeta[d,h]<-((2*ICA_all_ox_Dom1_dirvar[d,1,2,h]$gg^2)
+(2*ICA_all_ox_Dom1_dirvar[d,1,3,h]$gg^2)+(2*ICA_all_ox_Dom1_dirvar[d,1,4,h]$gg^2)
+(2*ICA_all_ox_Dom1_dirvar[d,1,5,h]$gg^2)+(2*ICA_all_ox_Dom1_dirvar[d,1,6,h]$gg^2)
+(2*ICA_all_ox_Dom1_dirvar[d,3,2,h]$gg^2)+(2*ICA_all_ox_Dom1_dirvar[d,4,2,h]$gg^2)
+(2*ICA_all_ox_Dom1_dirvar[d,5,2,h]$gg^2)+(2*ICA_all_ox_Dom1_dirvar[d,6,2,h]$gg^2)
+(2*ICA_all_ox_Dom1_dirvar[d,3,4,h]$gg^2)+(2*ICA_all_ox_Dom1_dirvar[d,3,5,h]$gg^2)
+(2*ICA_all_ox_Dom1_dirvar[d,3,6,h]$gg^2)+(2*ICA_all_ox_Dom1_dirvar[d,4,5,h]$gg^2)
+(2*ICA_all_ox_Dom1_dirvar[d,4,6,h]$gg^2)+(2*ICA_all_ox_Dom1_dirvar[d,5,6,h]$gg^2))
}
}

## Tau values for alr data ICA
ICA_all_alr_Dom1_omnitau<-array(rep(NA, 16))
for (h in 1:16){
U<-((2*abs(ICA_all_alr_Dom1_omnivar[1,1,2,h]$gg))+(2*abs(ICA_all_alr_Dom1_omnivar[1,1,3,h]$gg))
+(2*abs(ICA_all_alr_Dom1_omnivar[1,1,4,h]$gg))
+(2*abs(ICA_all_alr_Dom1_omnivar[1,1,5,h]$gg))+(2*abs(ICA_all_alr_Dom1_omnivar[1,3,2,h]$gg))
+(2*abs(ICA_all_alr_Dom1_omnivar[1,4,2,h]$gg))
+(2*abs(ICA_all_alr_Dom1_omnivar[1,5,2,h]$gg))+(2*abs(ICA_all_alr_Dom1_omnivar[1,3,4,h]$gg))
+(2*abs(ICA_all_alr_Dom1_omnivar[1,3,5,h]$gg))
```

```
+(2*abs(ICA_all_alr_Dom1_omnivar[1,4,5,h]$gg)))
D<-(abs(ICA_all_alr_Dom1_omnivar[1,1,1,h]$gg)+abs(ICA_all_alr_Dom1_omnivar[1,2,2,h]$gg)
+abs(ICA_all_alr_Dom1_omnivar[1,3,3,h]$gg)
+abs(ICA_all_alr_Dom1_omnivar[1,4,4,h]$gg)+abs(ICA_all_alr_Dom1_omnivar[1,5,5,h]$gg))
ICA_all_alr_Dom1_omnitau[h]<-U/D
}


ICA_all_alr_Dom1_dirtau<-array(rep(NA, (2*16)),dim=c(2,16))
for (d in 1:2){
for (h in 1:16){
U<-((2*abs(ICA_all_alr_Dom1_dirvar[d,1,2,h]$gg))+(2*abs(ICA_all_alr_Dom1_dirvar[d,1,3,h]$gg))
+(2*abs(ICA_all_alr_Dom1_dirvar[d,1,4,h]$gg))
+(2*abs(ICA_all_alr_Dom1_dirvar[d,1,5,h]$gg))+(2*abs(ICA_all_alr_Dom1_dirvar[d,3,2,h]$gg))
+(2*abs(ICA_all_alr_Dom1_dirvar[d,4,2,h]$gg))
+(2*abs(ICA_all_alr_Dom1_dirvar[d,5,2,h]$gg))+(2*abs(ICA_all_alr_Dom1_dirvar[d,3,4,h]$gg))
+(2*abs(ICA_all_alr_Dom1_dirvar[d,3,5,h]$gg))
+(2*abs(ICA_all_alr_Dom1_dirvar[d,4,5,h]$gg)))
D<-(abs(ICA_all_alr_Dom1_dirvar[d,1,1,h]$gg)+abs(ICA_all_alr_Dom1_dirvar[d,2,2,h]$gg)
+abs(ICA_all_alr_Dom1_dirvar[d,3,3,h]$gg)
+abs(ICA_all_alr_Dom1_dirvar[d,4,4,h]$gg)+abs(ICA_all_alr_Dom1_dirvar[d,5,5,h]$gg))
ICA_all_alr_Dom1_dirtau[d,h]<-U/D
}
}
```

```
## Kappa values for alr data ICA
ICA_all_alr_Dom1_omnikappa<-array(rep(NA, 16))
for (h in 1:16){
ICA_all_alr_Dom1_omnikappa[h]<-1-(ICA_all_alr_Dom1_omnizeta[h]/RAW_all_alr_Dom1_omnizeta[h])
}


ICA_all_alr_Dom1_dirkappa<-array(rep(NA, (2*16)),dim=c(2,16))
for (d in 1:2){
for (h in 1:16){
ICA_all_alr_Dom1_dirkappa[d,h]<-1-(ICA_all_alr_Dom1_dirzeta[d,h]/RAW_all_alr_Dom1_dirzeta[d,h])
}
}


## Tau values for alr data MAF
MAF_all_alr_Dom1_omnitau<-array(rep(NA, 16))
for (h in 1:16){
U<-((2*abs(MAF_all_alr_Dom1_omnivar[1,1,2,h]$gg))+(2*abs(MAF_all_alr_Dom1_omnivar[1,1,3,h]$gg))
+(2*abs(MAF_all_alr_Dom1_omnivar[1,1,4,h]$gg))
+(2*abs(MAF_all_alr_Dom1_omnivar[1,1,5,h]$gg))+(2*abs(MAF_all_alr_Dom1_omnivar[1,3,2,h]$gg))
+(2*abs(MAF_all_alr_Dom1_omnivar[1,4,2,h]$gg))
+(2*abs(MAF_all_alr_Dom1_omnivar[1,5,2,h]$gg))+(2*abs(MAF_all_alr_Dom1_omnivar[1,3,4,h]$gg))
+(2*abs(MAF_all_alr_Dom1_omnivar[1,3,5,h]$gg))
+(2*abs(MAF_all_alr_Dom1_omnivar[1,4,5,h]$gg)))
```

```
D<-(abs(MAF_all_alr_Dom1_omnivar[1,1,1,h]$gg)+abs(MAF_all_alr_Dom1_omnivar[1,2,2,h]$gg)
+abs(MAF_all_alr_Dom1_omnivar[1,3,3,h]$gg)
+abs(MAF_all_alr_Dom1_omnivar[1,4,4,h]$gg)+abs(MAF_all_alr_Dom1_omnivar[1,5,5,h]$gg))
MAF_all_alr_Dom1_omnitau[h]<-U/D
}


MAF_all_alr_Dom1_dirtau<-array(rep(NA, (2*16)),dim=c(2,16))
 for  (d  in  1:2){
 for  (h  in  1:16){
U<-((2*abs(MAF_all_alr_Dom1_dirvar[d,1,2,h]$gg))+(2*abs(MAF_all_alr_Dom1_dirvar[d,1,3,h]$gg))
+(2*abs(MAF_all_alr_Dom1_dirvar[d,1,4,h]$gg))
+(2*abs(MAF_all_alr_Dom1_dirvar[d,1,5,h]$gg))+(2*abs(MAF_all_alr_Dom1_dirvar[d,3,2,h]$gg))
+(2*abs(MAF_all_alr_Dom1_dirvar[d,4,2,h]$gg))
+(2*abs(MAF_all_alr_Dom1_dirvar[d,5,2,h]$gg))+(2*abs(MAF_all_alr_Dom1_dirvar[d,3,4,h]$gg))
+(2*abs(MAF_all_alr_Dom1_dirvar[d,3,5,h]$gg))
+(2*abs(MAF_all_alr_Dom1_dirvar[d,4,5,h]$gg)))
D<-(abs(MAF_all_alr_Dom1_dirvar[d,1,1,h]$gg)+abs(MAF_all_alr_Dom1_dirvar[d,2,2,h]$gg)
+abs(MAF_all_alr_Dom1_dirvar[d,3,3,h]$gg)
+abs(MAF_all_alr_Dom1_dirvar[d,4,4,h]$gg)+abs(MAF_all_alr_Dom1_dirvar[d,5,5,h]$gg))
MAF_all_alr_Dom1_dirtau[d,h]<-U/D
}
}

## Kappa values  for  alr  data  MAF
```

```
MAF_all_alr_Dom1_omnikappa<-array(rep(NA, 16))
for (h in 1:16){
MAF_all_alr_Dom1_omnikappa[h]<-1-(MAF_all_alr_Dom1_omnizeta[h]/RAW_all_alr_Dom1_omnizeta[h])
}


MAF_all_alr_Dom1_dirkappa<-array(rep(NA, (2*16)),dim=c(2,16))
for (d in 1:2){
for (h in 1:16){
MAF_all_alr_Dom1_dirkappa[d,h]<-1-(MAF_all_alr_Dom1_dirzeta[d,h]/RAW_all_alr_Dom1_dirzeta[d,h])
}
}

## Tau values for ox data ICA
ICA_all_ox_Dom1_omnitau<-array(rep(NA, 16))
for (h in 1:16){
U<-((2*abs(ICA_all_ox_Dom1_omnivar[1,1,2,h]$gg))+(2*abs(ICA_all_ox_Dom1_omnivar[1,1,3,h]$gg))
+(2*abs(ICA_all_ox_Dom1_omnivar[1,1,4,h]$gg))
+(2*abs(ICA_all_ox_Dom1_omnivar[1,1,5,h]$gg))+(2*abs(ICA_all_ox_Dom1_omnivar[1,3,2,h]$gg))
+(2*abs(ICA_all_ox_Dom1_omnivar[1,4,2,h]$gg))
+(2*abs(ICA_all_ox_Dom1_omnivar[1,5,2,h]$gg))+(2*abs(ICA_all_ox_Dom1_omnivar[1,3,4,h]$gg))
+(2*abs(ICA_all_ox_Dom1_omnivar[1,3,5,h]$gg))
+(2*abs(ICA_all_ox_Dom1_omnivar[1,4,5,h]$gg)))
D<-(abs(ICA_all_ox_Dom1_omnivar[1,1,1,h]$gg)+abs(ICA_all_ox_Dom1_omnivar[1,2,2,h]$gg)
+abs(ICA_all_ox_Dom1_omnivar[1,3,3,h]$gg)
```

```
+abs(ICA_all_ox_Dom1_omnivar[1,4,4,h]$gg)+abs(ICA_all_ox_Dom1_omnivar[1,5,5,h]$gg))
ICA_all_ox_Dom1_omnitau[h]<-U/D
}


ICA_all_ox_Dom1_dirtau<-array(rep(NA, (2*16)),dim=c(2,16))
for (d in 1:2){
for (h in 1:16){
U<-((2*abs(ICA_all_ox_Dom1_dirvar[d,1,2,h]$gg))+(2*abs(ICA_all_ox_Dom1_dirvar[d,1,3,h]$gg))
+(2*abs(ICA_all_ox_Dom1_dirvar[d,1,4,h]$gg))
+(2*abs(ICA_all_ox_Dom1_dirvar[d,1,5,h]$gg))+(2*abs(ICA_all_ox_Dom1_dirvar[d,3,2,h]$gg))
+(2*abs(ICA_all_ox_Dom1_dirvar[d,4,2,h]$gg))
+(2*abs(ICA_all_ox_Dom1_dirvar[d,5,2,h]$gg))+(2*abs(ICA_all_ox_Dom1_dirvar[d,3,4,h]$gg))
+(2*abs(ICA_all_ox_Dom1_dirvar[d,3,5,h]$gg))
+(2*abs(ICA_all_ox_Dom1_dirvar[d,4,5,h]$gg)))
D<-(abs(ICA_all_ox_Dom1_dirvar[d,1,1,h]$gg)+abs(ICA_all_ox_Dom1_dirvar[d,2,2,h]$gg)
+abs(ICA_all_ox_Dom1_dirvar[d,3,3,h]$gg)
+abs(ICA_all_ox_Dom1_dirvar[d,4,4,h]$gg)+abs(ICA_all_ox_Dom1_dirvar[d,5,5,h]$gg))
ICA_all_ox_Dom1_dirtau[d,h]<-U/D
}
}

## Kappa values for ox data ICA
ICA_all_ox_Dom1_omnikappa<-array(rep(NA, 16))
for (h in 1:16){
```

```
ICA_all_ox_Dom1_omnikappa[h]<-1-(ICA_all_ox_Dom1_omnizeta[h]/RAW_all_ox_Dom1_omnizeta[h])
}

ICA_all_ox_Dom1_dirkappa<-array(rep(NA, (2*16)),dim=c(2,16))
for (d in 1:2){
for (h in 1:16){
ICA_all_ox_Dom1_dirkappa[d,h]<-1-(ICA_all_ox_Dom1_dirzeta[d,h]/RAW_all_ox_Dom1_dirzeta[d,h])
}
}

# Tau values for ox data MAF
MAF_all_ox_Dom1_omnitau<-array(rep(NA, 16))

for (h in 1:16){
U<-((2*abs(MAF_all_ox_Dom1_omnivar[1,1,2,h]$gg))+(2*abs(MAF_all_ox_Dom1_omnivar[1,1,3,h]$gg))
+(2*abs(MAF_all_ox_Dom1_omnivar[1,1,4,h]$gg))
+(2*abs(MAF_all_ox_Dom1_omnivar[1,1,5,h]$gg))+(2*abs(MAF_all_ox_Dom1_omnivar[1,3,2,h]$gg))
+(2*abs(MAF_all_ox_Dom1_omnivar[1,4,2,h]$gg))
+(2*abs(MAF_all_ox_Dom1_omnivar[1,5,2,h]$gg))+(2*abs(MAF_all_ox_Dom1_omnivar[1,3,4,h]$gg))
+(2*abs(MAF_all_ox_Dom1_omnivar[1,3,5,h]$gg))
+(2*abs(MAF_all_ox_Dom1_omnivar[1,4,5,h]$gg)))
D<-(abs(MAF_all_ox_Dom1_omnivar[1,1,1,h]$gg)+abs(MAF_all_ox_Dom1_omnivar[1,2,2,h]$gg)
+abs(MAF_all_ox_Dom1_omnivar[1,3,3,h]$gg)
+abs(MAF_all_ox_Dom1_omnivar[1,4,4,h]$gg)+abs(MAF_all_ox_Dom1_omnivar[1,5,5,h]$gg))
MAF_all_ox_Dom1_omnitau[h]<-U/D
```

```
}

MAF_all_ox_Dom1_dirtau<-array(rep(NA, (2*16)),dim=c(2,16))
for (d in 1:2){
for (h in 1:16){
U<-((2*abs(MAF_all_ox_Dom1_dirvar[d,1,2,h]$gg))+(2*abs(MAF_all_ox_Dom1_dirvar[d,1,3,h]$gg))
+(2*abs(MAF_all_ox_Dom1_dirvar[d,1,4,h]$gg))
+(2*abs(MAF_all_ox_Dom1_dirvar[d,1,5,h]$gg))+(2*abs(MAF_all_ox_Dom1_dirvar[d,3,2,h]$gg))
+(2*abs(MAF_all_ox_Dom1_dirvar[d,4,2,h]$gg))
+(2*abs(MAF_all_ox_Dom1_dirvar[d,5,2,h]$gg))+(2*abs(MAF_all_ox_Dom1_dirvar[d,3,4,h]$gg))
+(2*abs(MAF_all_ox_Dom1_dirvar[d,3,5,h]$gg))
+(2*abs(MAF_all_ox_Dom1_dirvar[d,4,5,h]$gg)))
D<-(abs(MAF_all_ox_Dom1_dirvar[d,1,1,h]$gg)+abs(MAF_all_ox_Dom1_dirvar[d,2,2,h]$gg)
+abs(MAF_all_ox_Dom1_dirvar[d,3,3,h]$gg)
+abs(MAF_all_ox_Dom1_dirvar[d,4,4,h]$gg)+abs(MAF_all_ox_Dom1_dirvar[d,5,5,h]$gg))
MAF_all_ox_Dom1_dirtau[d,h]<-U/D
}
}

## Kappa values for ox data MAF
MAF_all_ox_Dom1_omnikappa<-array(rep(NA, 16))
for (h in 1:16){
MAF_all_ox_Dom1_omnikappa[h]<-1-(MAF_all_ox_Dom1_omnizeta[h]/RAW_all_ox_Dom1_omnizeta[h])
}
```

```
MAF_all_ox_Dom1_dirkappa<-array(rep(NA, (2*16)),dim=c(2,16))
for (d in 1:2){
for (h in 1:16){
MAF_all_ox_Dom1_dirkappa[d,h]<-1-(MAF_all_ox_Dom1_dirzeta[d,h]/RAW_all_ox_Dom1_dirzeta[d,h])
}
}

#End of Section
#----------------

# START OF SECTION
# Gneerates Zeta Tau and Kappa values for alr / oxide data, DIRECTIONAL MAF_alr / MAF_ox data
# Plots values for each decorrelation method


## Zeta Values for alr data DMAF
DMAF_all_alr_Dom1_omnizeta<-c(rep(NA, 16))
for (h in 1:16){
DMAF_all_alr_Dom1_omnizeta[h]<-((2*DMAF_all_alr_Dom1_omnivar[1,1,2,h]$gg^2)
+(2*DMAF_all_alr_Dom1_omnivar[1,1,3,h]$gg^2)+(2*DMAF_all_alr_Dom1_omnivar[1,1,4,h]$gg^2)
+(2*DMAF_all_alr_Dom1_omnivar[1,1,5,h]$gg^2)+(2*DMAF_all_alr_Dom1_omnivar[1,1,6,h]$gg^2)
+(2*DMAF_all_alr_Dom1_omnivar[1,3,2,h]$gg^2)+(2*DMAF_all_alr_Dom1_omnivar[1,4,2,h]$gg^2)
+(2*DMAF_all_alr_Dom1_omnivar[1,5,2,h]$gg^2)+(2*DMAF_all_alr_Dom1_omnivar[1,6,2,h]$gg^2)
+(2*DMAF_all_alr_Dom1_omnivar[1,3,4,h]$gg^2)+(2*DMAF_all_alr_Dom1_omnivar[1,3,5,h]$gg^2)
+(2*DMAF_all_alr_Dom1_omnivar[1,3,6,h]$gg^2)+(2*DMAF_all_alr_Dom1_omnivar[1,4,5,h]$gg^2)
```

```
+(2*DMAF_all_alr_Dom1_omnivar[1,4,6,h]$gg^2)+(2*DMAF_all_alr_Dom1_omnivar[1,5,6,h]$gg^2))
}

DMAF_all_alr_Dom1_dirzeta<-array(rep(NA, (2*16)),dim = c(2,16))
for (d in 1:2){
for (h in 1:16){
DMAF_all_alr_Dom1_dirzeta[d,h]<-((2*DMAF_all_alr_Dom1_dirvar[d,1,2,h]$gg^2)
+(2*DMAF_all_alr_Dom1_dirvar[d,1,3,h]$gg^2)+(2*DMAF_all_alr_Dom1_dirvar[d,1,4,h]$gg^2)
+(2*DMAF_all_alr_Dom1_dirvar[d,1,5,h]$gg^2)+(2*DMAF_all_alr_Dom1_dirvar[d,1,6,h]$gg^2)
+(2*DMAF_all_alr_Dom1_dirvar[d,3,2,h]$gg^2)+(2*DMAF_all_alr_Dom1_dirvar[d,4,2,h]$gg^2)
+(2*DMAF_all_alr_Dom1_dirvar[d,5,2,h]$gg^2)+(2*DMAF_all_alr_Dom1_dirvar[d,6,2,h]$gg^2)
+(2*DMAF_all_alr_Dom1_dirvar[d,3,4,h]$gg^2)+(2*DMAF_all_alr_Dom1_dirvar[d,3,5,h]$gg^2)
+(2*DMAF_all_alr_Dom1_dirvar[d,3,6,h]$gg^2)+(2*DMAF_all_alr_Dom1_dirvar[d,4,5,h]$gg^2)
+(2*DMAF_all_alr_Dom1_dirvar[d,4,6,h]$gg^2)+(2*DMAF_all_alr_Dom1_dirvar[d,5,6,h]$gg^2))
}
}

## Zeta Values for ox data DMAF
DMAF_all_ox_Dom1_omnizeta<-c(rep(NA, 16))
for (h in 1:16){
DMAF_all_ox_Dom1_omnizeta[h]<-((2*DMAF_all_ox_Dom1_omnivar[1,1,2,h]$gg^2)
+(2*DMAF_all_ox_Dom1_omnivar[1,1,3,h]$gg^2)+(2*DMAF_all_ox_Dom1_omnivar[1,1,4,h]$gg^2)
+(2*DMAF_all_ox_Dom1_omnivar[1,1,5,h]$gg^2)+(2*DMAF_all_ox_Dom1_omnivar[1,1,6,h]$gg^2)
+(2*DMAF_all_ox_Dom1_omnivar[1,3,2,h]$gg^2)+(2*DMAF_all_ox_Dom1_omnivar[1,4,2,h]$gg^2)
+(2*DMAF_all_ox_Dom1_omnivar[1,5,2,h]$gg^2)+(2*DMAF_all_ox_Dom1_omnivar[1,6,2,h]$gg^2)
```

```
+(2*DMAF_all_ox_Dom1_omnivar[1,3,4,h]$gg^2)+(2*DMAF_all_ox_Dom1_omnivar[1,3,5,h]$gg^2)
+(2*DMAF_all_ox_Dom1_omnivar[1,3,6,h]$gg^2)+(2*DMAF_all_ox_Dom1_omnivar[1,4,5,h]$gg^2)
+(2*DMAF_all_ox_Dom1_omnivar[1,4,6,h]$gg^2)+(2*DMAF_all_ox_Dom1_omnivar[1,5,6,h]$gg^2))
}

DMAF_all_ox_Dom1_dirzeta<-array(rep(NA, (2*16)),dim = c(2,16))
for (d in 1:2){
for (h in 1:16){
DMAF_all_ox_Dom1_dirzeta[d,h]<-((2*DMAF_all_ox_Dom1_dirvar[d,1,2,h]$gg^2)
+(2*DMAF_all_ox_Dom1_dirvar[d,1,3,h]$gg^2)+(2*DMAF_all_ox_Dom1_dirvar[d,1,4,h]$gg^2)
+(2*DMAF_all_ox_Dom1_dirvar[d,1,5,h]$gg^2)+(2*DMAF_all_ox_Dom1_dirvar[d,1,6,h]$gg^2)
+(2*DMAF_all_ox_Dom1_dirvar[d,3,2,h]$gg^2)+(2*DMAF_all_ox_Dom1_dirvar[d,4,2,h]$gg^2)
+(2*DMAF_all_ox_Dom1_dirvar[d,5,2,h]$gg^2)+(2*DMAF_all_ox_Dom1_dirvar[d,6,2,h]$gg^2)
+(2*DMAF_all_ox_Dom1_dirvar[d,3,4,h]$gg^2)+(2*DMAF_all_ox_Dom1_dirvar[d,3,5,h]$gg^2)
+(2*DMAF_all_ox_Dom1_dirvar[d,3,6,h]$gg^2)+(2*DMAF_all_ox_Dom1_dirvar[d,4,5,h]$gg^2)
+(2*DMAF_all_ox_Dom1_dirvar[d,4,6,h]$gg^2)+(2*DMAF_all_ox_Dom1_dirvar[d,5,6,h]$gg^2))
}
}

## Tau values for alr data DMAF
DMAF_all_alr_Dom1_omnitau<-array(rep(NA, 16))
for (h in 1:16){
U<-((2*abs(DMAF_all_alr_Dom1_omnivar[1,1,2,h]$gg))+(2*abs(DMAF_all_alr_Dom1_omnivar[1,1,3,h]$gg))
+(2*abs(DMAF_all_alr_Dom1_omnivar[1,1,4,h]$gg))
+(2*abs(DMAF_all_alr_Dom1_omnivar[1,1,5,h]$gg))+(2*abs(DMAF_all_alr_Dom1_omnivar[1,3,2,h]$gg))
```

```
+(2*abs(DMAF_all_alr_Dom1_omnivar[1,4,2,h]$gg))
+(2*abs(DMAF_all_alr_Dom1_omnivar[1,5,2,h]$gg))+(2*abs(DMAF_all_alr_Dom1_omnivar[1,3,4,h]$gg))
+(2*abs(DMAF_all_alr_Dom1_omnivar[1,3,5,h]$gg))
+(2*abs(DMAF_all_alr_Dom1_omnivar[1,4,5,h]$gg)))
D<-(abs(DMAF_all_alr_Dom1_omnivar[1,1,1,h]$gg)+abs(DMAF_all_alr_Dom1_omnivar[1,2,2,h]$gg)
+abs(DMAF_all_alr_Dom1_omnivar[1,3,3,h]$gg)
+abs(DMAF_all_alr_Dom1_omnivar[1,4,4,h]$gg)+abs(DMAF_all_alr_Dom1_omnivar[1,5,5,h]$gg))
DMAF_all_alr_Dom1_omnitau[h]<-U/D
}

DMAF_all_alr_Dom1_dirtau<-array(rep(NA, (2*16)),dim=c(2,16))
for (d in 1:2){
for (h in 1:16){
U<-((2*abs(DMAF_all_alr_Dom1_dirvar[d,1,2,h]$gg))+(2*abs(DMAF_all_alr_Dom1_dirvar[d,1,3,h]$gg))
+(2*abs(DMAF_all_alr_Dom1_dirvar[d,1,4,h]$gg))
+(2*abs(DMAF_all_alr_Dom1_dirvar[d,1,5,h]$gg))+(2*abs(DMAF_all_alr_Dom1_dirvar[d,3,2,h]$gg))
+(2*abs(DMAF_all_alr_Dom1_dirvar[d,4,2,h]$gg))
+(2*abs(DMAF_all_alr_Dom1_dirvar[d,5,2,h]$gg))+(2*abs(DMAF_all_alr_Dom1_dirvar[d,3,4,h]$gg))
+(2*abs(DMAF_all_alr_Dom1_dirvar[d,3,5,h]$gg))
+(2*abs(DMAF_all_alr_Dom1_dirvar[d,4,5,h]$gg)))
D<-(abs(DMAF_all_alr_Dom1_dirvar[d,1,1,h]$gg)+abs(DMAF_all_alr_Dom1_dirvar[d,2,2,h]$gg)
+abs(DMAF_all_alr_Dom1_dirvar[d,3,3,h]$gg)
+abs(DMAF_all_alr_Dom1_dirvar[d,4,4,h]$gg)+abs(DMAF_all_alr_Dom1_dirvar[d,5,5,h]$gg))
DMAF_all_alr_Dom1_dirtau[d,h]<-U/D
}
```

```
}

## Kappa values for alr data DMAF
DMAF_all_alr_Dom1_omnikappa<-array(rep(NA, 16))
for (h in 1:16){
DMAF_all_alr_Dom1_omnikappa[h]<-1-(DMAF_all_alr_Dom1_omnizeta[h]/RAW_all_alr_Dom1_omnizeta[h])
}

DMAF_all_alr_Dom1_dirkappa<-array(rep(NA, (2*16)),dim=c(2,16))

for (d in 1:2){
for (h in 1:16){
DMAF_all_alr_Dom1_dirkappa[d,h]<-1-(DMAF_all_alr_Dom1_dirzeta[d,h]/RAW_all_alr_Dom1_dirzeta[d,h])
}
}

## Tau values for ox data DMAF
DMAF_all_ox_Dom1_omnitau<-array(rep(NA, 16))
for (h in 1:16){
U<-((2*abs(DMAF_all_ox_Dom1_omnivar[1,1,2,h]$gg))+(2*abs(DMAF_all_ox_Dom1_omnivar[1,1,3,h]$gg))
+(2*abs(DMAF_all_ox_Dom1_omnivar[1,1,4,h]$gg))
+(2*abs(DMAF_all_ox_Dom1_omnivar[1,1,5,h]$gg))+(2*abs(DMAF_all_ox_Dom1_omnivar[1,3,2,h]$gg))
+(2*abs(DMAF_all_ox_Dom1_omnivar[1,4,2,h]$gg))
+(2*abs(DMAF_all_ox_Dom1_omnivar[1,5,2,h]$gg))+(2*abs(DMAF_all_ox_Dom1_omnivar[1,3,4,h]$gg))
+(2*abs(DMAF_all_ox_Dom1_omnivar[1,3,5,h]$gg))
```

```
+(2*abs(DMAF_all_ox_Dom1_omnivar[1,4,5,h]$gg)))
D<-(abs(DMAF_all_ox_Dom1_omnivar[1,1,1,h]$gg)+abs(DMAF_all_ox_Dom1_omnivar[1,2,2,h]$gg)
+abs(DMAF_all_ox_Dom1_omnivar[1,3,3,h]$gg)
+abs(DMAF_all_ox_Dom1_omnivar[1,4,4,h]$gg)+abs(DMAF_all_ox_Dom1_omnivar[1,5,5,h]$gg))
DMAF_all_ox_Dom1_omnitau[h]<-U/D
}

DMAF_all_ox_Dom1_dirtau<-array(rep(NA, (2*16)),dim=c(2,16))
 for  (d  in  1:2){
 for  (h  in  1:16){
U<-((2*abs(DMAF_all_ox_Dom1_dirvar[d,1,2,h]$gg))+(2*abs(DMAF_all_ox_Dom1_dirvar[d,1,3,h]$gg))
+(2*abs(DMAF_all_ox_Dom1_dirvar[d,1,4,h]$gg))
+(2*abs(DMAF_all_ox_Dom1_dirvar[d,1,5,h]$gg))+(2*abs(DMAF_all_ox_Dom1_dirvar[d,3,2,h]$gg))
+(2*abs(DMAF_all_ox_Dom1_dirvar[d,4,2,h]$gg))
+(2*abs(DMAF_all_ox_Dom1_dirvar[d,5,2,h]$gg))+(2*abs(DMAF_all_ox_Dom1_dirvar[d,3,4,h]$gg))
+(2*abs(DMAF_all_ox_Dom1_dirvar[d,3,5,h]$gg))
+(2*abs(DMAF_all_ox_Dom1_dirvar[d,4,5,h]$gg)))
D<-(abs(DMAF_all_ox_Dom1_dirvar[d,1,1,h]$gg)+abs(DMAF_all_ox_Dom1_dirvar[d,2,2,h]$gg)
+abs(DMAF_all_ox_Dom1_dirvar[d,3,3,h]$gg)
+abs(DMAF_all_ox_Dom1_dirvar[d,4,4,h]$gg)+abs(DMAF_all_ox_Dom1_dirvar[d,5,5,h]$gg))
DMAF_all_ox_Dom1_dirtau[d,h]<-U/D
}
}

## Kappa values  for  ox  data  DMAF
```

```
DMAF_all_ox_Dom1_omnikappa<-array(rep(NA, 16))
for (h in 1:16){
DMAF_all_ox_Dom1_omnikappa[h]<-1-(DMAF_all_ox_Dom1_omnizeta[h]/RAW_all_ox_Dom1_omnizeta[h])
}

DMAF_all_ox_Dom1_dirkappa<-array(rep(NA, (2*16)),dim=c(2,16))
for (d in 1:2){
for (h in 1:16){
DMAF_all_ox_Dom1_dirkappa[d,h]<-1-(DMAF_all_ox_Dom1_dirzeta[d,h]/RAW_all_ox_Dom1_dirzeta[d,h])
}
}

#End of Section
#---------------
%\end{verbatim}
```